AFFDL-TR-78-137

ENVIRONMENT-LOAD INTERACTION EFFECTS ON CRACK GROWTH

H.D. DILL
C.R. SAFF

MCDONNELL DOUGLAS CORPORATION
MCDONNELL AIRCRAFT COMPANY
P.O. BOX 516
ST. LOUIS, MISSOURI 63166

NOVEMBER 1978

Final Report
July 1976 - August 1978

AIR FORCE FLIGHT DYNAMICS LABORATORY
AIR FORCE WRIGHT AERONAUTICAL LABORATORIES
AIR FORCE SYSTEMS COMMAND
WRIGHT-PATTERSON AIR FORCE BASE, OHIO 45433

GP78-1063-1

NOTICE

When Government drawings, specifications, or other data are used for any purpose other than in connection with a definitely related Government procurement operation, the United States Government thereby incurs no responsibility nor any obligation whatsoever; and the fact that the government may have formulated, furnished, or in any way supplied the said drawings, specifications, or other data, is not to be regarded by implication or otherwise as in any manner licensing the holder or any other person or corporation, or conveying any rights or permission to manufacture, use, or sell any patented invention that may in any way be related thereto.

This report has been reviewed by the Information Office (OI) and is releasable to the National Technical Information Service (NTIS). At NTIS, it will be available to the general public, including foreign nations.

This technical report has been reviewed and is approved for publication.

Margery E. Artley

MARGERY E. ARTLEY,
Project Engineer

Philip A. Parmley

PHILIP A. PARMLEY, Actg Chief
Structural Integrity Br

FOR THE COMMANDER

Ralph L. Kuster, Jr.

RALPH L. KUSTER, JR., Col. USAF
Chief, Structural Mechanics Division

If your address has changed, if you wish to be removed from our mailing list, or if the addressee is no longer employed by your organization please notify, AFFDL/FBE, W-PAFB, OH 45433 to help us maintain a current mailing list.

Copies of this report should not be returned unless return is required by security considerations, contractual obligations, or notice on a specific document.

AIR FORCE/56780/9 February 1979 — 470

UNCLASSIFIED

SECURITY CLASSIFICATION OF THIS PAGE *(When Data Entered)*

REPORT DOCUMENTATION PAGE		READ INSTRUCTIONS BEFORE COMPLETING FORM
1. REPORT NUMBER AFFDL-TR-78-137	2. GOVT ACCESSION NO.	3. RECIPIENT'S CATALOG NUMBER
4. TITLE *(and Subtitle)* ENVIRONMENT - LOAD INTERACTION EFFECTS ON CRACK GROWTH		5. TYPE OF REPORT & PERIOD COVERED Final Report July 1976-August 1978 6. PERFORMING ORG. REPORT NUMBER
7. AUTHOR*(s)* H. D. Dill C. R. Saff		8. CONTRACT OR GRANT NUMBER*(s)* F33615-76-C-3133
9. PERFORMING ORGANIZATION NAME AND ADDRESS McDonnell Aircraft Company P.O. Box 516 St. Louis, Missouri 63166		10. PROGRAM ELEMENT, PROJECT, TASK AREA & WORK UNIT NUMBERS 486U0226
11. CONTROLLING OFFICE NAME AND ADDRESS Air Force Flight Dynamics Laboratory (FBE) Wright-Patterson Air Force Base Ohio 45433		12. REPORT DATE November 1978 13. NUMBER OF PAGES 208
14. MONITORING AGENCY NAME & ADDRESS*(if different from Controlling Office)*		15. SECURITY CLASS. *(of this report)* Unclassified 15a. DECLASSIFICATION/DOWNGRADING SCHEDULE
16. DISTRIBUTION STATEMENT *(of this Report)* Approved for public release: distribution unlimited.		
17. DISTRIBUTION STATEMENT *(of the abstract entered in Block 20, if different from Report)*		
18. SUPPLEMENTARY NOTES		
19. KEY WORDS *(Continue on reverse side if necessary and identify by block number)* Landing gear Initial flaws Crack growth Environmental acceleration Crack growth prediction Surface flaws Spectrum loads		
20. ABSTRACT *(Continue on reverse side if necessary and identify by block number)* The objective of this program was to systematically investigate chemical environment-load interaction effects on crack propagation. The program was focused by developing a set of design guidelines and criteria for a durability and damage tolerance control plan for landing gear. Current life prediction capability was assessed by comparison of prediction and test. A field survey was conducted to catalog the size, type, and locations of flaws in landing gear components. A crack growth prediction capability developed through analysis and test accounts for environment and load interaction effects.		

DD FORM 1 JAN 73 1473 EDITION OF 1 NOV 65 IS OBSOLETE

UNCLASSIFIED

SECURITY CLASSIFICATION OF THIS PAGE *(When Data Entered)*

20. Materials studied are HP-9Ni-4Co-.30 and 300M steels, and 7075-T6 and 7049-T73 aluminums. A flight-by-flight test stress history was developed for a landing gear component, and crack growth predictions prepared. Subsequently, spectrum tests were performed. A Durability/Damage Tolerance Control Plan for landing gear is outlined.

FOREWORD

This report was prepared by McDonnell Aircraft Company (MCAIR), St. Louis, Missouri, for the Structural Integrity Branch, Structural Mechanics Division, Air Force Flight Dynamics Laboratory, Wright-Patterson Air Force Base, Ohio under Contract F33615-75-C-3133, Project 486U "Advanced Metallic Structures", Work Unit 486U0226. The contract was administered by M. E. Artley, Project Engineer, AFFDL/FBE.

The Structural Research Department of McDonnell Aircraft Company had the responsibility for the performance of this program. The program manager for MCAIR was J. F. Schier. Principal authors of this report are H. D. Dill and C. R. Saff. Dr. J. P. Gallagher, AFFDL/FBE, and W. T. Fujimoto, MCAIR, conducted a field survey of landing gear initial flaws. J. E. Feeney, MCAIR, was a consultant for landing gear design and load spectra development. K. C. Garland and F. J. Coffey, MCAIR Metallurgical Laboratories, performed the test program.

This report covers work accomplished during the period July 1976 through August 1978.

This report was released by the authors in August 1978 for publication.

TABLE OF CONTENTS

TABLE OF CONTENTS (CONTINUED)

TABLE OF CONTENTS (CONCLUDED)

LIST OF ILLUSTRATIONS

LIST OF ILLUSTRATIONS (Continued)

LIST OF ILLUSTRATIONS (Continued)

LIST OF ILLUSTRATIONS (Continued)

LIST OF ILLUSTRATIONS (Continued)

LIST OF ILLUSTRATIONS (Concluded)

LIST OF TABLES

LIST OF TABLES (Continued)

SECTION I

INTRODUCTION

Throughout their service life, aircraft are subjected to the combination of environmental attack and varying loads. The structural integrity of the vehicle can be impaired by surface degradation due to corrosive action or when crack damage is developed or aggravated by the environment.

A major structural aircraft subsystem which experiences high maintenance cost due to the interactions of high load levels and environmental attack is the landing gear subsystem. This subsystem usually consists of a series of nonredundant structural elements that are exposed to numerous aggressive environments during their lives and yet have to be fabricated, for the most part, from materials which are known to be susceptible to environmentally assisted cracking.

Great care is taken during manufacturing and processing to ensure that these nonredundant structural elements are as flaw-free as possible. However, even with good quality control, minute cracks can be developed, for example during grinding and plating of high strength steel parts. Also, as with any aircraft structural subsystem, small cracks can be initiated during service life from latent damage sites developed by fretting, pitting, intergranular stress corrosion cracking (for aluminum alloys) and fatigue.

In landing gear structural components, the cracks of principal concern initiate on the surface of the component. Cracks, whether initially present or service developed, can propagate to failure in these highly-loaded nonredundant structural subsystems and cause system failure.

Therefore, this program was undertaken to systematically investigate chemical environment-load interaction effects on crack propagation behavior. It was focused by developing a set of design guidelines and criteria for a durability and damage tolerance control plan for landing gear structural components. Current life prediction capability was assessed in conjunction with experimentally developed crack growth behavior.

In Phase I, Initial Flaw Characterization, a field survey was conducted in order to catalog the size, type, and locations of flaws in landing gear components.

In Phase II, Algorithm Development, a crack growth prediction capability was developed through analysis and test that accounts for environment and load interaction effects. The Willenborg model was the basis of model development. A technique was developed for predicting the growth of semi-elliptic surface flaws. Materials studied were 7049-T73 and 7075-T6 aluminums and HP-9Ni-4Co-.30 and 300M steels. Crack growth tests were performed on seventy-six specimens.

In Phase III, Verification Test Program, a flight-by-flight test stress history was prepared for a landing gear component. The F-15 main landing gear was selected to establish the stress values and to estimate times associated with the stress conditions. This history is based on design loads for the gear, and not on field measurements. Using the prediction capability developed in Phase II, crack life predictions were prepared for the verification test specimens and 18 tests were conducted.

In Phase IV, Formulation of Guidelines, the experimental data were evaluated to develop recommendations for a Durability/Damage Tolerance Control Plan for landing gear structure. Structural criteria that can be used in landing gear design and the chemical environment for landing gears were outlined.

SECTION II

INITIAL FLAW CHARACTERIZATION

A field survey was conducted by AFFDL and McDonnell Douglas at Ogden ALC (Hill AFB), 21-24 September 1976. The objective was to identify crack-like damage that had resulted in structural failures in landing gear components. This survey is reported in greater detail in Reference 1. The term "crack-like damage" was used to describe latent damage sites from which there had been negligible crack initiation time to an initial crack configuration.

During the first phase of the survey, depot metallurgical laboratory reports from 1971 to Aug 1976 were reviewed to identify causes of damage and to obtain estimates of the range of flaw sizes and shapes for each cause. The reports consisted, in most cases, of a brief history of the problem, optical or transmission electron microscope photomicrographs of the fracture surfaces and pertinent metallurgical information such as alloy, chemical composition, surface condition and hardness. The basic sources of initial damage were found to be: 1) processing operations, 2) latent material defects, 3) mechanical damage, and 4) corrosion.

The next phase of the survey required the determination of a single initial flaw size and shape which was representative of the range of initial damage observed for each cause. To determine these geometries, "ball park" estimates of the sizes and shapes for each cause were prepared. These estimates were then critiqued and refined during separate group discussions with depot maintenance engineering personnel and laboratory metallurgists.

The initial flaw geometry estimates, as determined by this process, are summarized in Table 1. The flaw depth of 0.008 inches in steel caused by localized untempered martensite and the flaw depth of 0.010 inches in aluminum caused by a corrosion pit, as determined from this survey, were used to define test conditions for this program.

TABLE 1
INITIAL FLAWS FOR LANDING GEAR COMPONENTS

Cause of Damage	Dimensions (in)	Comments
Processing Operations		
• Localized Overtempered Martensite	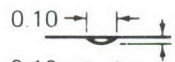	Occurs in steel during grinding operations
• Localized Untempered Martensite	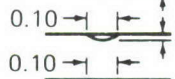	Occurs in steel during grinding operations
• Chrome Cracking		Crack depth equal to depth of chrome layer
Latent Material Defects		
• Inclusions		
• Forging Defects	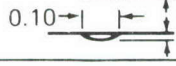	Dimensions shown are for forging laps
Mechanical Damage		
• Field Induced Damage in Steel	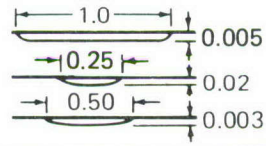	
• Field Induced Damage in Aluminum		
• Shop Induced Tool Marks		
Corrosion		
• Corrosion Pit as Initiation Site for Stress Corrosion Cracking in Aluminum	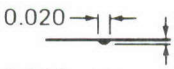	Depth of crack approximately half that of compressive layer induced by shot peening
• Corrosion Pits as Initiation Site for Stress Corrosion Cracking in Steel	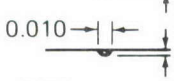	Depth of crack approximately half that of compression layer induced by shot peening
• Corrosion Pit as Initiation Site for Fatigue Crack Growth	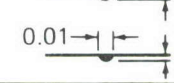	Occurs only in fatigue critical regions

GP78-0753-21

SECTION III

ALGORITHM DEVELOPMENT TEST PROGRAM

1. TEST PROGRAM SUMMARY - The purpose of this program was to obtain experimental data necessary for developing and evaluating a set of crack growth incrementation algorithms. Table 2 summarizes the test plan. Two steels (300M and HP-9-4-.30) and two aluminums (7075-T651 and 7049-T7351) were each subjected to 18 tests. Data was obtained to define material behavior, verify stress intensity solutions for part-through elliptical flaw geometries, and develop crack growth prediction algorithms. The test series was identical for each material with the exception of Specimen 12 for which test conditions were selected independently in each case. The tests had four objectives:

TABLE 2
ALGORITHM DEVELOPMENT AND EVALUATION TEST PROGRAM SUMMARY

Specimen Number	Specimen Type	Environment	Stress Ratio	Frequency cps	Wave Shape	Overload Test Type	Objectives
1	Center Cracked Panel	< 10% R.H. Air	0	10	Sinusoidal	–	Develop da/dn and Evaluate Stress Ratio
2	↓	↓	0.5	10	↓	–	
3	↓	↓	−1	10	↓	–	
4	↓	3.5% Salt Water	0	10	↓	–	Evaluate Frequency
5	↓	↓	0	1	↓	–	
6	↓	↓	0	0.1	↓	–	
7	↓	3.5% Salt Water	0	10	Trapezoidal	–	Evaluate Wave Shape
8	↓	↓	0	0.1	↓	–	
9	↓	↓	0.5	0.1	↓	–	
10	↓	↓	−1	0.1	↓	–	
11	Bolt-Loaded WOL	↓	–	–	Sustained	–	Develop da/dt
12	Center Cracked Panel	Both	–	–	–	–	Duplicate Test
13	↓	3.5% Salt Water	0	10	Sinusoidal	Const Amp	Determine Shut-Off Ratio Under Single Overloads and Under Spectrum Loading
14	↓	↓	0	10	↓	↓	
15	↓	< 10% R.H. Air	0	10	↓	↓	
16	↓	3.5% Salt Water	–	–	↓	Spectrum	
17	↓	< 10% R.H. Air	–	–	↓	↓	
18	Elliptical Flaw	< 10% R.H. Air	0	10	Sinusoidal	–	Evaluate K

Test series is identical for each material.

GP78-0753-44

• Characterize each material by developing constant amplitude fatigue crack growth rate data in a reference environment. (Specimens 1-3).

• Develop and evaluate a linear summation model of environmentally accelerated crack growth. (Specimens 4-12). Specimens 4-6 were used to evaluate the effects of frequency on environmentally assisted crack growth rates. Specimens 7-10 were used to evaluate wave shape effects under an aggressive environment and the interaction of wave shape with frequency and stress ratio. Specimen 11 was used to develop sustained load da/dt data and to determine if such data could be used to predict environmental acceleration with a linear summation model. Specimen 12 was used to duplicate any one test in each material which appeared to give results which were inconsistent with expected trends.

• Determine the overload ratio required to shut-off constant amplitude fatigue crack growth. Assess the interaction of environment and spectrum loading. (Specimens 13-17).

• Evaluate the stress intensity solution for part-through elliptical flaw specimens used in verification testing. (Specimen 18).

2. TEST SPECIMENS - The specimens were of three types: center crack panels, bolt-loaded WOL specimens, and panels containing elliptic surface flaws. Generally, the center crack panels were used for cyclic tests, bolt-loaded WOL specimens for sustained loading tests, and surface flaw panels for stress intensity calibration and subsequent spectrum tests. Test specimens are shown in Figures 1 through 4. The center crack panel shown in Figure 1 was used in the majority of tests.

The bolt-loaded WOL specimens, depicted in Figures 2 and 3, were used to develop sustained load crack growth rate data in a 3.5% NaCl water environment. These specimen configurations allow a constant displacement to be maintained. With a compliance gauge attached to the front face of the specimen, the bolt is torqued until the

desired compliance is obtained. As the crack propagates, the compliance of the specimen increases and the constant displacement provided by the bolt results in decreasing stress intensity. This arrangement does not require sustained load equipment and permits long-term tests to be performed economically.

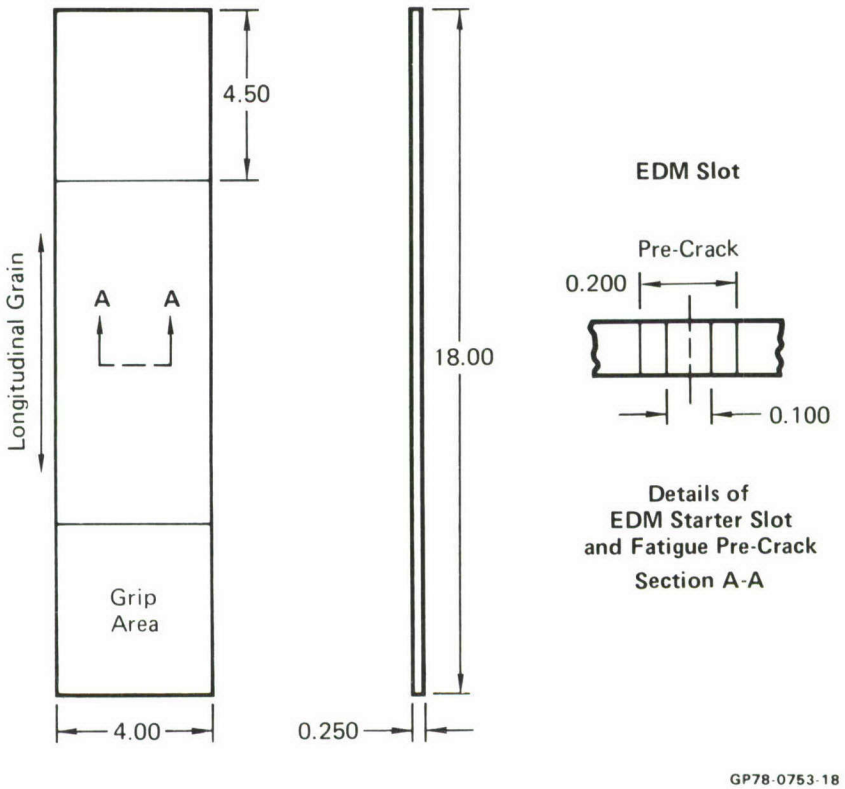

Figure 1
Center Crack Panel Specimen

During the sustained load tests using the bolt-loaded WOL specimen (Figure 2) with the aluminum alloys (7075-T6 adn 7049-T73) it was found that the cracks curved away from the midplane of the specimens. Sometimes the crack forked. In order to force the crack to remain in the midplane, specimens with side grooves (Figure 3) were used for subsequent testing in aluminum.

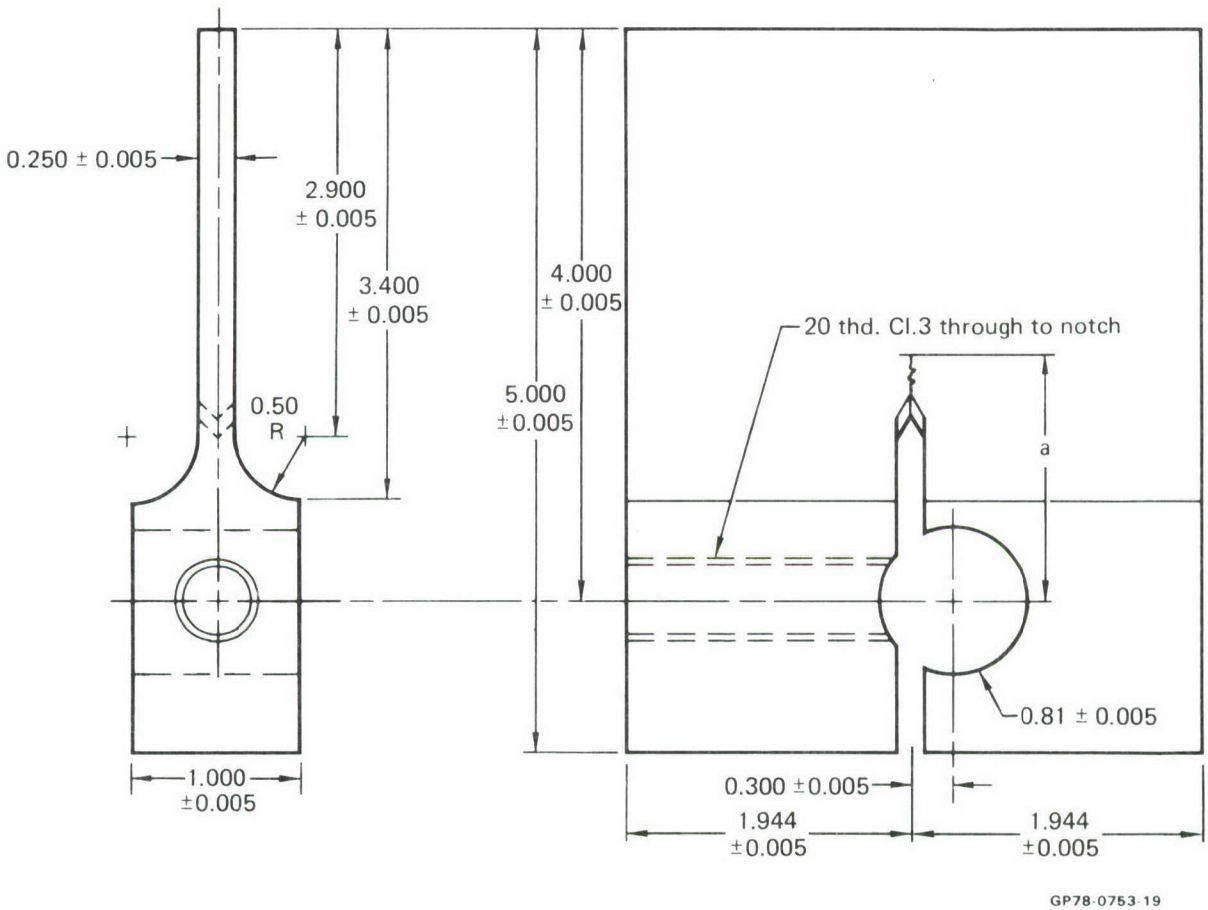

Figure 2
Bolt-Loaded WOL Specimen

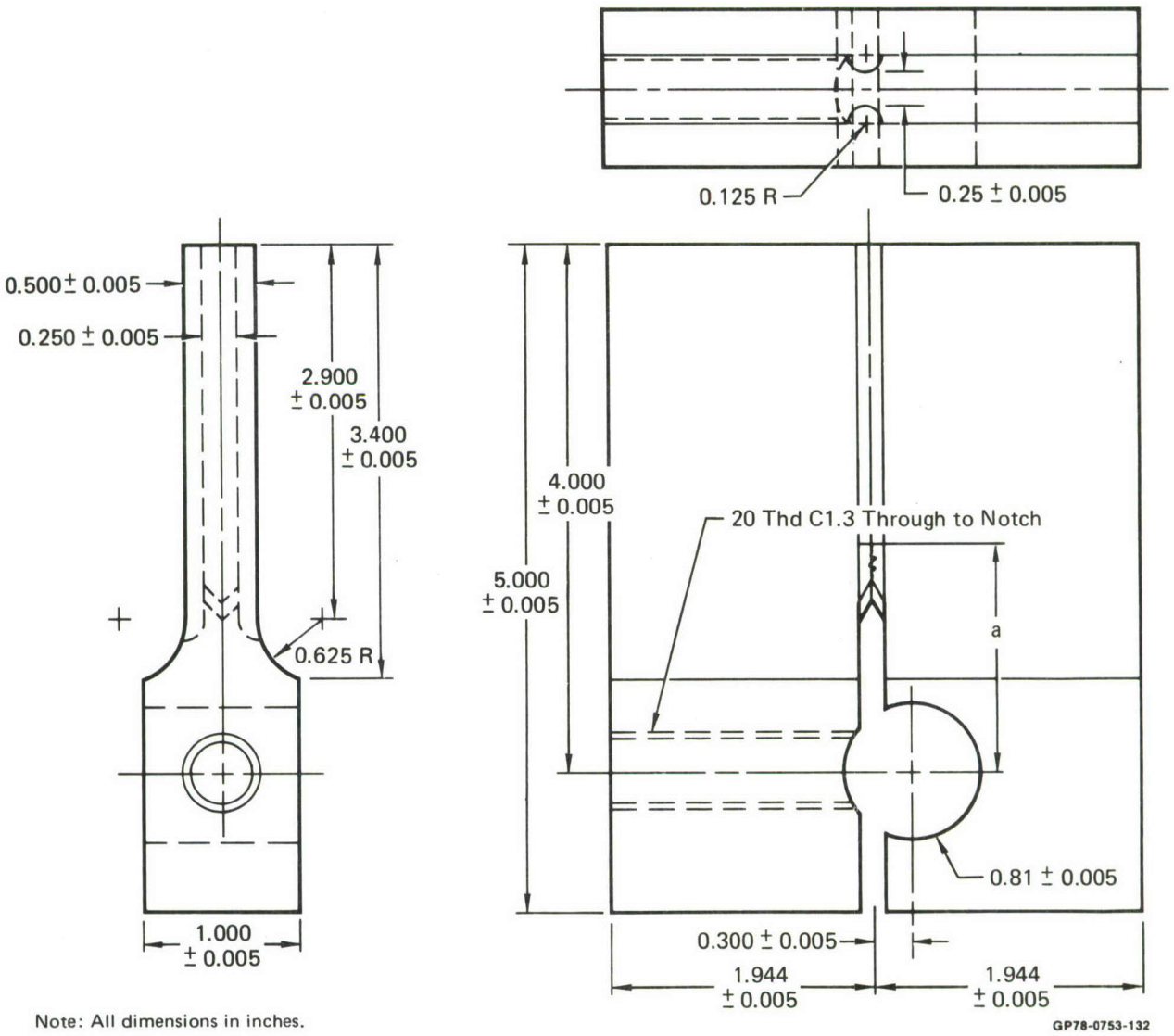

Figure 3
Modified Bolt-Loaded WOL Specimen for Aluminum

Prior to sustained load tests, the bolt-loaded WOL specimens were cyclically loaded through the bolt head and a transverse pin to develop compliance and da/dN versus ΔK measurements. This was necessary in order to characterize the bolt-loaded WOL specimen configurations. Specimens made from the environmentally resistant aluminum and steel materials (7049-T73 and HP-9-4-.30) were used to verify a stress intensity solution for the configuration shown in Figure 2. A specimen made from 7049-T73 was similarly used for the Figure 3 configuration.

The elliptic surface flaw specimens, Figure 4, were used for stress intensity calibration for the part-through crack, and have the basic configurations used for the verification test program (Section VI). The reduced section in the steel specimen was required in order to properly simulate stresses experienced in landing gear components, and maintain load levels within the capacity of available fatigue test equipment. The predicted finite width effect on crack growth was negligible.

3. TEST PROCEDURES

a. Pre-Cracking Procedures - Center-crack specimens were pre-cracked at a stress ratio of 0.02 until the total crack length was approximately 0.20 inches. The final 0.04 inches of crack extension were performed at a stress level equal to or less than that at which the subsequent test was performed.

Bolt-loaded WOL specimens were pre-cracked by cyclic loading, through the bolt head and a transverse pin, at a 0.02 stress ratio until a 0.20 inch crack was introduced at the chevron notch, Figures 2 and 3.

Elliptical-surface-flaw specimens had EDM notches of size and shape required to produce initial flaws on the surface at two locations. The initial flaw sizes and shapes, based on those found in landing gear components during the characterization phase of the program, are summarized in Table 1.

b. Specimen Loading and Instrumentation - Cyclic testing was performed in an MTS test system, consisting of a hydraulic power supply, load frame assembly, electronic control console, and tele-printer. The specimens were loaded through self-aligning hydraulic grips. Teflon roller guides were installed against the specimen surface to prevent buckling during application of compression loads.

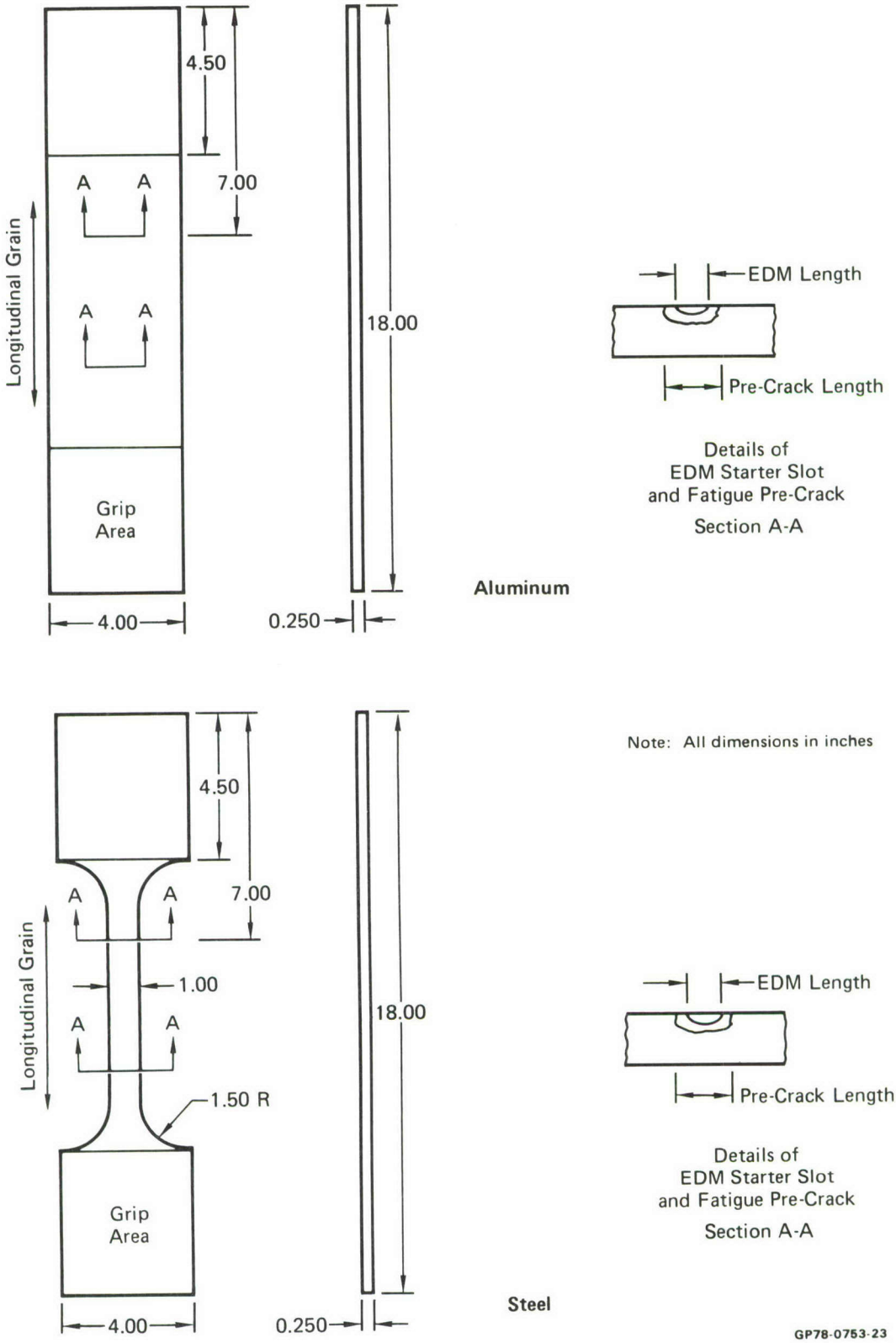

Figure 4
Elliptic Surface Flaw Specimen

During testing, surface crack lengths were optically monitored using a cathetometer with a 30X microscope. Crack growth measurements during constant amplitude tests were made after every .05 inches of crack growth (approximately). Subsequent to overload application, crack growth was monitored more closely to identify the transient behavior which occurs. During constant amplitude tests with overloads, the crack length was measured after each overload. Similar records were made after each .02 inches of growth after the overload until .20 inches of crack growth occurs. Thereafter, the measurements were made after every .04 inches of crack growth until .50 inches growth was obtained and the next overload applied.

Sustained load crack growth tests using bolt-loaded WOL specimens required compliance calibrations. A compliance gauge was used to measure the applied initial stress intensity, through the known relationship of displacement and stress intensity. The gauge was removed and crack growth was monitored every 15 minutes for two hours until enough data was obtained to estimate the time interval for .05 inches of crack growth. Crack lengths were subsequently measured at the end of the estimated time intervals.

Elliptic surface flaw lengths were recorded after each 0.02 inches of crack extension. After each 0.06 inches of crack extension the displacement gage was placed on knife edges across the crack mouth of the longest crack and displacement was measured at 10% load increments up to maximum load and returning to zero load. The gage then was removed and the specimen was subjected to marker band cycles at 65% of the constant amplitude test load. The procedure of measuring crack length after each 0.02 inch of extension and measuring displacement across the longest crack and applying marker band cycles after each 0.06 inches of crack extension was repeated for each specimen until specimen failure. The number of marker band cycles applied was reduced as the cracks grew longer. It was found that the best marker bands were produced by cycling at the 65% load level until minute surface

growth occurred. After completion of the test, the fracture surfaces of the specimens were examined and crack depth (a) measurements were made from the marker bands.

c. Environmental Control - The plastic pockets used to contain environmental solutions for cyclically loaded specimens are shown in Figure 5. This containment method was used for both the salt water (3.5 percent NaCl in distilled water) environment and the low humidity environment. Low humidity air environment (<10% R.H.) was provided using silica jell desiccant.

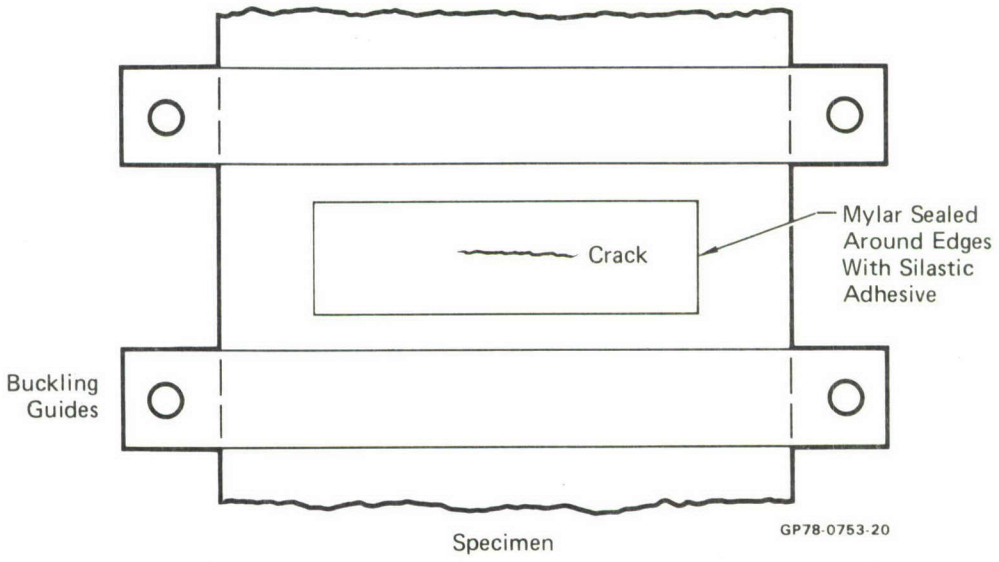

Figure 5
Environment Control System

4. CONSTANT AMPLITUDE FATIGUE STRESS RATIO EVALUATIONS - (Specimens 1-3) - Constant amplitude fatigue tests were performed on 12 center crack panels (three per material) to determine the effect of stress ratio on crack growth rate and to verify an analytical stress ratio correction. Tests were performed at stress ratios of 0, 0.5, and -1 for each of the four materials in a low-humidity air environment (10% R.H.). The wave shape used for these tests was a sinusoid, applied at a frequency of 10 Hz. During the tests, crack growth was visually monitored and crack length recorded at approximately 0.05 inch intervals.

The results of constant amplitude crack growth testing were summarized using the procedure shown in Figure 6. They are presented in Table 3 in terms of number of cycles to grow a center crack over the range of crack lengths shown for each material. In order to develop data over a wide range of stress intensities with a single specimen, the tests were performed with the stress level incrementally increasing as the crack length increased. The lives summarized in Table 3 are based on integration of the da/dN data obtained from test for a center crack in a 4 inch wide panel. For comparison, constant amplitude stress levels in steel were assumed to be 20 ksi and in aluminum to be 10 ksi. (The crack lengths at rupture varied predominately due to K_C variations among the materials.)

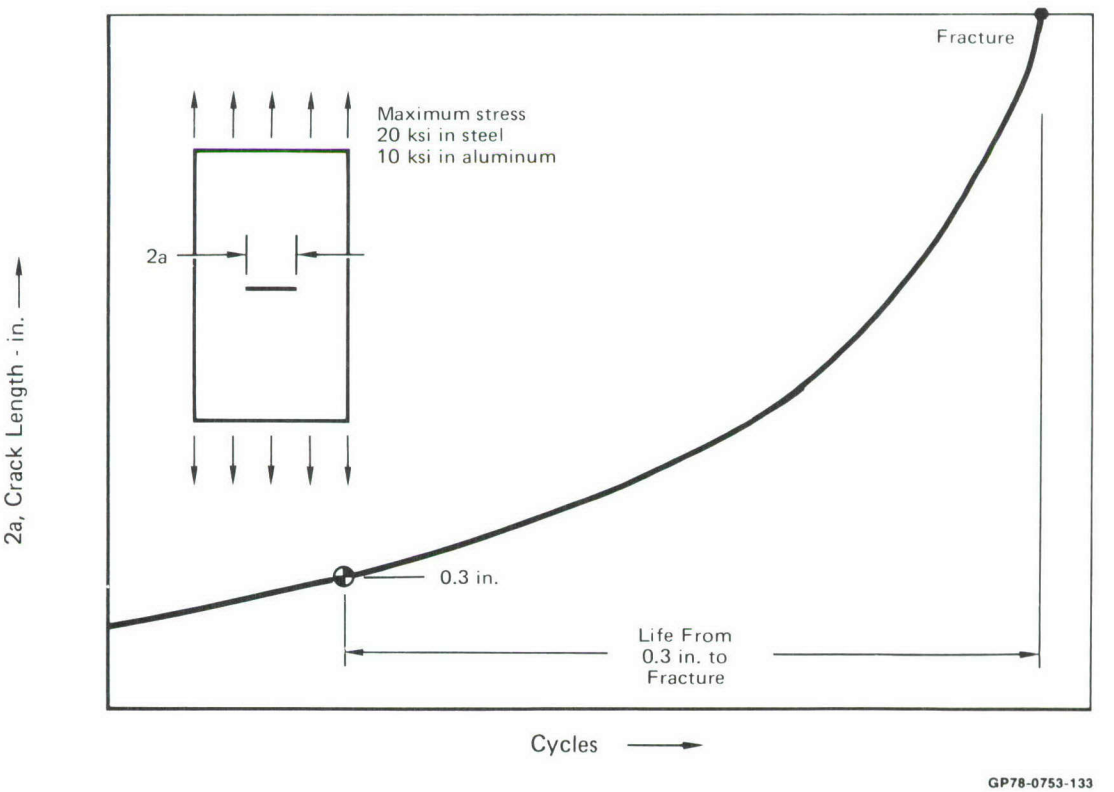

Figure 6
Algorithm Test Program Summary Procedure

TABLE 3
SUMMARY OF CONSTANT AMPLITUDE RESULTS FROM ALGORITHM TEST PROGRAM

Specimen Number	Objective	Environment	Stress Ratio	Cycle Rate	7049-T73 Cycles From 0.3 to 3.5	7075-T6 Cycles From 0.3 to 3.3	HP-9-4 Cycles From 0.3 to 3.5	300M Cycles From 0.3 to 2.0
1	Develop da/dN	<10% R.H. Air	0	10 cps	221000 (2)	102000	199000	128000
2	and Evaluate		0.5		658000	466000	706000	1097000
3	Stress Ratio		−1		161000	150000/ 107000	156000	167000
4	Evaluate	3.5% Salt Water	0	10 cps	29500/ 27500 (3)	31400	214000	298000/ 98300
	Frequency							
5			0	1 cps	15300	22200	148000	20000
6			0	0.1 cps	19100	22400	101000	4300
7	Evaluate (1)		0	10 cps	27900	28800	217000	83800
8	Trapezoidal		0	0.1 cps	45500	29200	157000	564
9	Wave Shape		0.5	0.1 cps	149000	104000	361000	765
10			−1	0.1 cps	31600	28000	180000	819

GP78-1063-5

Notes: (1) Tests 1 thru 6 use sinusoidal wave shape, tests 7 thru 10 use trapezoidal shape.

(2) Test lives are quoted as the number of cycles required to grow a center crack in a 4 inch wide panel from the smallest to the largest crack length shown. Stress levels in steel were assumed to be 20 ksi and in aluminum to be 10 ksi. Final crack lengths vary due to K_c variations among the materials.

(3) Second result, where shown, is result of duplicate test.

The results of the tests used to evaluate the effects of stress ratio are summarized in Table 3, and Figures 7 through 10. The figures also present predictions based on an analysis procedure discussed in Section IV.

5. CONSTANT AMPLITUDE FATIGUE FREQUENCY EVALUATIONS - (Specimens 4-6) - Constant amplitude fatigue tests were performed on 12 center crack panels (3 per material) to determine the effect of cyclic frequency on crack growth rate and to verify analytical results obtained with a linear superposition model (Section IV). Specimens were tested at frequencies of 10 cps, 1 cps, and 1/10 cps for each material. Each specimen was subjected to an aggressive environment (3.5% NaCl - distilled water) during test. The wave shape was sinusoidal. During the tests, crack growth was visually monitored and crack length recorded at approximately 0.05 inch intervals.

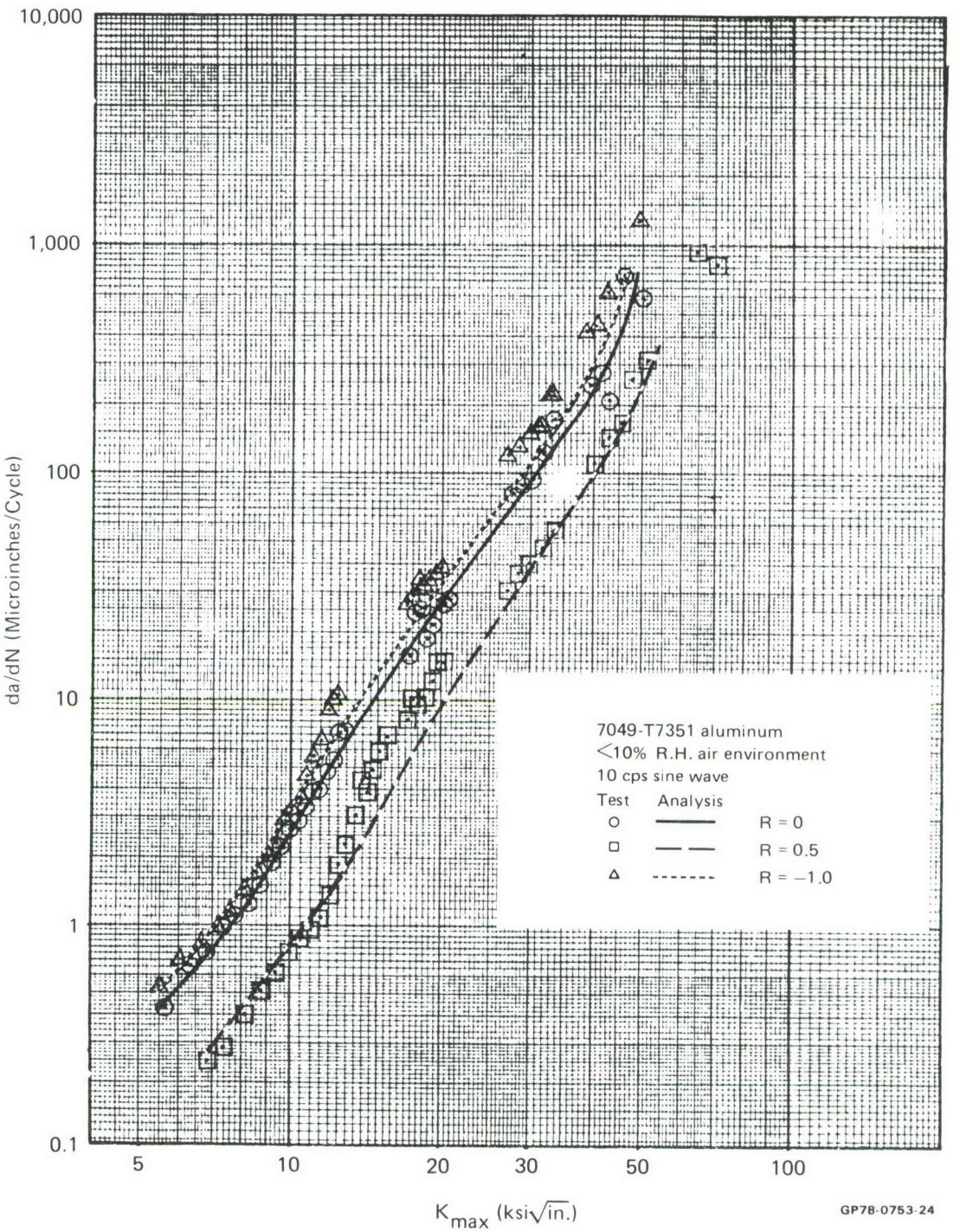

Figure 7
Effect of Stress Ratio on Crack Growth Rate in 7049 Aluminum

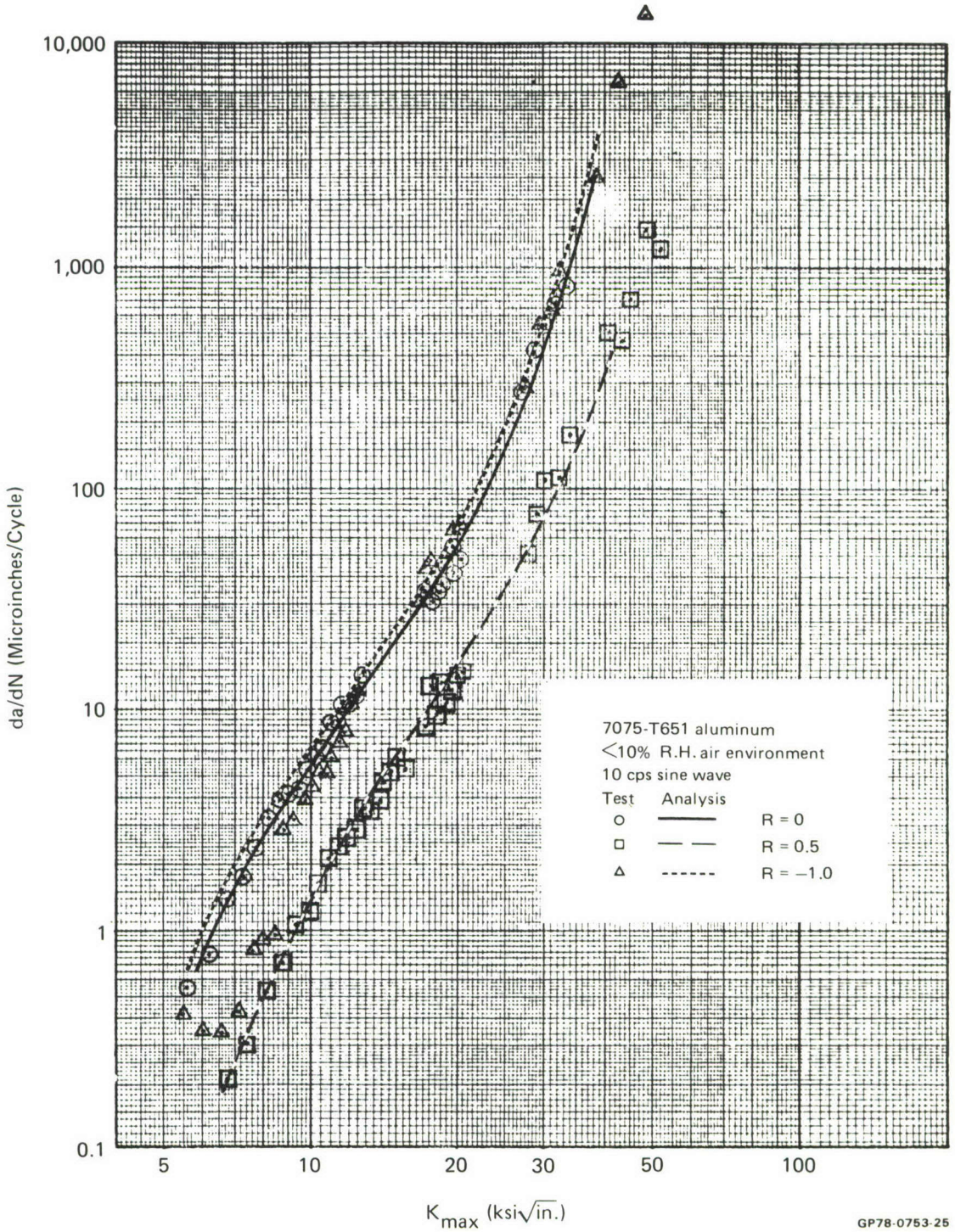

Figure 8
Effect of Stress Ratio on Crack Growth Rate in 7075 Aluminum

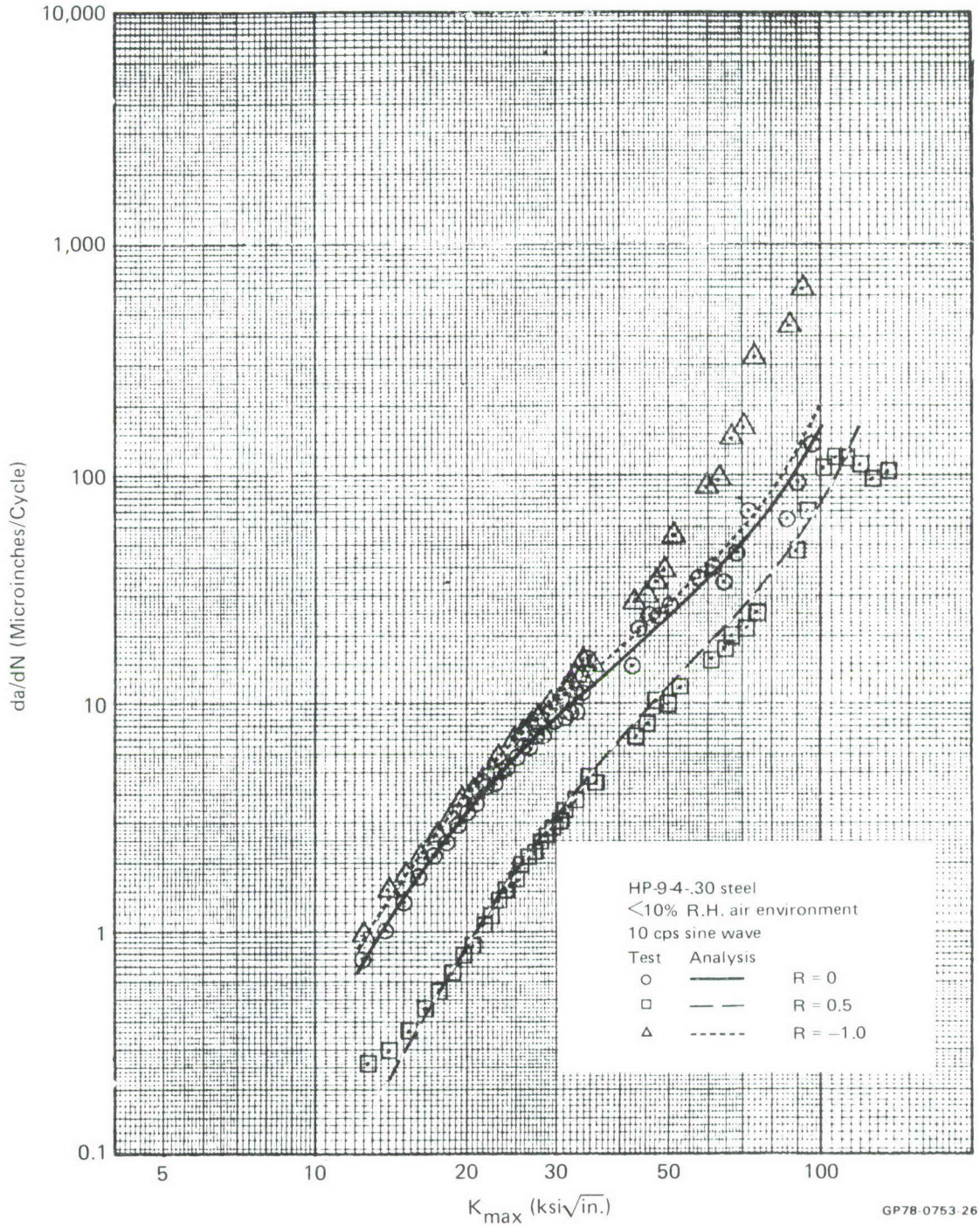

Figure 9
Effect of Stress Ratio on Crack Growth Rate in HP-9-4-.30 Steel

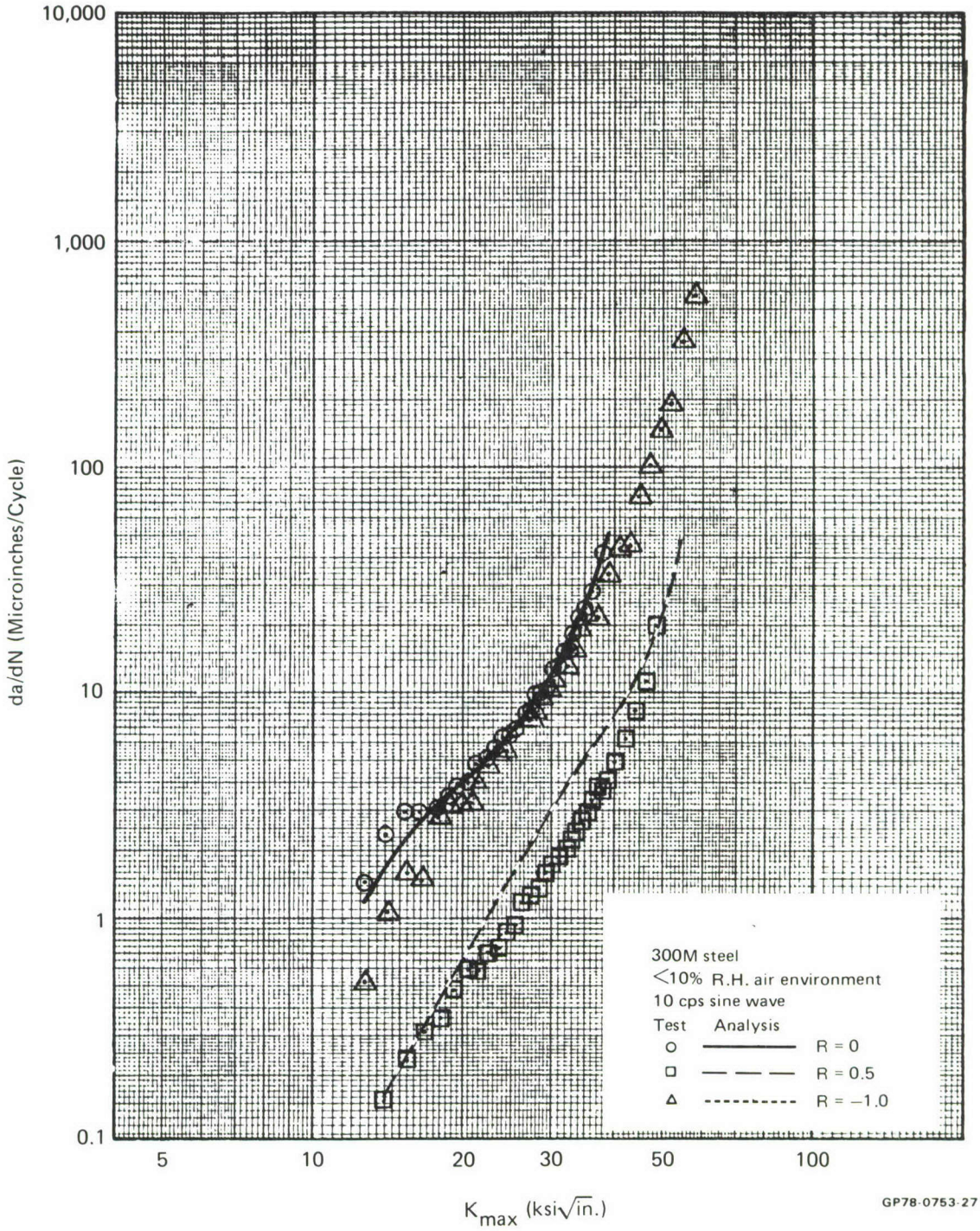

Figure 10
Effect of Stress Ratio on Crack Growth Rate in 300M Steel

The results of this series of tests are summarized in Table 3 and Figures 11 through 14. 300M steel shows a much larger effect of test frequency in the 3.5% salt water environment than any of the other materials. The 300M shows more than a factor of 20 decrease in crack growth life as the frequency is reduced from 10 cps to 0.1 cps. The other materials are affected by a factor of two or less, showing a decrease in life as the frequency decreases from 10 cps to 1 cps, but show only a small effect of further reduction in frequency from 1 cps to 0.1 cps.

6. CONSTANT AMPLITUDE FATIGUE WAVE SHAPE EVALUATIONS - (Specimens 7-10) - Sixteen constant amplitude fatigue tests were performed on center crack panels to assess the interaction of environment, stress ratio, cyclic frequency, and wave shape on crack growth. Four tests were performed on specimens from each material using a trapezoidal wave form, Figure 15, in which the load rate allowed a great portion of the cycle to be held at a constant peak stress. One test with the trapezoidal wave shape was run at 10 cps, the others were run at the frequency showing the largest environmental effect, 0.1 cps. These tests were run at stress ratios of 0, 0.5, and -1. All specimens were subjected to the aggressive environment (3.5% NaCl - water) during the test.

The results of these tests are summarized in Table 3, and in Figures 16 through 19. By comparing the trapezoidal and sine wave test results in Table 3, it can be seen that the trapezoidal wave has little effect except in 300M at the low frequency where the crack growth life is decreased by a factor of about 7. This is expected since, according to several sources, 300M exhibits large sustained load cracking rates in the salt water environment (e.g., References 2 and 3).

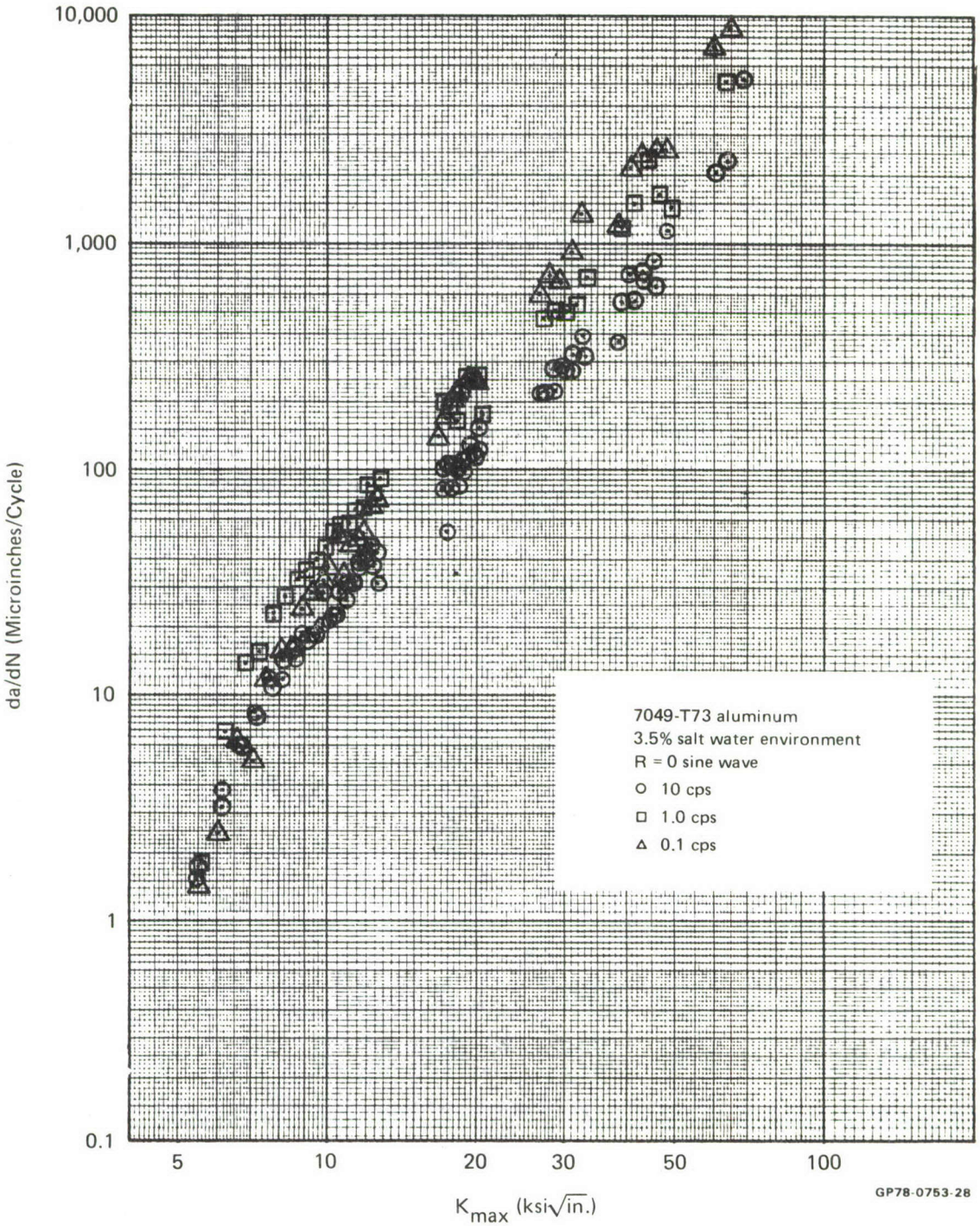

Figure 11
Effect of Frequency on Crack Growth Rate in Salt Water in 7049 Aluminum

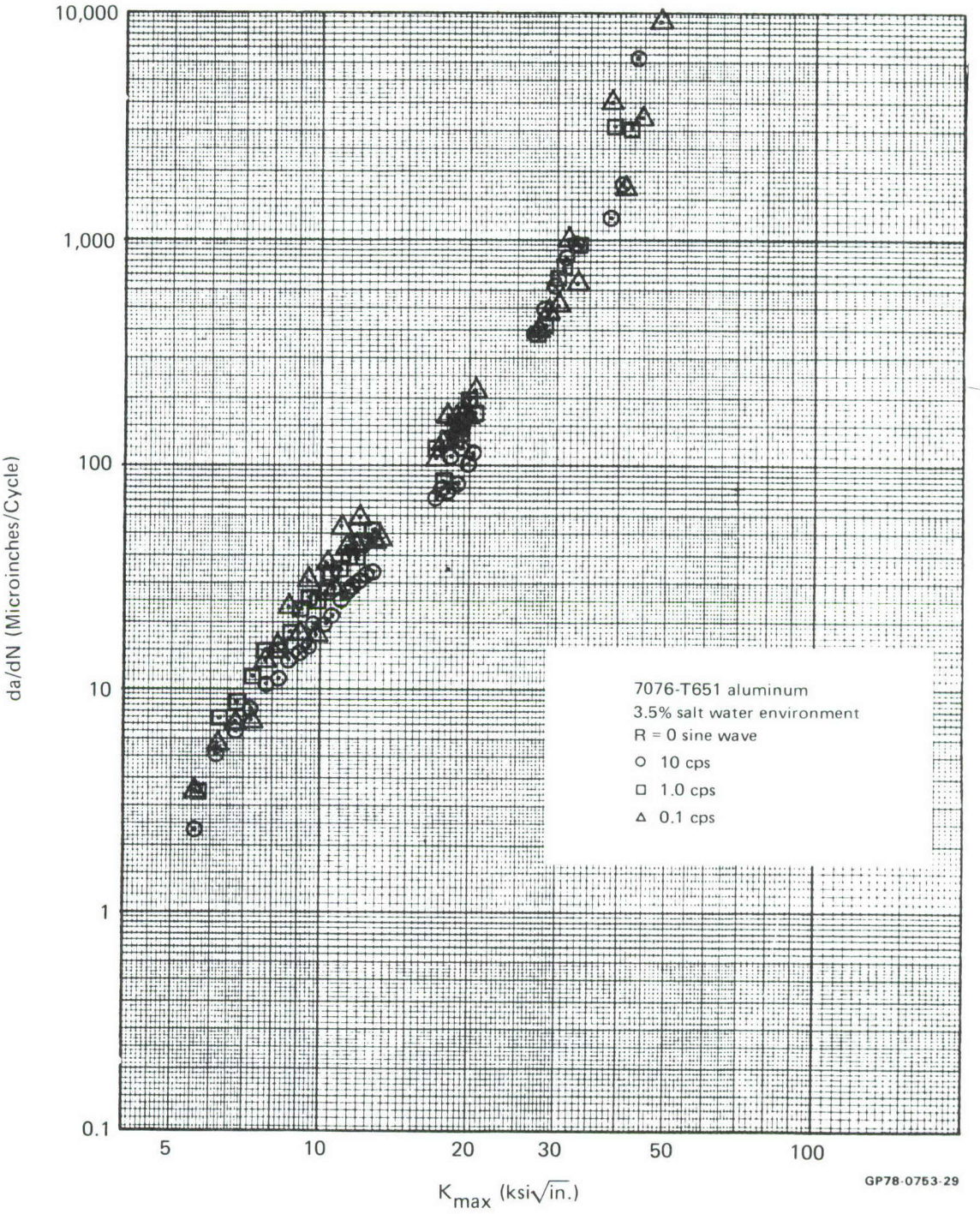

Figure 12
Effect of Frequency on Crack Growth Rate in Salt Water in 7075 Aluminum

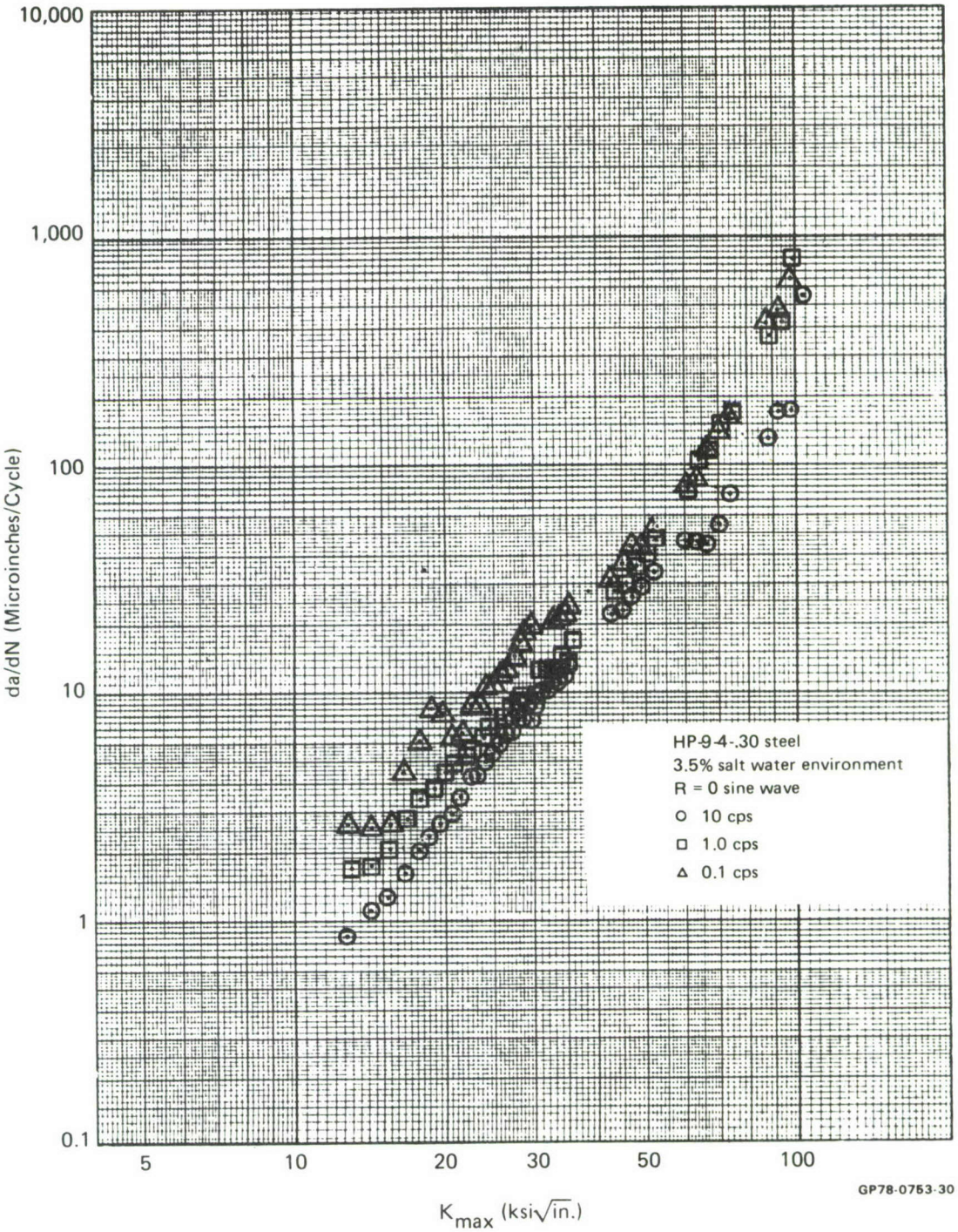

Figure 13
Effect of Frequency on Crack Growth Rate in Salt Water in HP-9-4-.30 Steel

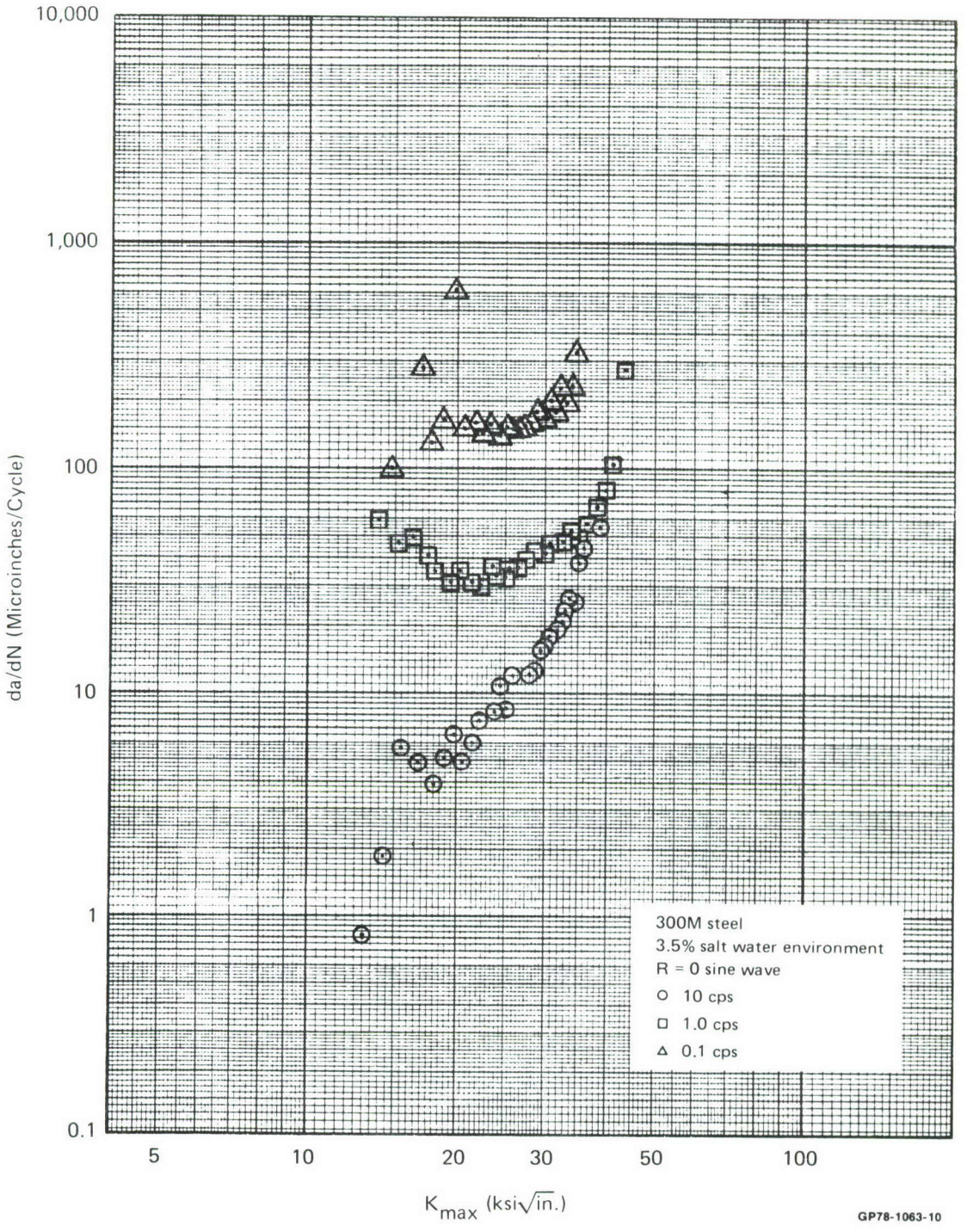

Figure 14
Effect of Frequency on Crack Growth Rate in Salt Water in 300M Steel

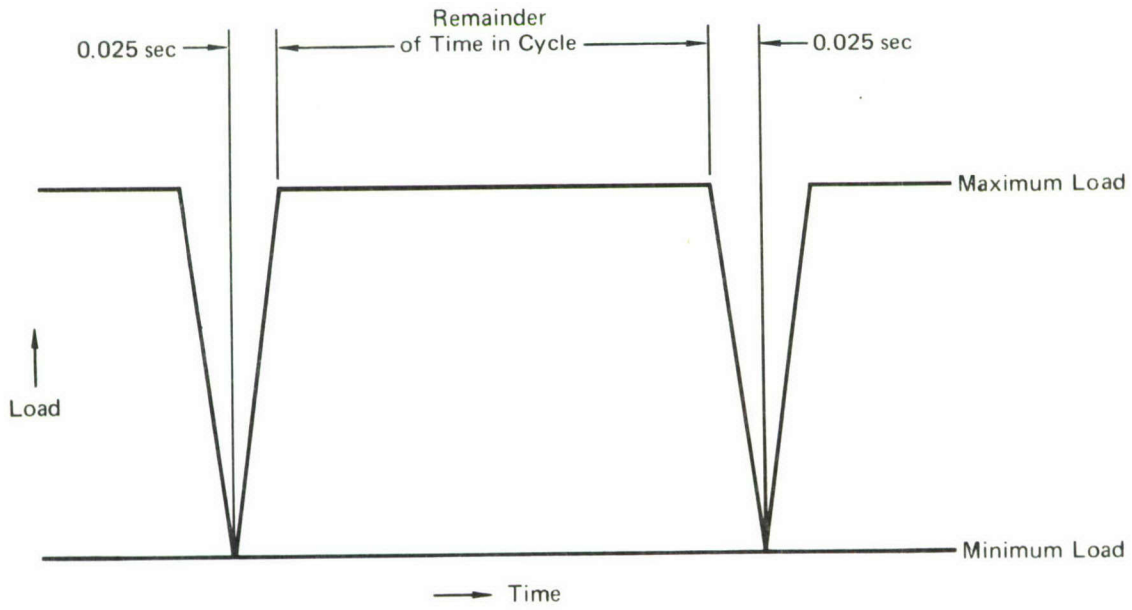

Figure 15
Trapezoidal Wave Shape

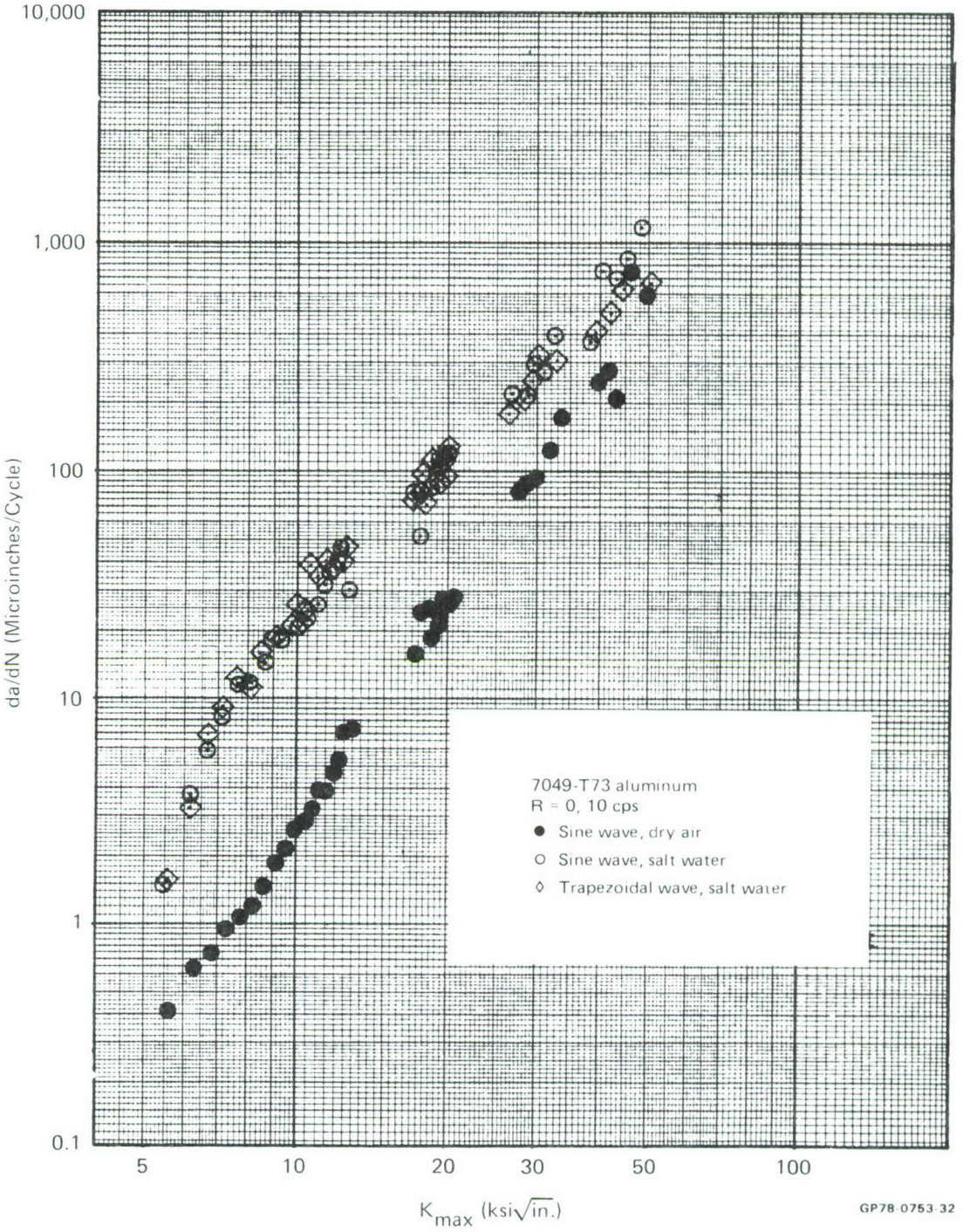

Figure 16
Effect of Wave Shape and Environment on Crack Growth Rate in 7049 Aluminum

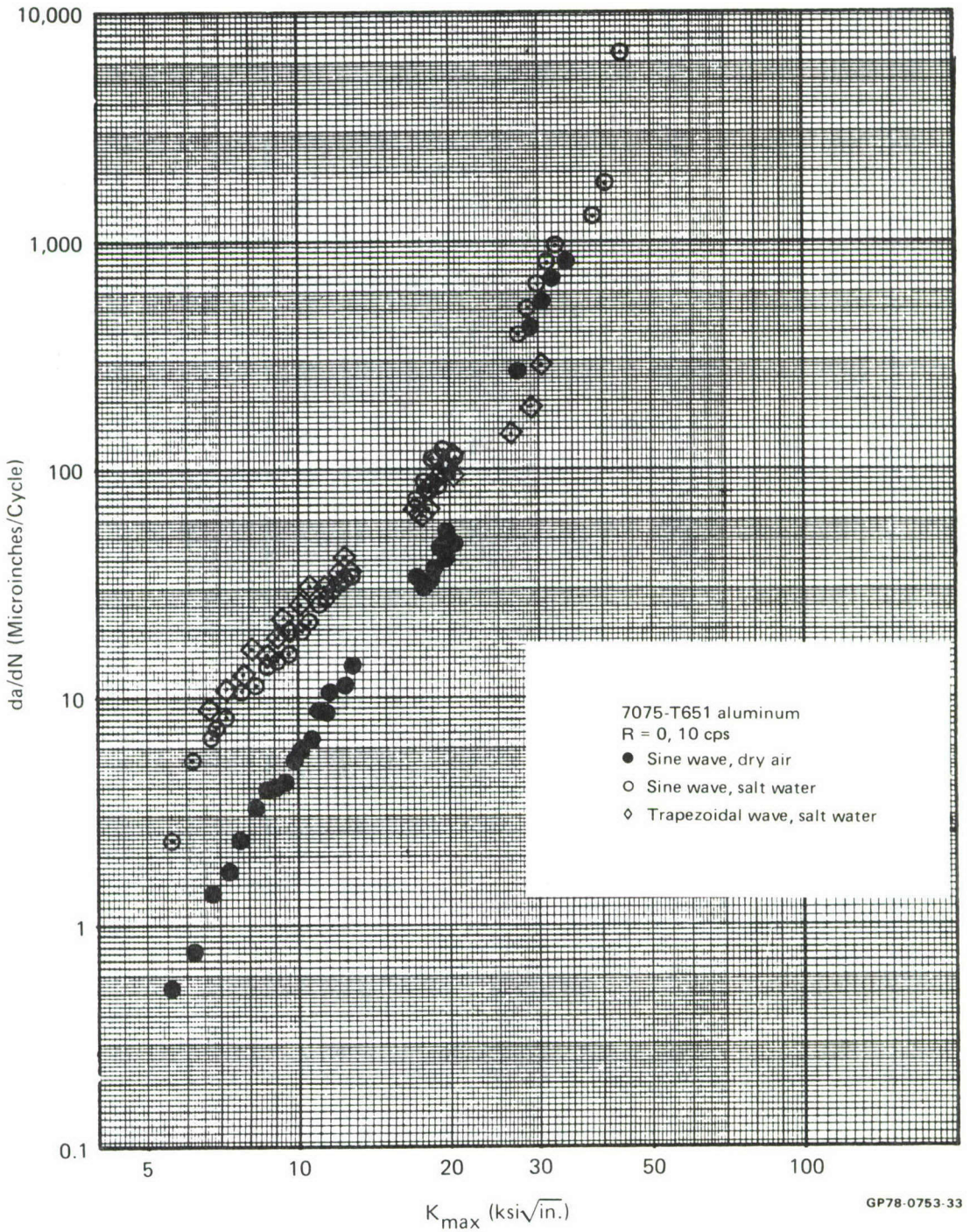

Figure 17
Effect of Wave Shape and Environment on Crack Growth Rate in 7075 Aluminum

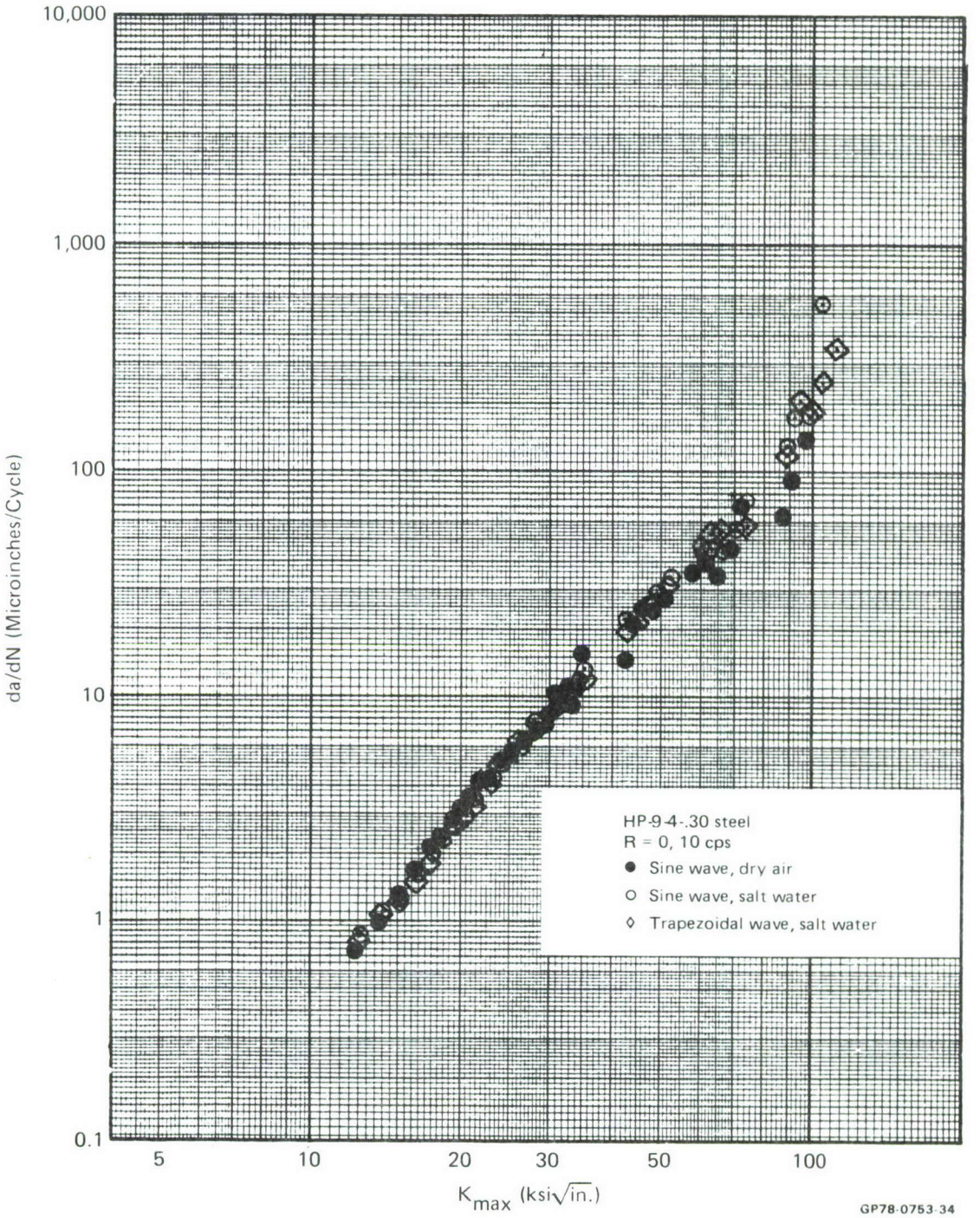

Figure 18
Effect of Wave Shape and Environment on Crack Growth Rate in HP-9-4-.30 Steel

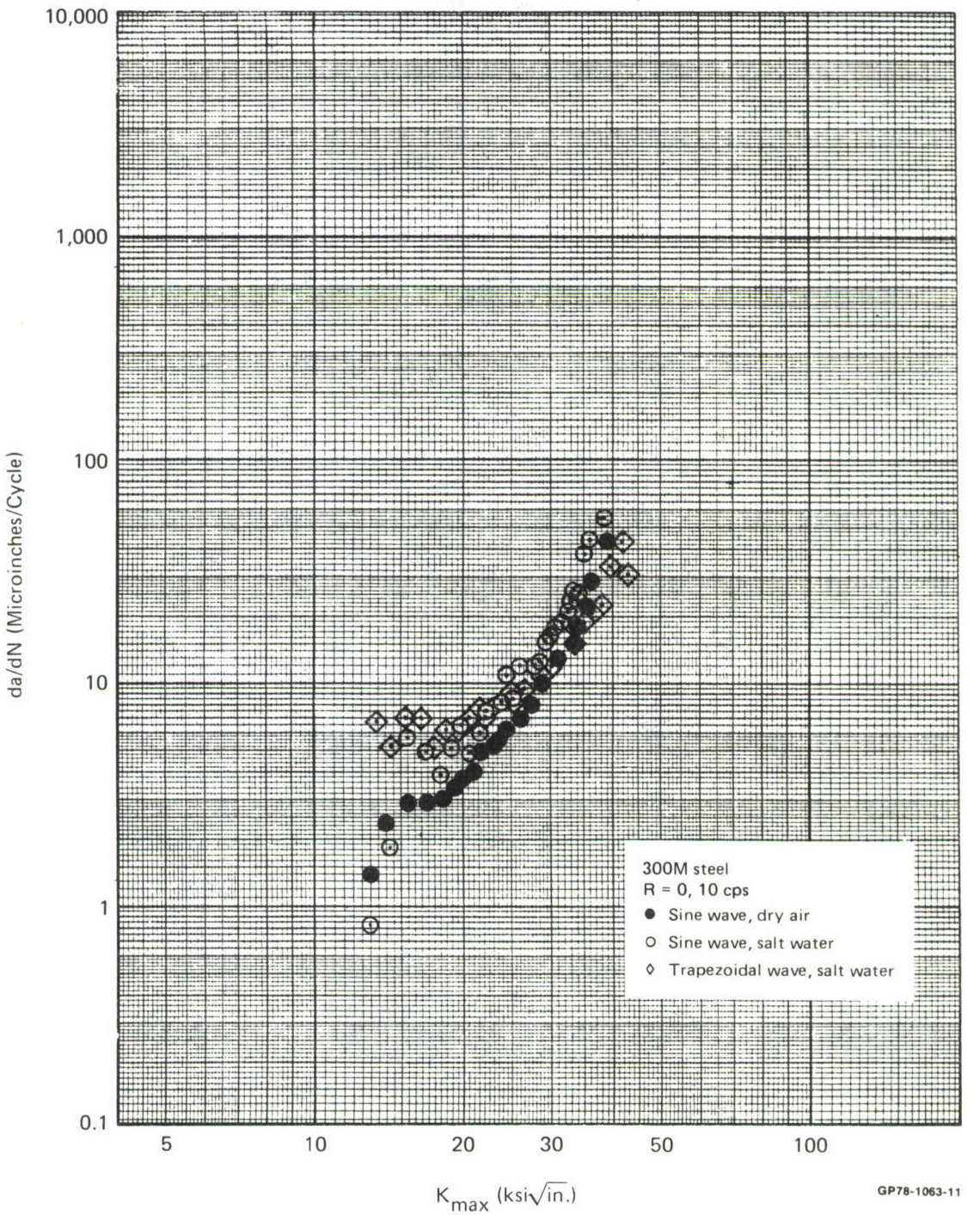

Figure 19
Effect of Wave Shape and Environment on Crack Growth Rate in 300M Steel

These trends are also evident in the data shown in Figures 16 through 19 where the growth rates at 10 cps are presented for the dry air environment, and for the salt water environment with sine wave and trapezoidal wave loading. The data show that even 300M is little affected by change in load wave shape at high frequencies. Similarly, Figures 20 through 23 present data indicating that there is little effect of frequency with the trapezoidal wave shape loading, except for 300M. This material exhibits a factor of 100 increase in growth rate as the frequency decreases from 10 cps to 0.1 cps (Figure 23).

The combined effects of wave shape and stress ratio are demonstrated in the test results presented in Figures 24 through 27. By comparing these data with those presented in Figures 7 through 10, it can be seen that the effects of stress ratio for tests performed in salt water with a trapezoidal wave shape loading are similar to those demonstrated in dry air with a sinusoidal wave shape loading.

7. SINGLE OVERLOAD AND SPECTRUM TESTS - (Specimens 13-17) - Two types of tests were used to determine the overload ratio which shuts-off subsequent constant amplitude crack growth. The first type of test was a series of increasing single overloads applied at intervals such that interactions of the overload effects were small. The second series of tests were spectrum tests of center cracked panels subjected to the accelerated stress history defined in Section V.

a. Single Overload Tests - (Specimens 13-15) - Ten tests of center crack panels were used to assess the effects of a single overload on constant amplitude crack growth, in both the inert and aggressive environments. The test procedure was to grow the crack under constant stress intensity amplitude cycling until .05 inches of growth was obtained, a single overload cycle ratio of 1.2 was applied, and, subsequently, the crack growth was monitored until .50

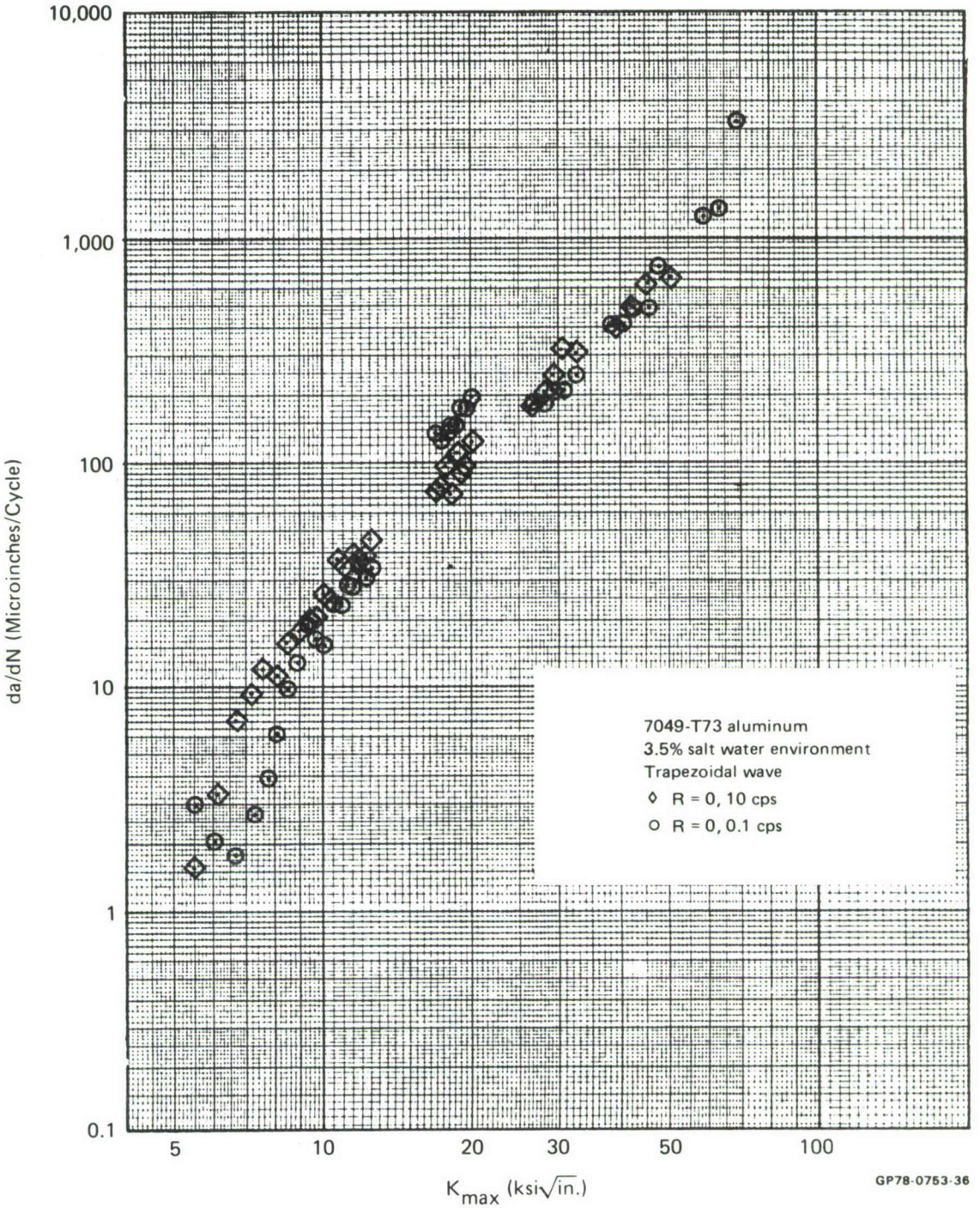

Figure 20
Effect of Frequency on Crack Growth Rate Under Trapezoidal Wave in 7049 Aluminum

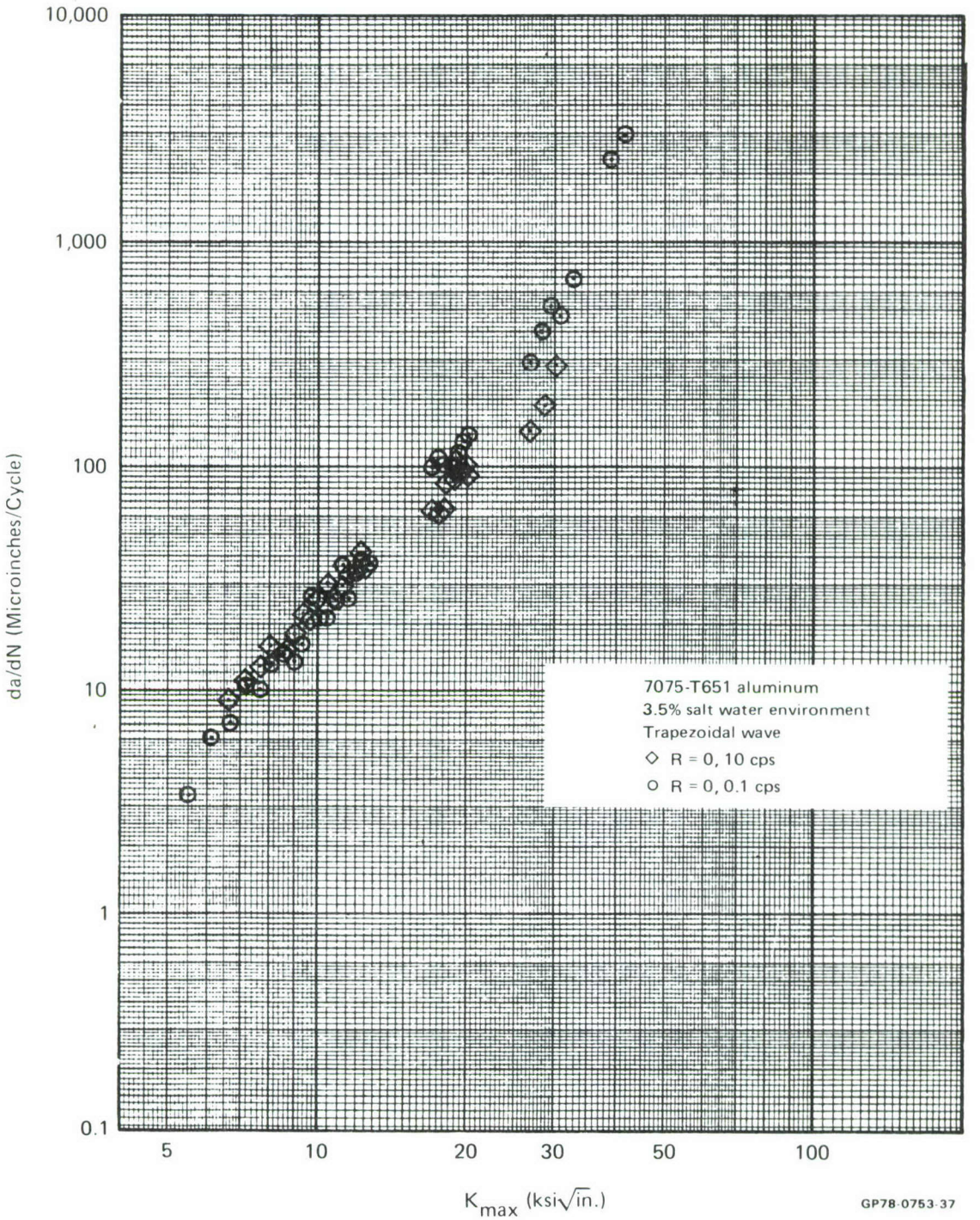

Figure 21
Effect of Frequency on Crack Growth Rate Under Trapezoidal Wave in 7075 Aluminum

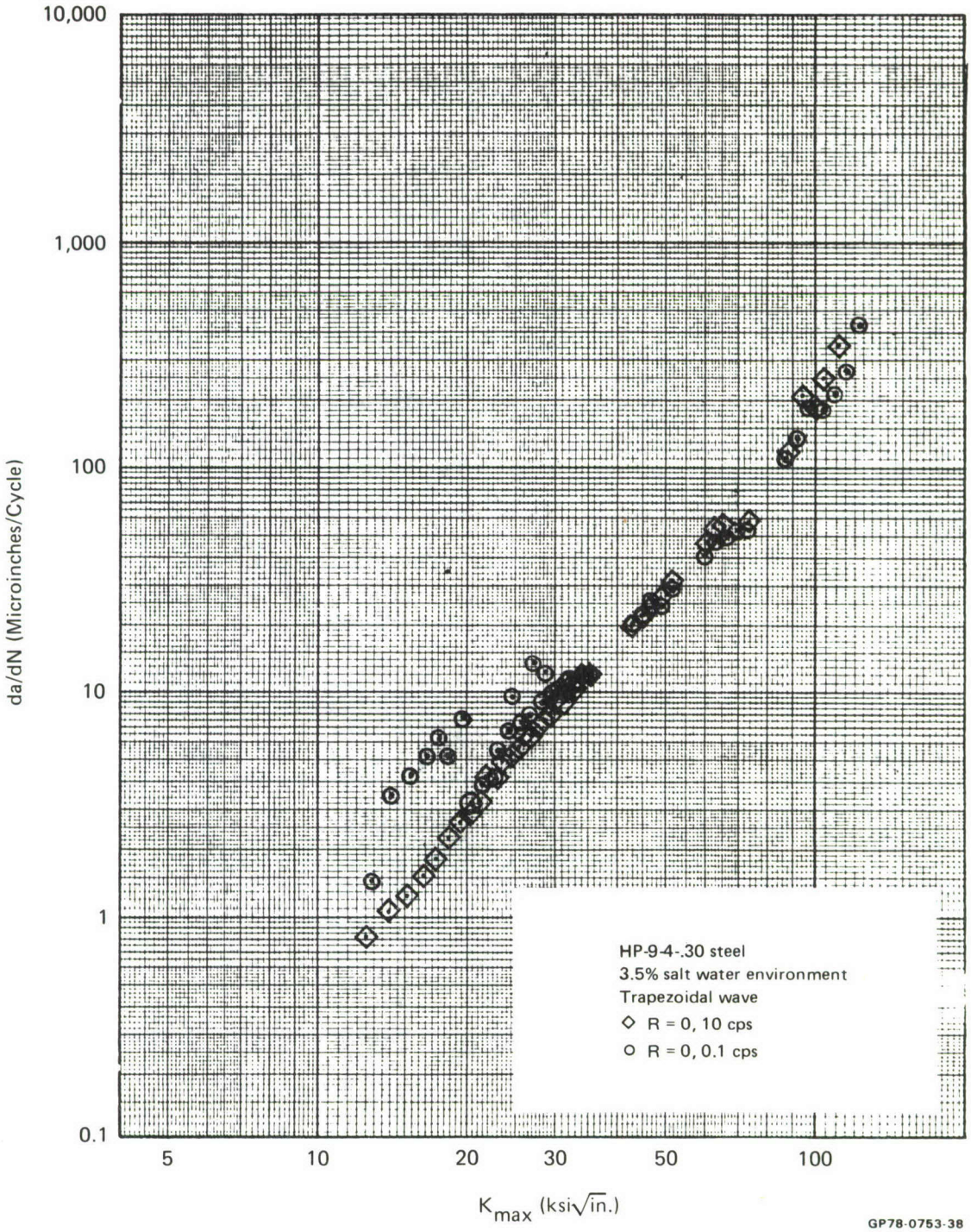

Figure 22
Effect of Frequency on Crack Growth Rate Under Trapezoidal Wave in HP-9-4-.30 Steel

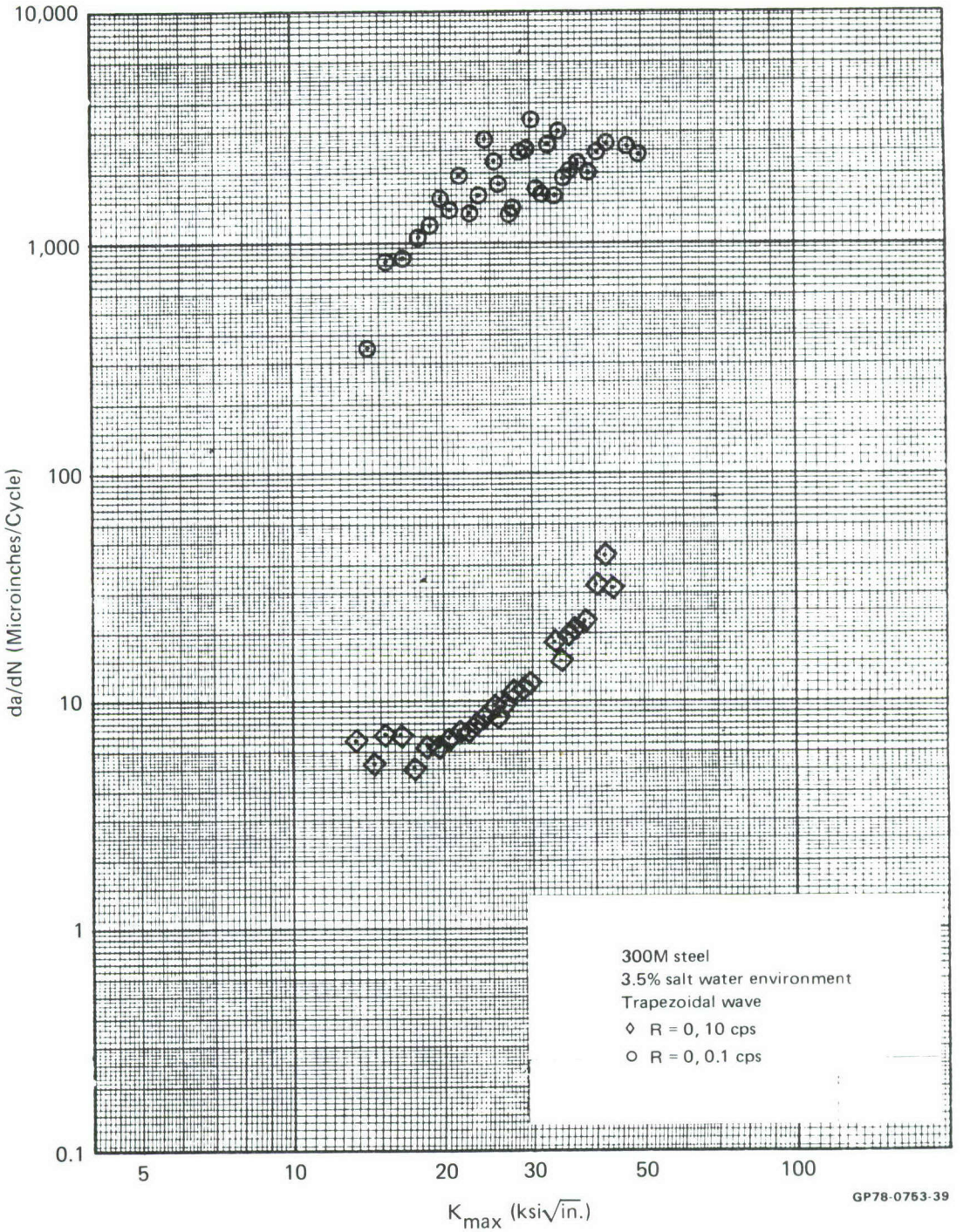

Figure 23
Effect of Frequency on Crack Growth Rate Under Trapezoidal Wave in 300M Steel

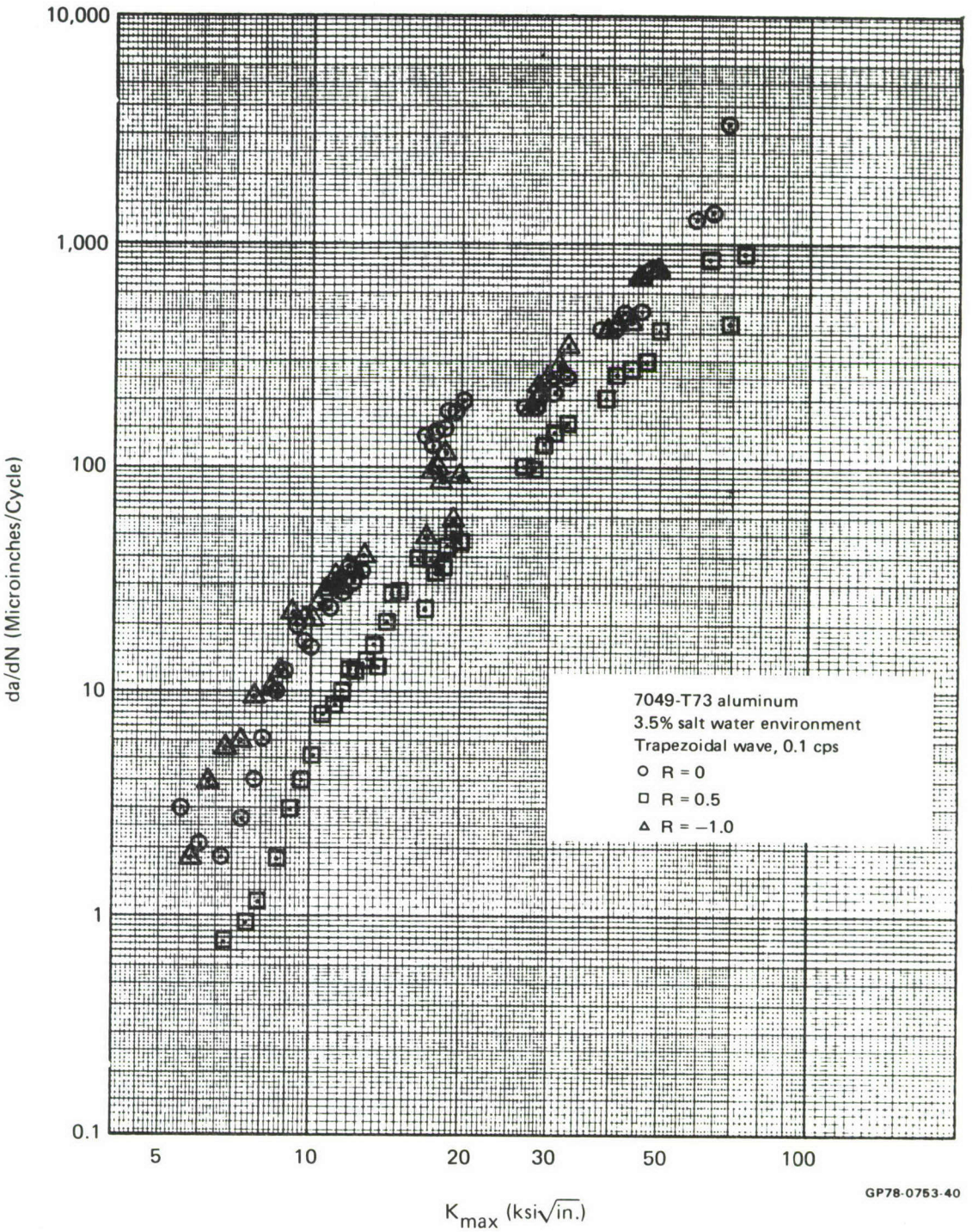

Figure 24
Effect of Stress Ratio on Crack Growth Rate Under Trapezoidal Wave in 7049 Aluminum

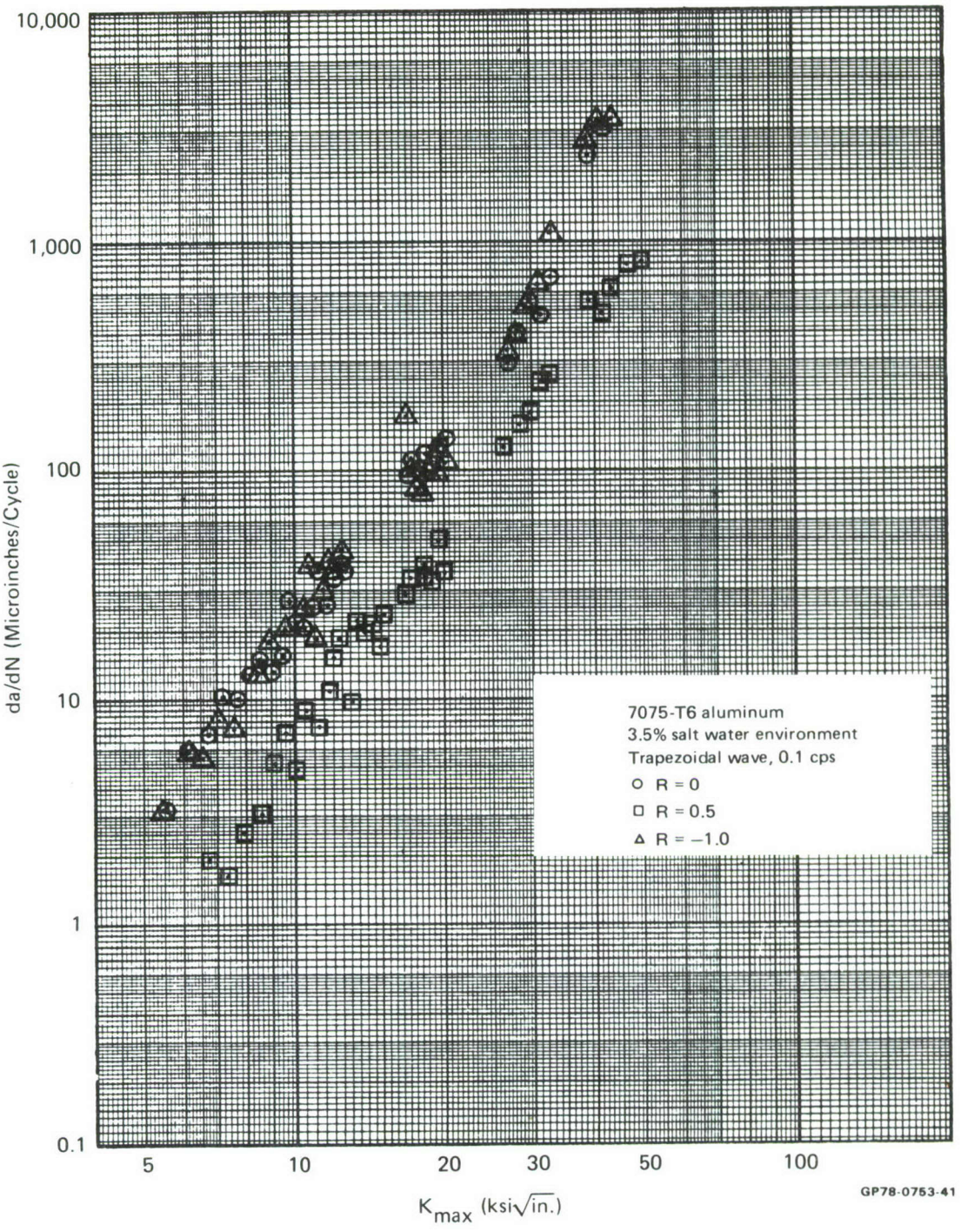

Figure 25
Effect of Stress Ratio on Crack Growth Rate Under Trapezoidal Wave in 7075 Aluminum

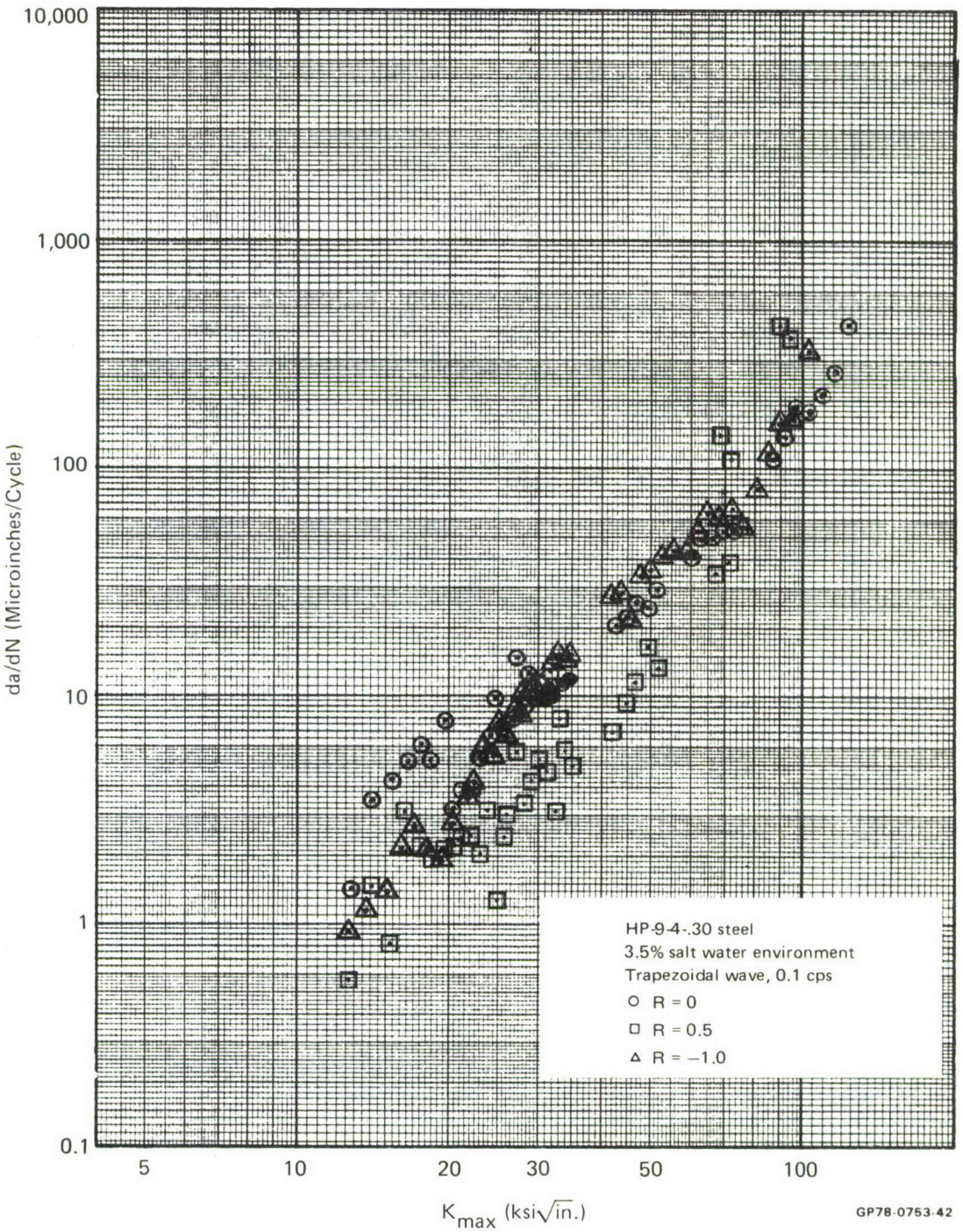

Figure 26
Effect of Stress Ratio on Crack Growth Rate Under Trapezoidal Wave in HP-9-4-.30 Steel

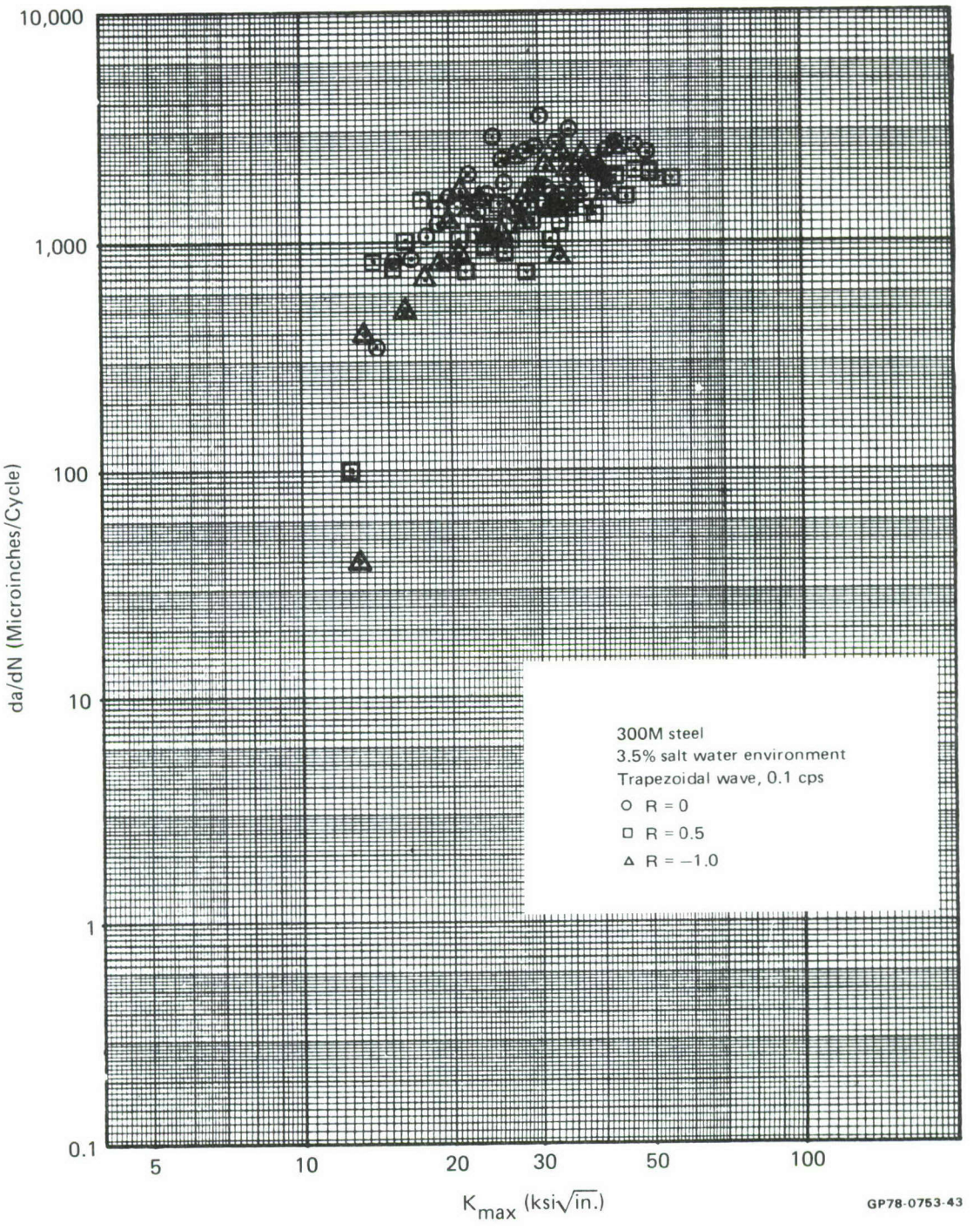

Figure 27
Effect of Stress Ratio on Crack Growth Rate Under Trapezoidal Wave in 300M Steel

inches of total growth occurred. After the crack had grown .50 inches, the next overload was applied. The overload ratios and stress intensities that were used are outlined in Table 4.

TABLE 4
SUMMARY OF OVERLOAD TEST CONDITIONS

Material	Constant Amplitude Stress Intensity Factor K_{max} ksi $\sqrt{in.}$ (1)	Environment	Overload Ratios Tested
7049-T73	15.3	Dry Air Salt Water	1.5, 2.0, 2.4, 2.8 1.2, 1.5, 1.8, 2.0, 2.2, 2.4, 2.6, 2.8, 3.0
7075-T6	15.3	Dry Air Salt Water	1.5, 2.0, 2.4, 2.8 1.2, 1.5, 1.8, 2.0, 2.2, 2.4, 2.6, 2.8
HP 9-4-.30	28.8	Dry Air Salt Water	1.5, 2.0, 2.4, 2.8 1.5, 2.0, 2.4, 2.8
300M	28.8	Dry Air Salt Water	1.5, 2.0, 2.4, 2.8 1.5, 2.0, 2.4, 2.8

Note: (1) Constant amplitude cycling was performed at R = 0.

GP78-0753-131

Detailed results for HP-9-4-.30 in air are shown in Figures 28-31. These figures demonstrate the technique used to determine the number of delay cycles for each overload ratio. Since the overload tests were performed under constant stress intensity amplitude cycling, the constant amplitude growth rate appears as a straight line on these figures. By fitting the constant amplitude slope to the recovery portion of the data, the total delay afforded by the overload is the number of cycles between the constant amplitude lines.

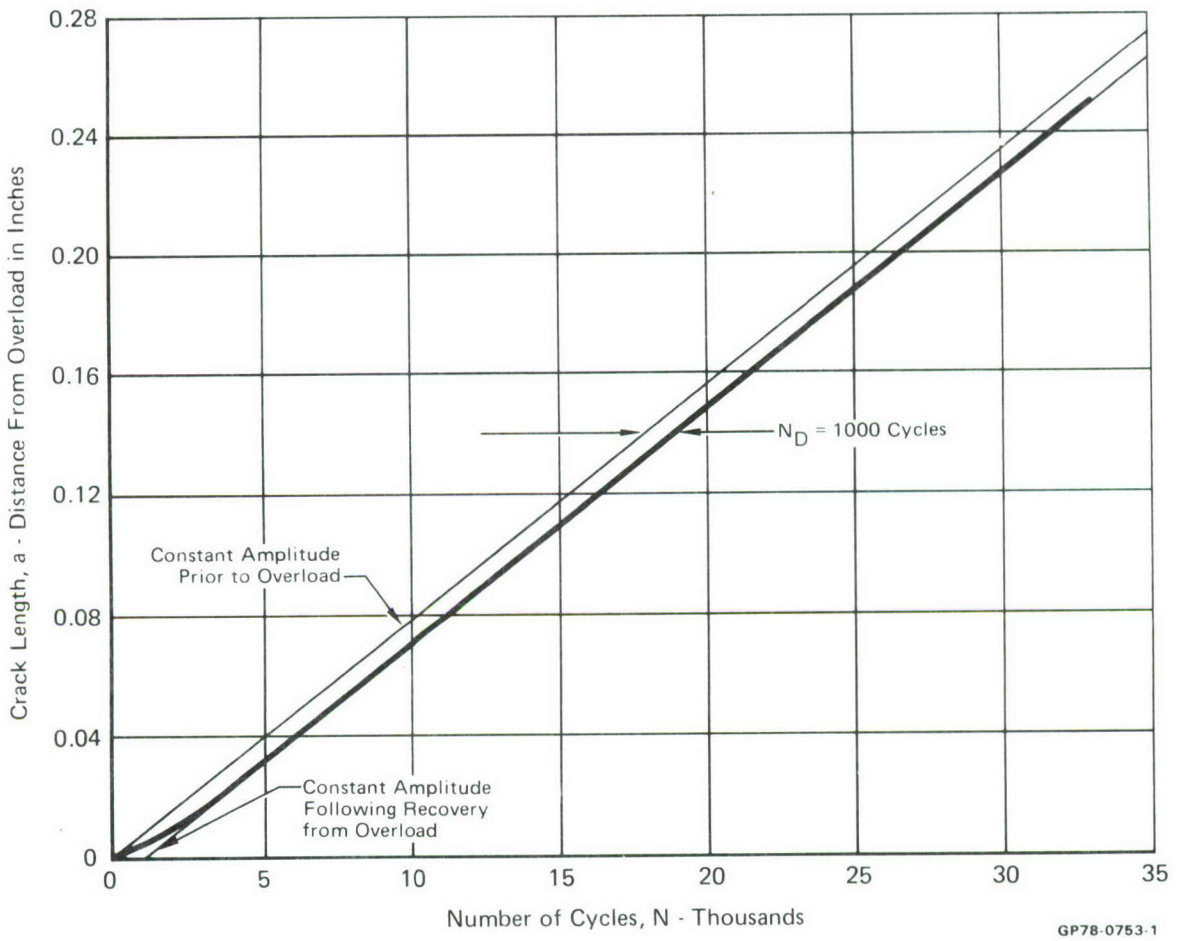

Figure 28
Crack Growth in HP-9-4-.30 After an Overload Ratio of 1.5 in Dry Air

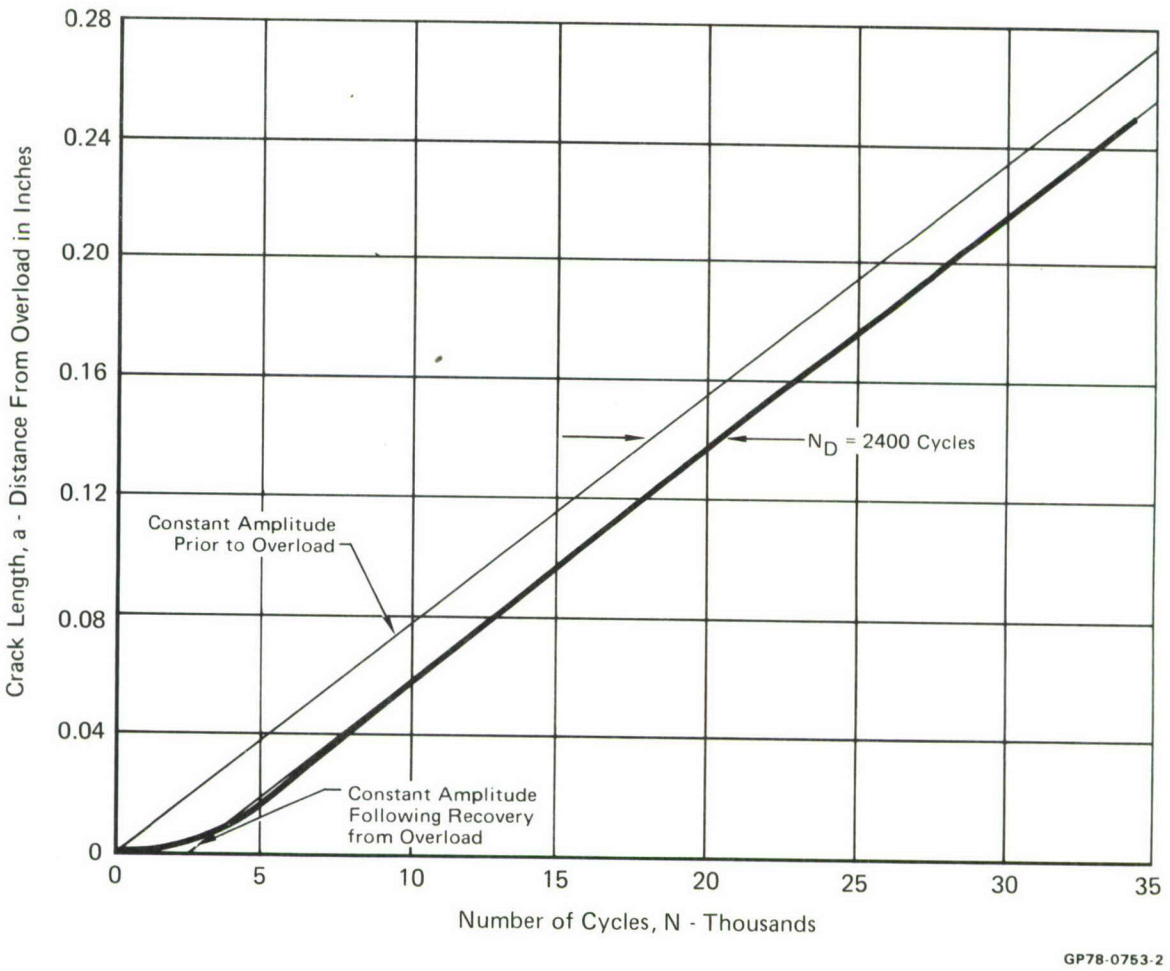

Figure 29
Crack Growth in HP-9-4-.30 After Overload Ratio of 2.0 in Dry Air

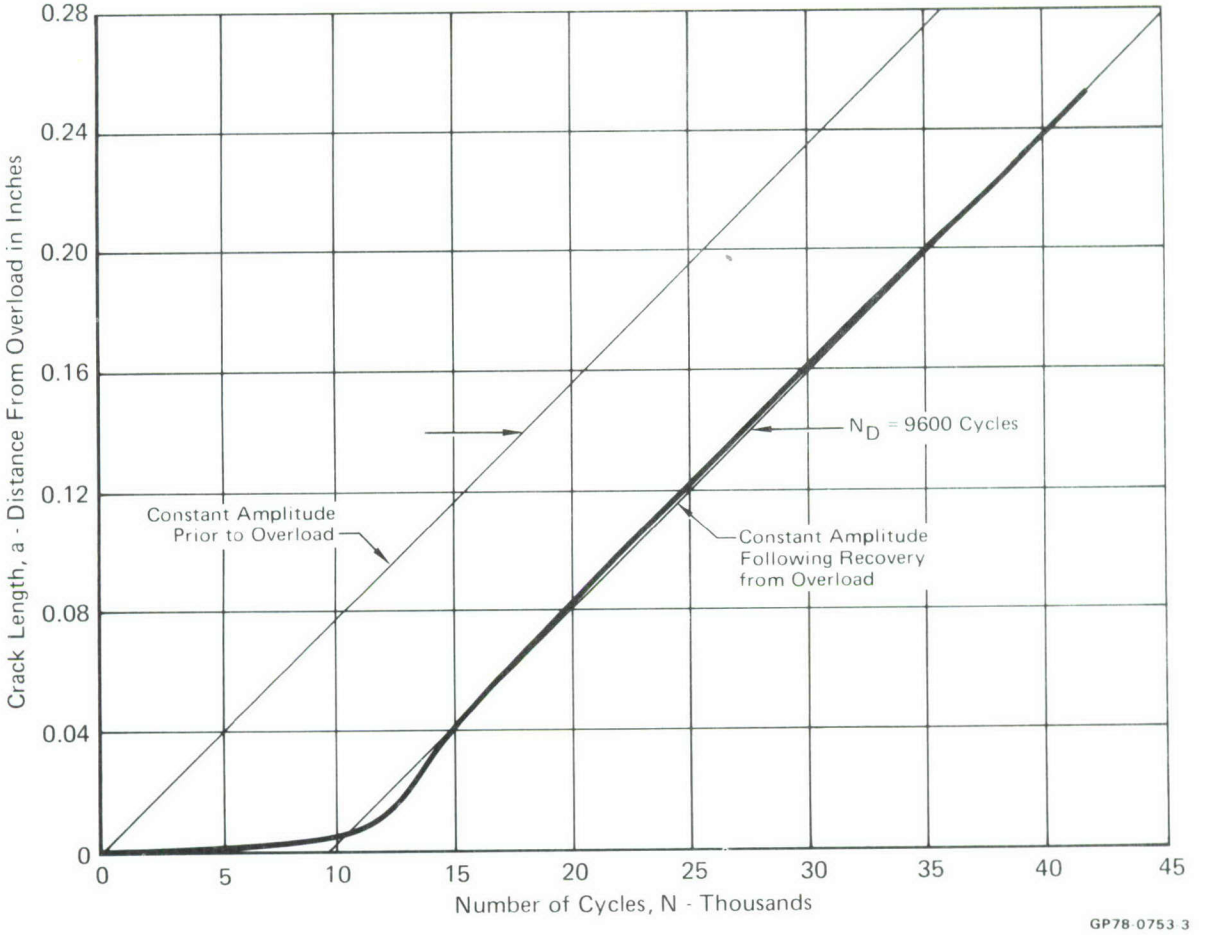

Figure 30
Crack Growth in HP-9-4-.30 After an Overload Ratio of 2.4 in Dry Air

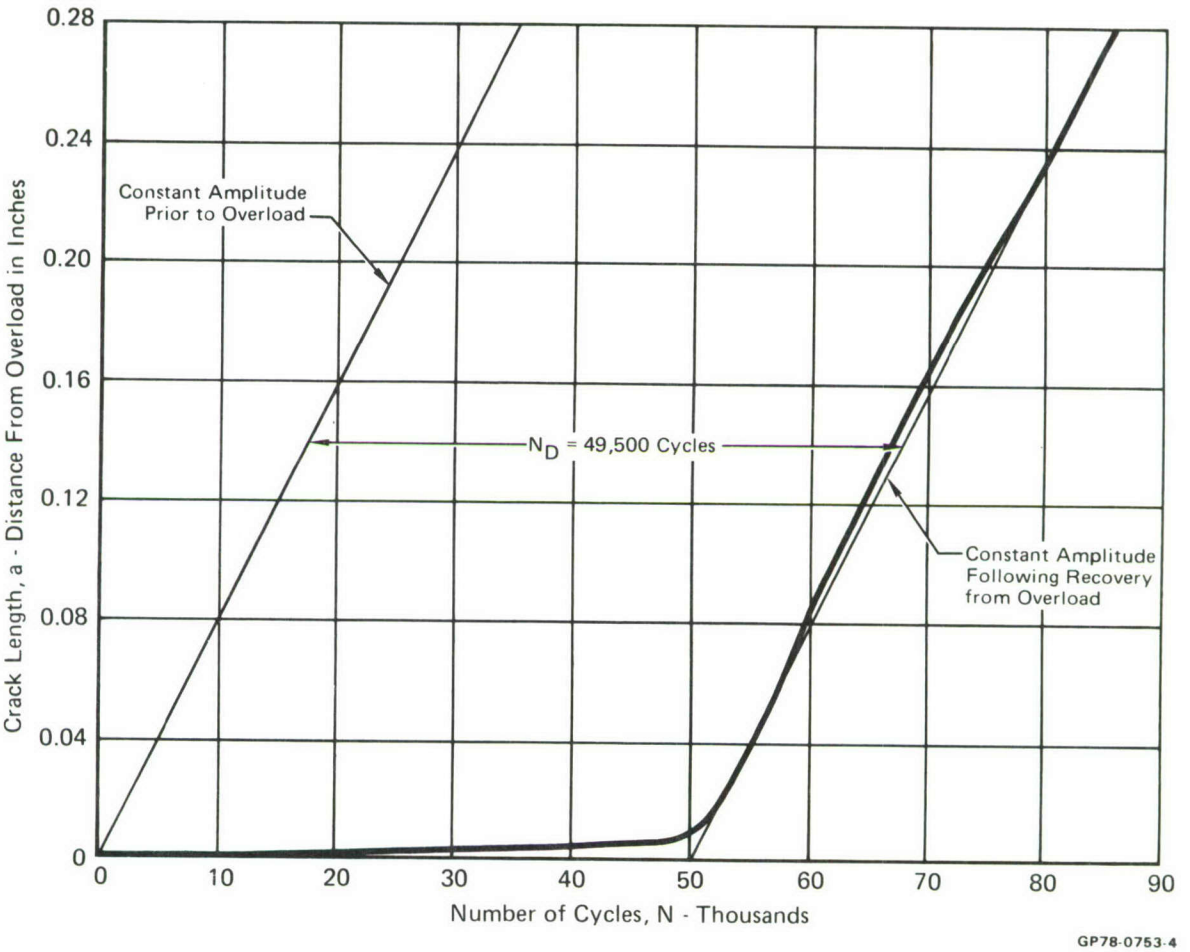

Figure 31
Crack Growth in HP-9-4-.30 After an Overload Ratio of 2.8 in Dry Air

Figures 32-35 summarize the delay cycles, N_D, for the overload tests both in air and in salt water. The acceleration of 300M crack growth in salt water following a 50% overload (see Figure 36) was not expected. The remainder of the 300M tests in salt water showed retardation but generally less than tests in air. Overload tests of HP-9-4-.30 steel showed slightly more retardation in salt water than in air while the other materials showed more retardation in air. In HP-9-4-.30 steel and 7049 aluminum, the resistant alloys, the retardation afforded by overloads in salt water seems to be very similar to that in air. In the susceptible alloys, 300M steel and 7075 aluminum, the

retardation produced by high overloads is significantly less in salt water than in air. This indicates that there may be a higher shut-off overload ratio in salt water than in air for these materials. For analytical purposes, shut-off overload ratios in salt water and air were considered equal.

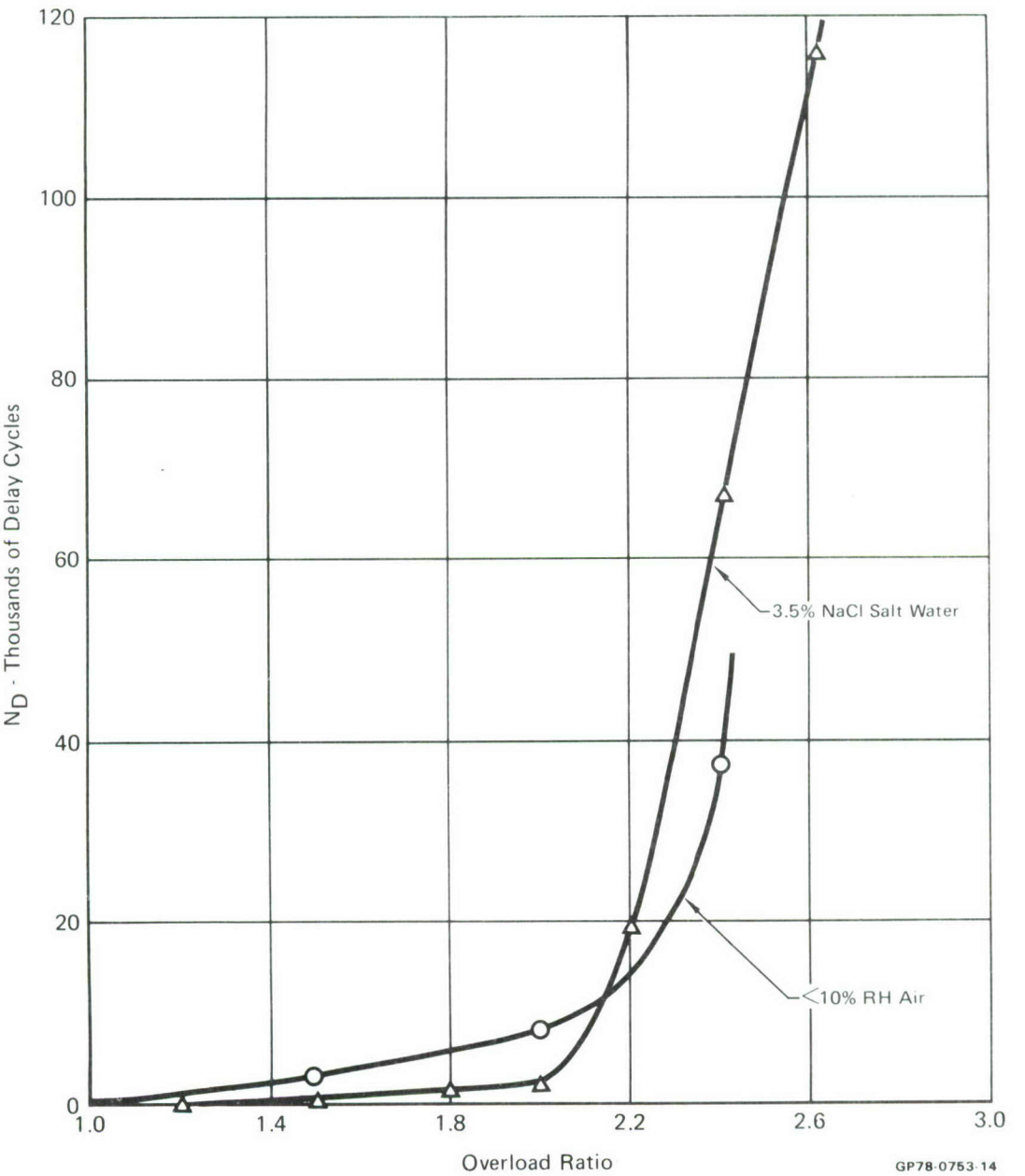

Figure 32
Crack Growth Delay Due to Single Overloads in 7049-T7351 Aluminum

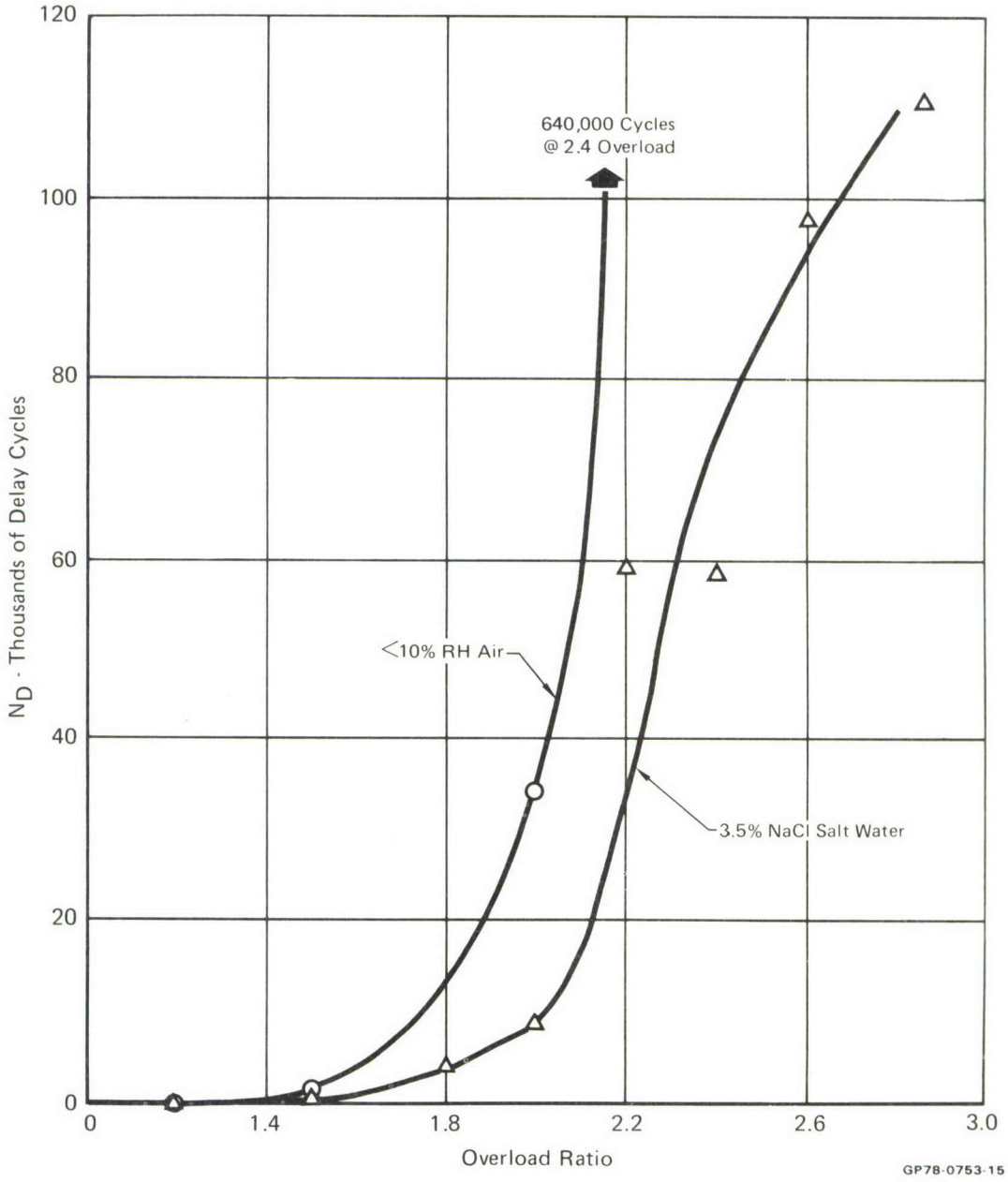

Figure 33
Crack Growth Delay Due to Single Overloads in 7075-T651 Aluminum

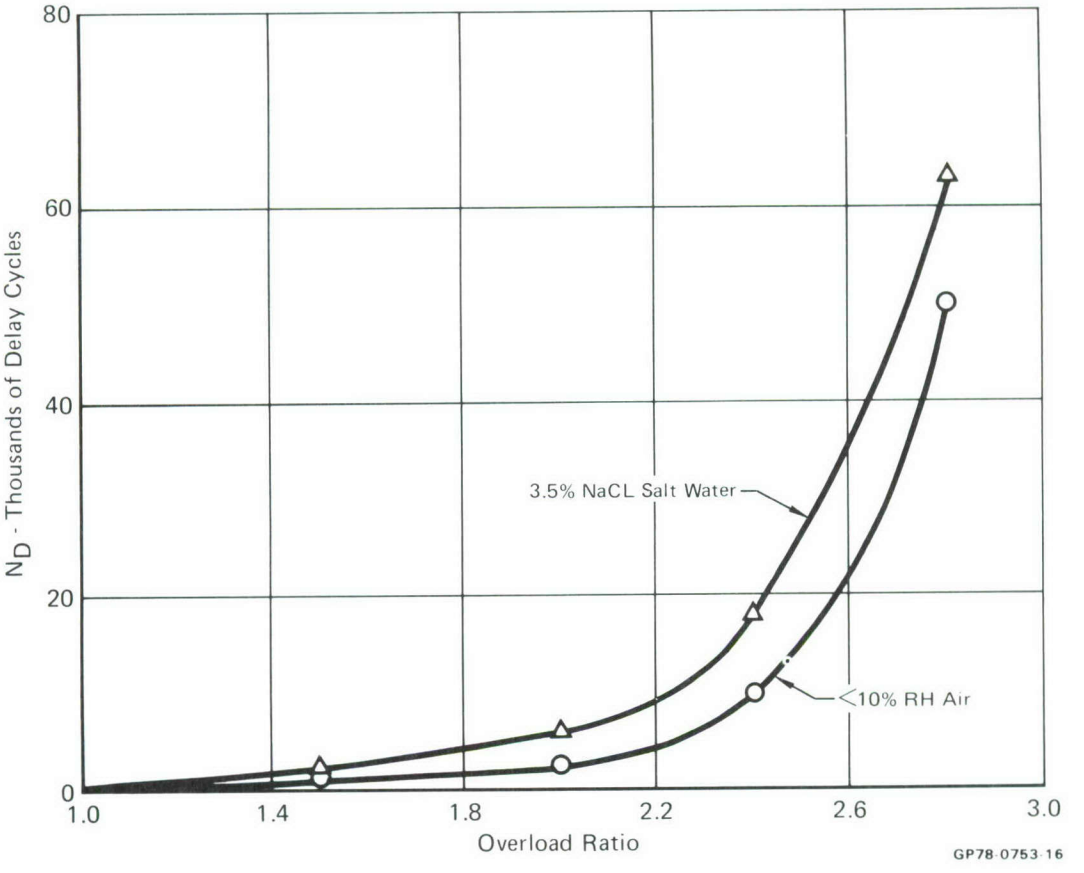

Figure 34
Crack Growth Delay Due to Single Overloads in HP-9-4-.30 Steel

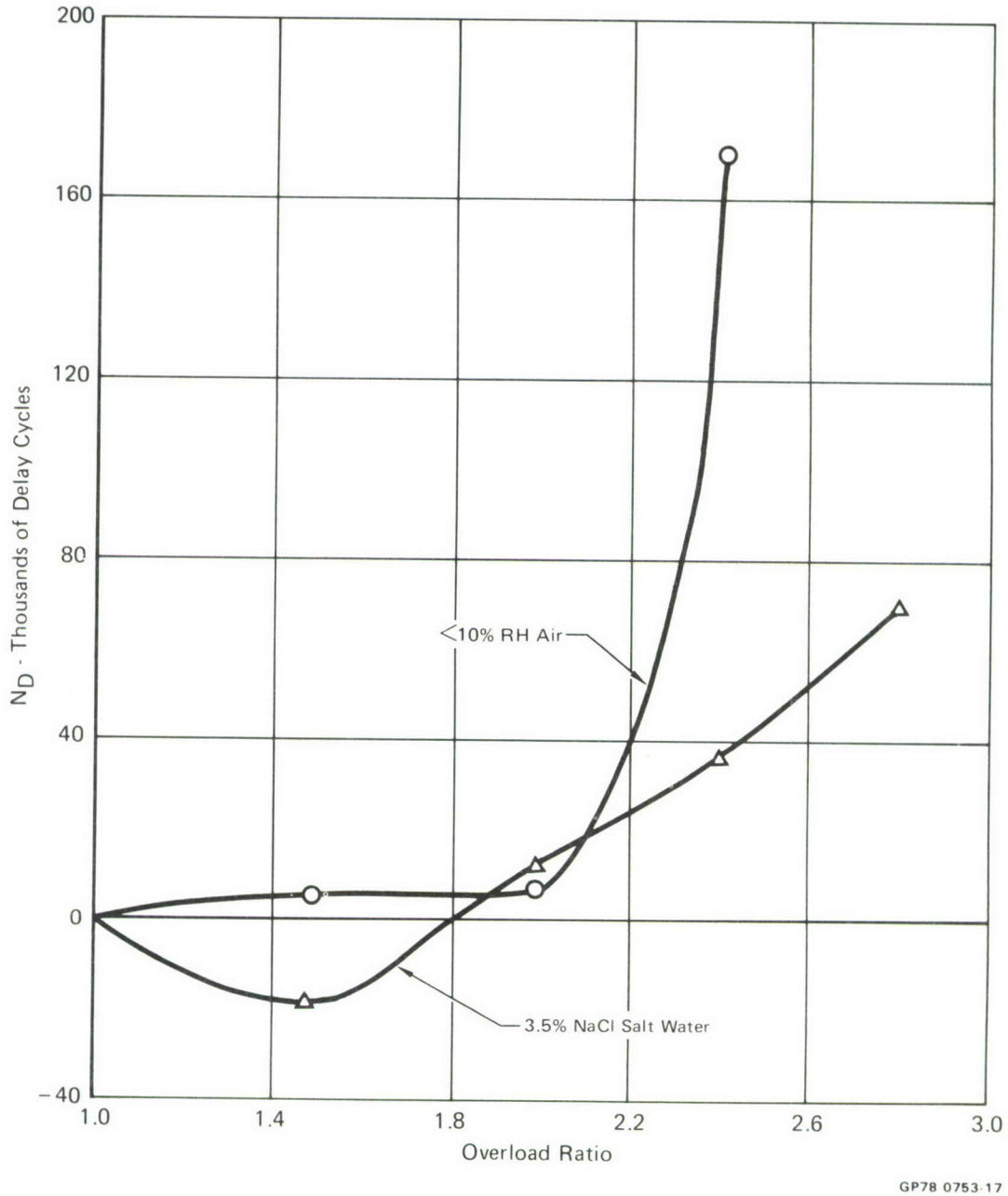

Figure 35
Crack Growth Delay Due to Single Overloads in 300M Steel

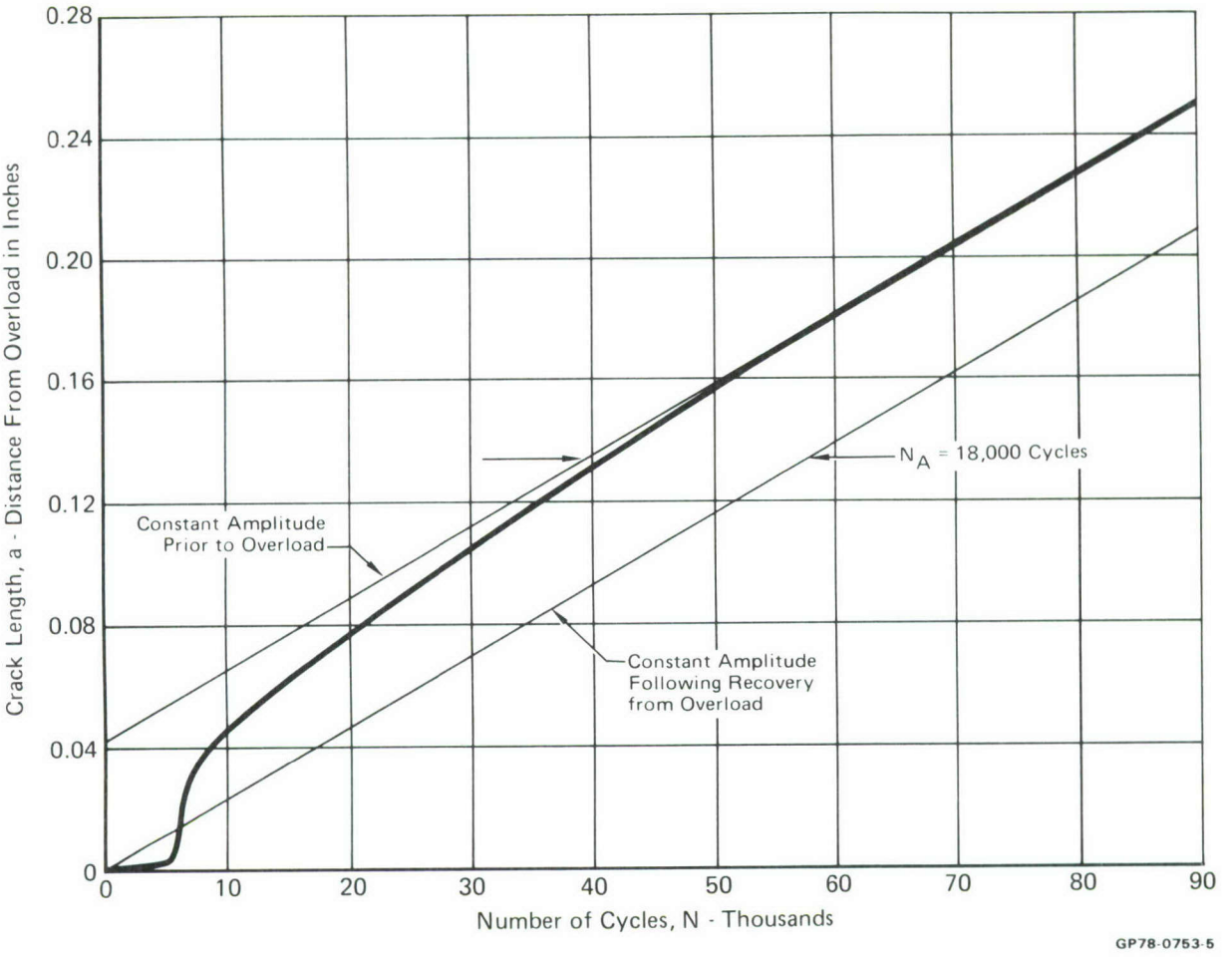

Figure 36
Crack Growth in 300M After an Overload Ratio of 1.5 in 3.5% Salt Water

b. Spectrum Tests - (Specimens 16-17) - Eight tests of center crack panels were used to evaluate retardation with spectrum loads. Two tests in each material were performed using the spectrum defined in Section V, in the dry air and in salt water environments. The test frequency was approximately 15 cps.

Test results in dry air permitted selection of overload interaction zone sizes for each of the four materials. The prediction methodology is discussed in Section V. Correlations of analysis and test are shown in Figure 37 through 44.

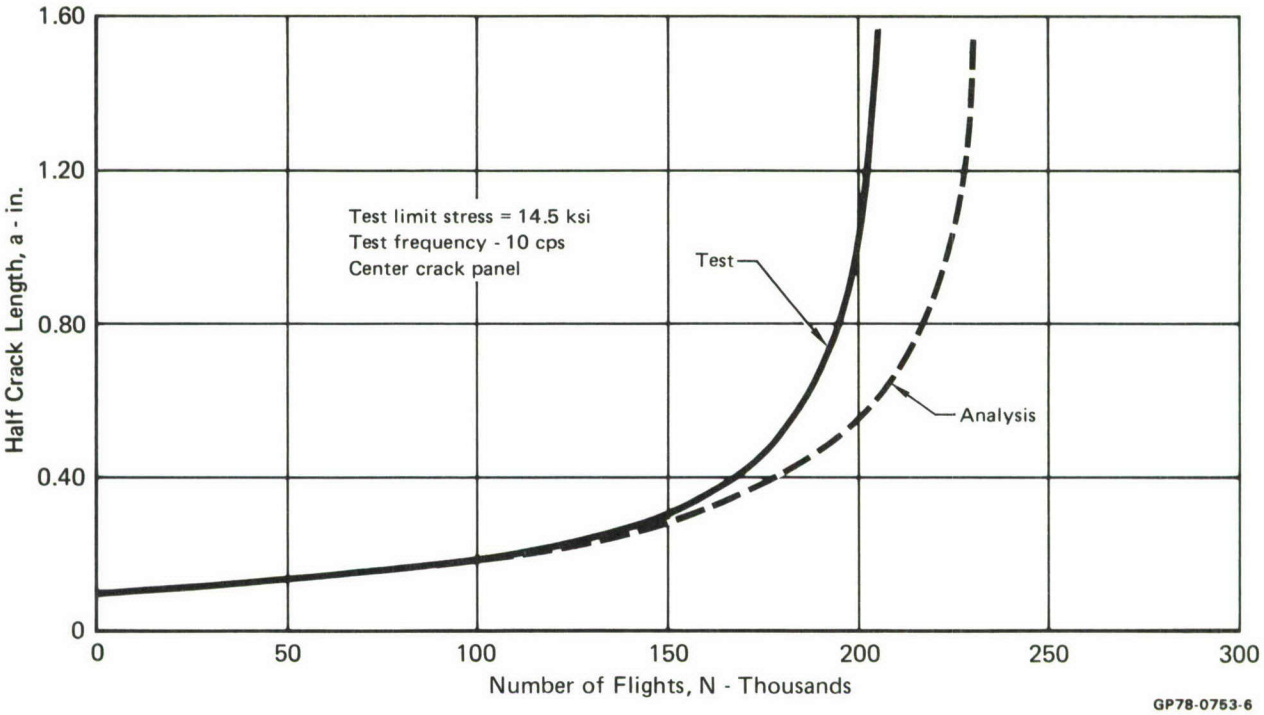

Figure 37
Spectrum Crack Growth of 7049-T73 in Dry Air

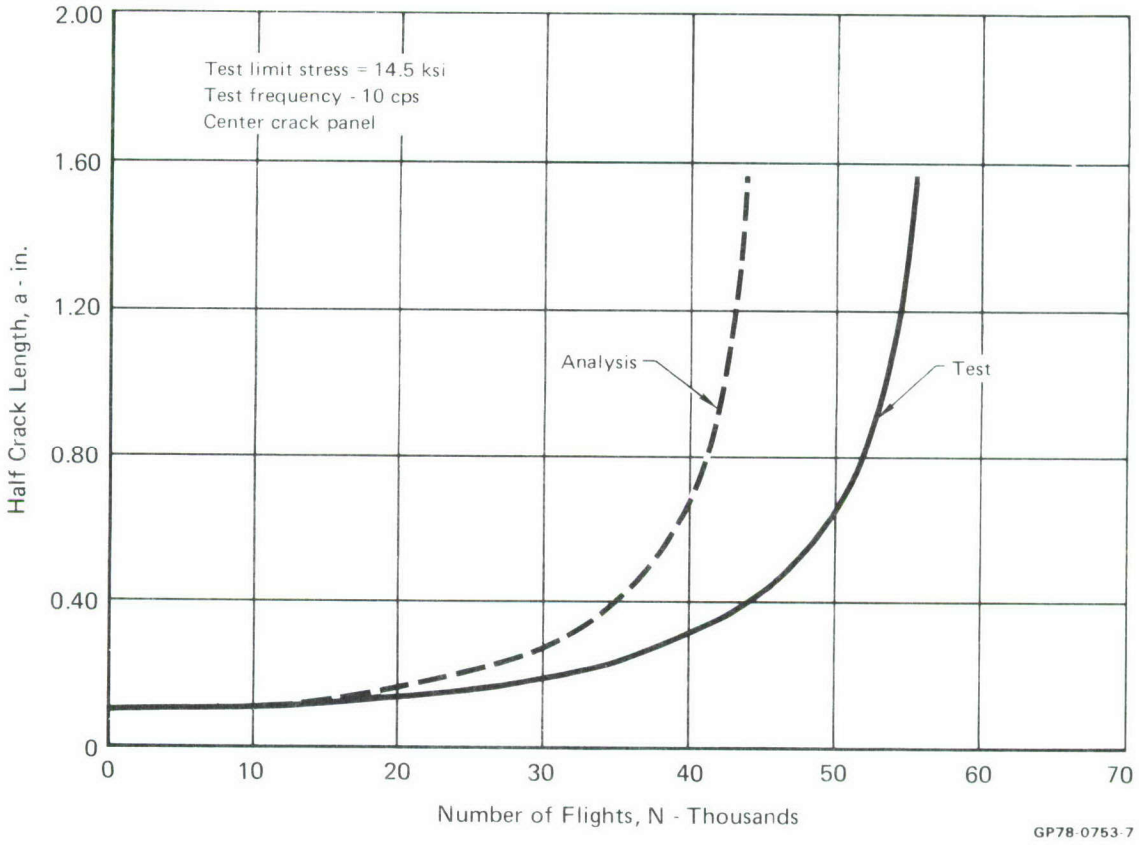

Figure 38
Spectrum Crack Growth of 7049-T73 in 3.5% Salt Water

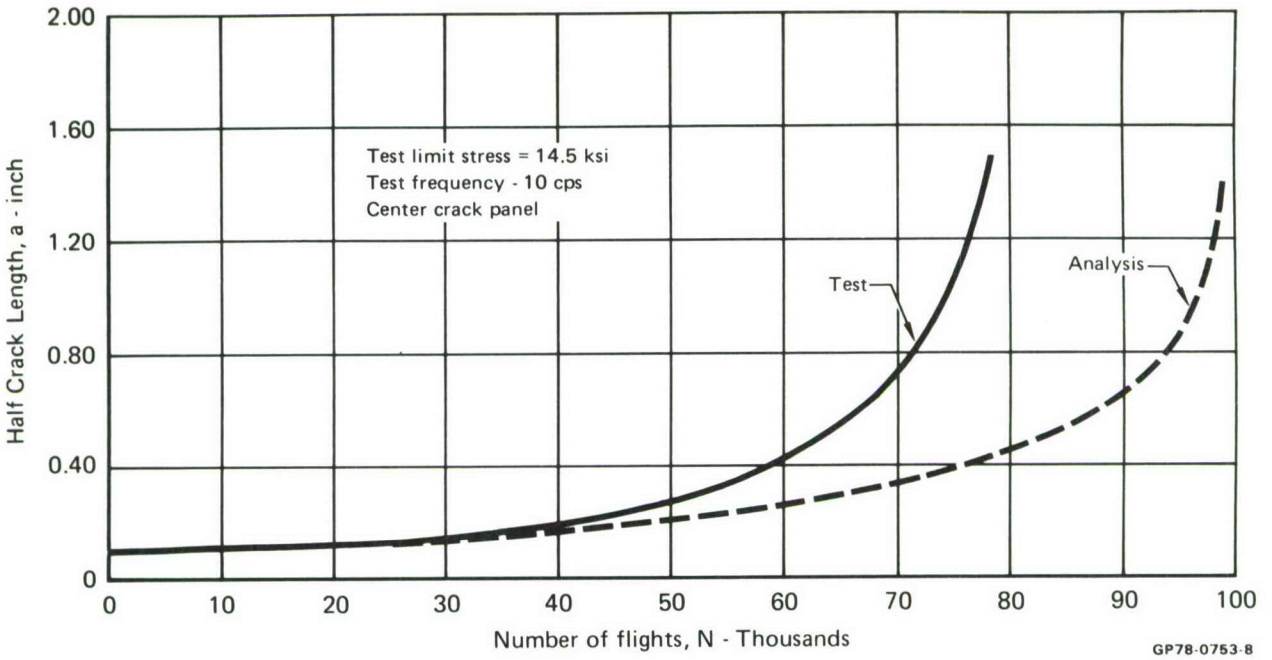

Figure 39
Spectrum Crack Growth of 7075-T6 in Dry Air

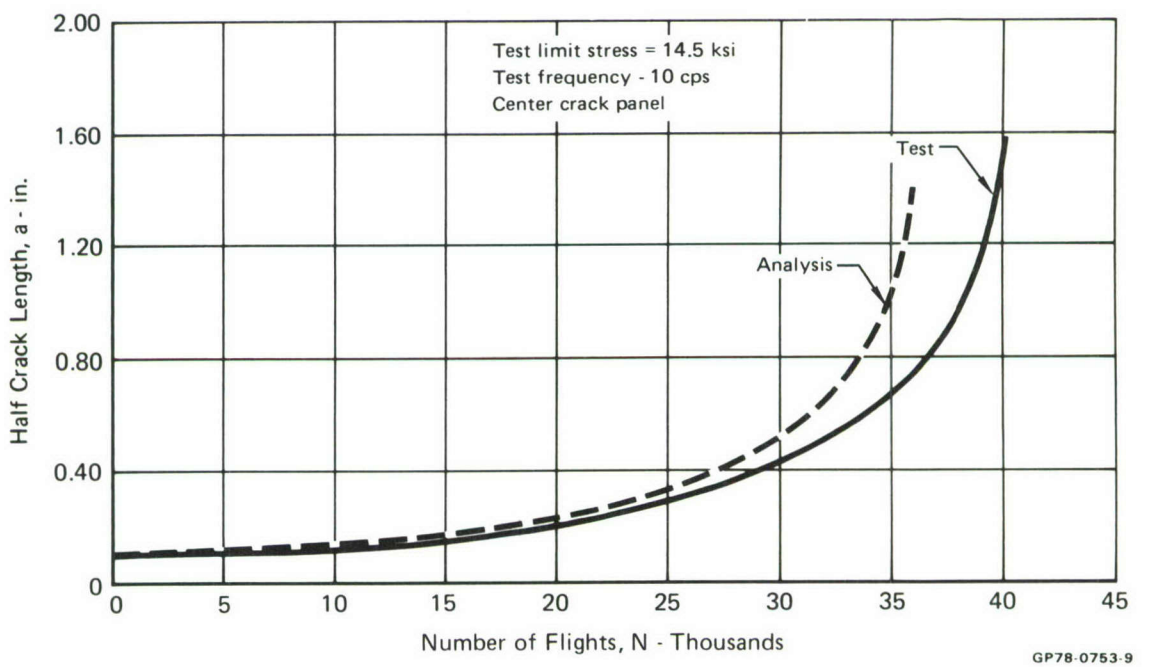

Figure 40
Spectrum Crack Growth of 7075-T6 in 3.5% Salt Water

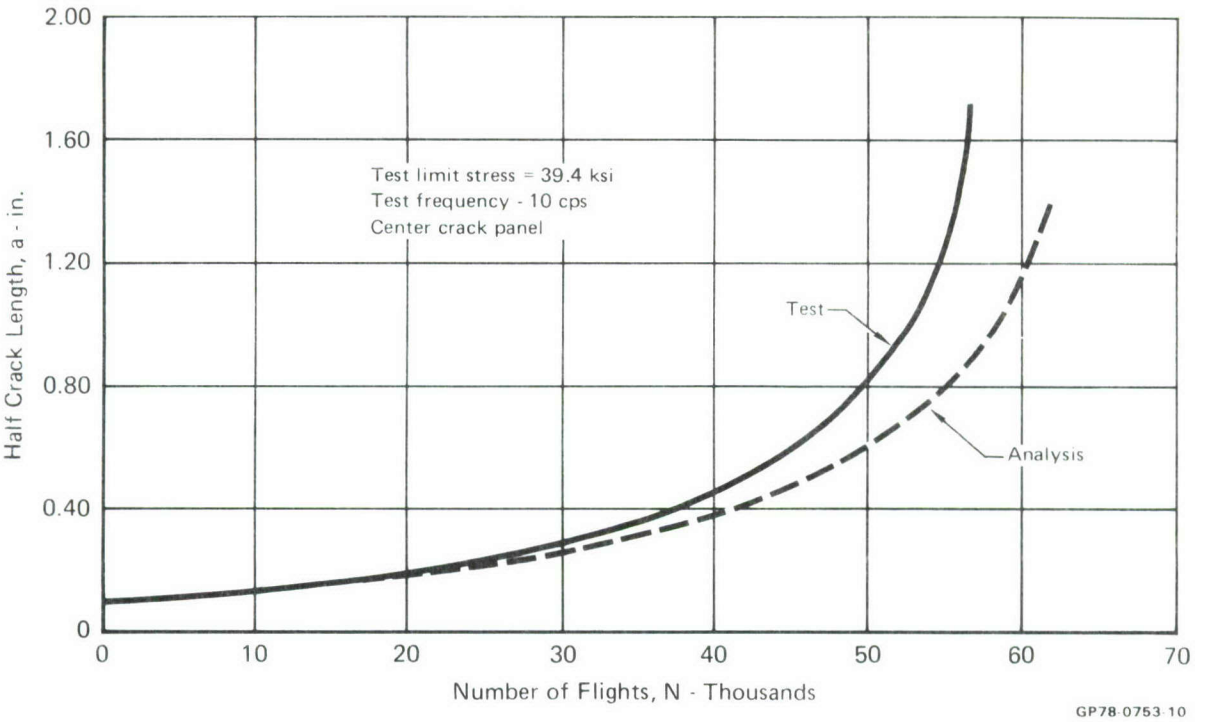

Figure 41
Spectrum Crack Growth of HP-9-4-.30 in Dry Air

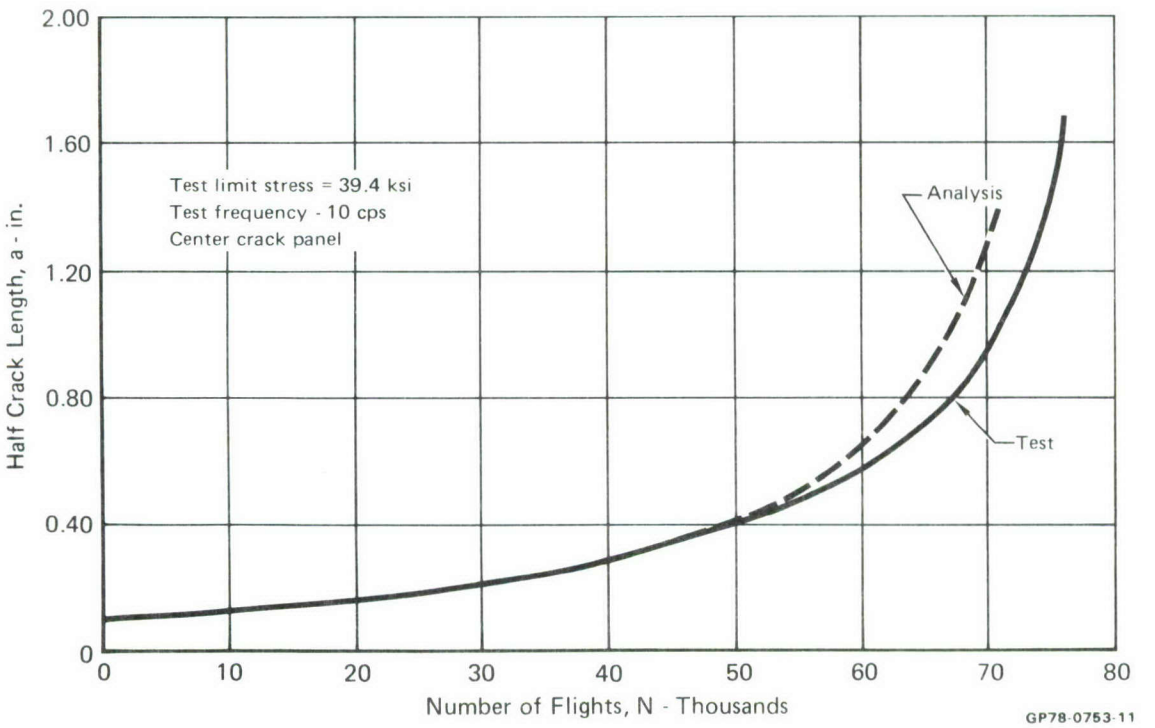

Figure 42
Spectrum Crack Growth of HP-9-4-.30 in 3.5% Salt Water

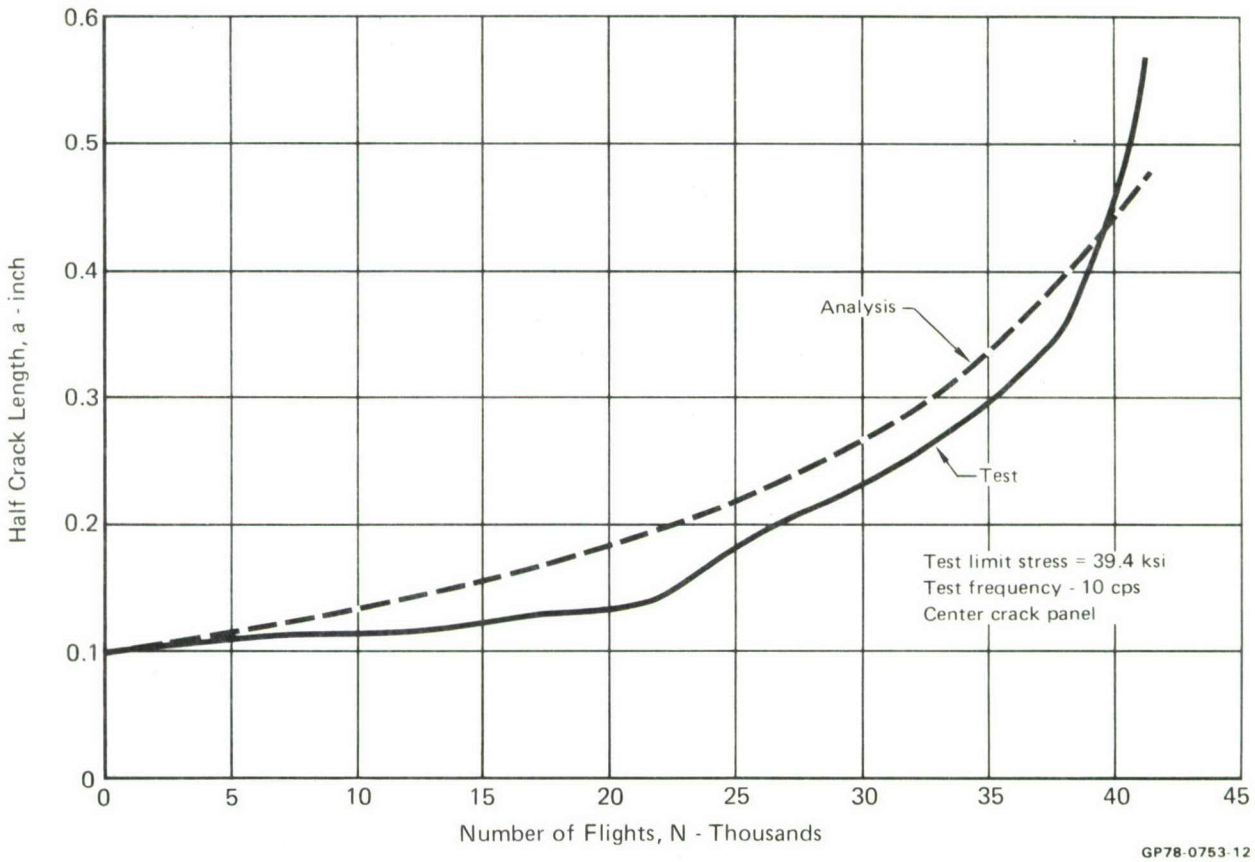

Figure 43
Spectrum Crack Growth of 300M in Dry Air

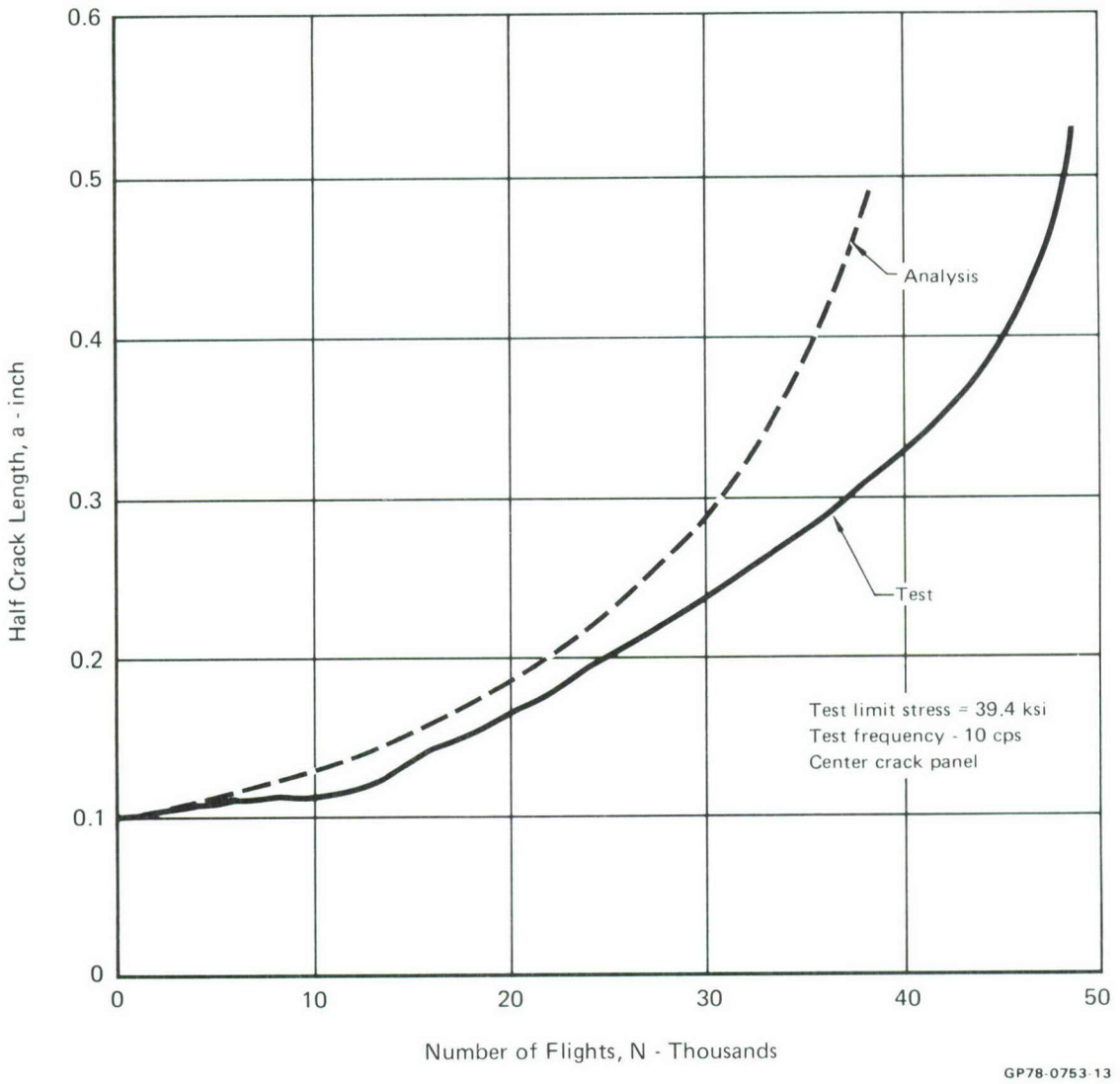

Figure 44
Spectrum Crack Growth of 300M in 3.5% Salt Water

8. SUSTAINED LOAD CRACK GROWTH - (Specimen 11) - Tests were performed using the bolt-loaded WOL specimens, Figures 2 and 3, to determine sustained load cracking rates. The modified bolt-loaded WOL specimen (Figure 3) was used for the aluminum alloys to force the crack to remain at the midplane, eliminating deviations that occurred in early testing. Only 300M developed measurable sustained load crack growth, the data is presented in Figure 45. The other alloys did not exhibit usable sustained-load cracking.

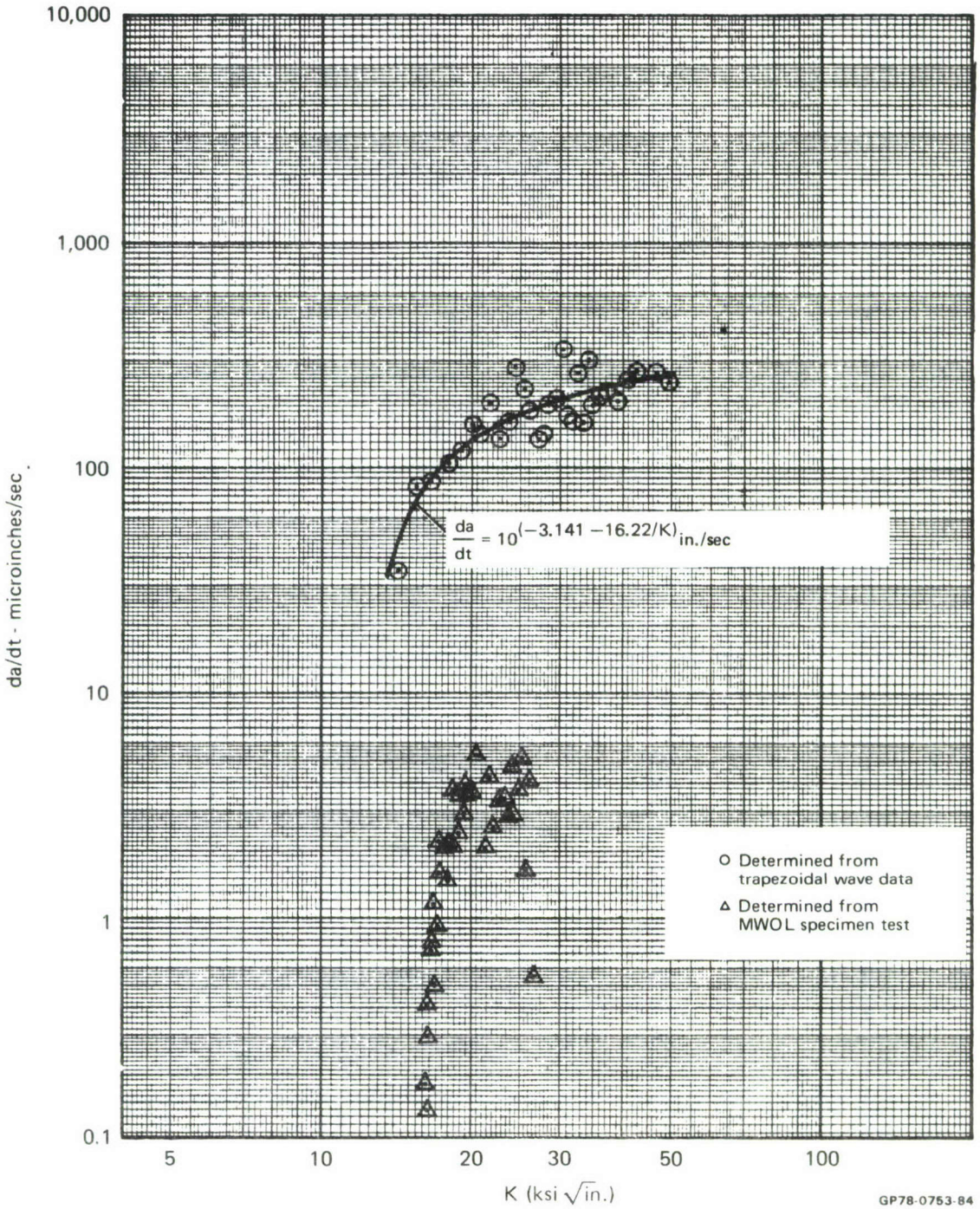

Figure 45
Sustained Load Crack Growth - 300M Steel

Sustained load crack growth rates were also determined from the cyclic tests by assuming that high frequency sine wave tests in the salt water environment result in cyclic growth only, and that any additional growth at low frequencies using a trapezoidal wave shape is due to sustained load growth. Sustained load crack growth rates determined from the cyclic tests are considerably higher than those obtained from the bolt-loaded WOL tests (Figure 45). Data obtained from the cyclic tests were used to correlate and predict load-environment interactions. The procedures used to derive sustained load crack growth rates from results of cyclic tests are described in Section IV.

9. DUPLICATE TESTS (Specimen 12) - One test in each material was repeated. The results obtained are compared with the original results in Figures 46 through 49. With the exception of the 300M steel data, the results of the duplicate tests match the original results very well. This indicates the small scatter expected between similar crack growth tests. In contrast, the 300M steel in salt water data, Figure 46, shows considerably greater variation in growth rate (almost a factor of three scatter). The second test agrees much more closely with the trends of the remaining data, indicating that the first specimen might have received improper heat treatment. A Rockwell hardness test on the specimens showed the original specimen to have an $R_C = 46.5$ while the remaining specimens varied from $R_C = 55$ to $R_C = 57$, which is the specification range. As a result of these tests, data from the duplicate test in 300M steel was used for all model development and comparisons reported herein.

Comparison of data on 7075 aluminum, Figure 48, shows higher growth rates at low ΔK's in the duplicate test than in the original test. The higher growth rates match predicted trends better and were used for subsequent life comparisons. Duplicate tests in HP-9-4-.30 steel and 7049 aluminum matched the original results so closely that

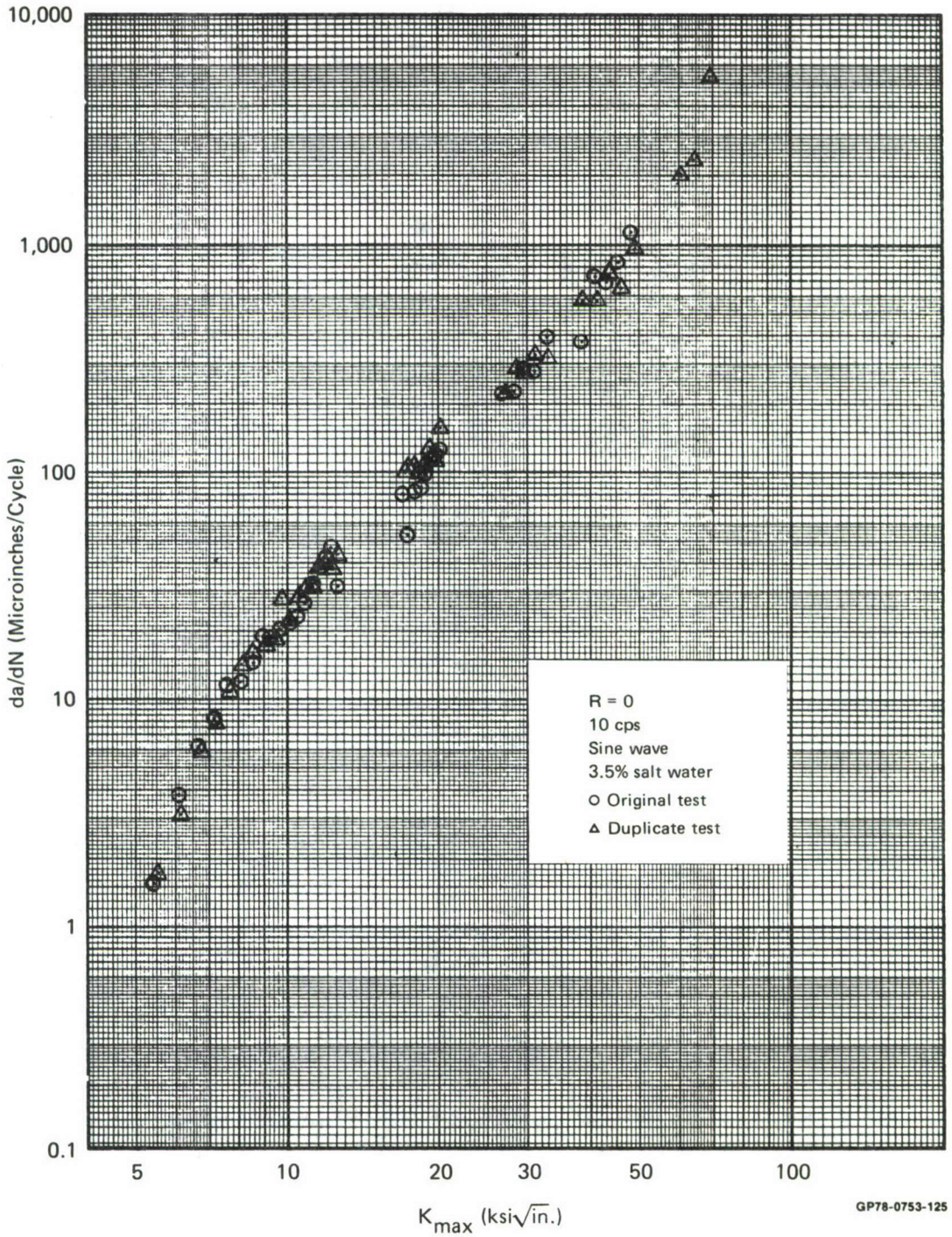

Figure 46
Comparison of Original and Duplicate Test Results in 7049-T7351 Aluminum

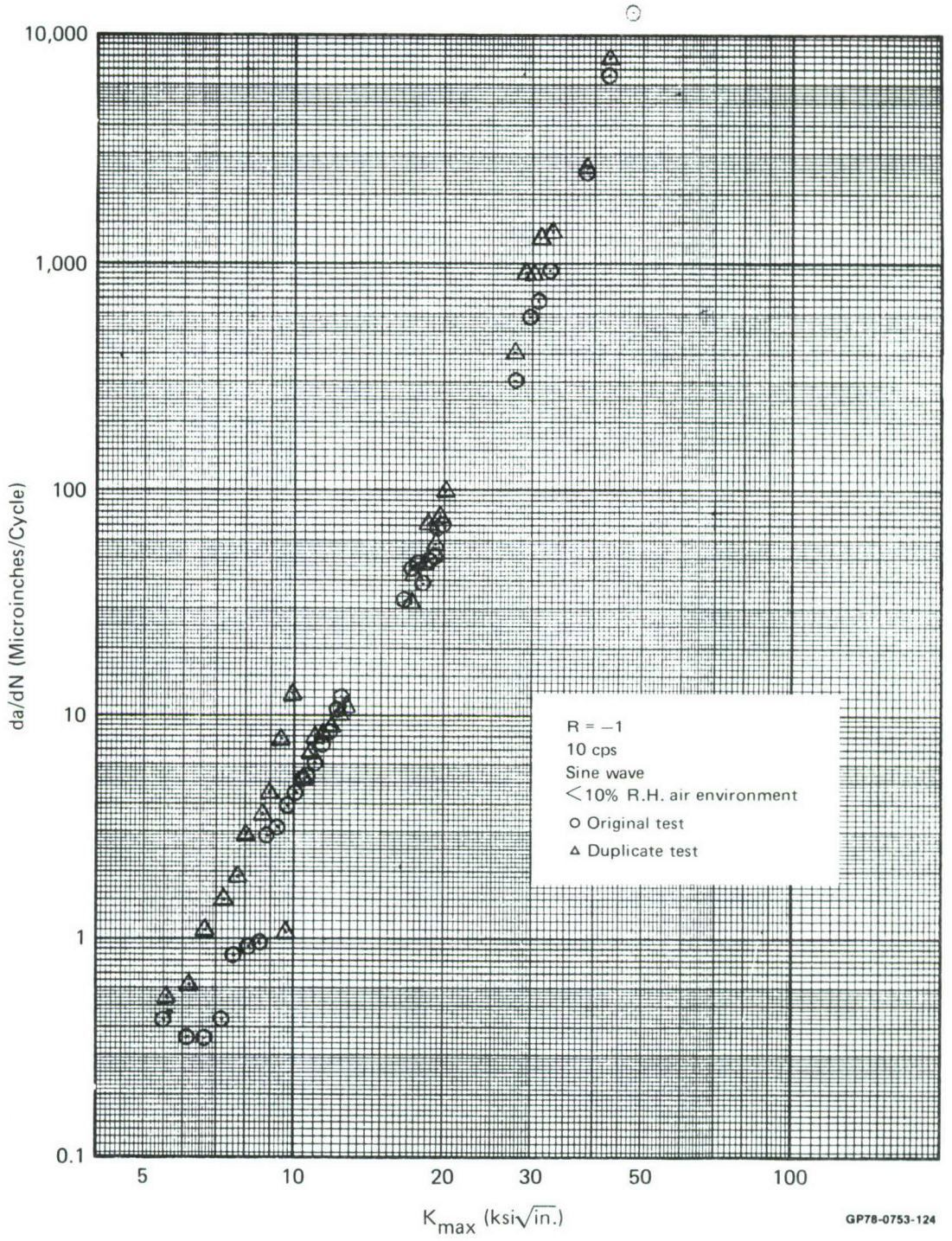

Figure 47
Comparison of Original and Duplicate Test Results in 7075-T651 Aluminum

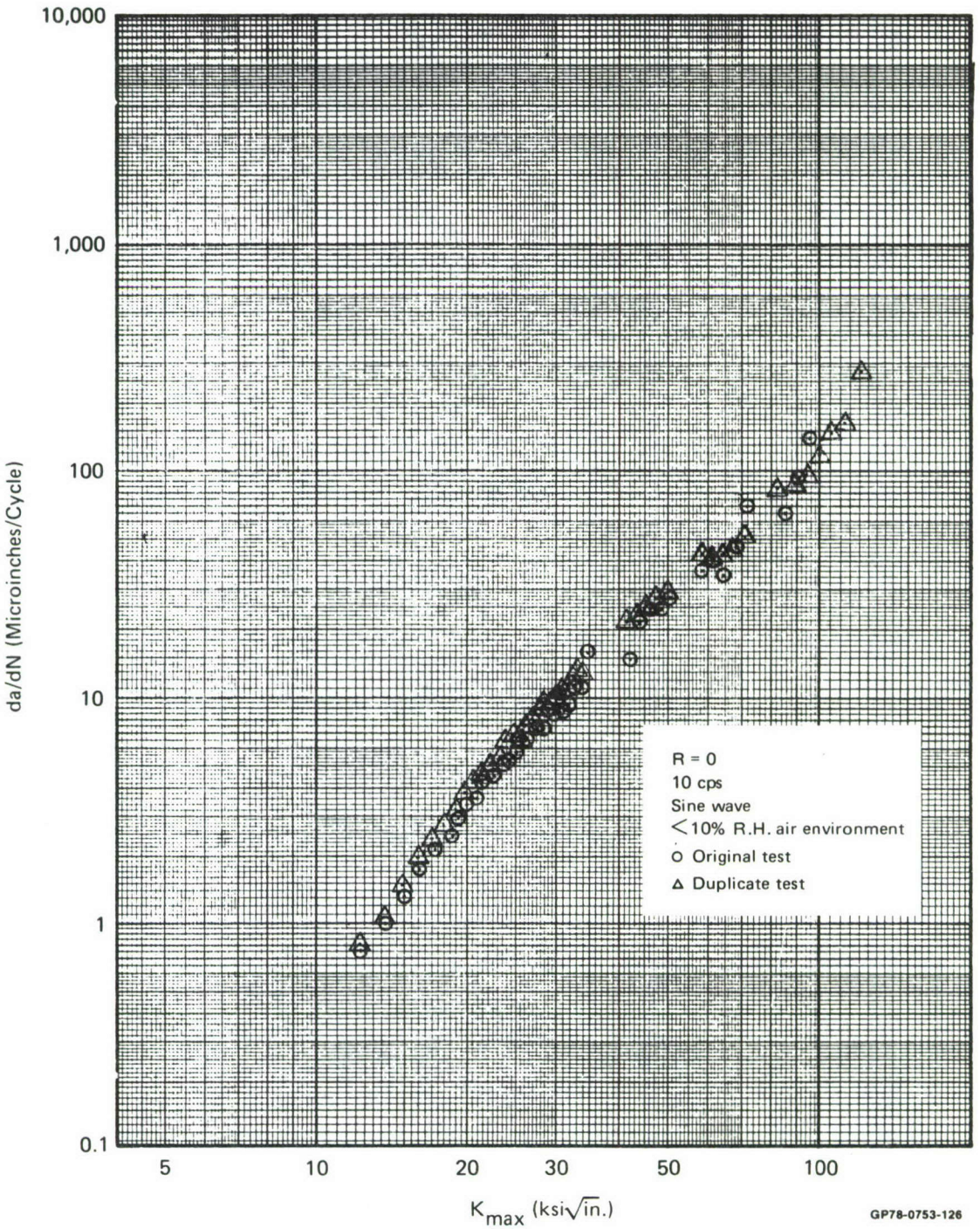

Figure 48
Comparison of Original and Duplicate Test Results in HP-9-4-.30 Steel

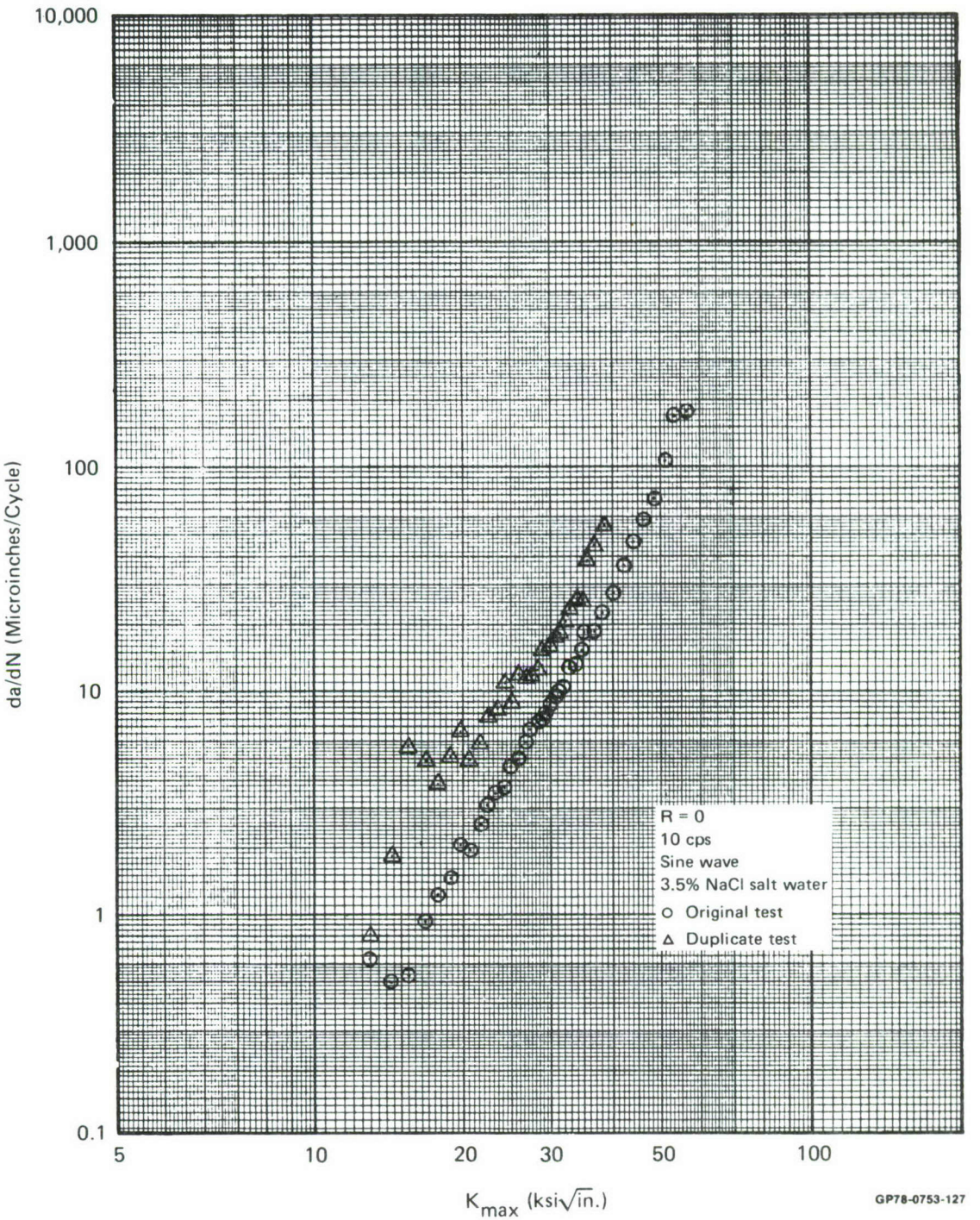

Figure 49
Comparison of Original and Duplicate Test Results in 300M Steel

life comparisons remained nearly unchanged. Table 3 shows test lives for all of the stress ratio, frequency, and wave shape variation tests. Lives based on duplicate test results are noted.

SECTION IV

ENVIRONMENT-LOAD INTERACTION MODEL

1. SUMMARY - The analysis of environmental acceleration of crack growth is based on a linear superposition of cyclic load and sustained load crack growth. Stress ratio effects are accounted for by using an effective stress intensity range concept based on closure. Crack growth analysis using the combination of these two algorithms shows good correlation with the results of the algorithm development tests.

The Willenborg model was the basis for extension of the crack growth analysis to spectrum loadings. Results of single overload tests and spectrum tests of center crack panels were used to calibrate the model for predictions of surface flaw crack growth under spectrum loadings. Stress intensity factor solutions for semi-elliptical surface flaws were determined using a slice synthesis model, and validated by comparisons with finite element solutions.

2. STRESS RATIO EFFECTS

a. Forman Equation - The Forman equation, Reference 4, has frequently been used to analyze stress ratio effects on crack growth rate. The growth rate at negative stress ratios is the same as that for R=0 so that the Forman equation becomes

$$da/dN = da/dN\Big|_{R=0} \frac{K_c-\Delta K}{(1-R)\ K_c-\Delta K} \quad \text{for } R \geq 0 \qquad (1)$$

$$= da/dN\Big|_{\substack{R=0 \\ \Delta K = K_{max}}} \quad \text{for } R \leq 0 \qquad (2)$$

In this formulation, the Forman equation has two limitations. First, Equation (1) predicts the same effect of stress ratio for all materials, except at stress intensities approaching the material-dependent value of K_c. Test data, such as developed in the program summarized in Section III, shows that there are material dependent differences in stress ratio effects which

cannot be predicted by Equation (1). Secondly, Equation (2) predicts no effect of compressive minimum stresses, whereas test data generally indicates that compression increases growth rates. Because the Willenborg Model predicts retardation by reducing the stress ratio for a retarded cycle, negative stress ratios frequently result within spectrum analyses. Therefore, it is important that the effects of compressive stresses be properly predicted.

Modifications to the Forman equation are possible, which would reduce these two limitations. Equation (1) could be re-written so that a material dependent coefficient could be introduced; Equation (2) could be modified to predict increases in growth rates with compressive stresses. An alternate approach, described in the following paragraph, does not have the limitations of the Forman equation.

b. Closure Based Solution - This prediction method is based on analysis of crack surface displacements. Crack closure determines the stress intensity range which is effective in propagating the crack. This effective stress intensity range is given by:

$$\Delta K_{eff} = \left(\frac{1-R}{1-K^\circ}\right) \quad [1 - (1-R) \quad K^\circ] \quad K_{max} \text{ for } R \geq 0 \qquad (3)$$

$$\Delta K_{eff} = \frac{1}{1-K^\circ} \; [1 - K^\circ e^{0.1R}] \; K_{max} \text{ for } R < 0 \qquad (4)$$

where R and K_{max} are defined by the remote loading conditions where K° is the ratio of closure stress intensity to K_{max} at R=0, generalized as

$$K^\circ = (0.33045 + 0.15164\alpha - 0.01476\alpha^2) \; [1 + 0.6 \; (f_c/f_m - 1) - 0.156 \; (f_c/f_m - 1)^2] \qquad (5)$$

where

f_m = monotonic yield stress

f_c = cyclic yield stress

The parameter, α, was used to "tune" Equations (4) and (5) for each material analyzed so that constant amplitude test lives for R=0 and R=0.5 were matched. In the closure analysis of Reference 5, α, was related to plastic zone conditions, α=1 for

plane stress, α=0 for plane strain. However, in this analysis α (and consequently K°) was used only to correlate the R=0 and R=0.5 crack growth rate data and was not related directly to plastic zone conditions. The parameters of Equation (5) used for both constant amplitude and spectrum analyses are presented in Table 5.

TABLE 5
PARAMETERS USED FOR STRESS RATIO CORRECTIONS

Material	α (1)	f_m ksi (2)	f_c ksi (3)	K° (4)
7049-T73	0.70	72	72	0.429
7075-T6	−0.55	80	80	0.242
HP 9-4-.30	−0.55	212	212	0.242
300M	−1.85	250	230	0

Notes:
(1) Plastic zone size correction factor.
(2) Monotonic yield stress.
(3) Cyclic yield stress.
(4) Ratio of $K_{max\text{-}eff} - \Delta K_{eff}$ to $K_{max\text{-}applied}$ for R = 0, constant amplitude loading.

GP78-0753-86

The closure based approach, as empirically used in this program, has two advantages over the Forman equation: (1) predicted effects of stress ratio on crack growth rate can be varied to account for variations in material behavior, and (2) negative stress ratios generally are predicted to accelerate crack growth. Because of these advantages, the closure based solution, Equations (4) and (5) were incorporated into the analysis routine to account for stress ratio effects.

c. Comparison of Constant Amplitude Analysis and Test Results - The constant amplitude lives determined from Forman's Equations (1) and (2) and the closure based Equations (4) and (5) are correlated with test lives in dry air in Table 6. This comparison shows that the closure based solution is more accurate at positive stress ratios than the Forman solution because it is empirically "tuned" to produce good correlation. The

closure based analysis for R=0.5 does not match the test life for 300M steel as well as it does for the other materials. To obtain this correlation with the closure based equations, it was assumed that 300M exhibits no closure at all ($K^{\circ}=0$) in Equations (4) and (5).

TABLE 6
SUMMARY OF STRESS RATIO EFFECTS IN DRY AIR

Material	Stress Ratio	Test Life (1)	Predicted Life Using Closure Model (2)	Predicted Life Using Forman's Eq (3)
7049-T73	0	221,000	221,000	221,000
	0.5	658,000	655,000	715,000
	−1.0	161,000	181,000	221,000
7075-T6	0	102,000	102,000	102,000
	0.5	466,000	464,000	598,000
	−1.0	107,000	93,700	102,000
HP 9-4-.30	0	199,000	199,000	199,000
	0.5	706,000	704,000	637,000
	−1.0	156,000	186,000	199,000
300M	0	128,000	128,000	128,000
	0.5	1,097,000	801,000	316,000
	−1.0	167,000	128,000	128,000

Notes:
(1) Test lives are based on constant amplitude testing of center cracked panels from a = 0.15 inches to fracture. Maximum stress levels were 10 ksi in aluminum and 20 ksi in steel.
(2) Test results for stress ratios of 0 and 0.5 were used to calibrate the model.
(3) Test results for stress ratio of 0 were used to calibrate the model.

GP78-0753-87

Life data resulting from negative stress ratio tests show both accelerated and decelerated growth rates with respect to the R=0 baseline data. Duplicate tests of 7075-T6 at R=-1 produced lives of 150,000 cycles and 107,000 cycles. Thus, some of the inconsistency may be due to test scatter. Generally, only one specimen per condition was tested. Figures 7 through 11 further demonstrate the ability of the closure based solution to correlate stress ratio effects.

3. LINEAR SUPERPOSITION APPROACH FOR PREDICTION OF ENVIRONMENTAL ACCELERATION

a. Modification of Wei-Landes Approach - The Wei-Landes linear summation hypothesis, Reference 6, suggests that environmentally accelerated crack growth rates can be predicted by adding the crack growth due to the individual mechanisms of environmental attack and cyclic loading. This hypothesis, when used to account for frequency effects, can be expressed:

$$\left(\frac{da}{dN}\right)_{total} = \frac{1}{f}\left(\frac{da}{dt}\right)_{environment} + \left(\frac{da}{dN}\right)_{fatigue} \tag{6}$$

The $\left(\frac{da}{dt}\right)_{environment}$ is obtained from sustained load or low frequency cyclic tests in the environment, and $\left(\frac{da}{dN}\right)_{fatigue}$ is obtained from cyclic load tests conducted at high frequencies in air or a non-aggressive environment.

The modification of the linear summation hypothesis used in this program is that for any environment the total crack growth rate for any cycle is the sum of two components; a cyclic component which is environment dependent but independent of frequency, and a sustained load component which is dependent on environment and time at load.

$$\left(\frac{da}{dN}\right)_{Total} = \left(\frac{da}{dN}\right)_{Cyclic} + \left(\frac{da}{dN}\right)_{Sustained} \tag{7}$$

Both crack growth rate components are dependent on the maximum stress intensity factor applied, K_{max}. To compute these components as functions of K_{max}, two inputs of $\left(\frac{da}{dN}\right)_{Total}$ are used; one a high frequency sine wave, the other a low frequency trapezoidal wave, both in the aggressive environment and at R=0. The sustained load growth rate is approximated for a given K_{max} by

$$\frac{da}{dt} = f\left\{\left(\frac{da}{dN}\right)_{Total} \text{ (trapezoidal wave)} - \left(\frac{da}{dN}\right)_{Total} \text{ (sinusoidal wave)}\right\} \tag{8}$$

where f is the frequency of the trapezoidal wave. This data is curve fit by the expression:

$$\frac{da}{dt} = 10^{A+B/K} \tag{9}$$

Equation (9) was numerically integrated for a 1 cps, R=0, sine wave loading to determine the sustained crack growth rate for sine waves of various K_{max} values. Only crack growth rates during the loading portion of the sine wave are integrated because it is assumed that the unloading portion of the cycle contributes no growth. The sustained load crack growth rates computed for the sine waves were curve fit with an expression similar to Equation (9). The sustained load crack growth rates are in the following forms:

$$\frac{da}{dN}_{Sustained} = \frac{1}{f} 10^{C+D/K_{max}} \quad \text{for sinusoidal loading}$$
$$= t10^{A+B/K_{max}} \quad \text{for sustained loading} \tag{10}$$

The fatigue crack growth rate due only to cyclic loading is determined for a given K_{max}:

$$\frac{da}{dN}_{Cyclic} = \frac{da}{dN}_{Total} \quad \text{(sinusoidal wave)}$$
$$- \frac{da}{dN}_{Sustained} \quad \text{(sinusoidal wave)}$$

Sustained load crack growth rates were determined using both Equation (9) and sustained load tests using bolt-loaded WOL specimens. The bolt-loaded WOL test in 300M steel was the most successful. However, as shown in Figure 45, growth rates determined from the cyclic tests were considerably higher than those obtained from the bolt-loaded WOL tests. Data obtained from the cyclic tests were used to correlate and predict load-environment interactions.

Sustained load cracking during a cycle is assumed to occur only during the loading portion of the cycle. When a trapezoidal

wave is applied, growth is the sum of three components; cyclic growth during loading, sustained load growth during loading (analyzed as a sine wave), and sustained load growth during the hold time. The unloading portion of a cycle is assumed to produce no crack growth and is ignored in the analysis.

As shown in Figure 45 for 300M, the coefficients A and B were determined to be -3.14 and -16.22. The predictions shown in Figures 50 and 51 are obtained by applying Equations (7) and (10) to the test conditions. Considering the large effect of environment on the growth rates in 300M, and the scatter that can be expected, the correlation of predictions and tests demonstrated in Figures 50 and 51 is reasonable.

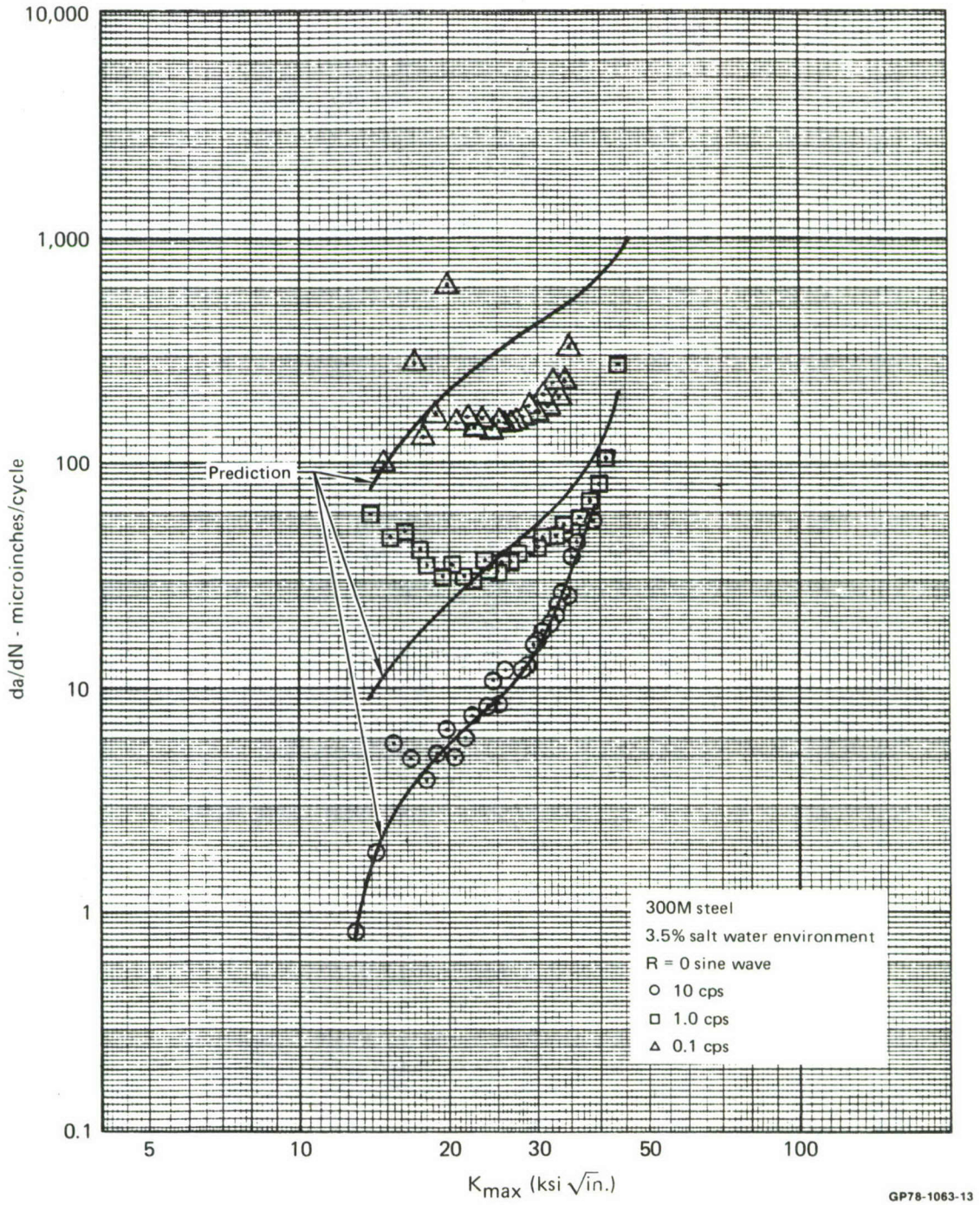

Figure 50
Comparison of Predicted and Measured Crack Growth - Sinusoidal Loading - 300M Steel

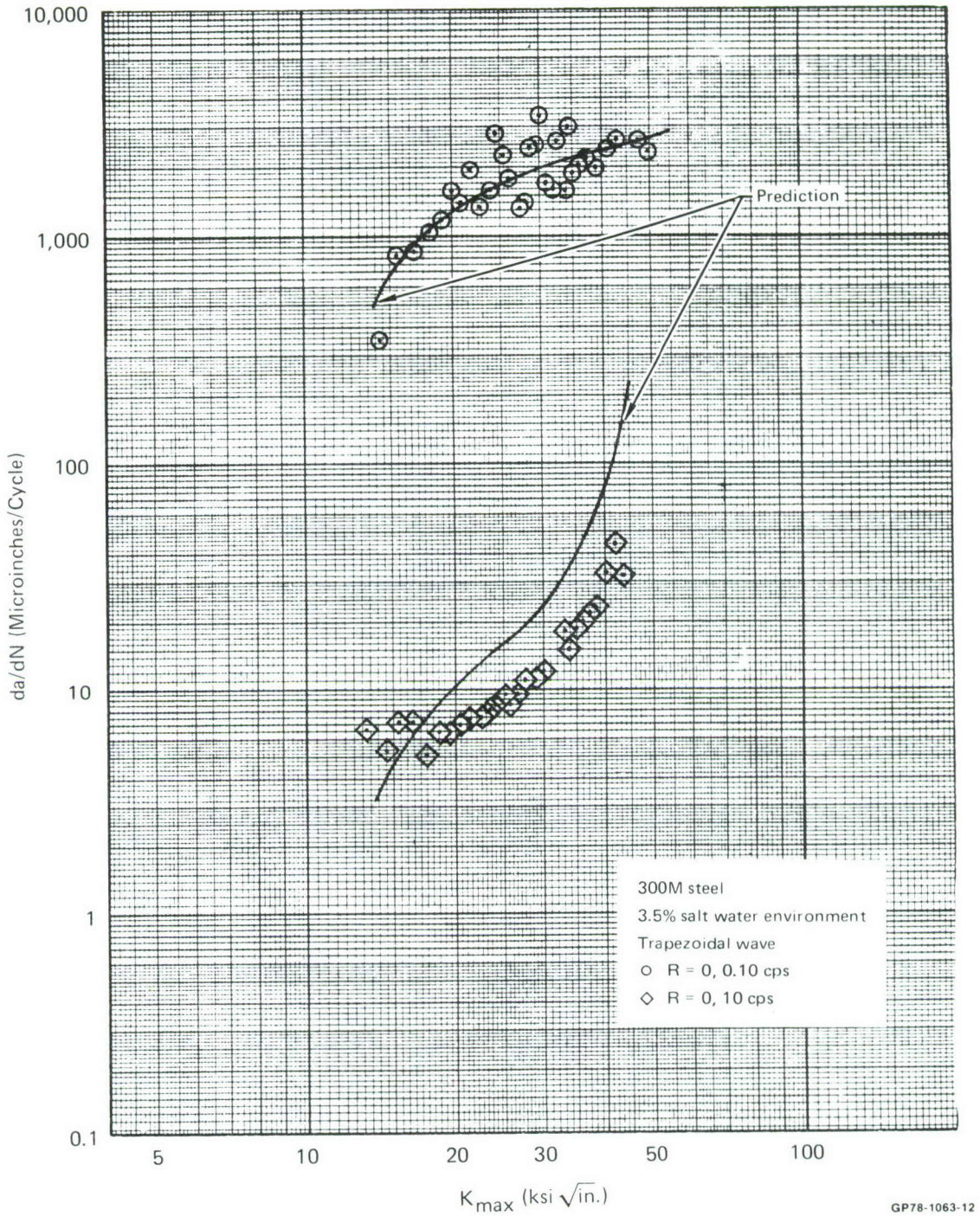

Figure 51
Comparison of Predicted and Measured Crack Growth - Trapezoidal Loading - 300M Steel

The apparent high crack growth rates measured at low K_{max} and low frequencies (shown in Figure 50) might be due to precracking the specimens in the air environment. In the aggressive environment the crack growth rates are very high and decrease slowly to levels nearer those analytically determined. The initial deceleration shown may be due to (a) a slow build up of residue on crack faces which would increase closure, (b) some other change in fracture surface increasing closure, (c) development of crack tip blunting in the aggressive environment, or (d) a combination of these effects. Precracking in the aggressive environment may have removed the transient behavior and produced initial growth rates in better agreement with the predictions shown in Figure 50.

Constant amplitude analysis results are compared with test results in Table 7. The correlation is good in most cases.

TABLE 7
COMPARISON OF ALGORITHM TEST AND ANALYSIS RESULTS

Specimen Number	Objective	Environment	Stress Ratio	Cycle Rate	7049-T73 Test Life/ Predicted Life	7075-T6 Test Life/ Predicted Life	HP 9-4-.30 Test Life/ Predicted Life	300M Test Life/ Predicted Life
1	Develop da/dN	10% R.H. Air	0	10 cps	1.16	1.09	1.06	1.07
2	and Evaluate	↓	0.5	↓	1.16	1.09	1.06	1.47
3	Stress Ratio	↓	−1	↓	1.03	1.24	0.89	1.40
4	Evaluate	3.5% Salt Water	0	10 cps	1.06	1.06	1.05	1.03
5	Frequency	↓	0	1 cps	0.55	0.75	0.73	0.84
6		↓	0	0.1 cps	0.69	0.76	0.55	1.38
7	Evaluate (1)	↓	0	10 cps	1.01	0.97	1.07	1.56
8	Trapezoidal	↓	0	0.1 cps	1.64	1.06	1.14	0.93
9	Wave Shape	↓	0.5	0.1 cps	1.84	0.80	1.28	1.23
10		↓	−1	0.1 cps	1.14	1.03	1.37	1.35

Notes: (1) Tests 1 through 6 use sinusoidal wave shape, tests 7 through 10 trapezoidal shape.

GP78-1063-4

b. Spectrum Analysis with Environmental Acceleration - Application of the crack growth algorithms to spectrum analysis was straightforward. The spectrum was input as a series of stresses and corresponding time increments to peak stress (Section V). Stress levels were joined by haversine waves as shown in the sketch. Sustained stress levels are represented by two adjoining peaks having the same stress level, the peak to peak time being the hold time.

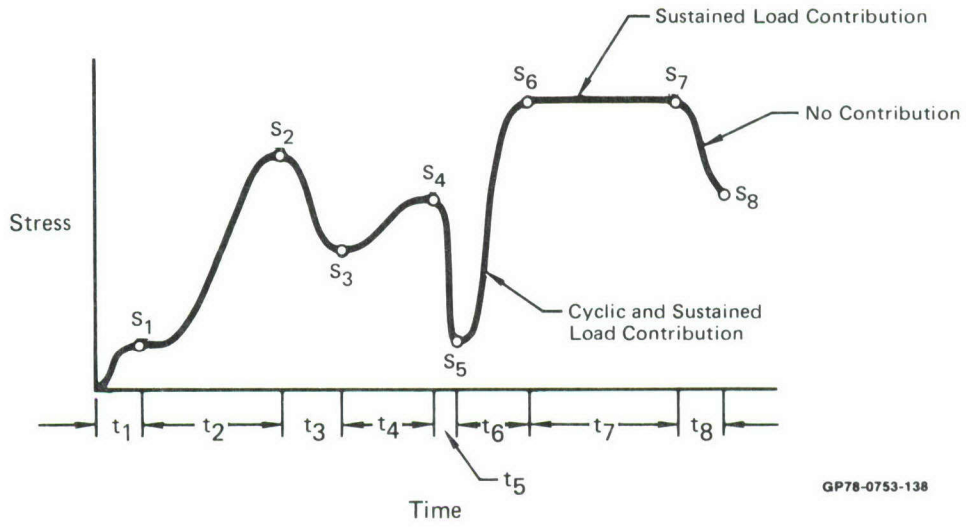

The stress history was simplified so that it contains only peaks and valleys and the times at which they are applied. Thus, during simplification, the stress level s_o is the first valley, stress level s_1 is dropped and s_2 is the peak for the first half cycle. The time increment for the first cycle is the sum of t_1 and t_2.

Under spectrum loadings, $\frac{da}{dN}_{Cyclic}$ and $\frac{da}{dN}_{Sustained}$ are assumed to depend on the effective loading parameters computed by the Willenborg model. Thus

$$\left(\frac{da}{dN}\right)_{Cyclic} = f(K_{max\text{-}eff}, R_{eff})$$

$$\left(\frac{da}{dN}\right)_{Sustained} = t\ 10^{A+B/K_{max\text{-}eff}} \quad \text{for sustained loading}$$

$$= \frac{1}{f}\ 10^{C+D/K_{max\text{-}eff}} \quad \text{for sinusoidal loading}$$

The following assumptions are also inherent in the analysis:

(a) The unloading portion of the stress cycle produces no crack growth and is ignored in the analysis. The stress intensity range and stress ratio used for analysis are determined by a valley stress and the subsequent peak stress.

(b) Any half cycle having a stress ratio greater than 0.9 is treated as a sustained load.

(c) In the computation of sustained load crack growth, a cycle has a peak stress intensity factor of $K_{max\text{-}eff}$, as determined by the Willenborg model, and $R_{eff}=0$.

(d) Fracture is assumed to occur whenever the stress intensity factor exceeds K_c.

Computation of cyclic crack growth considers only the loading portion of the cycle, i.e., s_5 to s_6 is a load cycle, s_6 to s_7 or s_7 to s_8 are assumed to produce no cyclic growth. Similarly, computation of sustained load crack growth uses only the loading half cycle and sustained load, the growth is predicted by Equations (19) through (21). The cyclic frequency is determined from the loading period, i.e.,

$$f = \frac{1}{2t_4} \quad \text{for } s_3 \text{ to } s_4,$$

For sustained loads, i.e., half cycles having $R \geq 0.90$,

$$\left(\frac{da}{dN}\right)_{Environmental} = \Delta t 10^{A+B/K_{max\text{-}eff}} \tag{11}$$

where for s_6 to s_7, $\Delta t = t_7$.

4. WILLENBORG MODEL

a. Generalized Willenborg Model - The Willenborg, et al, model, Reference 7, as generalized by Gallagher and Hughes (Reference 8) is the load interaction model extended to the analysis of environmental effects. The original Willenborg Model was developed to describe crack growth retardation following high-low block loadings. It is based on observations of the following phenomena:

(a) Retarded crack growth occurs whenever the maximum applied stress intensity is reduced.

(b) Such retardation is directly related to the reduction in maximum stress intensity.

(c) The length over which crack growth is retarded, i.e., the load interaction zone, is proportional to the plastic zone created by the maximum stress intensity.

(d) There is no retardation of growth if the current maximum stress creates a load interaction zone which extends out to or beyond a previously established interaction zone.

Based on these observations, Willenborg, et al, assumed that the load interaction effects were caused by variations in local stress intensity as the crack grows through the residual stress field produced by the overload(s).

Mathematically, the effective stress intensity for the Willenborg model is expressed in Reference 7 as:

$$K_{eff} = K^{\infty} - K_{RED} \tag{12}$$

$$K_{RED} = K_{max}^{OL} \left(1 - \frac{\Delta a}{z_{OL}}\right)^{1/2} - K_{max}^{\infty} \tag{13}$$

where K^{∞} is the applied stress intensity, K_{RED} is the additional stress intensity required to extend the current interaction zone to that created by the overload, Δa is the growth following the overload, and z_{OL} is the overload interaction zone size. The effective stress intensity range and stress ratio are computed as,

$$\Delta K_{eff} = K_{eff}^{max} - K_{eff}^{min} = K_{max}^{\infty} - K_{RED} - (K_{min}^{\infty} - K_{RED}) = \Delta K^{\infty} \quad (14)$$

$$R_{eff} = \frac{K_{eff}^{min}}{K_{eff}^{max}} = \frac{K_{min} - K_{RED}}{K_{max} - K_{RED}} \quad (15)$$

Thus, as noted in Reference 7, the Willenborg model predicts retardation by depressing the effective stress ratio below that remotely applied while leaving the stress intensity range intact. Since K_{RED} decreases as the crack grows through the overload interaction zone, the Willenborg model predicts that maximum retardation will occur just after the overload and that the growth rate will return to constant amplitude when the current interaction zone extends to the end of the overload interaction zone.

Due to the dependence of the Willenborg retardation on effective stress ratio, a crack growth rate relationship which interrelates the influence of stress ratio with stress intensity range must be used. This relationship is discussed in Paragraph 2. Overload ratio is defined as the ratio of overload stress intensity to maximum stress intensity, for the current load, and shut-off ratio as the overload ratio that prevents subsequent crack growth.

The Willenborg model predicts zero value for the maximum effective stress intensity, and thus no growth should occur, when the overload ratio is two, that is, when K_{RED} equals K_{max}^{∞} in Equation (12). This can be shown by rewriting (12) for the maximum effective stress intensity as:

$$K_{max}^{eff} = K_{max}^{\infty} - [K_{max}^{OL} \left(1 - \frac{\Delta a}{z_{OL}}\right)^{1/2} - K_{max}^{\infty}] \quad (16)$$

where K_{max}^{OL} is the maximum overload stress intensity, Δa is growth following overload and z_{OL} is overload interaction zone size. Immediately following the overload, Δa is usually very close to zero so that K_{max}^{eff} is zero when K_{max}^{OL} is twice K_{max}^{∞}.

Test results obtained by several investigators, References 9 through 12, show that the actual crack growth shut-off ratio can be greater than two. Gallagher and Hughes, Reference 8, generalized the Willenborg model to correct prediction of the overload to maximum load ratio required to produce cessation of crack growth. They proposed modifying Equation (5) so that for R = 0:

$$K_{max}^{eff} = K_{max}^{\infty} - \Phi \left[K_{max}^{OL} \left(1 - \frac{\Delta a}{z_{OL}}\right)^{1/2} - K_{max}^{\infty}\right] \tag{17}$$

For the condition of no growth, $\Delta a=0$, $K_{max}^{eff} = K_{maxTH}$ (threshold stress intensity) so that,

$$\Phi = \frac{1 - \dfrac{K_{maxTH}}{K_{max}^{\infty}}}{\dfrac{K_{max}^{OL}}{K_{max}^{\infty}} - 1} \tag{18}$$

where the shut-off overload ratio $\left(\dfrac{K_{max}^{OL}}{K_{max}^{\infty}}\right)$ must be obtained from tests for the given material, thickness, and stress ratio (underload condition).

Gallagher and Hughes used the generalized model quite successfully to predict the number of cycles required to return to constant amplitude growth rate following an overload in two steels having different yield strengths. Gallagher and Stalnaker, Reference 13, also used the generalized model to predict magnitude and trends of crack growth rate data generated under transport-wing simulation loading. The correlation of test and analysis was significantly improved over that of the original model.

The computer routine for the generalized Willenborg Model was extracted from the Air Force's CRACKS II computer program, Reference 14.

b. Compression Loads Analysis - There are two effects of compression loading. One effect is to increase the stress intensity amplitude of the cycle following compression; analysis of this stress ratio effect was discussed in Paragraph 2. The second, and frequently greater effect is to accelerate the growth caused by subsequent load cycles. In the program "Effects of Fighter Attack Spectrum on Crack Growth", Reference 15, modifications were made to the Willenborg model to better account for the accelerated growth following compression. The approach is to reduce the overload plastic zone size based on the minimum stress intensity applied prior to the overload:

$$z_{OL} = [(K^{\infty}_{max})^2 - \frac{3}{32} (K^{\infty}_{min})^2] \frac{\gamma}{2\pi} F^2_{ty}$$

where K^{OL}_{min} is the minimum stress intensity applied prior to the overload, F_{ty} is the material yield strength, and γ is the plane stress-plane strain coefficient; $\gamma = 1$ for plane stress and $\gamma = \frac{1}{2\sqrt{2}}$ for plane strain. The multiplier 3/32 was empirically selected to correlate predictions with the compression loads test data presented in Reference 16.

The improvement in prediction accuracy obtained by including compression in spectrum loading analysis is shown in Figure 52. The test data was obtained from the program "Effects of Fighter Attack Spectrum on Crack Growth", and in this series of tests the ground load was varied to investigate the effects of compression. The earlier Willenborg model predicted small impact of this variation, the improved model more accurately predicted the acceleration observed in test.

The complete environment-load interaction analysis routine is presented in the form of a user's manual in Appendix C.

5. MODEL CALIBRATION - The generalized Willenborg model was used to account for the effect of high loads in a spectrum to retard the crack growth produced by subsequent low load cycles. The Willenborg model accounts for this retardation by using two parameters; the overload interaction zone size, z_{OL}, and the shut-off overload ratio. The overload interaction zone size

determines the amount of crack growth affected by an overload. Increasing the interaction zone size retards the predicted crack growth. The shut-off overload ratio determines the magnitude of the retardation caused by a given overload level. Increasing the shut-off overload ratio accelerates the predicted crack growth.

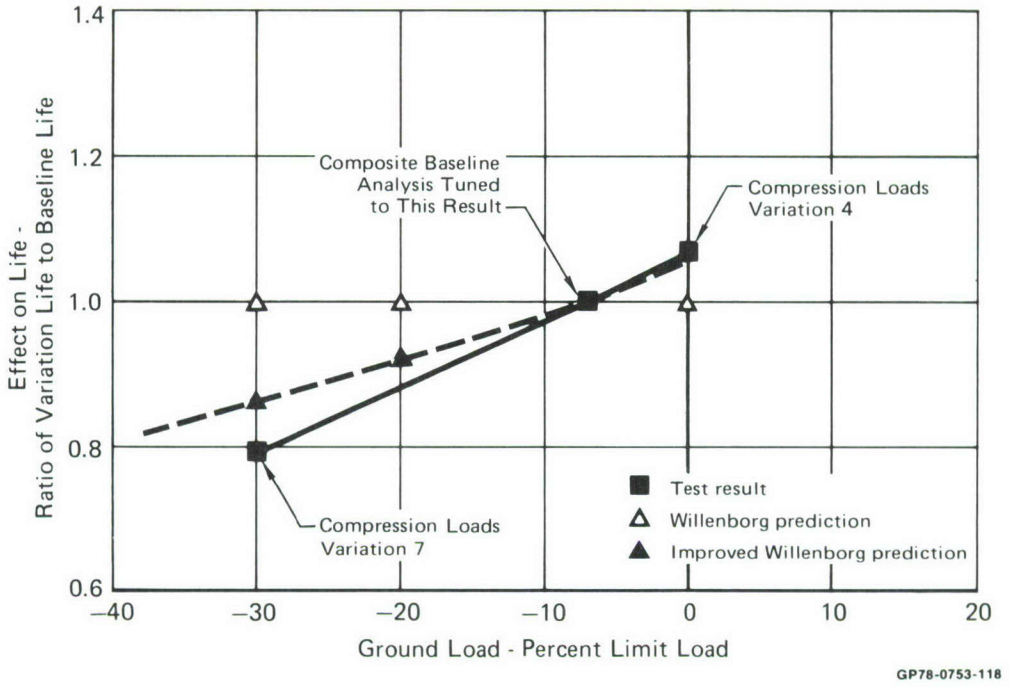

Figure 52
Improved Analysis of Compression Effects with Residual Stress Intensity Model

Values of both of these parameters were selected by correlation with results obtained with tests of center crack panels. The shut-off overload ratio selection was based on results of single overload tests. The overload interaction zone size was selected to correlate with the spectrum tests in dry air. The premise of the Willenborg model application in this program was that once parameter values were found which correlated spectrum analysis and test results, they could be used with confidence to predict the results of similar spectrum tests. The Willenborg model parameters used to make all spectrum crack growth predictions presented herein are shown in Table 8.

TABLE 8
WILLENBORG MODEL PARAMETERS USED FOR ANALYSIS

Material	ROOT2 (1)	OLMAX (2)
7049-T73	0.400	2.65
7075-T6	0.100	2.65
HP 9-4-.30	0.100	3.50
300M	0.028	3.50

Notes:

(1) ROOT2 is an overload interaction zone size factor
The interaction zone size is defined as

$$Z_{OL} = \frac{ROOT2}{2\pi} \left\{ \frac{K^{OL}_{max}}{F_{ty}} \right\}^2$$

(2) OLMAX is the overload ratio $\frac{K^{OL}_{max}}{K^{\infty}_{max}}$ which is determined from tests to shut-off subsequent crack growth.

GP78-0753-22

a. Determination of Shut-off Ratio Using Overloads Tests - To determine the overload ratio which shuts-off subsequent constant amplitude crack growth, a series of increasing single overloads was applied during constant amplitude tests. The constant amplitude crack growth between overload applications was sufficient to preclude interactions of the overload effects. Results of these tests were presented in Section III.

Results of overload tests in steels indicated that overload ratios of up to 2.8 will not cause crack growth shut-off in either air or salt-water. In aluminum, overload ratios of 2.8 did shut-off crack growth both in air and salt-water while ratios of 2.5 did not cause shut-off. These results were used to select shut-off ratios of 2.65 in the aluminum alloys and 3.5 in both steel alloys.

The correlation of predicted and measured delay cycles for the HP-9-4-.30 overload tests in both air and salt water is shown in Figure 53. As shown, the shut-off ratio of 3.5 used for analysis of HP-9-4-.30 steel correlates well with the higher overload ratios but predicts much less delay than measured for lower overload ratios. This should result in conservative analysis when applied to spectrum loadings.

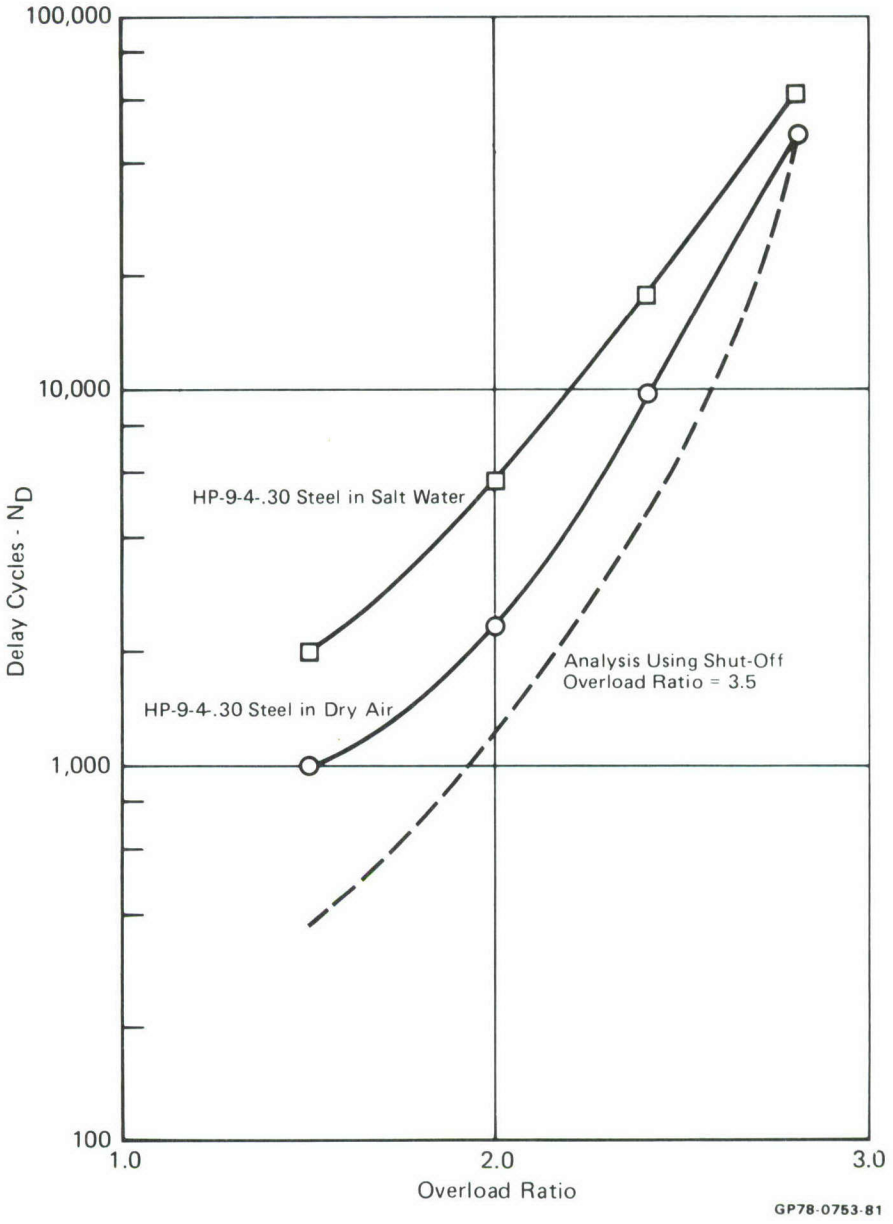

Figure 53
Effect of Overload Ratio on Delay in HP-9-4-.30 Steel

b. Determination of Overload Interaction Zone Size Using Spectrum Test Data - The overload interaction zone size selected for the analyses was based on the retardation measured in spectrum tests in dry air. Once the shut-off ratios were determined from the overload test results, overload interaction zone sizes were determined by correlating analyses results with re-

sults obtained from the center crack panel spectrum tested in dry air to the accelerated stress history. Results of these correlations are discussed in Section VIII.

6. SEMI-ELLIPTIC SURFACE FLAW ANALYSIS

a. Stress Intensity Solutions - Stress intensity solutions for elliptic surface flaws were determined using a slice synthesis technique described in Reference 17. A comparison of these solutions with others is presented in Figure 54. In Figures A-1 and A-2 of Appendix A, the solutions are graphically summarized and in Table A-1 are presented as closed form polynomial expressions which can be readily used in crack growth prediction computer routines.

The slice synthesis technique described in Appendix A was used to obtain stress intensity solutions. In this approach, the flaw is idealized as a series of center crack "slices" joined through the thickness with edge crack slices to account for the shear coupling between the center crack slices. The results presented in Figure 54 show good agreement with those obtained using fine mesh finite element models which are the most detailed employed thus far in the analysis of the surface flaw. The slice synthesis technique has the advantage over current models in that finite width as well as thickness can be included in the analysis.

b. Prediction of Flaw Shape Change - The elliptic surface flaw requires analysis of the growth in both the surface and depth directions. Because the crack aspect ratio changes as the crack grows, the stress intensity relationships at the surface and depth change. It would be unnecessarily complicated in spectrum analysis to track the growth at both locations on a cycle-by-cycle basis. Instead, the changing aspect ratio can be predicted, based on constant amplitude loading analysis. With the aspect ratio known, growth at only one location needs to be tracked, simplifying spectrum crack growth prediction. Figure 55 presents an example of the predicted change in shape, as a function of surface growth. With this data pre-determined,

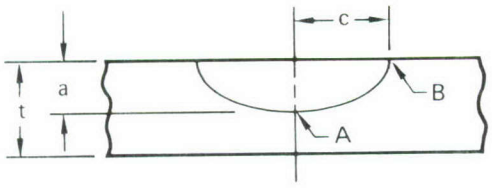

Semielliptical Surface Flaw a/2c = 0.1

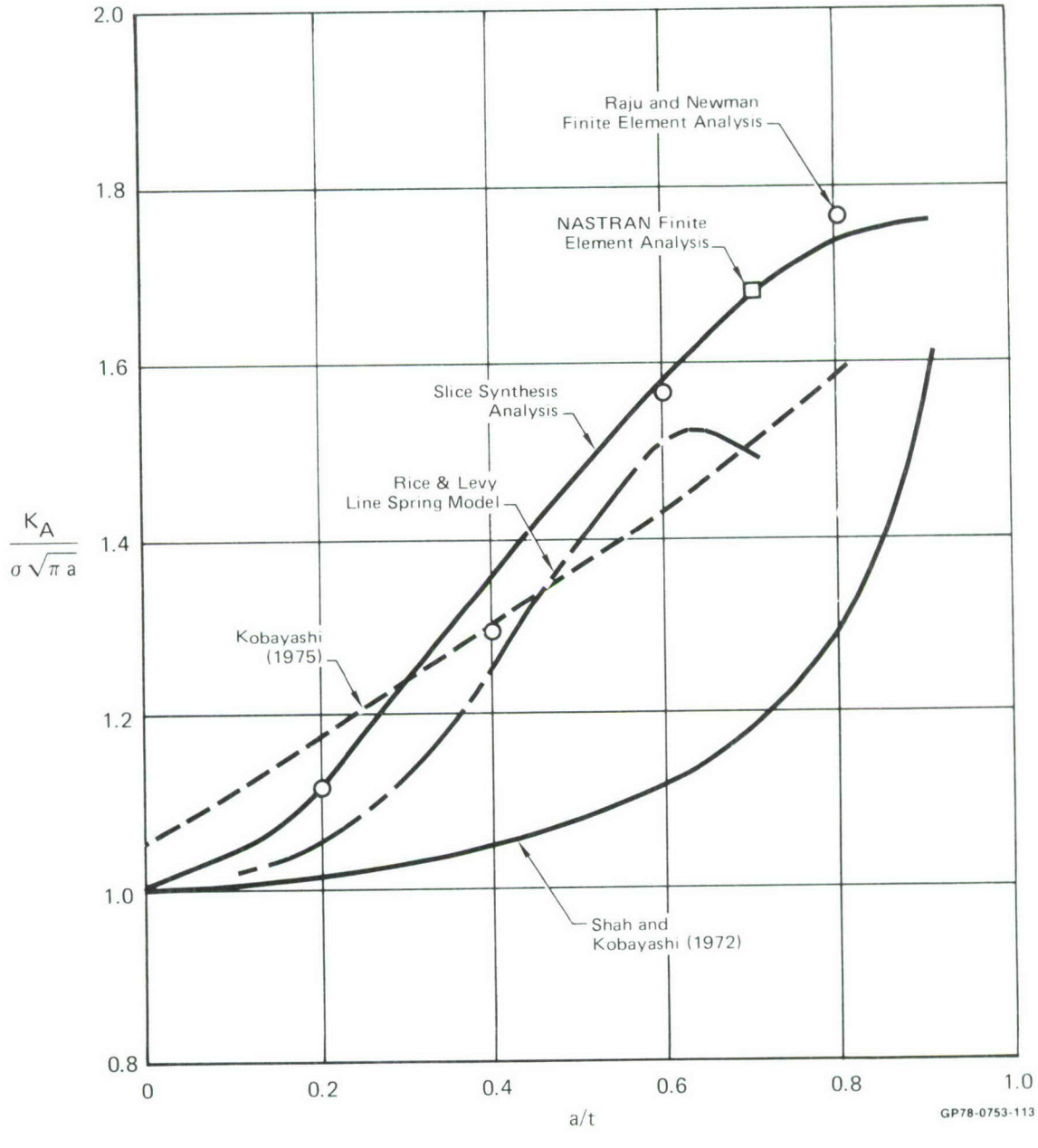

Figure 54
Comparison of Surface Flaw Stress Intensity Solutions

it is then possible to predict stress intensity relationships as a function of surface length, permitting the two dimensional growth to be characterized by surface growth.

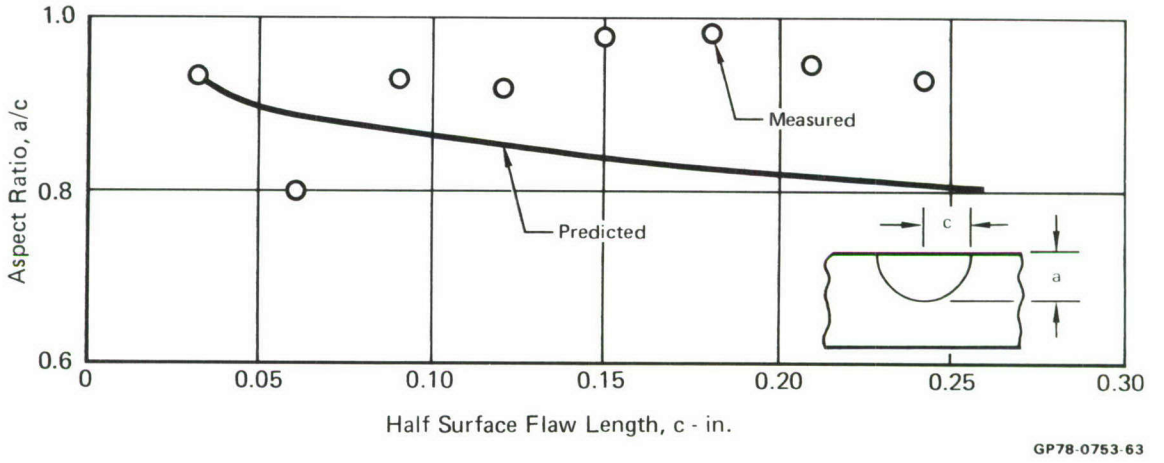

Figure 55
Shape Change of Surface Flaw in 7049-T73 Aluminum

Appendix B describes a routine used to predict growth, shape changes, and stress intensity factor corrections for a semi-elliptical surface flaw under constant amplitude loading. This routine was used to determine flaw shape changes and stress intensity factors for both constant amplitude and spectrum crack growth analyses. For spectrum crack growth analyses the highest stress level in the spectrum and initial flaw size and shape were used for analysis.

Computation of stress intensity factors at the crack depth and plate surface is based on results from the slice synthesis technique described in Appendix A. These results are summarized in Table A-1 of Appendix A. Stress intensity factors and crack growth both at flaw depth and surface are computed on a cycle-by-cycle basis. The following assumptions are inherent in this routine:

(a) Constant amplitude, R=0, sinusoidal loading is applied.
(b) Crack growth rates at plate surface and flaw depth are dependent on the ΔK which is applied at those points.

(c) Crack growth rate versus ΔK relationship obtained from a center cracked panel can be used to predict flaw growth at any point along the crack front.

(d) Stress intensity factor expressions are assumed valid until flaw depth exceeds 90% of plate thickness. Values of K_A and K_B at a/t=0.8 and a/t=0.9 are used for extrapolations beyond a/t=0.9.

(e) Fracture is assumed to occur when the stress intensity factor for the input constant amplitude stress level is equal to K_C.

c. Correlation of Analysis and Test - Figures 55 through 58 compare measured and predicted crack aspect ratio as a function of crack surface growth. The test data was obtained from the constant amplitude elliptic flaw testing summarized in Section III. Agreement between test and prediction does not appear very good.

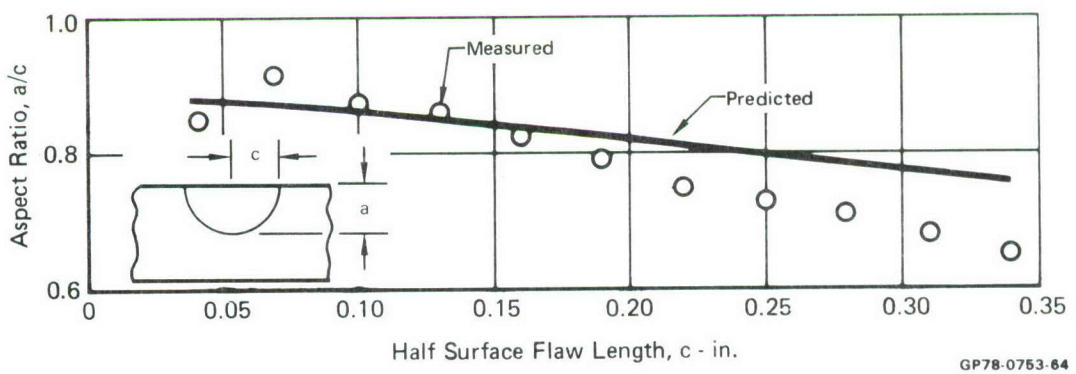

Figure 56
Shape Change of Surface Flaw in 7075-T6 Aluminum

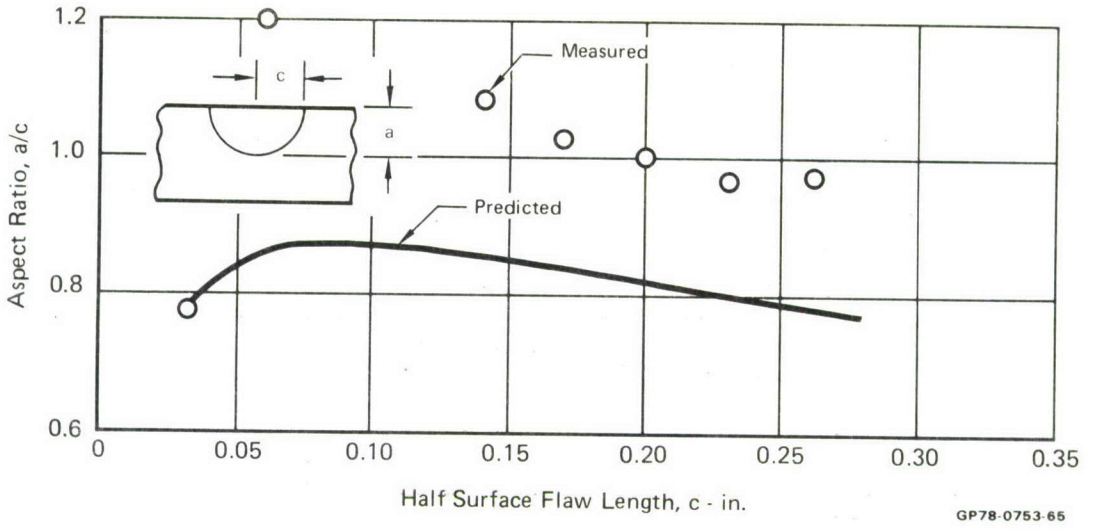

Figure 57
Shape Change of Surface Flaw in HP-9-4-.30 Steel

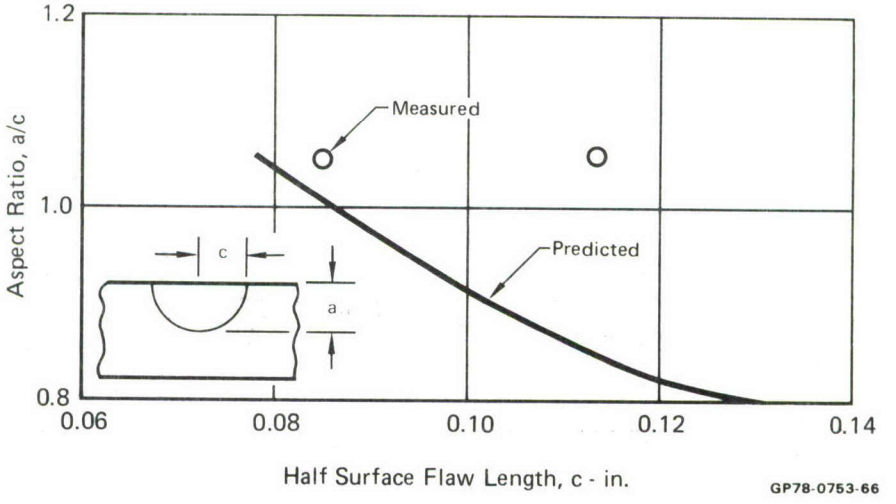

Figure 58
Shape Change of Surface Flaw in 300M Steel

However, the impact of crack aspect ratio on stress intensity factor is not as great as that of size. Figures 59 through 62 present comparisons of stress intensity factors determined from both the predicted and measured flaw shapes. The comparison is somewhat better than that obtained for flaw shape alone.

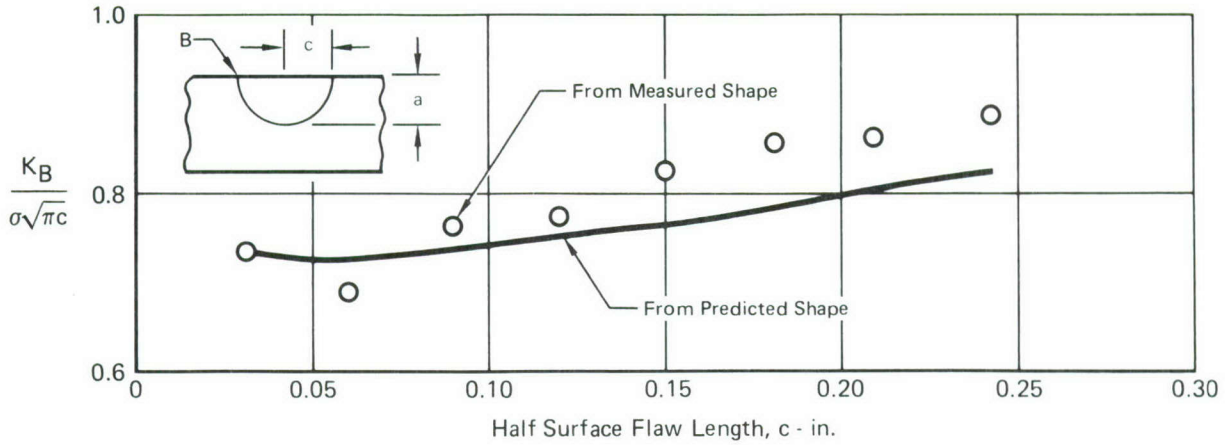

Figure 59
Stress Intensity Factors From Measured and Predicted Flaw Shapes for 7049-T73 Surface Flaw Test

GP78-0753-67

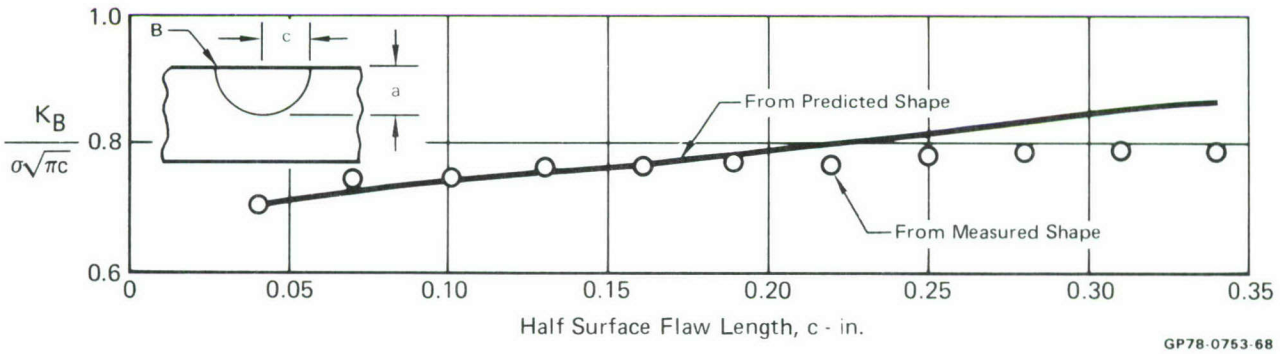

GP78-0753-68

Figure 60
Stress Intensity Factors From Measured and Predicted Flaw Shapes for 7075-T6 Surface Flaw Test

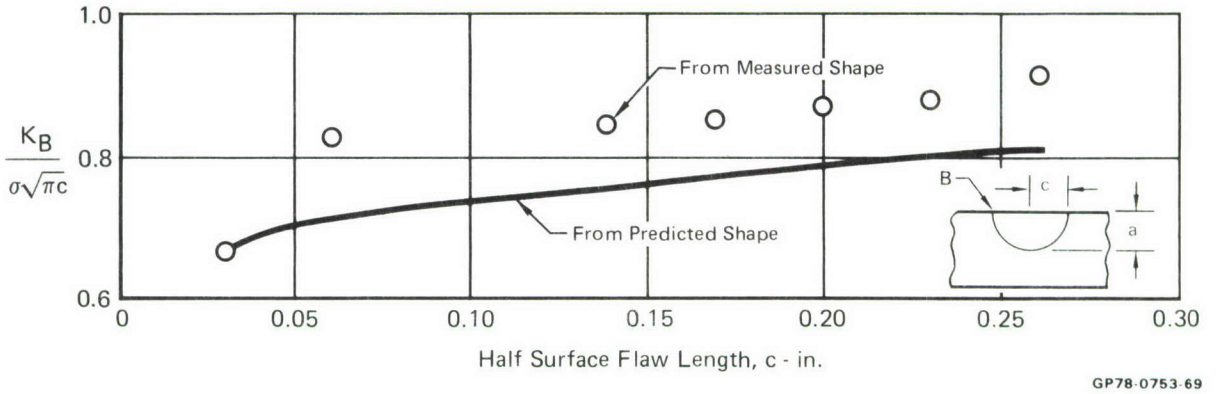

Figure 61
Stress Intensity Factors From Measured and Predicted Flaw Shapes for HP-9-4-.30 Surface Flaw Test

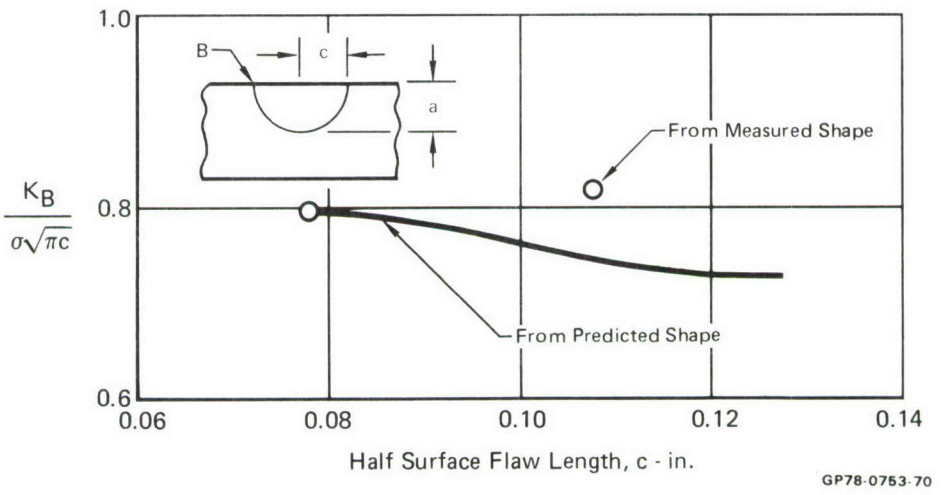

Figure 62
Stress Intensity Factors From Measured and Predicted Flaw Shapes for 300M Surface Flaw Test

More direct comparisons of the accuracy of the analysis procedures are shown in Figures 63 through 66. In those figures, the predicted and measured crack growths are compared, and good agreement is apparent for all materials except 300M steel. 300M steel may have been undergoing an initial retardation caused by insufficient precracking. This delay occurred randomly in the verification tests also, as described in Section VII.

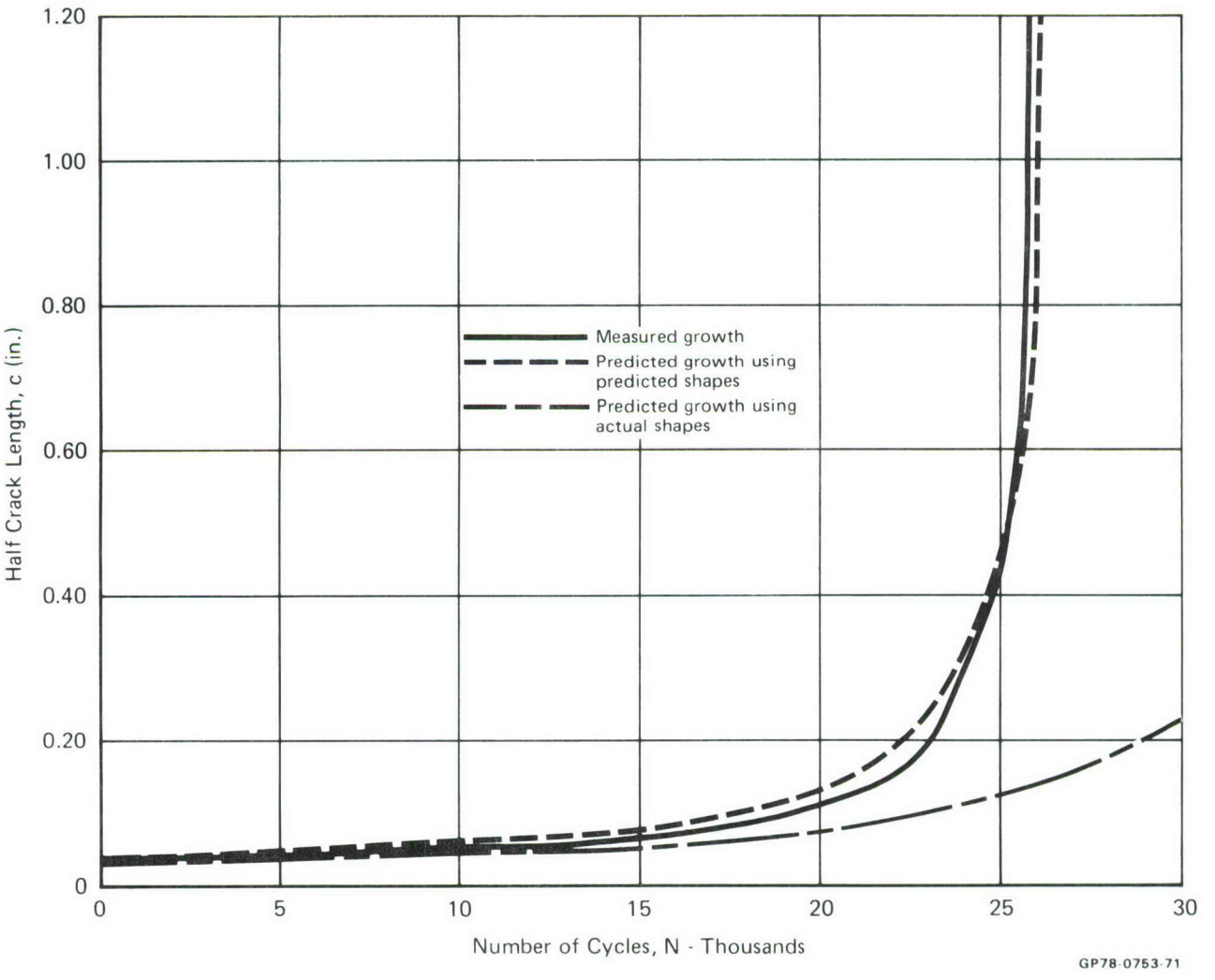

Figure 63
Surface Flaw Crack Growth in 7049-T73 Aluminum

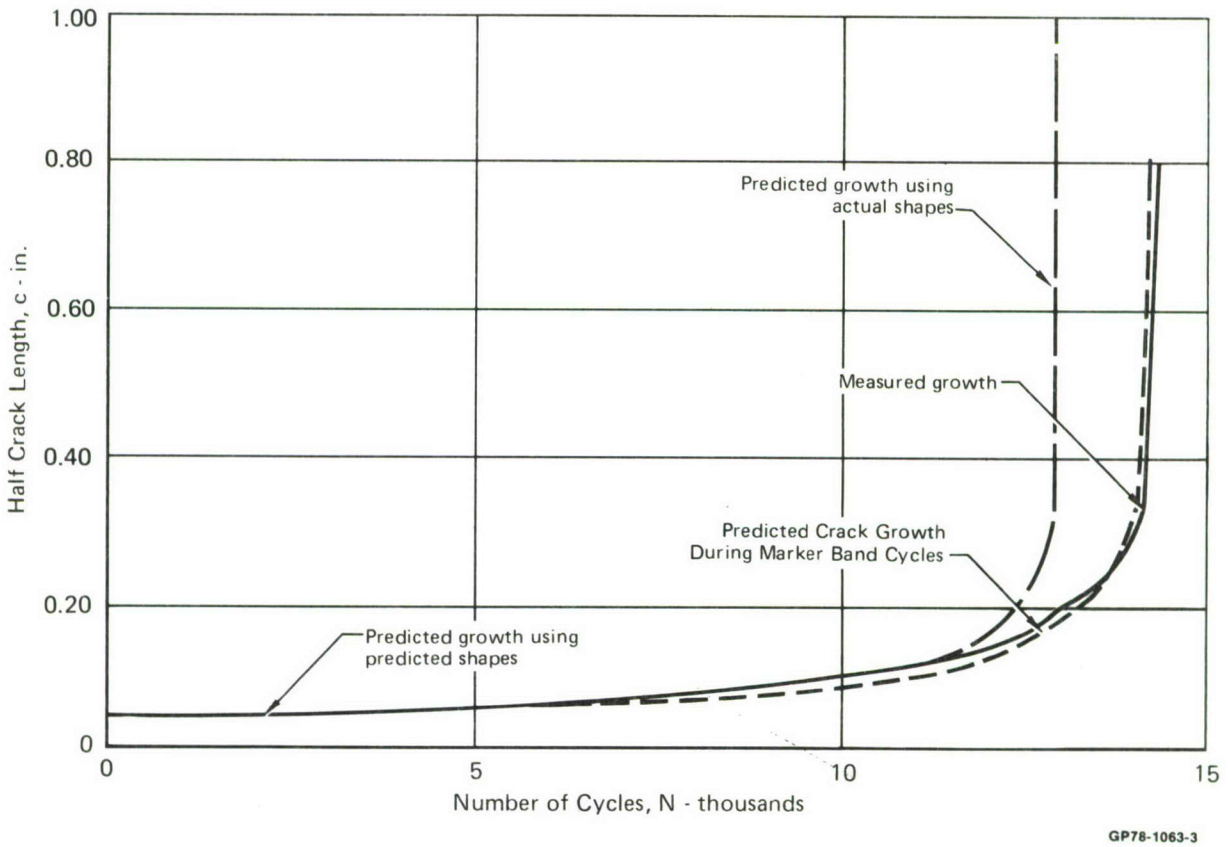

Figure 64
Surface Flaw Crack Growth in 7075-T6 Aluminum

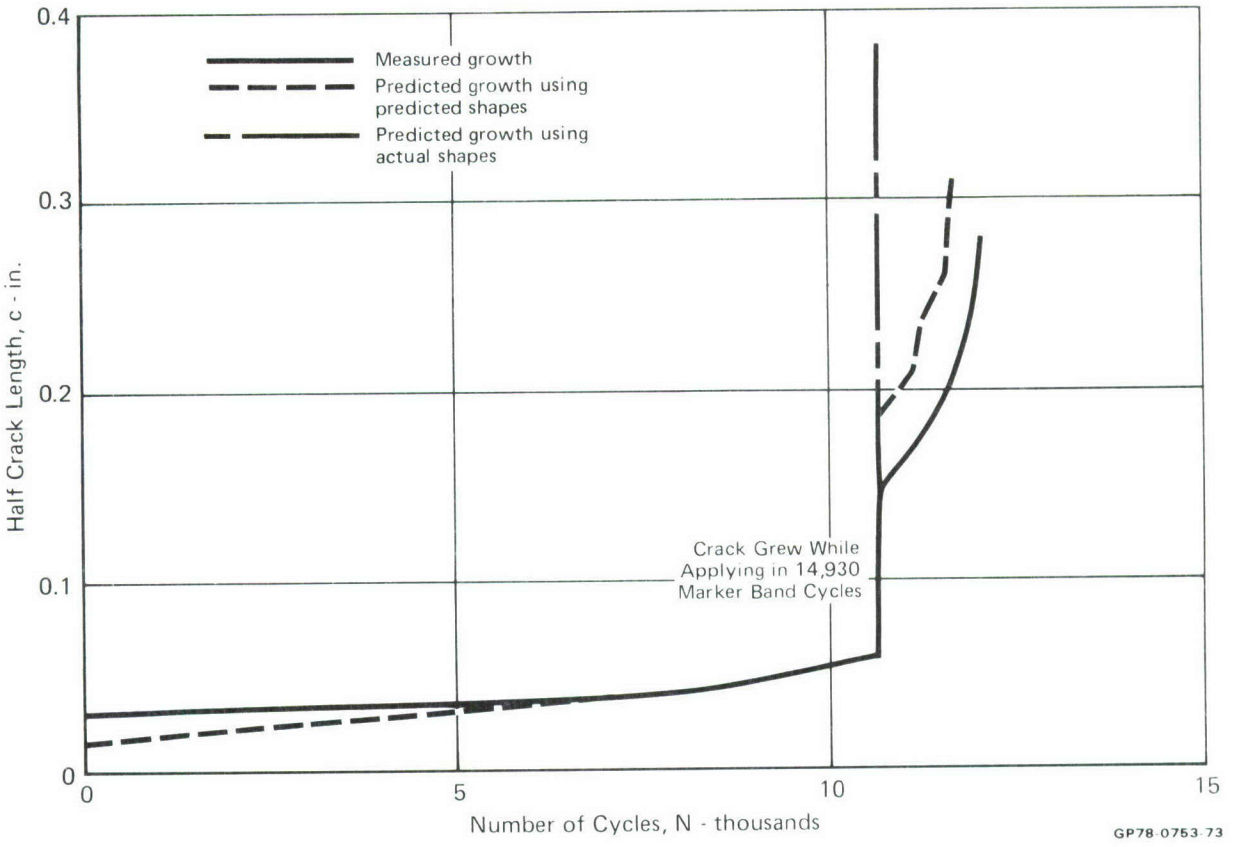

Figure 65
Surface Flaw Crack Growth in HP-9-4-.30 Steel

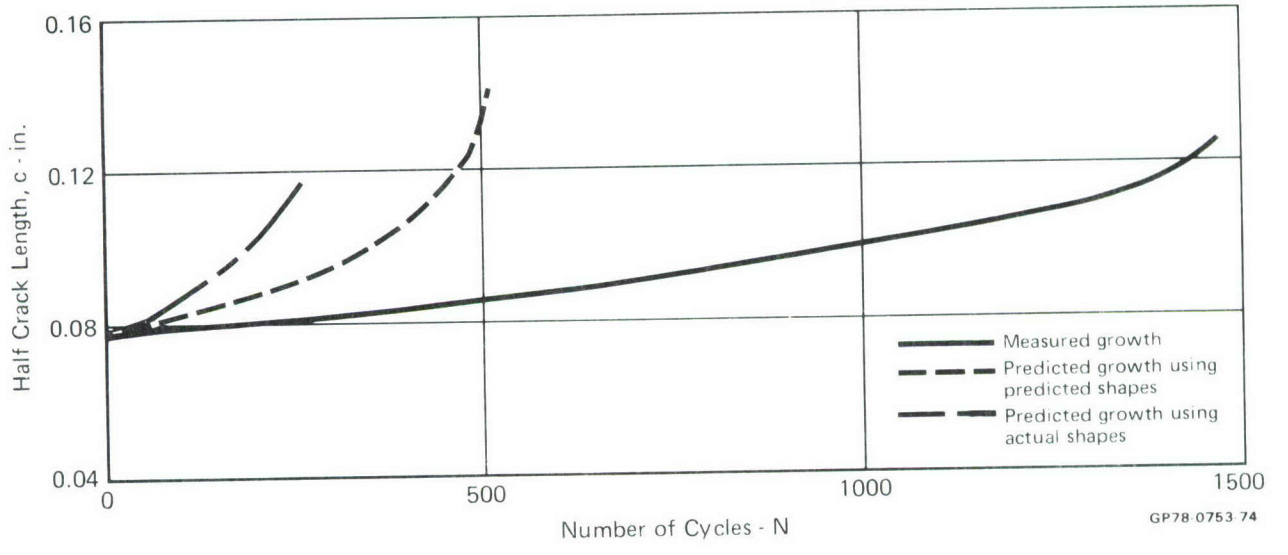

Figure 66
Surface Flaw Crack Growth in 300M Steel

SECTION V

LANDING GEAR STRESS HISTORY

A flight-by-flight stress history used in the verification test phase (Section VI) was derived, based on the outboard trunnion of the F-15 main landing gear system. It was derived from the design fatigue load spectrum employed in ground test verification of F-15 landing gears and includes estimated times of stress applications. The times required to attain the various landing gear loading conditions can vary widely, especially during braking where the pilot establishes load duration. The times computed were the maximum possible for each braking condition.

1. F-15 LANDING GEAR DESCRIPTION - The F-15 main landing gear (Figure 67) is a conventional air-oil landing gear system utilizing a folding drag brace, a side brace that is an integral part of the outer cylinder, and a one piece axle-fork-piston. The strut retracts forward and the wheel swivels 88.3° during retraction into the fuselage.

The F-15 landing gear has a cantilevered piston that transfers ground drag and side loads into the outer cylinder by socket action and vertical loads are reacted by pneumatic and metered oil pressures. Loads transferred into the outer cylinder are reacted by: a) the outboard trunnion which is an integral part of the outer cylinder, b) the inboard trunnion, also an integral part of the outer cylinder, and c) the drag brace, which is bolted to the lower end of the outer cylinder. The drag brace, which folds in the center to permit gear retraction, is made in two sections. All the structural components discussed above are fabricated from 300M steel (heat treated to 230 ksi yield strength, 280 ksi ultimate strength) except for the upper portion of the drag brace which is 6Al-6V-2Sn annealed titanium.

The main landing gear outer cylinder was selected as a representative highly loaded fatigue critical component. A fatigue spectrum was derived for the outboard trunnion region of this outer cylinder (Figure 68). The outboard

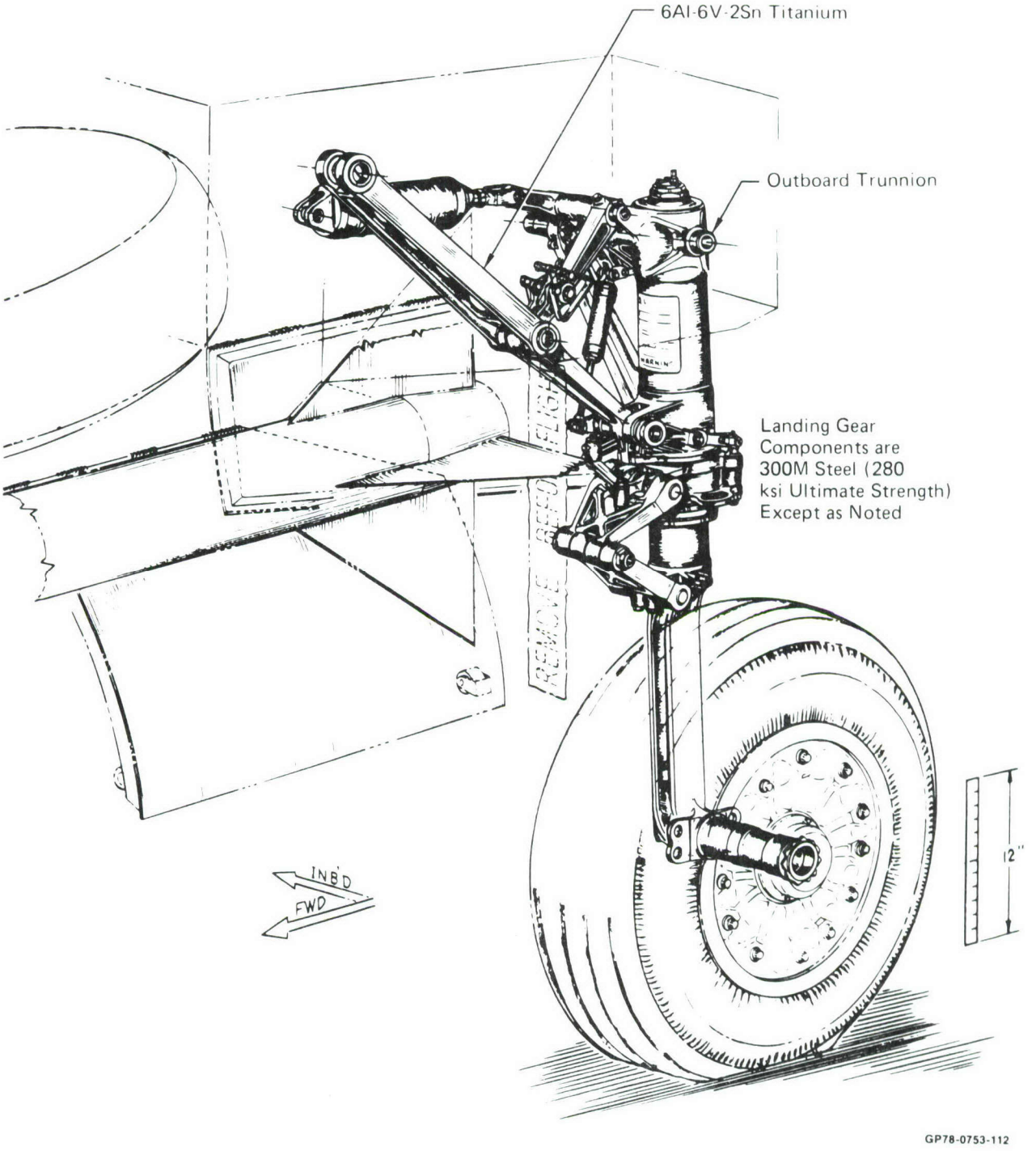

Figure 67
F-15 Main Landing Gear Selected as Study Base

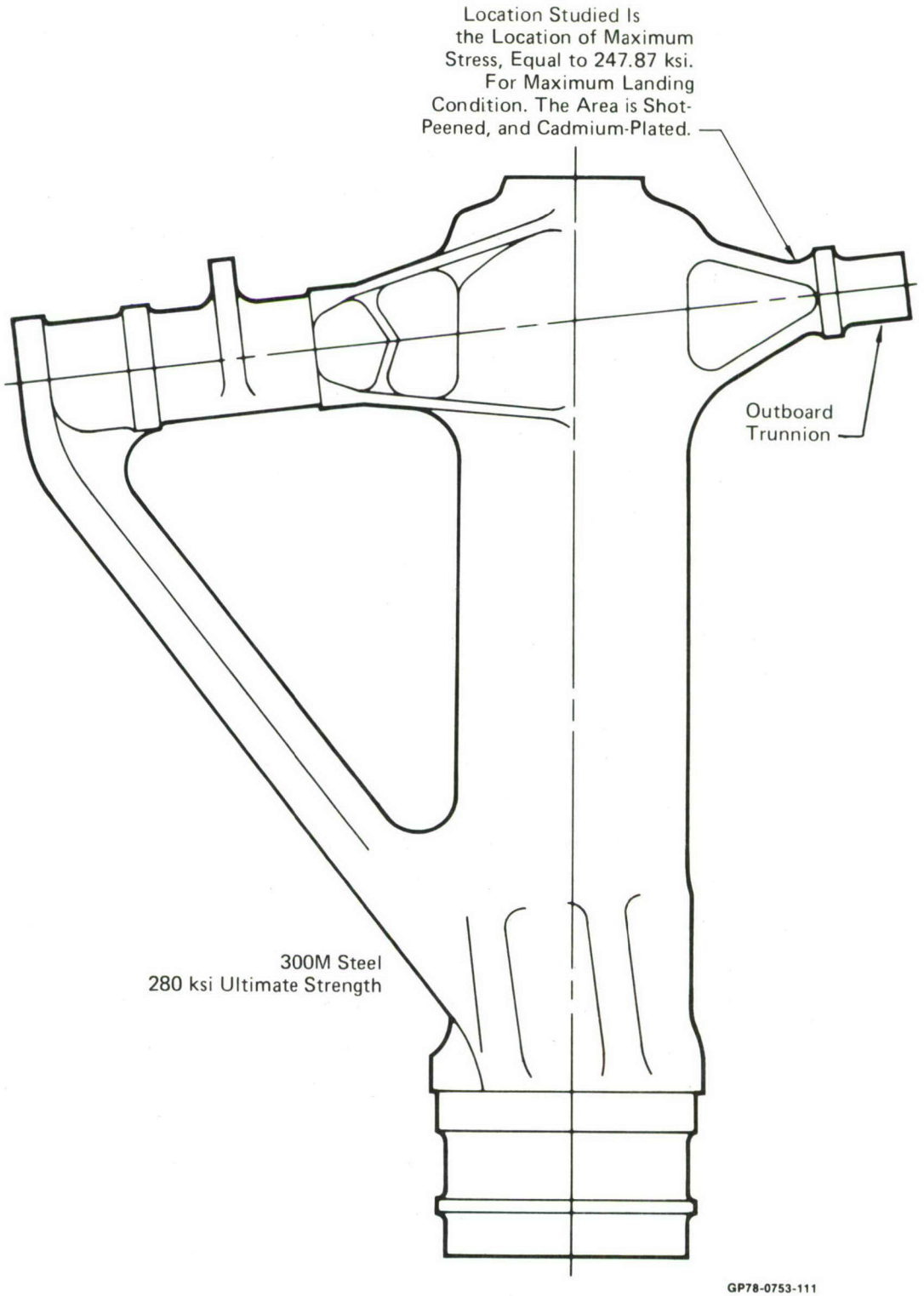

Figure 68
F-15 Main Landing Gear Outer Cylinder

trunnion experiences high loads in each of the major loading conditions for the gear; i.e., landing, braking, turning, etc., and is subject to most of the 1g sustained loads when the aircraft is parked.

2. DESIGN FATIGUE LOADS - The F-15 landing gear is designed to the ultimate strength requirements of MIL-A-8862 and the repeated loads requirements of MIL-A-8866. A large portion of the gear was designed by ultimate strength criteria. The one-lifetime design fatigue spectrum for F-15 landing gears included 5000 take-offs and landings. A scatter factor of four was used in the design so that 20,000 take-offs and landings were demonstrated in ground fatigue tests.

The F-15 landing gear loads design criteria are summarized in Table 9. All of these design criteria are in accordance with MIL-A-8866 except the taxiing loads which result from runway dips and bumps during typical takeoff and landings. Bumps and dips were specified by the Air Force as being those at Travis Air Force Base.

Ground load reactions were determined using methods of statics for braking, turning, and pivoting conditions and using a dynamic analysis for taxiing and landing conditions. Results of these analyses are summarized in Table 10 with load-time history diagrams which define the sequence in which various loads are applied to the landing gear. The resultant loads and corresponding maximum stresses for the outboard trunnion are summarized in Table 11.

3. OUTBOARD TRUNNION FLIGHT-BY-FLIGHT STRESS HISTORY - A simple flight-by-flight spectrum was developed containing the significant features of the design spectrum. This design spectrum was not based on actual measurements on field hardware. The 26 conditions summarized in Table 11 were rearranged into two flights, grouped by aircraft weight, as shown in Table 12. Flight 1 contains conditions corresponding to lighter aircraft weights and higher landing sink rates. Infrequently occurring landing conditions 21 and 22 were periodically introduced because they have the maximum

TABLE 9
F-15 LANDING GEAR REPEATED LOADS DESIGN CRITERIA

Description	Condition	Aircraft Weight	Number of Cycles [1]	Parameters Defining Loads
Hard Braking	1-2 10-11	Takeoff	20,000	Vertical Reaction = Weight Drag Reaction = 0.8 Vertical Reaction
		Landing	20,000	
Medium Braking	3-4 12-13	Takeoff	50,000	Vertical Reaction = Weight Drag Reaction = 0.4 Vertical Reaction
		Landing	50,000	
Turning	5-6-7 14-15-16	Takeoff	25,000	Vertical Reaction = Weight Side Reaction = 0.4 Vertical Reaction
		Landing	25,000	
Pivoting	8-9 17-18	Takeoff	500	Vertical Reaction = Weight Torque Based on Friction Coefficient = 0.4 Between Ground and Tire
		Landing	500	
Taxiing	19 20	Takeoff	123,000	Vertical Reactions Based on a PSD Analysis Where the Maximum Bump Heights were 1.0 in. and Maximum Dips Measured 1.2 in.
		Landing	29,000	

Landing Conditions				
	Condition	Sink Rate (ft/sec)	Number of Cycles	Additional Parameters Defining Loads
Landing	26	1	3,600	Landing Speeds Vary from 138 to 146 kts Landing Weights Vary from 26,000 to 36,000 lb
		2	5,800	
		3	5,200	
	25	4	3,100	
		5	1,560	
	24	6	520	
		7	160	
	23	8	30	
	22	9	20	
	21	10	10	

GP78-0753-110

Note:

[1] Number of cycles represent 20,000 takeoffs and landings. Loads criteria, and number of cycles of hard braking, medium braking, turning and pivoting are those specified by Mil. Spec A-008866A (USAF) "Airplane Strength and Rigidity Reliability Requirements, Repeated Loads, Fatigue," 21 January 1974. Taxiing criteria were separately specified.

TABLE 10
F-15 MAIN LANDING GEAR DESIGN FATIGUE SPECTRUM

Description	Weight	Condition	Gear Stroke Inches from Extended	V_S	V_G	V_{G_1}	V_{G_2}	D_G	D_{S_1}	D_{S_2}	S_{G_1}	S_{G_2}	S_{S_1}	S_{S_2}	T_G	W	Loading Diagram
Hard Braking	Takeoff	2	7.0	–	23,400	–	14,600	11,700	–	–	–	–	–	–	–	44,000	
		1	7.0	–	23,400	–	16,880	13,500	–	–	–	–	–	–	–	50,000	
	Landing	11	5.5	–	16,000	–	10,600	8,400	–	–	–	–	–	–	–	33,000	
		10	5.5	–	16,000	–	12,040	9,630	–	–	–	–	–	–	–	36,000	
Medium Braking	Takeoff	4	7.0	–	23,400	–	16,600	6,550	–	–	–	–	–	–	–	44,000	
		3	7.0	–	23,400	–	18,980	7,540	–	–	–	–	–	–	–	50,000	
	Landing	13	5.5	–	16,000	–	12,100	4,800	–	–	–	–	–	–	–	33,000	
		12	5.5	–	16,000	–	13,675	5,470	–	–	–	–	–	–	–	36,000	
Turning	Takeoff	6	7.0	–	23,400	31,015	7,130	–	–	–	12,405	−2,850	–	–	–	44,000	
		7	7.0	–	23,400	29,730	4,935	–	–	–	11,890	−1,975	–	–	–	40,000	
		5	7.0	–	23,400	35,305	8,050	–	–	–	14,120	−3,720	–	–	–	50,000	
	Landing	16	5.5	–	16,000	22,130	4,180	–	–	–	8,850	−1,675	–	–	–	29,000	
		15	5.5	–	16,000	24,515	4,500	–	–	–	9,805	−1,800	–	–	–	33,000	
		14	5.5	–	16,000	26,560	5,095	–	–	–	10,620	−2,040	–	–	–	36,000	
Pivoting	Takeoff	9	7.0	–	19,075	–	–	–	–	–	–	–	–	–	26,870	44,000	
		8	7.0	–	21,675	–	–	–	–	–	–	–	–	–	32,660	50,000	
	Landing	18	5.5	–	13,155	–	–	–	–	–	–	–	–	–	15,295	29,000	
		17	5.5	–	15,825	–	–	–	–	–	–	–	–	–	20,235	36,000	
Taxiing	Takeoff	19	6.5	–	20,000	29,000	16,000	–	–	–	–	–	–	–	–	46,000	
	Landing	20	4.4	–	12,700	18,200	10,700	–	–	–	–	–	–	–	–	28,000	
Landing		26a	4.8	19,500	–	–	–	–	3,100	−4,800	–	–	200	−1,500	–	36,000	
		26b	5.5	19,500	–	–	–	–	2,330	−3,600	–	–	200	−1,500	–	36,000	
		25a	4.8	21,500	–	–	–	–	4,800	−7,800	–	–	400	−2,500	–	26,000	
		25b	5.5	21,500	–	–	–	–	3,600	−5,850	–	–	400	−2,500	–	26,000	
		24a	4.8	27,500	–	–	–	–	7,500	−12,200	–	–	700	−4,000	–	26,000	
		24b	5.5	27,500	–	–	–	–	5,620	−9,100	–	–	700	−4,000	–	26,000	
		23a	4.8	32,500	–	–	–	–	9,500	−15,500	–	–	1,000	−5,000	–	26,000	
		23b	5.5	32,500	–	–	–	–	7,120	−11,600	–	–	1,000	−5,000	–	26,000	
		22a	4.8	38,500	–	–	–	–	12,200	−19,800	–	–	1,400	−6,200	–	26,000	
		22b	5.5	38,500	–	–	–	–	9,100	−14,800	–	–	1,400	−6,200	–	26,000	
		21a	4.8	46,000	–	–	–	–	15,500	−23,500	–	–	1,700	−7,500	–	26,000	
		21b	5.5	46,000	–	–	–	–	11,600	−19,150	–	–	1,700	−7,500	–	26,000	

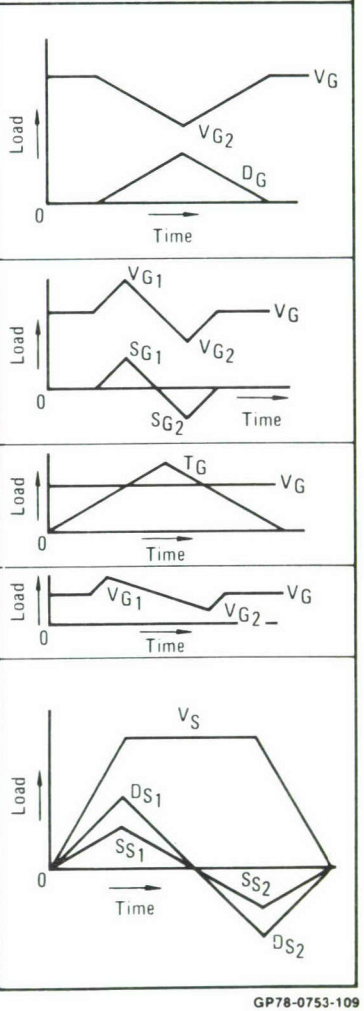

GP78-0753-109

Notes: 1. All loads are in pounds.
2. Landing gear tire rolling radii: Takeoff = 15.1 in., Landing = 15.65 in.

V = Vertical Load
S = Side Load
D = Drag Load
T = Torque

Subscripts: G = Ground Coordinate System
S = Strut Coordinate System
W = Aircraft Weight

TABLE 11
DESIGN LOADS AND STRESS SPECTRUM FOR OUTBOARD TRUNNION

Description	Weight	Condition	Resultant Trunnion Load (kips) Max/Min	Maximum Trunnion Stress (ksi) Max/Min	Percent of Spectrum Maximum Stress	Number of Cycles (1)
Hard Braking	Takeoff	2	34.58/25.46	157.33/74.24	63.5/29.9	8,800
		1	39.93/25.46	181.68/74.24	73.3/29.9	11,200
	Landing	11	25.68/17.41	117.96/50.80	47.5/20.5	8,800
		10	29.33/17.41	134.86/50.80	54.4/20.5	11,200
Medium Braking	Takeoff	4	27.93/25.61	114.79/74.24	46.2/29.9	28,000
		3	32.05/25.46	131.77/74.24	53.1/29.9	22,000
	Landing	13	20.81/17.41	86.63/50.80	35.0/20.5	28,000
		12	23.60/17.41	98.38/50.80	39.7/20.5	22,000
Turning (2)	Takeoff	6	15.83/−1.90	47.43/−9.73	19.1/−3.9	9,240
		7	10.98/−1.81	32.90/−9.34	13.3/−3.8	4,780
		5	19.30/−2.15	57.85/−11.05	23.4/−4.5	11,000
	Landing	16	9.50/−2.21	28.59/−10.19	11.5/−4.1	11,000
		15	10.23/−2.46	30.69/−11.29	12.4/−4.5	3,000
		14	11.59/−2.65	34.82/−12.18	14.1/−4.9	11,000
Pivoting (3)	Takeoff	9	20.75/20.69	65.01/60.47	26.2/24.4	280
		8	23.58/23.51	74.28/68.75	30.0/27.7	220
	Landing	18	14.33/14.31	44.43/41.73	17.9/16.8	220
		17	17.23/17.22	53.78/50.20	21.7/20.3	280
Taxiing	Takeoff	19	31.55/17.41	92.00/50.80	37.1/20.5	122,604
	Landing	20	19.91/11.71	58.07/34.14	23.5/13.8	29.180
Landing		26	24.36/0.0	86.74/0.0	35.0/0.0	14,600
		25	27.94/0.0	103.14/0.0	41.6/0.0	4,660
		24	36.80/0.0	139.21/0.0	56.2/0.0	680
		23	43.81/0.0	167.36/0.0	67.5/0.0	32
		22	52.46/0.0	202.77/0.0	81.8/0.0	20
		21	63.65/0.0	247.87/0.0	100.0/0.0	8

Notes:

GP78-0753-108

(1) Number of cycles represent 20,000 takeoffs and landings. (4 design life times)

(2) Pivoting conditions are subsequently deleted in the flight-by-flight stress history because they are infrequently applied, and the resulting stresses are comparatively small.

(3) See Table 12 for combined conditions and cycle counts used to develop the flight-by-flight history.

TABLE 12
STRESS SEQUENCE FOR OUTBOARD TRUNNION

Description	Condition	Weight-KIPS	Cycles per 20,000 Flights	Cycles per Flight
Flight 1				
Hard Braking at Take-off Weight	2	44	8,800	1
Medium Braking at Take-off Weight	4	44	28,000	3
Turning at Take-off Weight	6,7	44-40	11,630	1 (1)
Pivoting at Take-off Weight	9	44	280	0
Taxiing at Take-off Weight	19	46	61,302	6
Landing at Landing Weight	21,22,25	26	10,000	1 (2)
Taxiing at Landing Weight	20	28	14,590	1
Hard Braking at Landing Weight	11	33	8,800	1
Medium Braking at Landing Weight	13	33	28,000	3
Turning at Landing Weight	15,16	33-36	12,500	0 (3)
Pivoting at Landing Weight	18	29	220	0 (6)
Flight 2				
Hard Braking at Take-off Weight	1	50	11,200	1
Medium Braking at Take-off Weight	3	50	22,000	2
Turning at Take-off Weight	5,7	50-40	13,390	1 (4)
Pivoting at Take-off Weight	8	50	220	0
Taxiing at Take-off Weight	19	46	61,302	6
Landing at Landing Weight	26	36	10,000	1
Taxiing at Landing Weight	20	28	14,590	2
Hard Braking at Landing Weight	10	36	11,200	1
Medium Braking at Landing Weight	12	36	22,000	2
Turning at Landing Weight	14,15	36-33	12,500	2 (5)
Pivoting at Landing Weight	17	36	280	0 (6)

Notes:

(1) Cycles for condition 6 and half the cycles for condition 7 are combined, using loads for condition 6.

(2) Cycles for conditions 23 and 24 and 25 are combined, using loads for condition 25.

(3) Cycles for condition 16 and half the cycles for condition 15 are combined, using loads for condition 15.

(4) Cycles for condition 5 and half the cycles for condition 7 are combined, using loads for condition 5.

(5) Cycles for condition 14 and half the cycles for condition 15 are combined, using loads for condition 14.

(6) Pivoting loads have been removed because they are infrequently applied and the resulting trunnion loads are comparatively small, less than 30% of the maximum load.

7 Where conditions are combined, the loads for the more severe conditions are used, with the exception of conditions 23 and 24 which occur infrequently.

GP78-0753-97

stresses in the spectrum. The infrequently occurring conditions 23 and 24 were replaced by condition 25 to simplify the history; this had minimal effect on the spectrum because the hard braking conditions have similar stresses and occur much more frequently.

Flight 2 contains those conditions corresponding to higher aircraft weights and lower landing sink rates. Both flights were repeated in sequence throughout the stress history. The sequence of conditions in Table 12, though arbitrary, could be expected within a takeoff and landing.

A repeating block of two flights met the need for a simple flight-by-flight stress history to be used in test. The effect on crack growth caused by a repeating rather than random stress sequence was minimal, because a large number of blocks was employed in test.

The ground fatigue test of the F-15 gears used a block spectrum. A comparison of the computed stress exceedance of the outboard trunnion for the blocked design spectrum with the flight-by-flight spectrum presented in this report is shown in Figure 69. The occurrences of each condition are compared in Table 13. These comparisons show there are no significant differences in the stress exceedances between the two spectra.

4. TIMES FOR STRESS APPLICATION - The spectrum tests include simulation of the times of stress application as well as the value of stresses. Therefore, an evaluation of the times required to attain the landing gear loading conditions was performed. Load application times vary widely, especially during braking where the pilot dictates the duration of the load. The times for stress application computed herein are the maximum possible times for each braking condition. Two stress-time histories were created - one having the greatest possible duration of stress application, the other having the same stress levels applied as quickly as possible without sustained loads. The time estimates are design estimates and not based on actual measurements on field hardware.

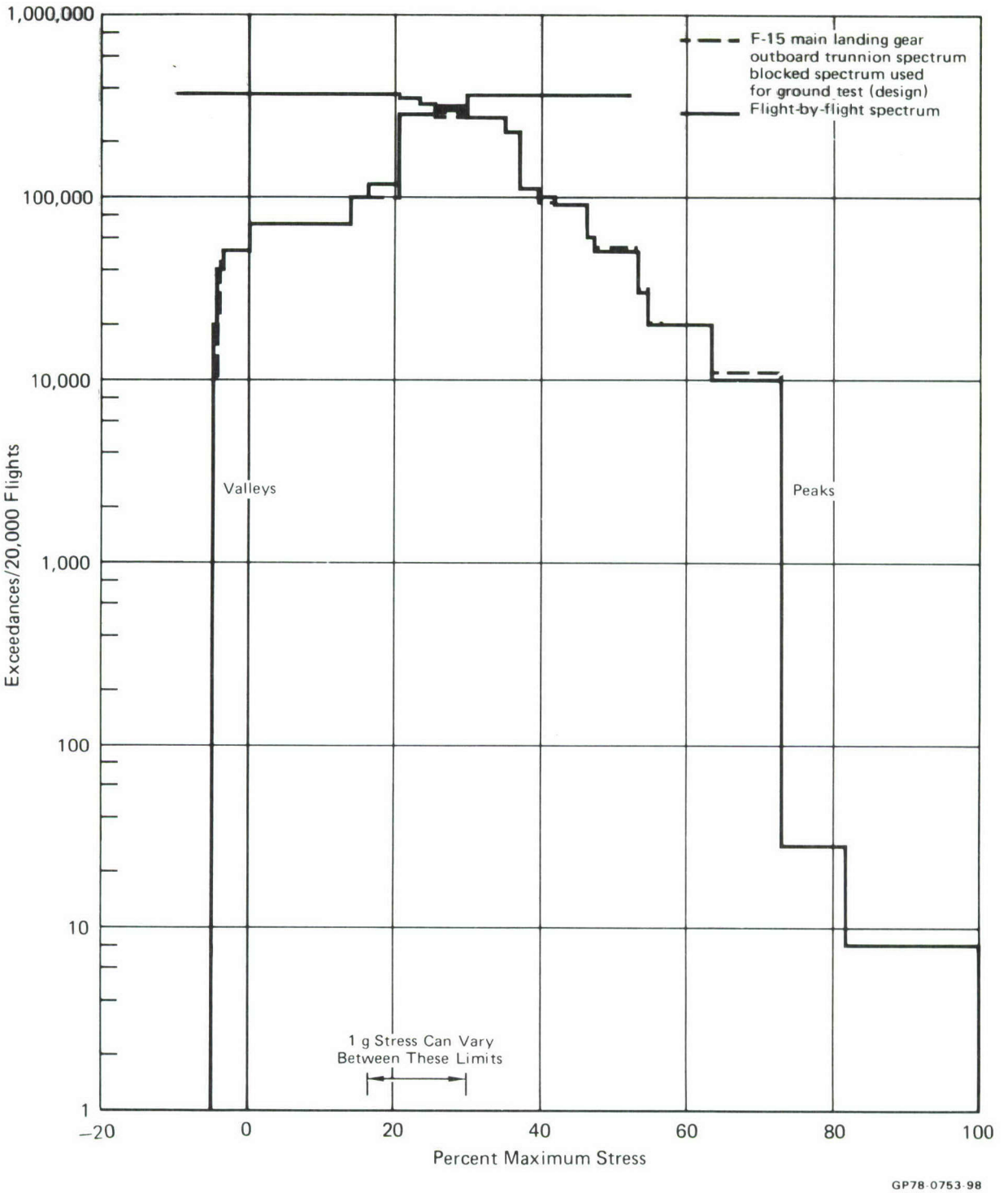

FIGURE 69
COMPARISON OF DESIGN AND FLIGHT-BY-FLIGHT STRESS SPECTRA

TABLE 13
COMPARISON OF DESIGN AND FLIGHT-BY-FLIGHT STRESS SPECTRA

F-15 Main Landing Gear Outboard Trunnion Spectra
20,000 Takeoffs and Landings

Description	Condition	Percent of Spectrum Maximum Stress	(1) Design Number of Cycles	(2) Flight-by-Flight Number of Cycles
Hard Braking	2	63.5/29.9	8,800	10,000
	1	73.3/29.9	11,200	10,000
	11	47.5/20.5	8,800	10,000
	10	54.4/20.5	11,200	10,000
Medium Braking	4	46.2/29.9	28,000	30,000
	3	53.1/29.9	22,000	20,000
	13	35.0/20.5	28,000	30,000
	12	39.7/20.5	22,000	20,000
Turning	6	19.1/−3.9	9,240	10,000
	7	13.3/−3.8	4,780	0
	5	23.4/−4.5	11,000	10,000
	16	11.5/−4.1	11,000	0
	15	12.4/−4.5	3,000	10,000
	14	14.1/−4.9	11,000	20,000
Pivoting	9	26.2/24.4	280	0
	8	30.0/27.7	220	0
	18	17.9/16.8	220	0
	17	21.7/20.3	280	0
Taxiing	19	37.1/20.5	122,604	120,000
	20	23.5/13.8	29,180	30,000
Landing	26	35.0/0.0	14,600	10,000
	25	41.6/0.0	4,660	9,972
	24	56.2/0.0	680	0
	23	67.5/0.0	32	0
	22	81.8/0.0	20	20
	21	100.0/0.0	8	8

GP78-0753-75

Notes:

(1) Blocked spectrum used for verification ground test (design)

(2) Flight-by-flight spectrum

a. Hard and Medium Braking - Braking times can vary from very short pulses to the time required to stop the aircraft during a high speed landing or a rejected takeoff. The effect of aerodynamic drag is small in comparison to braking forces and the deceleration was computed as:

$$\ddot{x} = \frac{2\mu V_G}{W} g$$

where x = distance
μ = coefficient of friction between tire and ground
V_G = main gear vertical load
g = acceleration constant
W = aircraft weight

The total main gear load is

$$2V_G = 0.86W$$

Hence $\ddot{x} = 0.86\mu g$

$$t = \frac{v}{\ddot{x}} = \frac{v}{0.86\mu g}$$

where v = initial velocity
t = time to stop
μ = 0.80 for hard braking
= 0.40 for medium braking

The velocity for a landing touchdown is:

$$v = 66.5 + .00205\ W, \text{ Kts.}$$

$$v = 66.5 + .00205 \frac{2V_G}{0.86} = 66.5 + 0.00477\ V_G$$

The resulting times for the braking conditions are summarized in Table 14. The time to apply and release the brakes were estimated to be one second.

b. Turning - Turning loads were based on a side load factor, n_y, equal to 0.40, and nose gear lateral forces for a coefficient of friction, μ, equal to 0.40. The turning torque acting on the aircraft due to nose gear force, is:

$$T = \mu V_{G-N} L$$

TABLE 14
BRAKING CONDITIONS DECELERATION TIMES

Description	Condition	V_G Pounds	ν Kts	μ	t Sec
Hard Braking at Take-off Weight	1	23,400	178	0.8	13.6
Hard Braking at Take-off Weight	2	23,400	178	0.8	13.6
Medium Braking at Take-off Weight	3	23,400	178	0.4	27.2
Medium Braking at Take-off Weight	4	23,400	178	0.4	27.2
Hard Braking at Landing Weight	10	16,000	143	0.8	10.9
Hard Braking at Landing Weight	11	16,000	143	0.8	10.9
Medium Braking at Landing Weight	12	16,000	143	0.4	21.8
Medium Braking at Landing Weight	13	16,000	143	0.4	21.8

GP78-0753-99

where μ = coefficient of friction

V_{G-N} = nose gear veritical load

L = distance

and $V_{G-N} = 0.14 \times W$

where W = aircraft weight

$T = 0.40 \times 0.14\ W \times 17.42 = 0.976xW$, ft-lb

The rotational acceleration of the aircraft is

$$\dot{\omega} = T/I$$

where ω = yaw rotation rate

I = moment of inertia

and $I = \frac{W}{g} \rho^2$

$\rho = 12.45$ ft

$$\dot{\omega} = \frac{0.976W \times 32.2}{W \times 12.45^2} = 0.203 \text{ rad/sec}^2$$

The relationships of velocities and accelerations are

$v = R\omega$

$a = R\omega^2$ hence $\omega = a/v$

where v = velocity

R = turning radius

The velocity was assumed to be 50 knots, 84.4 ft/sec

$$\omega = \frac{0.4 \times 32.2}{84.4} = 0.1526 \text{ rad/sec}$$

The time required to attain this angular rate was determined by:

$$\omega = t\dot{\omega} = t \times 0.203 \text{ rad/sec}^2$$

hence $t = \omega/\dot{\omega} = \frac{0.1526}{0.203} = 0.75$ seconds

The load factor history assumed a right turn followed by a left turn. All turning conditions were defined as follows:

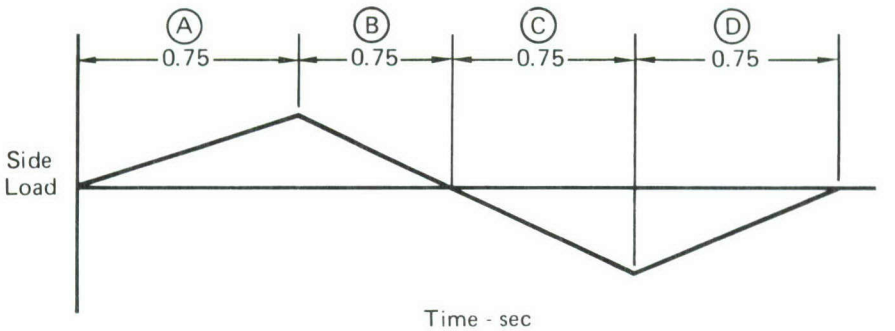

Ⓐ = time to initiate right turn
Ⓑ = time to recover from right turn
Ⓒ = time to initiate left turn
Ⓓ = time to recover from left turn

GP78-0753-104

c. Taxiing - Taxiing loads were derived from taxies, take-offs and landings on runways with specified roughness. Speeds varied from 30 knots for taxi, to lift-off speeds for take-off. Analysis of load-time records indicated that larger loads (condition 19) occur at a frequency of 1.25 cycles per second and the smaller loads (condition 20) occur at a frequency 2.5 cycles per second.

d. Landing - Summarized below are times for landing cycles, obtained from drop tests. As shown in the table, and in the following sketch, the time to reach the peak vertical load is significantly greater than the time over which side and drag loads occur.

Landing Sink Rate	Period of Drag Load	Time to Peak Vertical Load (1)
Ft/sec.	Sec.	Sec.
6	0.066	0.20
8	0.066	0.15
10	0.066	0.15
12	0.066	0.15

(1) Time to end of gear stroke.

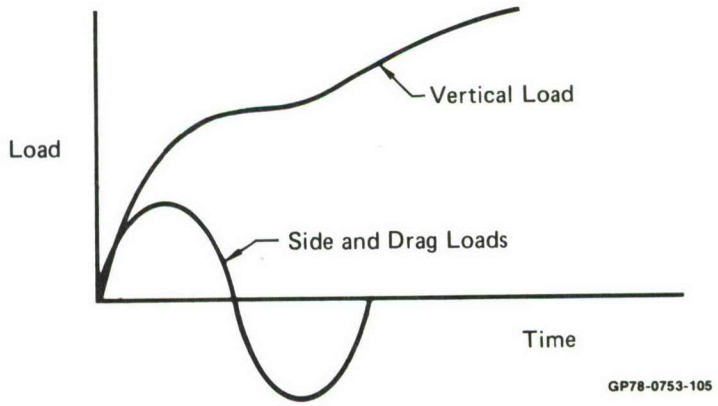

An average of the drag and vertical load times was used as the period for all landing loads, $\frac{0.066 + 0.15}{2} \approx 0.11$ sec. The assumed time profile is depicted below. This procedure conservatively superimposed the maximum vertical load on

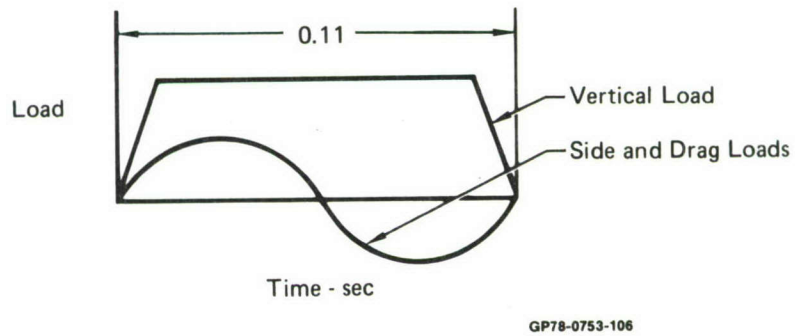

the maximum side and drag loads, and is the procedure that was employed in the ground test verification of the F-15 landing gears.

5. CYCLE-BY-CYCLE STRESS SPECTRA - Table 11 summarizes the stresses, and Table 12 summarizes the sequence of stresses used in this program. The stress history for each condition in Table 13 is described by a series of four stresses:

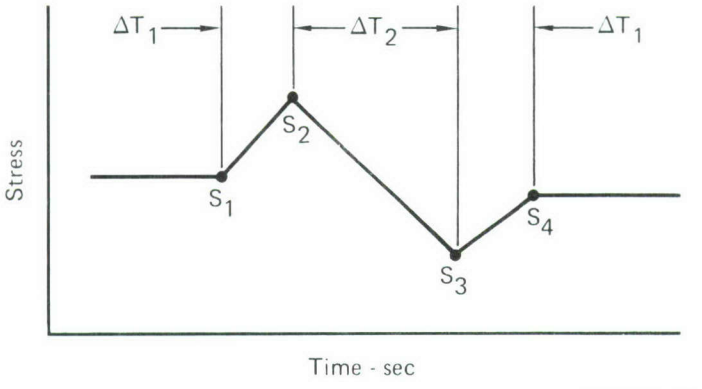

GP78-0753-107

The stresses S_2 and S_3 represent the maximum and minimum in the history for a cycle and S_1 and S_4 represent the sustained stress levels before and after the cyclic stress applications. The times represented by ΔT_1 and ΔT_2 for each condition were described in Paragraph 3.

The data from Tables 11 and 12 were combined to develop the cycle-by-cycle stress spectra. The results are presented in Table 15 and shown in Figures 70 and 71. Stresses numbered 1 through 144 represent the stresses for two take-offs and landings. The majority of landing loads presented in Table 3 had the same magnitude, defined by condition 26. The infrequently occurring conditions, 21 and 22, were periodically introduced. Their application in the test spectra was important because they represent the maximum stresses in the spectra. Infrequently occurring landing conditions, 23 and 24, were replaced in the cycle-by-cycle stress definition with condition 25. This simplified the final stress definition, and had minimal impact on the spectra because braking conditions 1 through 4 and 10 and 11 have similar magnitudes, and occur much more frequently. A sustained 1g stress was arbitrarily added, in equal time intervals of 0.33 seconds between conditions.

TABLE 15
CYCLE-BY-CYCLE SPECTRA

Stress Number	Delta Time	Percent of Maximum Stress	Condition	Description
1 (1)	0.33	29.9	2	Take-off Flight 1
2	1.00	63.5	2	Hard
3	13.60	63.5	2	Braking
4	1.00	29.9	2	↓
5	0.33	29.9	4	Medium
6	1.00	46.2	4	Braking
7	27.20	46.2	4	↓
8	1.00	29.9	4	
9	0.33	29.9	4	
10	1.00	46.2	4	
11	27.20	46.2	4	
12	1.00	29.9	4	
13	0.33	29.9	4	
14	1.00	46.2	4	
15	27.20	46.2	4	
16	1.00	29.9	4	↓
17	0.33	29.5	6	Turning
18	0.75	19.1	6	↓
19	1.50	−3.9	6	
20	0.75	29.5	6	↓
21	0.33	25.6	19	Taxiing
22	0.20	37.1	19	↓
23	0.40	20.5	19	
24	0.20	25.6	19	
25	0.33	25.6	19	
26	0.20	37.1	19	
27	0.40	20.5	19	
28	0.20	25.6	19	
29	0.33	25.6	19	
30	0.20	37.1	19	
31	0.40	20.5	19	
32	0.20	25.6	19	
33	0.33	25.6	19	
34	0.20	37.1	19	
35	0.40	20.5	19	
36	0.20	25.6	19	
37	0.33	25.6	19	
38	0.20	37.1	19	
39	0.40	20.5	19	
40	0.20	25.6	19	
41	0.33	25.6	19	
42	0.20	37.1	19	
43	0.40	20.5	19	
44	0.20	25.6	19	
45	0.33	25.6	25	*Landing* (2)

GP78-0753-100

TABLE 15 (Continued)
CYCLE-BY-CYCLE STRESS SPECTRA

Stress Number	Delta Time	Percent of Maximum Stress	Condition	Description
46	0.03	0.0	25	Landing
47	0.05	41.6	25	
48	0.03	16.2	25	
49	0.33	16.2	20	Taxiing
50	0.10	23.5	20	
51	0.20	13.8	20	
52	0.10	16.2	20	
53	0.33	20.5	11	Hard-Braking
54	1.00	47.5	11	
55	10.90	47.5	11	
56	1.00	20.5	11	
57	0.33	20.5	13	Medium-Braking
58	1.00	35.0	13	
59	21.80	35.0	13	
60	1.00	20.5	13	
61	0.33	20.5	13	
62	1.00	35.0	13	
63	21.80	35.0	13	
64	1.00	20.5	13	
65	0.33	20.5	13	
66	1.00	35.0	13	
67	21.80	35.0	13	
68	1.00	20.5	13	
69	0.33	20.2	15	Turning
70	0.75	12.4	15	
71	1.50	−4.5	15	
72	0.75	20.2	15	Park
73	0.33	29.9	1	*Take-Off Flight 2*
74	1.00	73.0	1	Hard-Braking
75	13.60	73.0	1	
76	1.00	29.9	1	
77	0.33	29.9	3	Medium-Braking
78	1.00	53.1	3	
79	27.20	53.1	3	
80	1.00	29.9	3	
81	0.33	29.9	3	
82	1.00	53.1	3	
83	27.20	53.1	3	
84	1.00	29.9	3	
85	0.33	29.5	5	Turning
86	0.75	23.4	5	
87	1.50	−4.5	5	
88	0.75	29.5	5	
89	0.33	25.6	19	Taxiing
90	0.20	37.1	19	

GP78-0753-101

TABLE 15 (Continued)
CYCLE-BY-CYCLE STRESS SPECTRA

Stress Number	Delta Time	Percent of Maximum Stress	Condition	Description
91	0.40	20.5	19	Taxiing
92	0.20	25.6	19	
93	0.33	25.6	19	
94	0.20	37.1	19	
95	0.40	20.5	19	
96	0.20	25.6	19	
97	0.33	25.6	19	
98	0.20	37.1	19	
99	0.40	20.5	19	
100	0.20	25.6	19	
101	0.33	25.6	19	
102	0.20	37.1	19	
103	0.40	20.5	19	
104	0.20	25.6	19	
105	0.33	25.6	19	
106	0.20	37.1	19	
107	0.40	20.5	19	
108	0.20	25.6	19	
109	0.33	25.6	19	
110	0.20	37.1	19	
111	0.40	20.5	19	
112	0.20	25.6	19	
113	0.33	25.6	26	*Landing*
114	0.03	0.0	26	
115	0.05	35.0	26	
116	0.03	16.2	26	
117	0.33	16.2	20	Taxiing
118	0.10	23.5	20	
119	0.20	13.8	20	
120	0.10	16.2	20	
121	0.33	16.2	20	
122	0.10	23.5	20	
123	0.20	13.8	20	
124	0.10	16.2	20	
125	0.33	20.5	10	Hard-Braking
126	1.00	54.4	10	
127	10.90	54.4	10	
128	1.00	20.5	10	
129	0.33	20.5	12	Medium-Braking
130	1.00	39.7	12	
131	21.80	39.7	12	
132	1.00	20.5	12	
133	0.33	20.5	12	
134	1.00	39.7	12	
135	21.80	39.7	12	

GP78-0753-102

TABLE 15 (Concluded)
CYCLE-BY-CYCLE STRESS SPECTRA

Stress Number	Delta Time	Percent of Maximum Stress	Condition	Description
136	1.00	20.5	12	Medium Braking
137	0.33	20.5	14	Turning
138	0.75	20.2	14	↓
139	1.50	14.1	14	
140	0.75	−4.9	14	
141	0.33	20.2	14	
142	0.75	14.1	14	
143	1.50	−4.9	14	
144	0.75	20.2	14	Park
		Random Landing Conditions (2)		
145	0.41	25.6	21	Special Landing No. 1
146	0.03	0.0	21	↓
147	0.05	100.0	21	
148	0.03	16.2	21	
149	0.33	25.6	22	Special Landing No. 2
150	0.03	0.0	22	↓
151	0.05	81.8	22	
152	0.03	16.2	22	

Notes:

(1) Repeat stress numbers 1 thru 144 10,000 times to achieve 4 design lifetimes.

(2) Replace stresses 45 thru 48 with stresses 145 thru 148, respectively on the 1250th landing, on the 3750th, on the 6250th, and every 2500 landings thereafter. Replace stresses 45 thru 48 with stresses 149 thru 152 on the 500th landing, on the 1500th, on the 2500th, and every 1000 landings thereafter.

GP78-0753-103

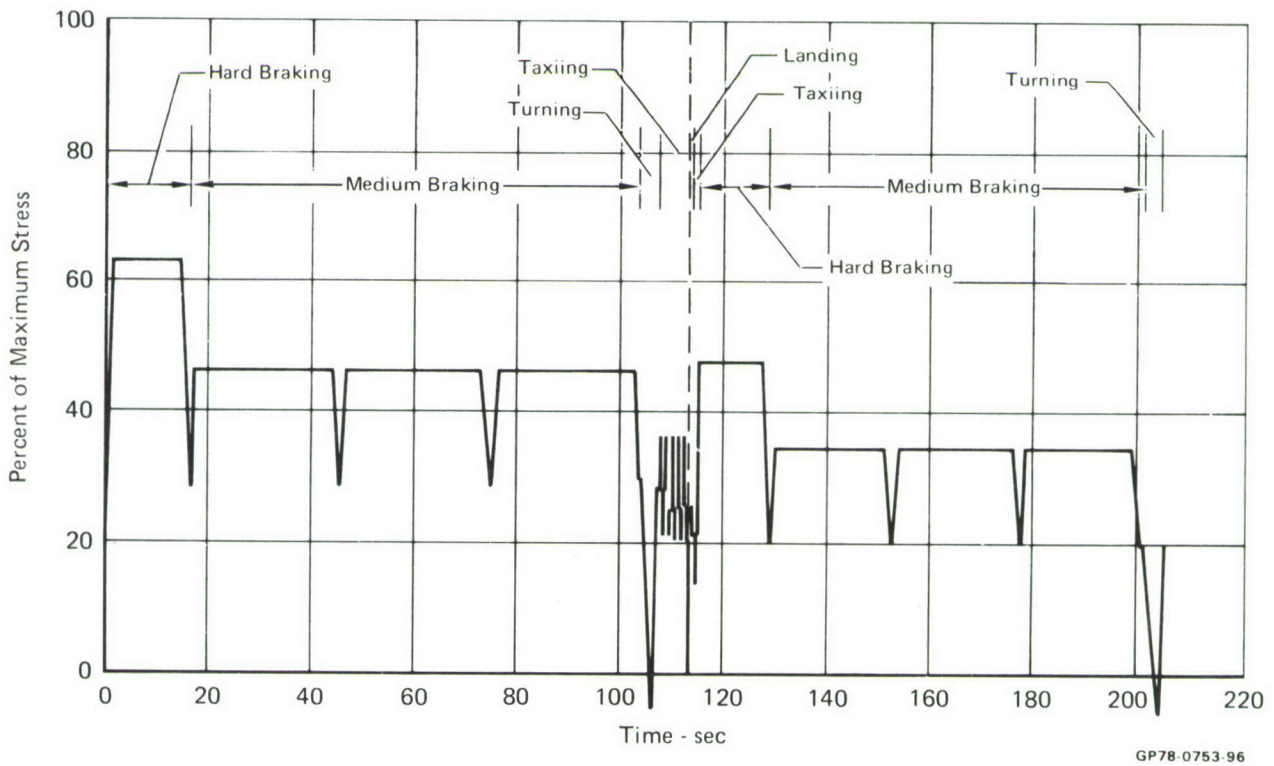

Figure 70
Stress-Time History for Flight 1

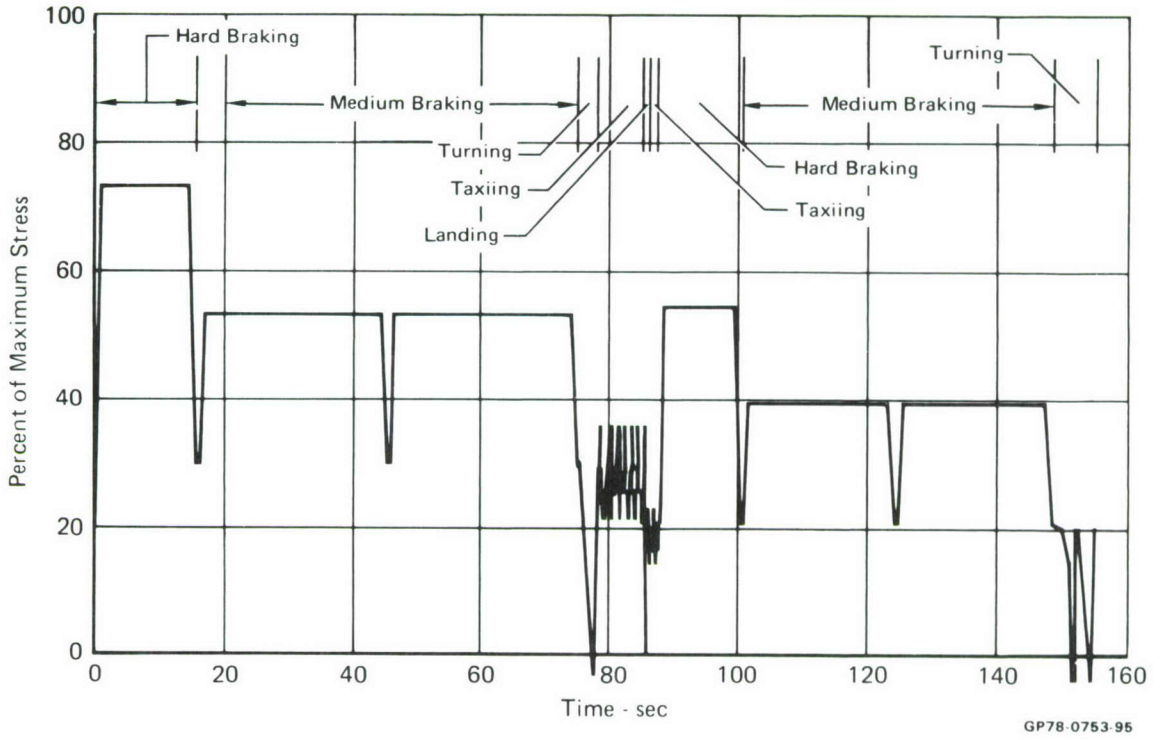

Figure 71
Stress-Time History for Flight 2

SECTION VI

VERIFICATION TEST PROGRAM

1. TEST PROGRAM SUMMARY - Table 16 summarizes the test plan. Three types of tests were performed in each of the four materials to obtain the data to validate the crack growth prediction algorithms. Each specimen had a single elliptic surface flaw, as shown in Figures 12 and 13.

TABLE 16
ALGORITHM VERIFICATION TEST PROGRAM SUMMARY

Specimen Number	Environment	Load Frequency cps	Objective
1	10% R.H. Air	~10	Evaluate crack growth in inert environment.
2	3.5% Salt Water	~10	Evaluate crack growth in agressive environment.
3	3.5% Salt Water	~0.1 (1)	Evaluate crack growth with sustained load in agressive environment.

Notes: (1) The time sequence of loads is defined in section 5.

GP78-0753-89

Test Type 1 - One test evaluating spectrum crack growth at a comparatively high load frequency (10 cps) in a dry air environment, permitting an assessment of the prediction algorithms with only the effects of overloads considered.

Test Type 2 - One test evaluating spectrum crack growth at a comparatively high load frequency (10 cps) in a 3.5% salt water environment, permitting an assessment of the predictive ability of the prediction algorithms, including environmental effects but minimizing sustained load effects.

Test Type 3 - One test evaluating spectrum crack growth with load hold times typical for fighter landing gear (0.1 cps) permitting an assessment of the predictive ability of the prediction algorithms with the effects of sustained load and aggressive environment maximized.

After completion of the initial series of 12 tests (3 test types for each of 4 materials) additional duplicate tests were performed.

2. TEST SPECIMENS AND TEST CONDITIONS

a. Test Specimens - The elliptic surface flaw specimens, Figures 72 and 73, were used for the testing. These specimens had configurations similar to those used in the Phase II alogrithm development test program. The reduced sections in the specimens were required in order to properly simulate the stresses experienced in landing gear components, and maintain load levels within the capacity of available fatigue test equipment. For all alloys, there was minimal specimen width effect on predicted critical flaw sizes, or on the predicted crack growth rates in developing those critical flaw sizes.

b. Initial Flaw Sizes - The target initial flaw geometries for steel alloys were of the size and shape that characterize cracks induced by grinding burns. For aluminum alloys, the target initial flaw geometries were of the size and shape that could originate from a corrosion pit. Table 1 summarizes the results of the survey of landing gear initial flaws - causes and geometries. The table shows that for steel, localized untempered martensite caused by grinding burns results in an initial flaw 0.008 inches deep by 0.100 inches long. For aluminum, a corrosion pit results in an initial flaw 0.010 inches deep by 0.020 inches long. The landing gear initial flaw survey is reported in Reference 1.

For surface cracks with lengths greater than twice the depth, the most significant dimension in controlling growth is depth. Consistent with the requirements of the program, initial depths of 0.008 inches in steel and 0.010 inches in aluminum were used as target values. The surface length was selected such that crack growth in depth was accompanied by growth on the surface. This enabled visual crack growth measurements to be made during the test, and eliminated

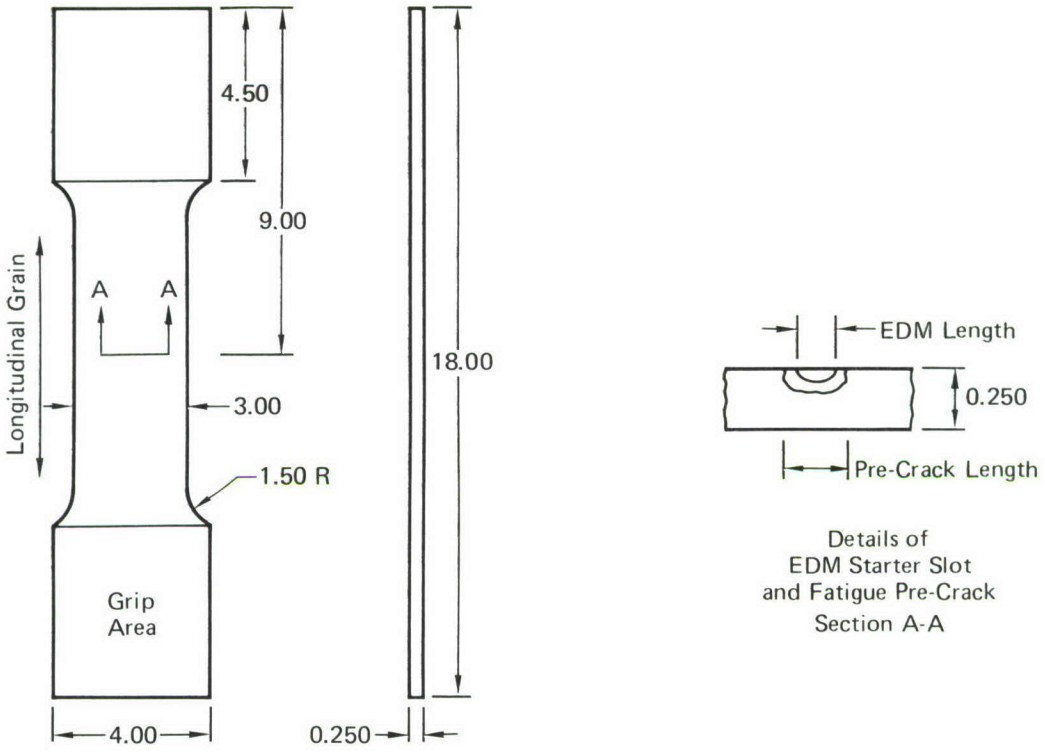

Figure 72
Elliptic Surface Flaw Specimen - Aluminum

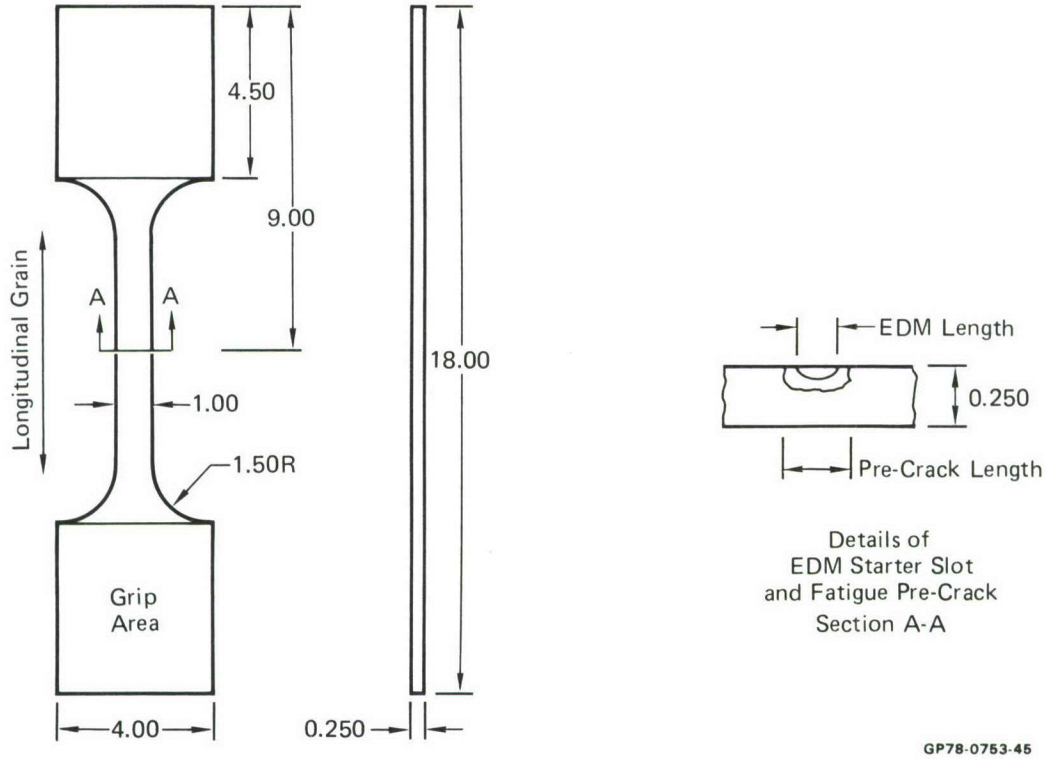

Figure 73
Elliptic Surface Flaw Specimen - Steel

dependence upon compliance or post-test fractographic measurements of crack growth. In order to enhance the probability of surface growth, the initial flaw geometries shown in Figure 74 were used as target values. Flaws with these aspect ratios have nearly equal stress intensities at the depth and surface, and simultaneous growth in both directions was expected.

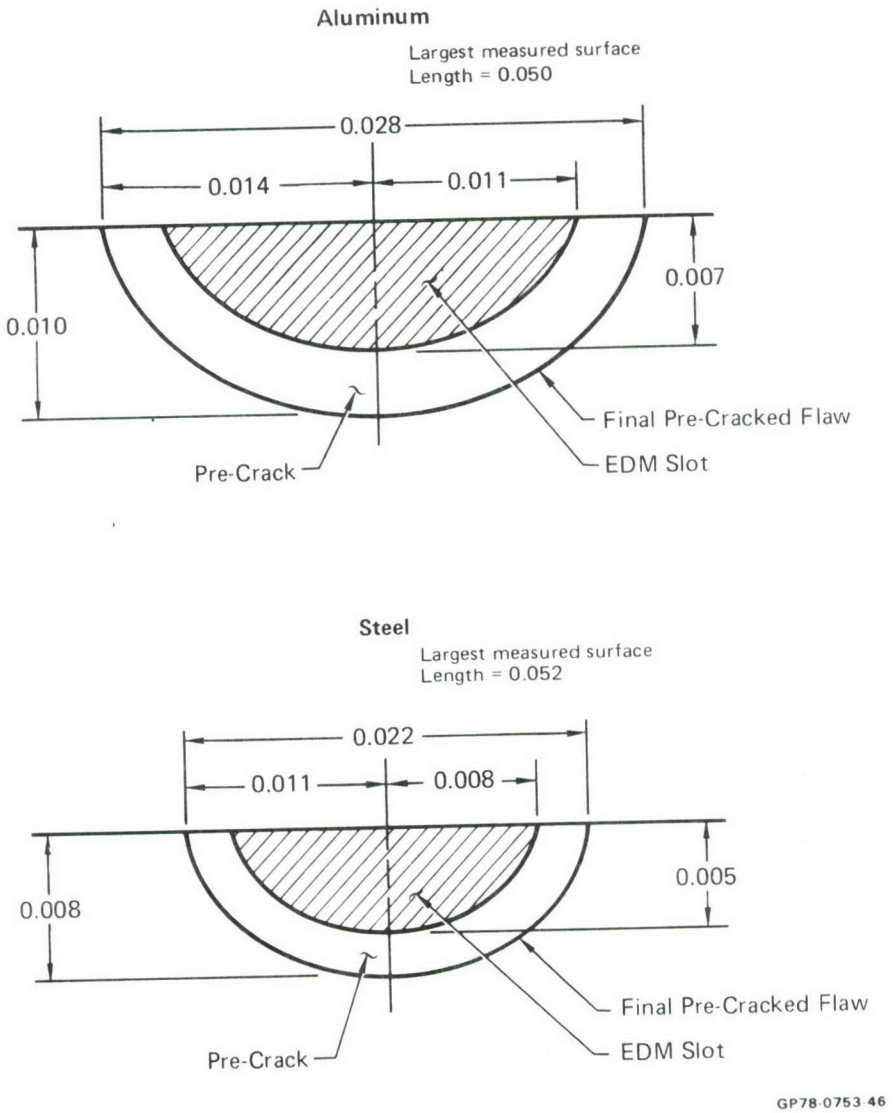

Figure 74
Development of Initial Flaws

c. Spectrum Stress Levels - The spectrum used in the testing is defined in Section V. The cycle-by-cycle stress history was derived for the outboard trunnion of the F-15 main landing gear system. In order to achieve the desired life (1,000 hours and 20,000 take-offs and landings), consistent stress levels had to be selected. The maximum spectrum stress level in the trunnion is 247 ksi, approximately 85% of the ultimate strength of the 300M material. This percentage is representative of the maximum stress level in a landing gear component. To permit direct comparison of crack growth rates, it is desirable to use the same maximum stress in both steel materials. However, 247 ksi is greater than the ultimate strength of the HP-9-4-.30 steel (220 ksi). Therefore 185 ksi, which is 85% of the ultimate strength of the HP-9-4-.30 steel, was selected as the maximum spectrum stress level for both steels.

The ultimate strengths of the two aluminum alloys investigated are similar (77 ksi and 71 ksi for 7075-T651 and 7049-T63, respectively). A maximum spectrum stress level of 60 ksi, which is 80% of the ultimate strength of the 7049-T73 alloy, was selected for both aluminums.

3. PRECRACKING PROCEDURES - An Electrical Discharge Machined (EDM) notch of size and shape expected to produce the desired initial flaw was introduced on the specimen surface. Specimens were then precracked to obtain the desired surface length. The target EDM and precrack sizes and shapes are indicated in Figure 74. The precracking stress levels were 30 ksi for aluminum, and 100 ksi for steel. The EDM slot was enlarged 0.006 by precracking, to obtain a sharp crack, regardless of EDM slot sizes. Difficulties in obtaining the desired EDM slot size resulted in larger than desired precrack sizes, as noted in Figure 74.

4. TEST PROCEDURES, CRACK GROWTH MONITORING, INSTRUMENTATION, AND ENVIRONMENTAL CONTROL - Cyclic testing was performed in a Materials Testing System (MTS) test system. The specimen was loaded through self-aligning hydraulic grips. The load spectrum application was controlled through a mini-computer; the time-sequence load spectrum was defined by the load levels and the time point at which each load was to be applied. A haversine wave shape was used between consecutive loads. Sustained load was defined by two consecutive loads of equal magnitude applied at the beginning and end of the sustained load period.

Specimens were clamped in the machine grips and Teflon roller guides installed against the specimen to prevent buckling during application of compression loads.

During the testing, surface crack lengths were optically monitored using a cathetometer with a 30X microscope. Crack growth measurement tests were made after every .01 inches of growth (approximately). After completion of the test, fractographic measurements of the crack surface were made.

The chamber used to contain environmental solutions is shown in Figure 5. This containment method was used for both the 3.5 percent NaCl in distilled water environment and the low humidity environment. Low humidity air was obtained by using silica jell dessicant to give <10% R.H. air.

5. TEST RESULTS - Table 17 summarizes the measured and predicted crack growth lives for each test condition. The crack growth lives shown in Table 17 are presented for growth to fracture from the largest initial flaw length in each material type. In steels this flaw length (2c) was 0.052 inches and in aluminum the flaw length was 0.050 inches. In two-thirds of the cases the predictions are within 30% of the test lives. The most noteworthy exceptions are the duplicate tests of 300M steel in salt water at both high and low frequencies. These results vary considerably from both predictions and the original test results. The spectrum predictions are discussed in Section VII.

TABLE 17
SUMMARY OF PREDICTED AND TEST LIVES FOR ELLIPTIC SURFACE FLAWS

Material	Test Type	Predicted Life Landings	Test Life Landings	Duplicate Test Life Landings
7049-T73	15 cps-dry	14,900	11,500	–
	15 cps-3.5% NaCl	2,630	3,900	–
	0.1 cps-3.5% NaCl	2,620	2,200	–
7075-T6	15 cps-dry	7,080	10,400	8,650
	15 cps-3.5% NaCl	2,600	3,200	–
	0.1 cps-3.5% NaCl	2,300	2,570	–
HP-9-4-.30	15 cps-dry	3,690	4,850	4,800
	15 cps-3.5% NaCl	3,770	4,310	–
	0.1 cps-3.5% NaCl	2,090	1,060	1,850
300M	15 cps-dry	1,440	1,240	1,680
	15 cps-3.5% NaCl	1,090	915	565
	0.1 cps-3.5% NaCl	5	16	104

Notes: 1. Lives for steels are presented for growth from 0.026 in. (c, half surface length) to fracture. Lives for aluminum are presented for growth from 0.025 in. to fracture.

GP78-0753-90

Comparisons of predicted and measured crack growth for each test condition are presented in Figures 75 through 86. In these figures the initial flaw length corresponds to the largest initial flaw for the particular test condition. One duplicate test was performed in 7075-T6 aluminum in a dry air environment as shown in Figure 78. In HP-9-4-.30 steel the duplicate test results are considerably closer to the predicted behavior than were the original results. In dry air the original test (Figure 81) crack growth appears to be retarded at small crack lengths, although from 0.026 inches to fracture the results are very close (Table 17). In salt water with sustained spectrum loadings the original test behavior is considerably different from that predicted or from that measured during the duplicate test. Fracture surfaces for the two specimens were compared but, other than showing a slightly shallower flaw for the original test specimen at fracture, the surfaces were too corroded to yield information about the behavior variations at small crack

lengths. In Figures 85 and 86 the variation in test results for 300M steel is evident and is discussed later. Agreement between the duplicate test data and prediction is very good.

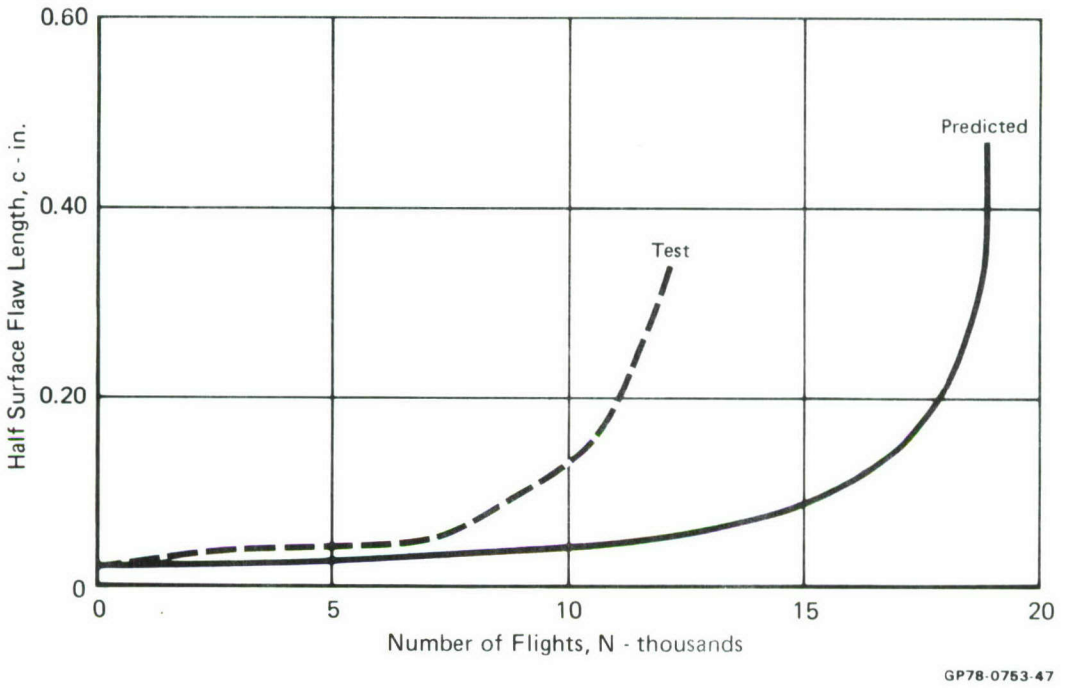

Figure 75
Surface Flaw Growth in 7049-T73 Aluminum in Dry Air - Spectrum Tested Without Sustained Loads

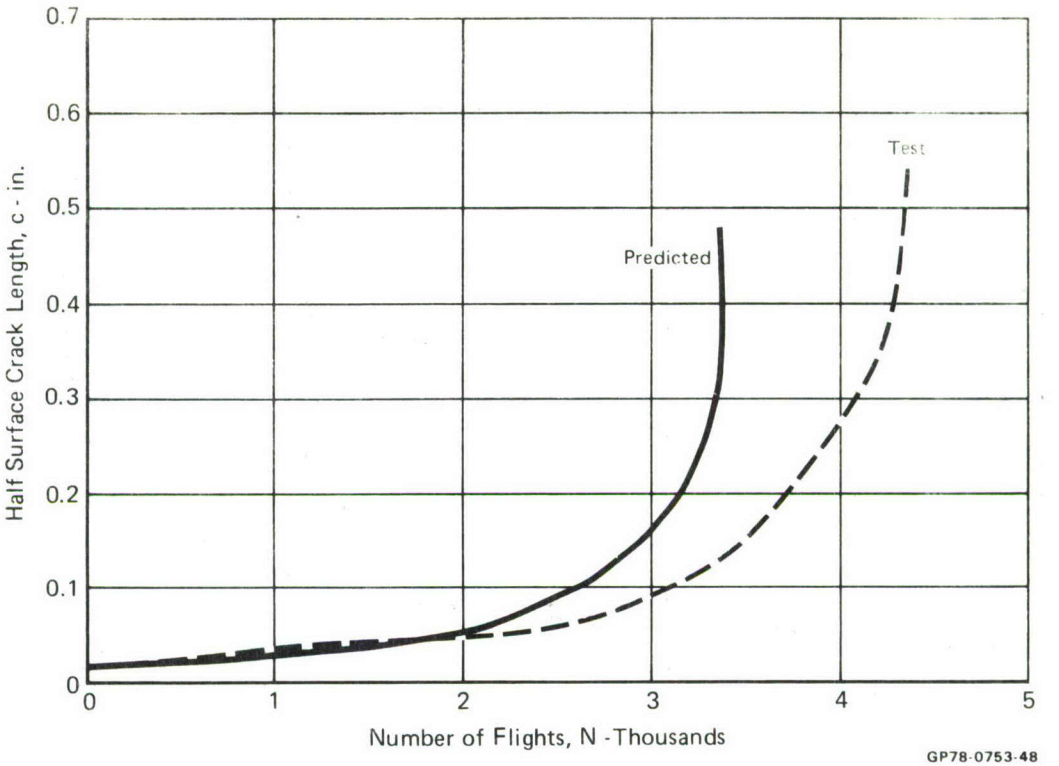

Figure 76
Surface Flaw Growth in 7049-T73 Aluminum
in Salt Water - Spectrum Tested without Sustained Loads

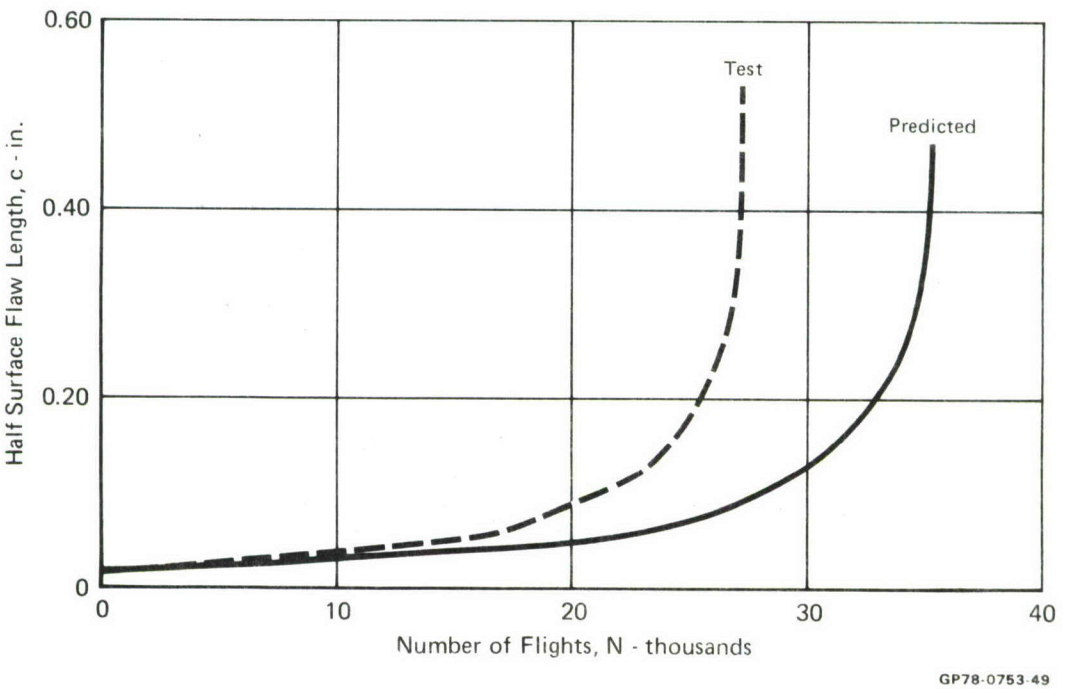

Figure 77
Surface Flaw Growth in 7049-T73 Aluminum
in Salt Water - Spectrum Tested Including Sustained Loads

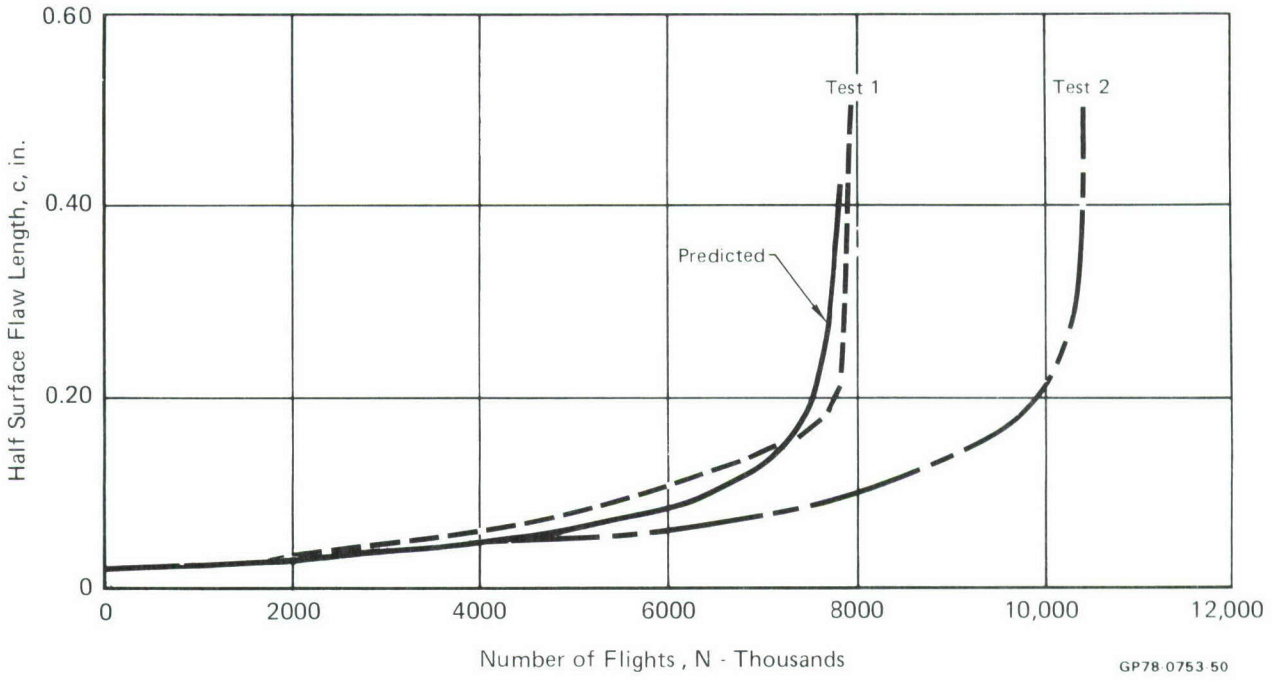

Figure 78
Surface Flaw Growth in 7075-T6 Aluminum
in Dry Air - Spectrum Tested Without Sustained Loads

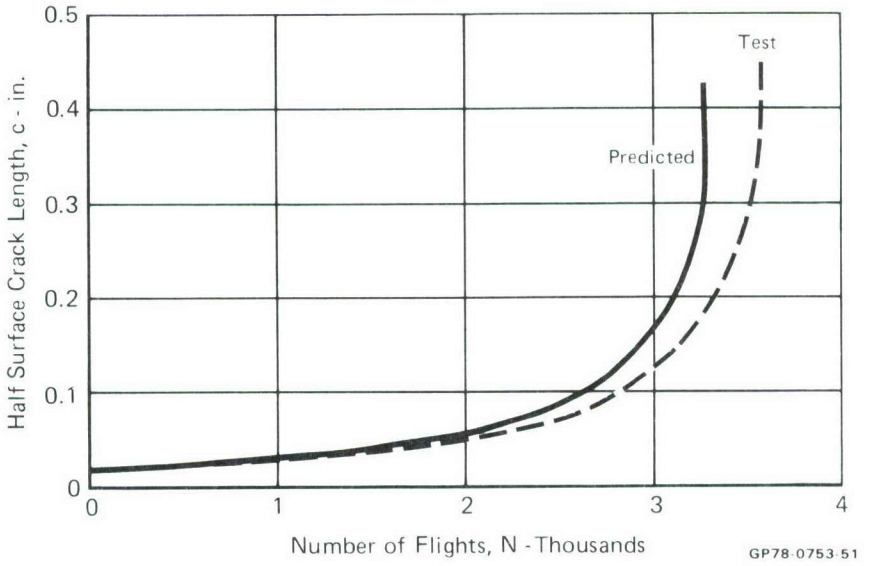

Figure 79
Surface Flaw Growth in 7075-T6 Aluminum
in Salt Water - Spectrum Tested without Sustained Loads

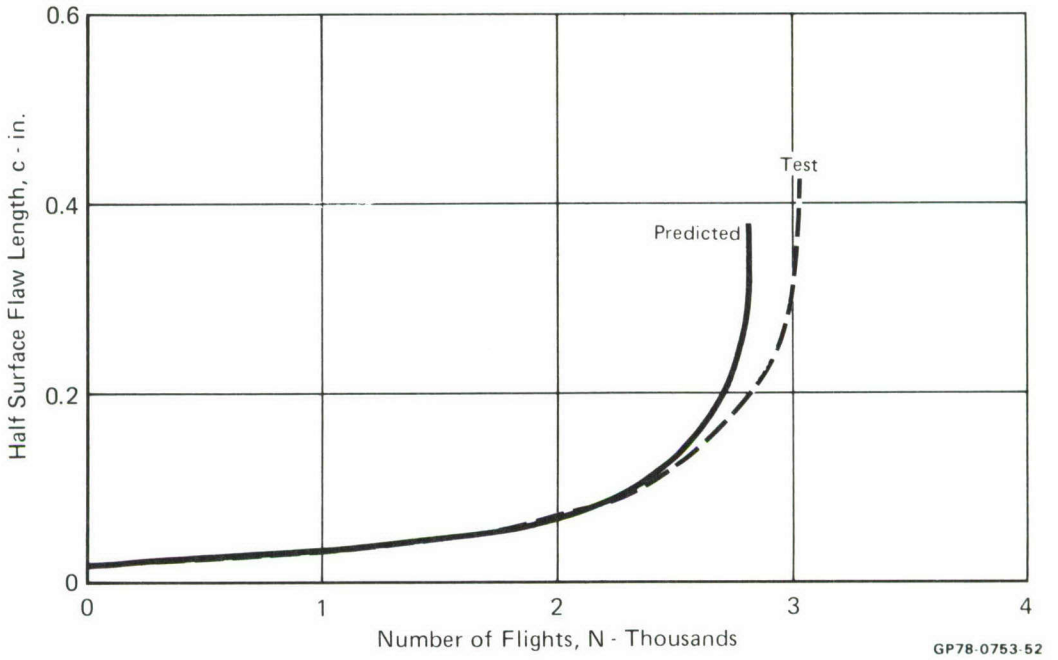

Figure 80
Surface Flaw Growth in 7075-T6 Aluminum
in Salt Water - Spectrum Tested Including Sustained Loads

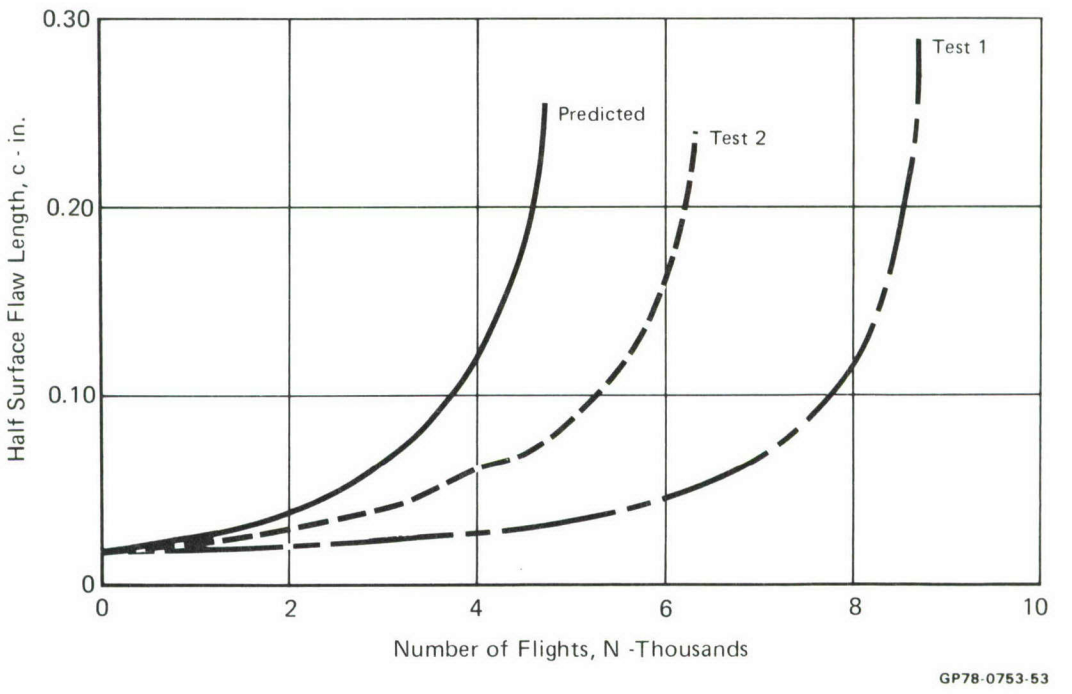

Figure 81
Surface Flaw Growth in HP-9-4-.30 Steel
in Dry Air - Spectrum Tested Without Sustained Loads

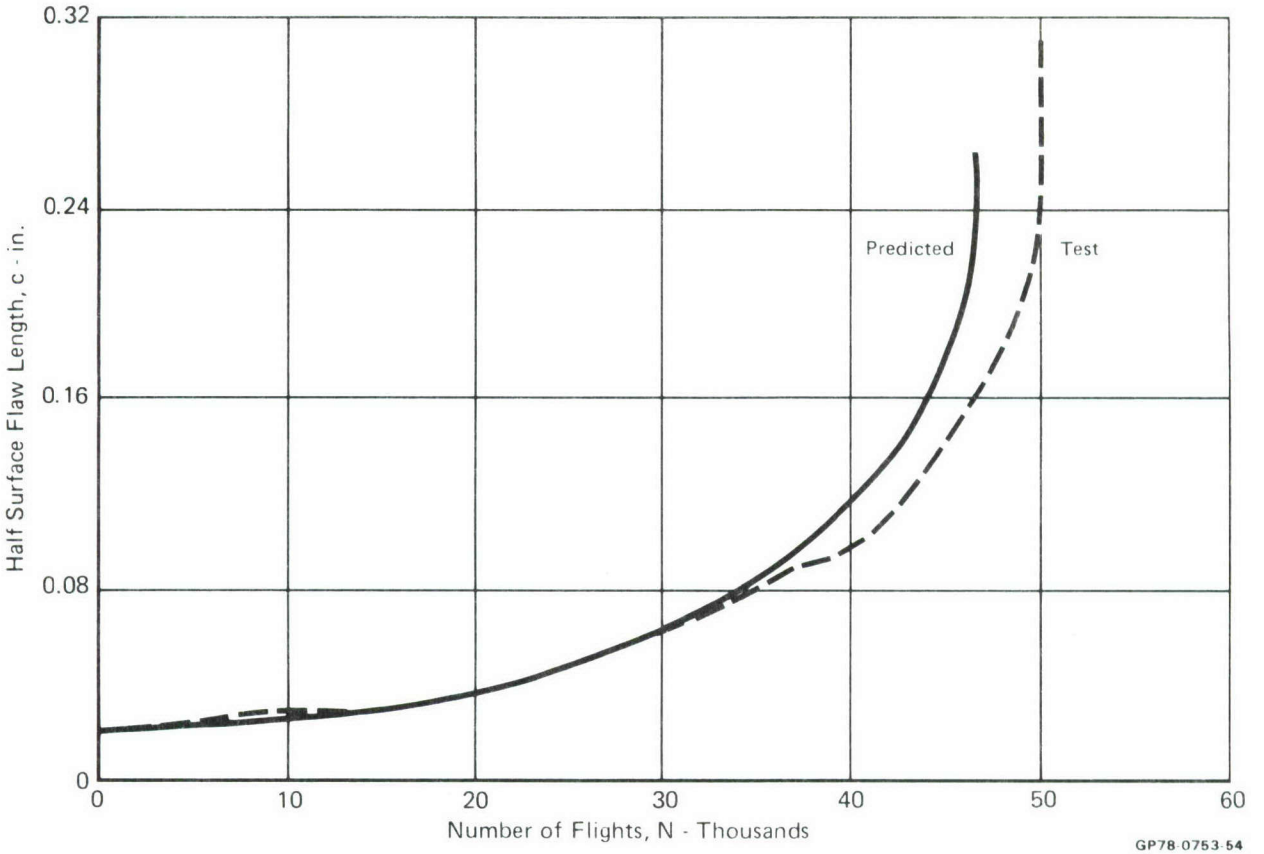

Figure 82
Surface Flaw Growth in HP-9-4-.30 Steel
in Salt Water - Spectrum Tested Without Sustained Loads

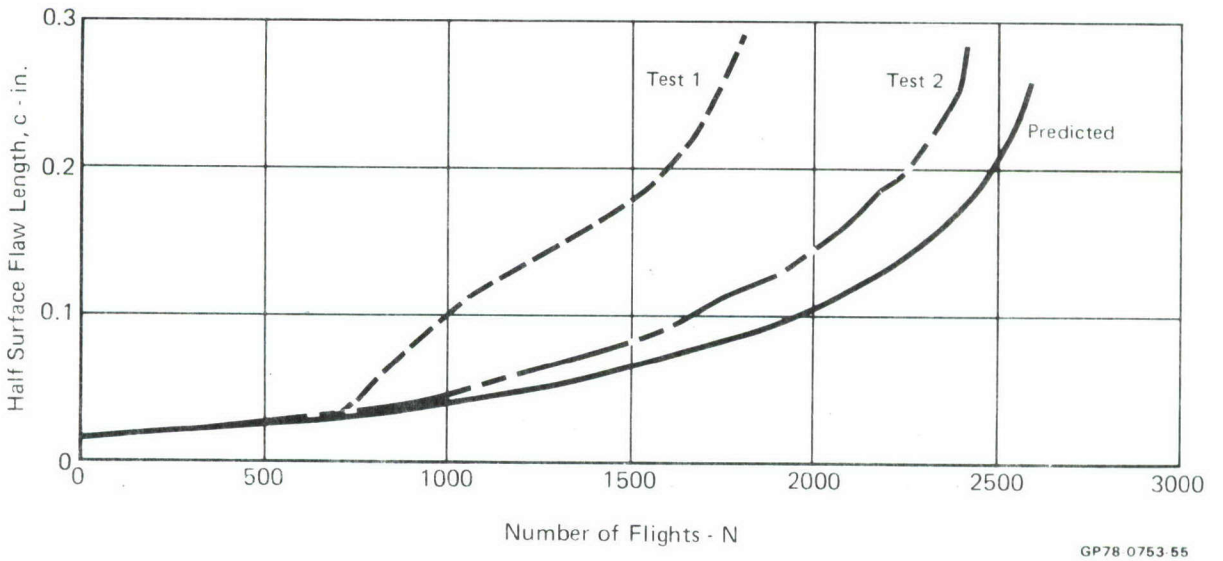

Figure 83
Surface Flaw Growth in HP-9-4-.30 Steel
in Salt Water - Spectrum Tested Including Sustained Loads

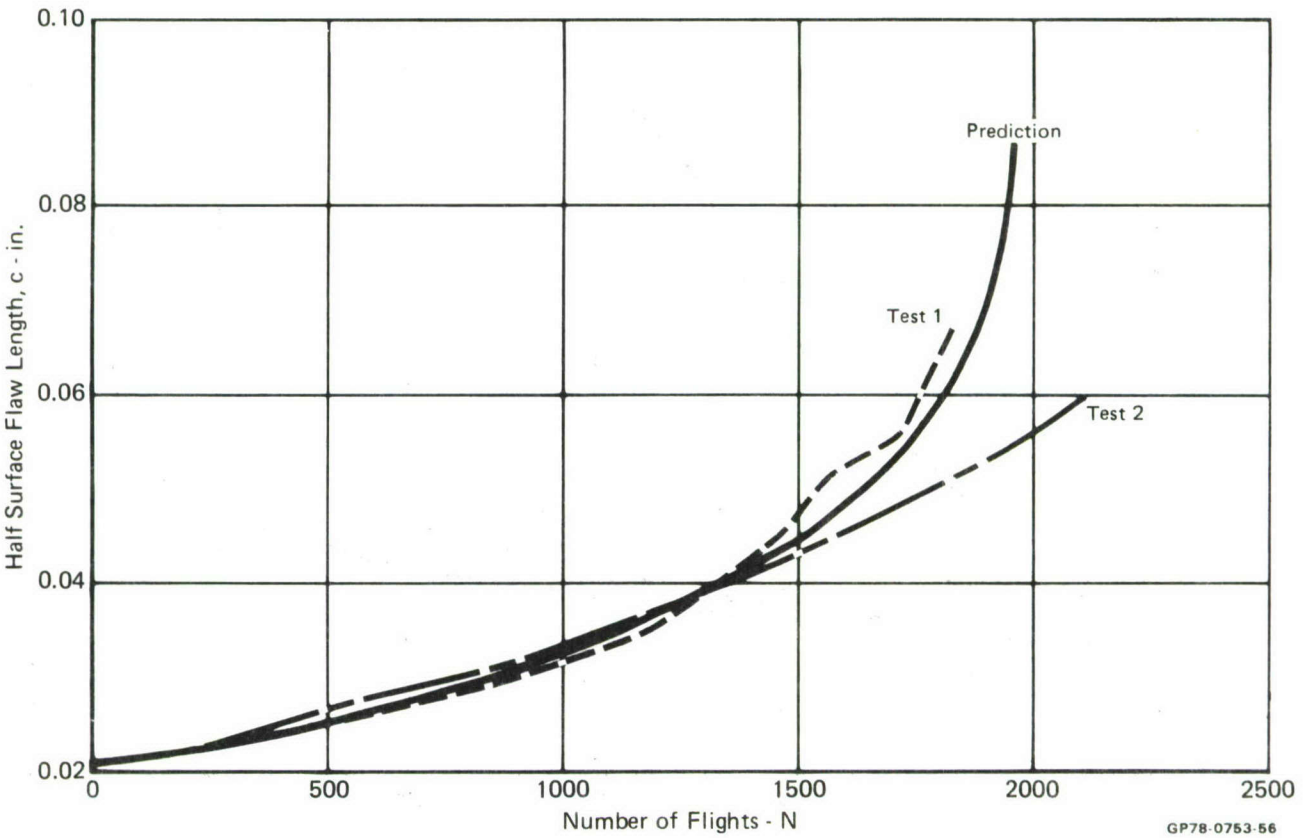

Figure 84
Surface Flaw Growth in 300M Steel
in Dry Air - Spectrum Tested Without Sustained Loads

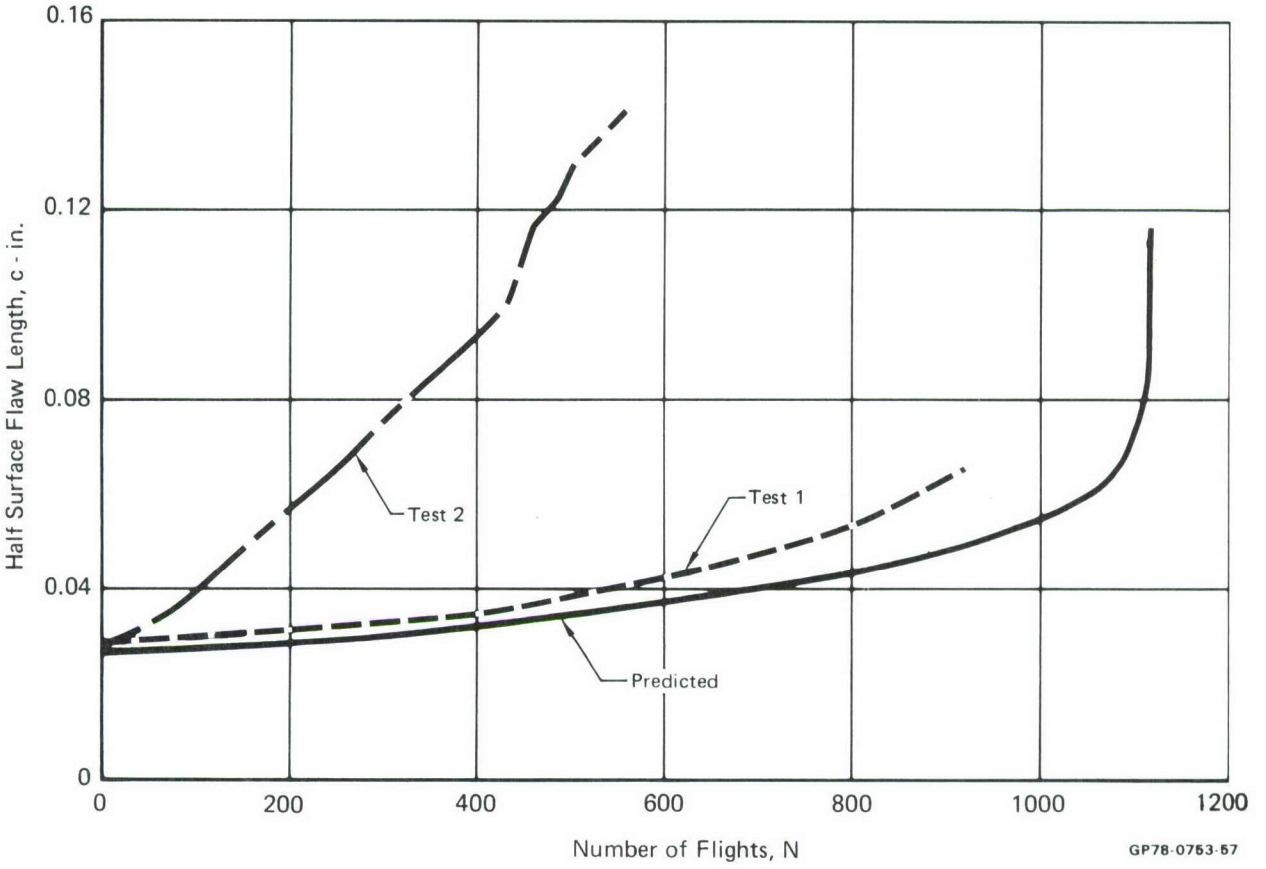

Figure 85
Surface Flaw Growth in 300M Steel
in Salt Water Spectrum Tested Without Sustained Loads

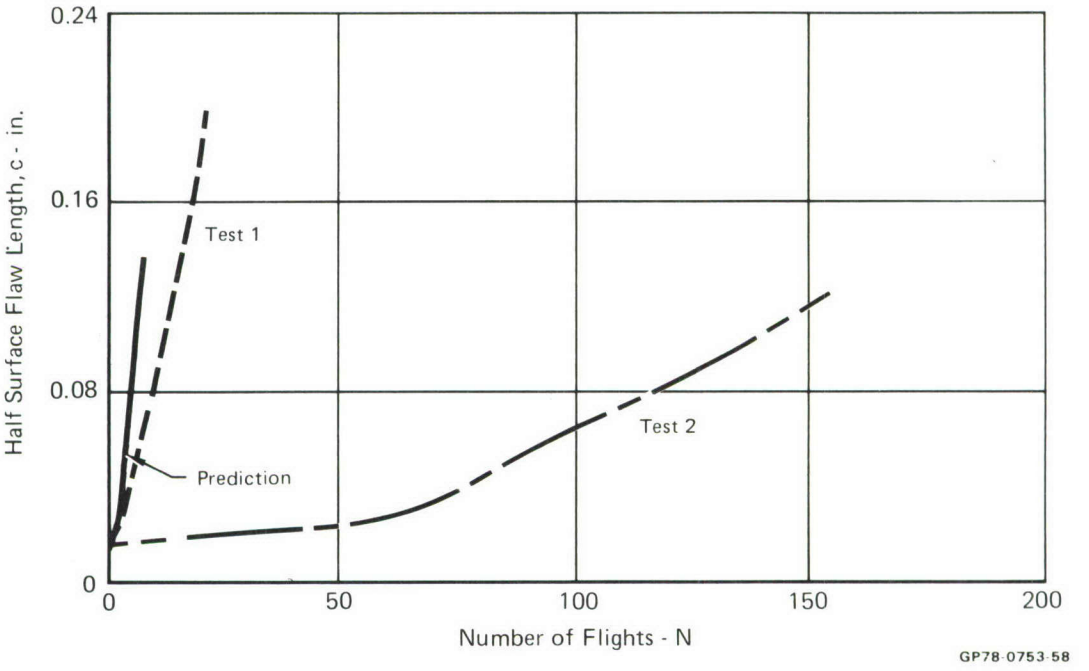

Figure 86
Surface Flaw Growth in 300M Steel in Dry Air - Spectrum Tested Including Sustained Loads

Because comparisons of crack growth were made from initial flaw sizes which were larger than those originally desired, they overlooked the long delay period found in certain 300M steel tests. At the beginning of several of these tests, no detectable crack growth occurred for several thousand take-offs and landings. Examples of this delay are shown in Figures 87 and 88. These figures show that considerable delay occurs following precracking before the crack abruptly begins to grow at a rate closer to that predicted. This delay occurred in both original tests in air and salt water when the specimens were spectrum tested without sustained loading. The delay did not occur in the original test which included sustained loading.

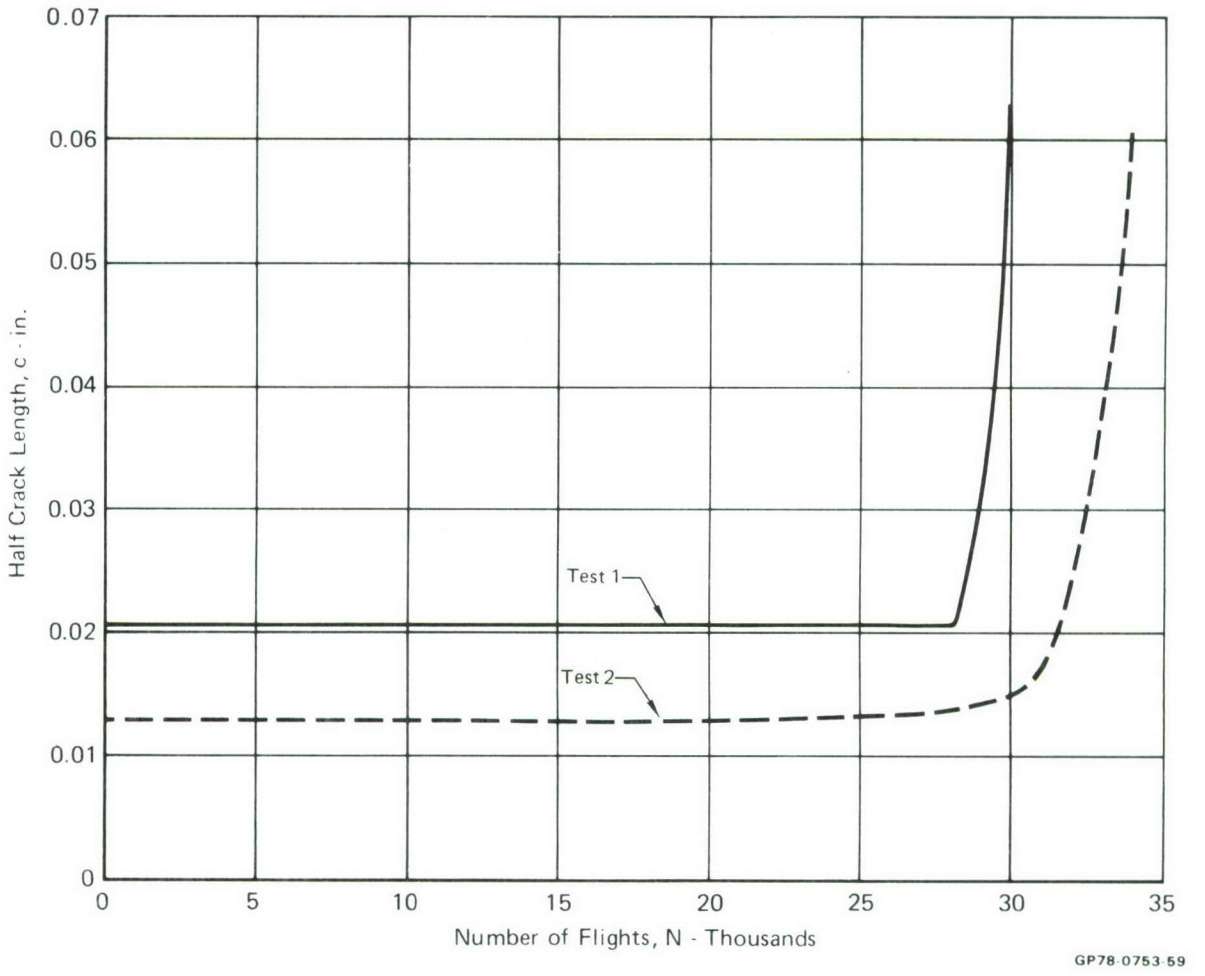

Figure 87
Surface Flaw Growth in 300M Steel in Dry Air -
Spectrum Tested Without Sustained Loads - Showing Delay Time

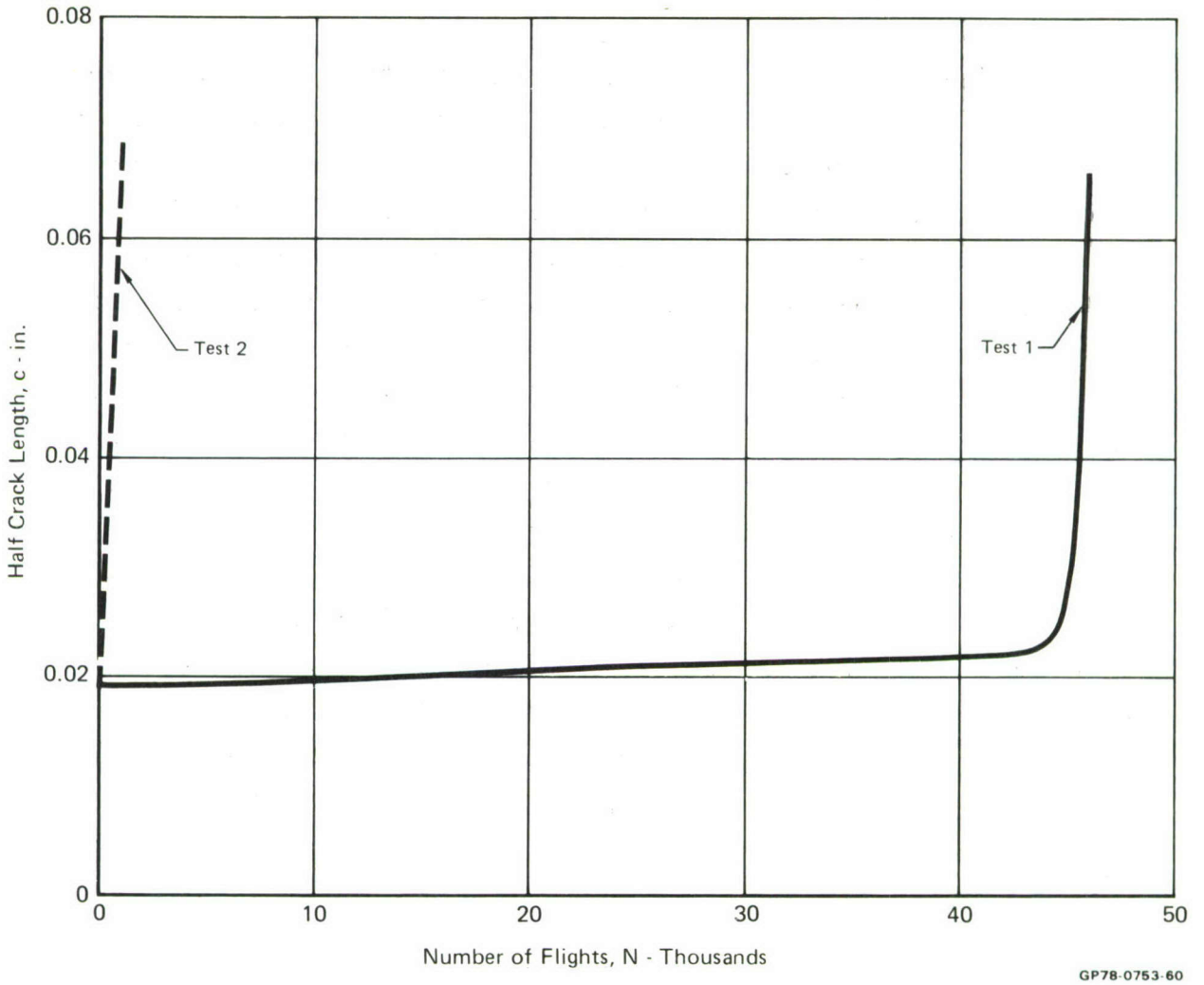

Figure 88
Surface Flaw Growth in 300M Steel in Salt Water
Spectrum Tested Without Surface Loads - Showing Delay Time

The duplicate tests of 300M, starting with small initial flaw sizes, show varying behavior. In dry air the duplicate test shows delay and subsequent growth which are very similar to the original test (Figures 84 and 87). In salt water, tested without sustained loads, the duplicate test did not show any delay but grew faster than either the predicted rate or that of the original test (Figures 85 and 88). The duplicate test with sustained loads did not show any

delay, however, the growth rate was significantly slower than that of the original test (Figure 86).

Studies of the fracture surfaces of the 300M specimens did not reveal the cause of delay or the variation in growth rates for these tests. Striations on the fracture surfaces due to high stress levels are difficult to distinguish in 300M. Indeed, because of its rapid corrosion in salt water it is unusual to find any identifiable markings other than those caused by fracture. A comparison of predicted and measured crack depth to surface half length (a/c) ratios at fracture is presented in Table 18. In those cases in which the fracture length dimensions could be determined, the crack shapes at fracture in the duplicate tests are closer to the predictions than are those in the original tests. However, the crack growth curves for the original tests are much closer to the predicted curves than are the growth rates for the duplicate tests. Based on the data presented in Table 18 and Figures 87 and 88, there appears to be no correlation between crack aspect ratio at fracture and crack growth rate in this test series.

TABLE 18
FLAW ASPECT RATIO OF 300M STEEL SPECIMENS AT FRACTURE

Environment	Frequency cps	Test Number	Predicted a/c	Measured a/c
Air	~10	1	0.857	1.570
		2	0.857	0.991
Salt Water	~10	1	0.867	1.420
		2	0.867	(1)
Salt Water	~0.1	1	0.867	0.239
		2	0.867	0.956

Note: (1) Crack dimensions at fracture could not be determined from the fracture surface.

GP78-0753-91

The specimens fabricated for the duplicate tests had EDM slot sizes much closer to those originally desired (about 0.016 inches in length rather than the 0.028 inches in the original specimens). All the flaws were precracked 0.006 inches under constant amplitude loading at 100 ksi prior to spectrum fatigue testing (maximum spectrum loading is 185 ksi, 135 ksi is applied once per flight). However, since all EDM slot sizes for the duplicate test specimens were about the same size, this does not explain the variation in crack growth rates obtained.

The delay in some 300M steel tests, and perhaps the variation in growth rates in that test series may have been caused by insufficient precracking of the EDM slot prior to spectrum testing. In some cases, the precrack length may not have been sufficient to ensure that the crack had initiated from the EDM slot at all points along the slot boundary. The delay then represents the time required to initiate a fatigue crack long enough that the EDM slot does not influence the crack growth. Uneven growth from the slot may also be reflected in the variation in crack growth rates, noted in 300M steel tests. Because such growth variation affects the damage tolerance and durability criteria described in Section VIII, the problem of introducing surface flaws reliably and repeatably is addressed in that section.

Even with the initial flaw variation problems encountered in the verification testing, the results obtained provide validation of the analytical algorithms developed in this program. Generally, it appears that such techniques can be used with confidence to predict the effect of environment-load interaction effects on crack growth.

SECTION VII

SPECTRUM LIFE PREDICTIONS

1. SUMMARY - The crack growth algorithms described in Section IV were calibrated to correlate with the spectrum crack growth data obtained from center crack panels tested in dry air. The calibrated model was then used to predict the crack growth in the center crack panels tested to the accelerated stress history in the salt water environment. Good correlation was obtained between the predicted growth behavior and the measured behavior in the aggressive (salt water) environment.

The calibrated model was also used to predict crack growth for the verification test series. Verification test results confirm the ability of the model to predict the growth of semi-elliptical surface flaws under spectrum loading both in inert and aggressive environments. The sensitivity of the predictions to selected crack growth model parameters was investigated.

2. CENTER CRACK PANEL SPECIMEN RESULTS

a. Model Calibration - Model calibration is discussed in greater detail in Section IV. The load-environment interaction algorithms were calibrated through correlation with constant amplitude test results from the development test program. The Willenborg spectrum crack growth analysis parameters were determined from single overloads tests in dry air and salt water and through correlation with the results of tests of center cracked panels tested to the accelerated stress history in the dry air environment.

b. Crack Growth Analyses and Test Results - Spectrum crack growth was predicted for center crack panels in the salt water environment under the accelerated stress history using the calibrated crack growth algorithms. Results of analysis and tests in each material are presented in Section III. Table 17 summarizes these results. Correlation with dry air test results is very good because the model was calibrated to correlate with those results. The analysis of 7075-T6 aluminum in dry air

resulted in a longer life than that given by test even though the analysis parameters were selected to produce a conservative life prediction.

Predictions of salt water test results were all slightly conservative, but very good agreement was obtained. The correlation of analysis and test results provides additional verification of the ability of the load-environment interaction algorithms to predict these effects.

3. SURFACE FLAW SPECIMEN TEST RESULTS

a. Crack Growth Analyses and Results - Using the analysis algorithms described in Section IV, spectrum crack growth predictions were made for the surface flaw geometries and loading conditions recommended for use in the verification tests, Section VI. These predictions were based on cycle-by-cycle analyses of the stress spectrum of the F-15 main landing gear outboard trunnion. This spectrum involves peak loads sustained for up to 27 seconds, as well as periods of rapidly applied sinusoidal stress. The verification tests included application of the stress history both in real time and at accelerated rates to specimens containing surface flaws. Tests were conducted both in lab air and in 3.5% salt water.

Predictions of the shape change occurring during growth from the given initial flaw geometries are obtained from constant amplitude analysis, as described in Section IV. At any surface crack length, the crack aspect ratio is assumed equal to that obtained with constant amplitude analysis.

Table 17 summarizes the predicted and measured crack growth lives for each test condition. The crack growth lives shown in the table are presented for growth to fracture from the largest initial flaw length in each material type. In steels, this flaw length was 0.026 inches; and in aluminum, it was 0.025 inches. In two-thirds of the cases, the predictions are within 30 percent of the test lives. The most noteworthy exceptions are the duplicate tests of 300M steel in salt water at both high and low frequencies. These results vary considerably both from predictions and from the original test results. The cause for the erratic behavior of 300M steel in this test series has not been

determined. We believe that difficulty in developing a sharp pre-crack with the proper shape may cause the erratic behavior.

Comparisons of predicted and measured crack growth for each test condition are presented in Figures 75 to 86. In these figures, the initial flaw length corresponds to the largest initial flaw for the particular test condition. The results are discussed in Section VI.

b. Sensitivity Analysis - There are many variables which can have considerable effect on the accuracy of the predictions presented in Section IV. These variables include initial flaw size and shape, assumptions of plastic zone size, overload shut-off ratio, hold time in the environment, and stress level. The impact of these parameters on the predicted lives was assessed to determine their relative significance. In all cases, crack growth sensitivity analyses were performed using the real time stress history and salt water environment and so represent minimum lives.

(1) Initial Flaw Size and Shape - As depicted in Table 1, initial flaw sizes and shapes can vary considerably depending on the mechanism of their formation. Even in the verification test program, considerable variations in EDM slot sizes and initial flaw sizes and shapes occurred. Thus, it is important to assess the sensitivity of the predictions to initial flaw sizes and shapes.

To evaluate initial flaw size sensitivity, surface flaws were selected to have the dimensions shown in Table 19. The surface lengths of the baseline analyses were selected as the longest initial flaw lengths measured in test. They correspond to the lengths used for the comparisons of analysis and test results presented in Table 17. The flaw depths were those predicted by the elastic surface flaw analysis of Appendix B. Baseline flaw sizes were selected to be the same for both steels and for both aluminums. The variations used in the sensitivity study represent flaws 10 percent smaller in both length and depth and 10 percent larger in both length and depth.

TABLE 19
EFFECT OF INITIAL FLAW SIZE AND SHAPE ON CRACK GROWTH

Material	Initial Flaw Size		Life in Flights (3)
	a (1)	2c (2)	
Initial Flaw Size			
HP 9-4-.30 Steel	0.0205	0.0236	2258
Baseline	0.0225	0.0260	2146
	0.0248	0.0286	2029
7075 Aluminum	0.0191	0.0227	2531
Baseline	0.0210	0.0250	2350
	0.0231	0.0275	2166
Initial Flaw Shape			
HP 9-4-.30 Steel	0.0248	0.0236	2152
Baseline	0.0225	0.0260	2146
	0.0205	0.0286	2143
7075 Aluminum	0.0231	0.0227	2256
Baseline	0.0210	0.0250	2350
	0.0191	0.0275	2398

Notes: (1) a is crack depth

(2) 2c is crack surface length

(3) Lives are predicted for real time (~0.1 cps) application of main gear stress history in 3.5% NaCl salt water environment.

GP78-0753-136

The crack growth lives presented in Table 19 were based on analyses of flaw growth from the initial dimensions to failure using the real time stress history and salt water environment. The results of Table 19 indicate that 10 percent increase or decrease in initial surface flaw size results in about a 6 percent decrease or increase in life, respectively, in steel. In aluminum, those variations cause an over 8 percent variation in crack growth life.

To assess the effects of initial flaw shape, two cases were considered: the first was based on increasing the initial crack length 10 percent while decreasing the initial depth by 10 percent from the baseline dimensions; and the second was based on decreasing the length 10 percent from the baseline and increasing the depth by 10 percent. As shown in Table 19, the effect of these variations is very small in both materials. Initial shape variations of this small magnitude have little

effect on life because the stress intensity factor along the crack front rapidly drives the flaw toward a "natural shape" in which growth at both surface and depth occur in proportion to those dimensions. This will be true as long as plasticity effects at front and back surfaces of the plate can be ignored and that breakthrough occurs after the "natural shape" has been attained.

(2) Interaction Zone Size Assumptions - Interaction zone size is a parameter of the Willenborg model which relates to the crack length over which an overload is effective in producing retardation. It is therefore related to the condition of the overload plastic zone, plane stress or plane strain. The interaction zone sizes used in all of the comparisons shown thus far were presented in Table 5, Section IV. These sizes were increased and decreased by 10 percent in this study, and comparisons of crack growth lives are shown in Table 20. The parameter has very little impact on these analyses. The greatest effect is less than one-half percent in 7075-T6 aluminum.

TABLE 20
EFFECT OF INTERACTION ZONE SIZE ASSUMPTION ON CRACK GROWTH LIFE

Material	Interaction Zone Size Assumption (ROOT 2) (1)	Life in Flights (2)
7049-T73 Aluminum Baseline	0.3640	2753
	0.4000	2755
	0.4400	2756
7075-T6 Aluminum Baseline	0.0909	2338
	0.1000	2350
	0.1100	2359
HP 9-4-.30 Steel Baseline	0.0909	2139
	0.1000	2146
	0.1100	2154
300M Steel Baseline	0.0255	5
	0.0280	5
	0.0308	5

Notes: (1) Interaction zone size is defined as

$$z_a = \frac{\text{ROOT 2}}{2\pi}\left\{\frac{K^{OL}_{max}}{F_{ty}}\right\}^2$$

(2) Lives are predicted for real time (~0.1 cps) application of the main gear stress history in 3.5% NaCl salt water environment.

GP78-1063-2

(3) Shut-Off Overload Ratio - The shut-off overload ratios used for the baseline analyses were determined as described in Section IV. Table 21 shows the effect of ±10 percent variations of the selected ratios on crack growth life. This parameter has considerably greater impact than the interaction zone size parameter, resulting in over 6 percent variation in life for 7049-T73 aluminum.

TABLE 21
EFFECT OF SHUT-OFF OVERLOAD RATIO ON CRACK GROWTH LIFE

Material		Shut-Off Overload Ratio	Life in Flights (1)
7049-T73	Aluminum Baseline	2.41 2.65 2.92	2614 2755 2947
7075-T6	Aluminum Baseline	2.41 2.65 2.92	2267 2350 2480
HP 9-4-.30	Steel Baseline	3.18 3.50 3.85	2073 2146 2233
300M	Steel Baseline	3.18 3.50 3.85	5 5 5

Note: (1) Lives are predicted for real time (~0.1 cps) application of main gear stress history in 3.5% NaCl salt water environment.

GP78-0753-134

(4) Sustained Load Hold Time - The effect of sustained load hold time in the 3.5 NaCl salt water environment is indicated by comparing the lives predicted for the real time stress history and the accelerated stress history, shown for each material in Table 17. These comparisons indicate that 300M steel has an unusually high susceptibility to sustained loads; HP-9-4-.30 shows considerably smaller variation and the two aluminums show almost no effect of hold time.

(5) Stress Level - Figures 89 and 90 show the effect of reducing stress level on lives of the four materials in the salt water environment under the real time stress history. These figures indicate that the stress levels required to produce crack growth lives in excess of 20,000 flights in each material would be predicted to be approximately 90 ksi in HP-9-4-.30 steel and 40 ksi in aluminum. Apparently, from the baseline initial flaw size, no reasonable stress level will result in lives exceeding 20,000 flights for 300M steel.

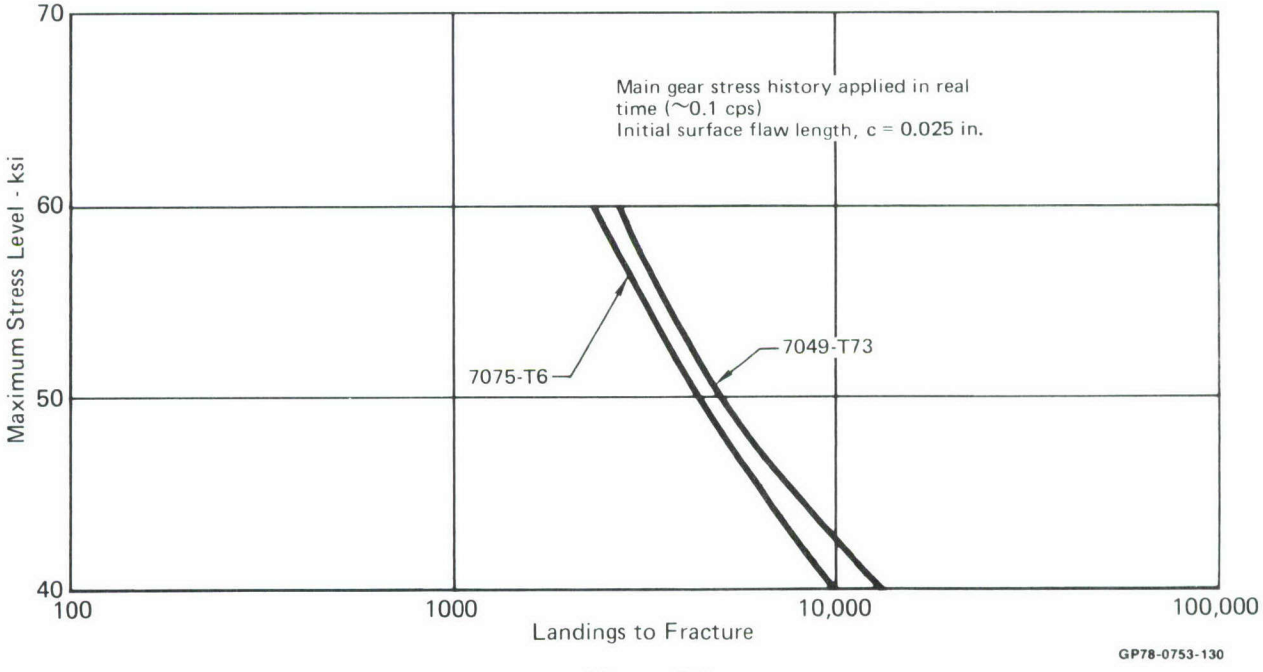

Figure 89
Effect of Stress Level on Crack Growth Life in Aluminum

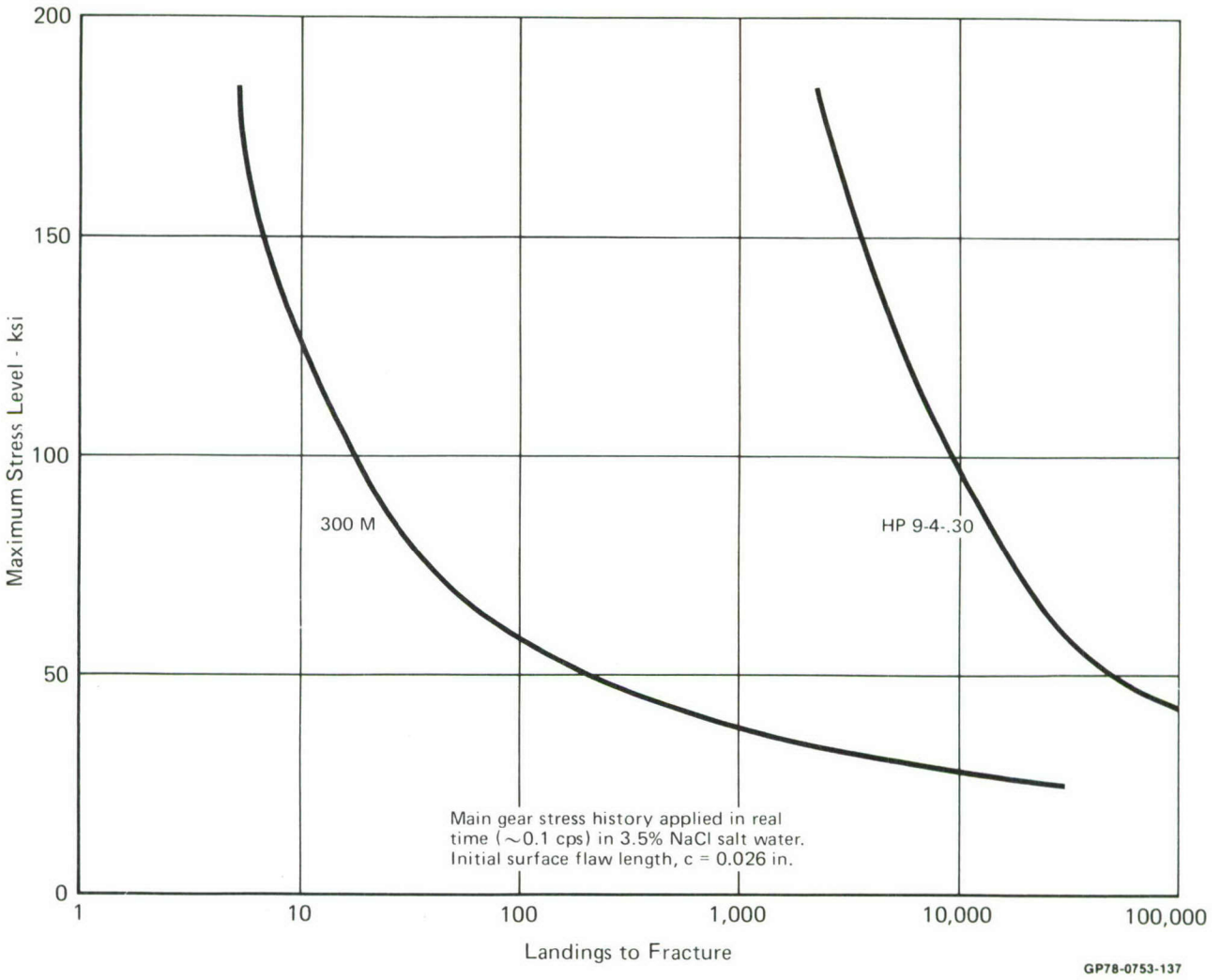

Figure 90
Effect of Stress Level on Crack Growth Life in Steel

These analyses indicate that the effect of sustained loads and aggressive environment on 300M steel is to accelerate crack growth to the point that other variations, which can be shown to be major factors in other materials under the same environment and stress history, have insignificant effect.

c. Conclusions - In spite of the initial flaw variation problems encountered in the verification testing, the results obtained provide validation of the analytical algorithms developed in this program. Generally, it appears that such techniques can be used with confidence to predict the effect of environment-load interaction effects on crack growth.

SECTION VIII

OUTLINE - DURABILITY/DAMAGE TOLERANCE CONTROL PLAN

A durability and damage tolerance control plan is outlined that could be applied to landing gear structural components (excluding wheels, tires, and brakes). Areas are identified that require further research or development before implementation of the plan could be accomplished. Structural design criteria that could be utilized in the design of landing gear components are summarized.

There is no current requirement for damage tolerance control of landing gear. Implementation of a damage tolerance control plan could have significant weight and cost impact. The control plan as outlined below is perhaps idealistic. Further research, studies, and evaluation of weight penalties and system pay-off are recommended before implementation of any plan. The basic design approach for durability should be to prevent degradation of wear surfaces, and crack initiation and growth. The basic design approach for damage tolerance should be based on the assumption that the primary landing gear structure can contain pre-existing flaws. Specific areas to be addressed in a durability and damage tolerance control plan are outlined in Figure 91.

1. MATERIALS AND PROCESSES

a. Durable Metals - Alloy selection is an important step in the prevention of degradation of wear surfaces. The selection of alloys and heat treatments to obtain long fatigue lives (cycles to formation of a crack), resistance to corrosion, stress corrosion cracking, and hydrogen embrittlement is required.

Properties that require characterization are:

F_{tu}

F_{ty}

S-N (Constant amplitude loading - initiation life)

Crack initiation life under spectrum loading

1. **Materials and Processes**
   - 1.1 Durable Metals Selection Criteria
   - 1.2 Damage Tolerant Metals Selection Criteria
   - 1.3 Durability and Damage Tolerance Enhancement Processes

2. **Design**
   - 2.1 Design Criteria
     - –Ultimate Strength
     - –Crack Initiation
     - –Crack Growth
     - –Environment, Spectrum - Load History
   - 2.2 Slow Crack Growth Structure
   - 2.3 Fail Safe Structure
   - 2.4 Critical Parts Selection
     - –Fracture Critical Area Identification
     - –Inspection Zoning Procedure

3. **Manufacturing Control**
   - 3.1 Material Quality Control
   - 3.2 Manufacturing Quality Control
   - 3.3 Parts Traceability

4. **Nondestructive Inspection**
   - 4.1 Manufacturing Quality Assurance Forging Inspection
     - –Finished Part Inspection
     - –Demonstration of NDI Capability
   - 4.2 In-Service Evaluation
     - –Inspection Interval Determination
     - –NDI Manual

5. **Durability and Damage Tolerance Analysis**
   - 5.1 Materials Data
     - –Stress - Life (S-N)
     - – da/dN
     - – F_{ty}
     - – F_{cy}
     - – F_{tu}
     - –Stress-strain Curve
     - –Spectrum Crack Initiation Data
     - –Spectrum Crack Growth Data
   - 5.2 Detail Stress Analysis
     - –Finite Element Analysis
     - –Strain Survey
   - 5.3 Stress Spectrum
     - –Load - Time Spectrum
     - –Load to Stress Conversion
   - 5.4 Environment
     - –Chemical
     - –Temperature
   - 5.5 Durability and Crack Growth Analysis Procedures

6. **Testing**
   - 6.1 Materials Testing
   - 6.2 Sub-Component Testing
   - 6.3 Component Testing

GP78-1063-6

Figure 91
Outline of Durability/Damage Tolerance Control Plan

For an initiation/propagation approach, S-N data are required to permit evaluation of candidate alloys, and provide a basis for predicting spectrum crack initiation lives for critical areas. Tests for crack initiation life under spectrum loading are required to validate spectrum life predictions, and confirm the ranking of alloys based on constant amplitude data.

b. Damage Tolerant Metals - The assumption that the structure contains pre-existing flaws will require long crack growth life. Therefore, selection of metals with low crack growth rates, high toughness, and resistance to environmental crack growth acceleration is desired.

Properties that require characterization are:

F_{tu}

F_{ty}

K_{IC}, K_C

da/dN - Dry air environment

da/dN - Aggressive environment

Crack growth in a dry air environment under spectrum loading

Crack growth in an aggressive environment under spectrum loading

In most alloys, especially steels, high strength is usually accompanied by low toughness and environmental resistance. Figure 92 shows critical flaw sizes for the alloys studied in this program, indicating that smaller sizes accompany higher strengths. The figure demonstrates the need for a balance of toughness and strength in order to achieve damage tolerance.

Within a metal system (aluminum, steel, titanium) the differences in inert environment crack growth rates, da/dN, are not as dramatic as the differences caused by aggressive environments. Table 3 (Section III) summarizes the constant amplitude crack growth rate for the alloys studied in this program, demonstrating the significant reduction in life of 300M when subjected to 3.5% salt water. Aggressive environment acceleration of crack growth can best be measured by cyclic load tests. Tests of 300M steel have shown the time dependent crack growth rate in cyclic testing to be much greater than the time dependent crack

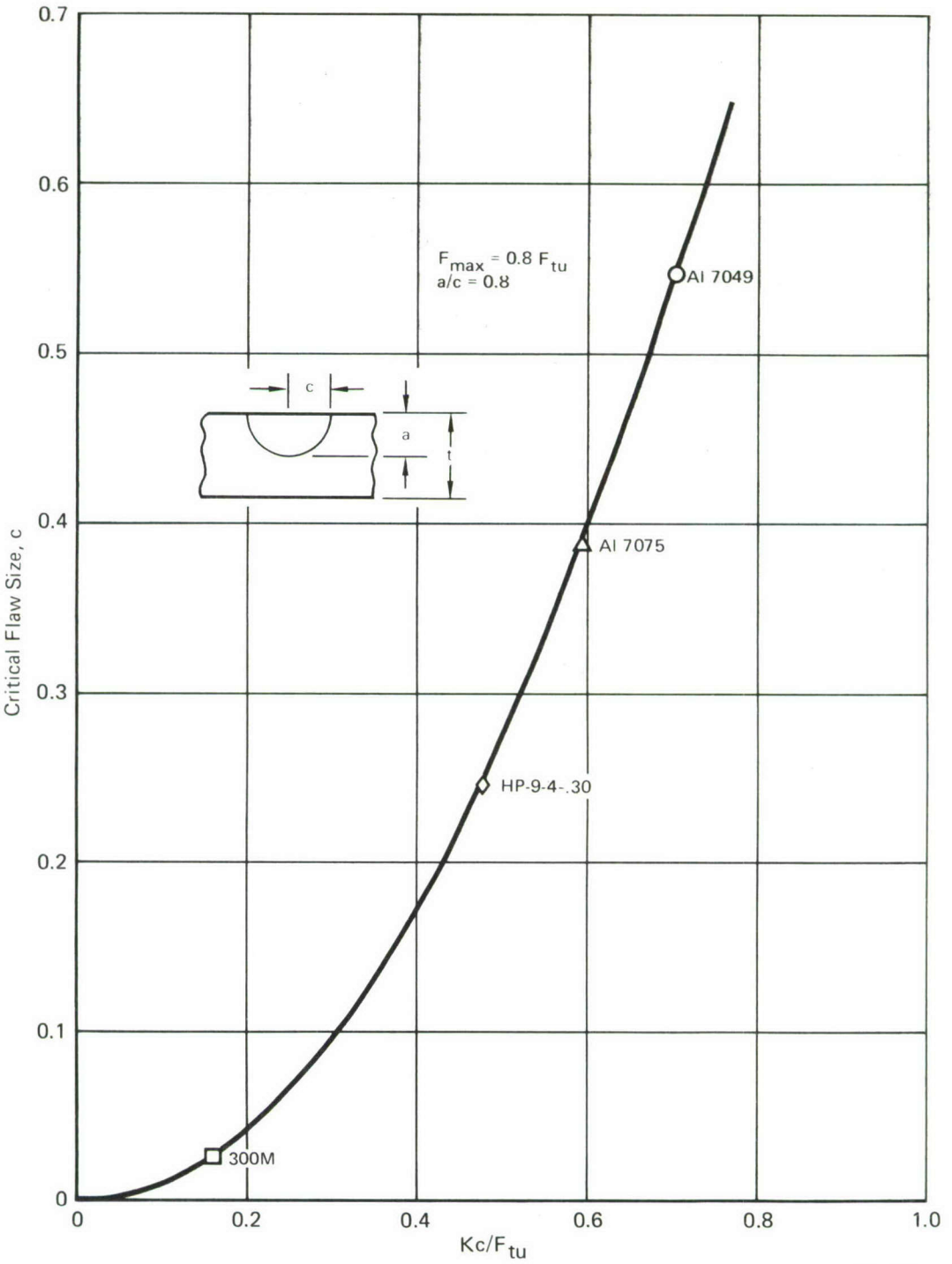

Figure 92
Critical Flaw Sizes

growth rates observed in sustained load tests (Figure 45 of Section III). Therefore, cyclic tests at a low cycle rate in an aggressive environment are recommended as a basis for evaluating environmental crack growth resistance, by comparison to results of tests performed at higher frequencies ($\sim$ 10 cps).

The final tests required to characterize damage tolerance of a metal are spectrum tests in inert and aggressive environments. These tests provide further validation of environmental resistance, and measure the crack growth retardation caused by overloads. The latter knowledge is required for accurate life prediction of the gear, for the many combinations of flaw size and shape, and stress levels, that must be considered in design.

Based on the damage tolerance selection criteria previously discussed and the results of the tests performed in this program, steel alloy HP-9-4-.30, and aluminum alloy 7049-T73 exhibit good combinations of properties. From the viewpoint of damage tolerance, including environmental resistance, 300M steel exhibits poor properties. Other high strength steels (D6AC, 4340, H-11) would probably exhibit very similar behavior.

There is need for development of a high strength steel with a better balance of strength and damage tolerance. The medium strength steels typified by HP-9-4-.30 exhibit good tolerance, but use of these steels instead of the higher strength steels would result in significant weight increases. The weight and damage tolerance of intermediate strength steels, ($F_{tu} \sim 260$ ksi) needs to be systematically evaluated.

c. Durability and Damage Tolerant Enhancement Processes - Production of gears with controlled durability and damage tolerance requires an organized manufacturing plan. Included in this plan should be techniques for material control, processing control, inspection, and parts traceability through production and in service. Corrosion and wear protection requirements are outlined in MIL-STD-1568 and MIL-STD-1587.

The use of carefully selected processes can enhance the inherent durability and damage tolerance created by structural design and material choice. The creation of compressive

residual stresses at surfaces can increase crack initiation life and reduce crack growth rates, increasing life with flaws. Techniques to develop these residual stresses include shot-peening, cold-working of holes, installation of interference fit bushings, and roll burnishing.

2. DESIGN

a. Design Criteria - The structural design of Air Force landing gears has been based on the ultimate strength requirements of MIL-A-8862, and the requirements for repeated operation (durability) of MIL-A-8866. Damage tolerance requirements for airframes are specified in MIL-STD-1530 and MIL-A-83444. MIL-A-83444 excludes application of that specification to landing gear.

Modifications that could permit MIL-A-83444 to be applied to landing gear are outlined below. The paragraphs requiring modification are primarily those containing requirements for initial flaw size assumptions. Based on the survey summarized in Reference 1, the initial flaws typical of landing gear are smaller than those permitted for airframe structure by MIL-A-83444. Paragraphs where modifications are recommended are 3.1.1.1 (a) and (b) and 6.1. Paragraph 3.1.1.1 (a) specifies initial flaw sizes for slow crack growth structure. At holes and cutouts it specifies a 0.05 inch through thickness or corner flaw depending on material thickness. At locations other than holes, a 0.25 inch flaw length is specified, either through thickness or semi-circular surface flaw (surface length = 0.25 inch, depth = 0.125 inch) dependent on material thickness. Paragraph 3.1.1.1 (b) specifies initial flaw sizes for fail safe structure. At holes and cutouts it specifies a 0.02 inch through thickness or corner flaw dependent on material thickness. At locations other than holes a 0.100 inch flaw length is specified, either through thickness or semicircular surface flaw dependent on material thickness. Paragraph 6.1 specifically excludes application of the specification to landing gear, and would have to be modified.

These paragraphs in MIL-A-83444 that specify initial flaw sizes require modification before application to landing gear.

The study summarized in Reference 1 identified initial surface flaws up to 0.02 inches deep. The testing in this

program employed target depths of 0.008 inches in steel, and 0.010 inches in aluminum as representative of initial flaws in landing gear. These are significantly smaller than the MIL-A-83444 specified value of 0.125 inch depth for surface flaws in slow crack growth structure. Landing gear components are primarily slow crack growth structure within the definitions of MIL-A-83444. Use of an assumed initial flaw depth of 0.125 inches would require stress levels significantly lower than currently employed, and would be accompanied by weight increases.

There is a need for further definition of initial flaw depths to be permitted for landing gear structure. The values of 0.008 inches in steel, and 0.010 inches in aluminum used for testing in this program are based on the study summarized in Reference 1. But that study was limited in scope and intended to be used as a basis for initiating a more complete evaluation. This evaluation could be based on metallurgical inspections of landing gear components as a continuing procedure at the Ogden Air Logistics Center, permitting refinement of the geometry estimates in Reference 1.

Crack growth predictions should be performed for each critical gear component. These predictions would be utilized in material selection, in the design of critical components, in the establishment of flaw sizes to be detected by NDE procedures during fabrication, and in the establishment of in-service inspection intervals.

It is important that a realistic landing gear load spectrum be used as the basis for crack growth predictions. For metals that demonstrate frequency dependent crack growth rates, such as 300M steel, times of load application are also important. As a basis for developing loads spectra MIL-8866 appears to be conservative, but does not provide estimates of load duration. MIL-A-8866 should be reviewed to ensure its realism. Over the last several years there have been substantial advances in the technologies associated with fatigue life tracking systems. By taking advantage of current recorder technology, and advanced data reduction techniques, it is feasible to track landing gear

load history on an aircraft fleet. Such a program can have a substantial payoff in terms of more precise estimates of useful life for current gear and more precise definition of design loads for future gear, leading to a more optimal balance of weight and damage tolerance.

The chemical environment encountered by landing gear includes dry and moist air, hydraulic fluid, water, and salt water. The latter environment is usually the most aggressive. It can be present on aircraft operating near oceans, and also near salt deserts. Salt water is created in the latter situation by condensation of water on the gear cooled by high altitude operation of the aircraft, with subsequent salt entrapment. In selecting materials for use on gears, attention should be given to those materials which display good fatigue and crack growth qualities as well as stress corrosion and exfoliation resistance in salt water. Metals that are comparatively resistant have been shown in this program to exhibit crack growth rates that are nearly independent of cyclic frequency and load hold time. Selection of corrosion resistant materials reduces the need for precise definition of the environment, and times of load duration.

b. Slow Crack Growth Structure - Single load path structure (safe-life) and structure which is not readily inspectable should be designed such that initial manufacturing or material defects will not propagate to failure during a time period established by specification. Initial flaws should be assumed to exist at bolt holes or other areas of stress concentration. The analysis should be based on spectrum crack growth data obtained from element or sub-component tests. Crack growth predictions using the methods described in Section V should be correlated with spectrum test data to substantiate prediction accuracy.

c. Fail Safe Structure - The majority of landing gear structure is single-load path structure without crack arrest features. MIL-A-83444 specifies that for airframe use, such structure must be qualified as slow crack growth structure. Landing gear design details utilizing multiple load paths and crack arrest features could be qualified as fail safe structure.

The inspection intervals, residual strength requirements, and damage growth limits specified in Paragraph 3.2.2 of MIL-A-83444 could be employed for landing gear fail safe structure. As with slow growth structure, a program should be performed to determine initial flaw sizes. The initial flaw size assumption for fail safe structure, using the concepts of MIL-A-83444, would be smaller than for slow growth structure.

d. Critical Part Selection - Design for durability is concerned with minimizing maintenance costs, whereas design for damage tolerance is concerned with ensuring safety of landing. Separate lists of durability and damage-tolerance critical components should be prepared. The critical component lists should be prepared early in the design phase, and updated periodically. Selection of parts for the lists requires preliminary ultimate strength, durability, and damage tolerance analyses.

Durability considerations include expense of replacement, inspection, and repairs. If the design stress levels are constrained by durability or environmental considerations (corrosion, wear, hydrogen embrittlement) the part should be placed on the durability critical parts list. If special processes are required to achieve the life requirements the part should be placed on the durability list.

Components required for safety, or whose design stress levels are established by damage tolerance requirements, should be placed on the damage tolerance critical part list.

3. MANUFACTURING CONTROL

a. Material Quality Control - The processing sequence for all critical parts should receive a step-by-step review to ensure proper NDI sequencing and to verify that all processing operations will not have uncontrolled or unexpected effects on the durability or toughness of the part, or will induce undesirable residual stresses.

There are a few components for which damage tolerance requires a minimum-guaranteed-toughness material. For those components, material specifications should be prepared which

will specify a guaranteed minimum K_{Ic}. For those materials which have toughness properties included in the material specifications, fracture toughness tests should be conducted. Implementation could be via drawing callout of the material specification number, which in turn would become a part of the purchase order.

Material specifications controlling the toughness of the material should also require that the material be marked with the specification number. Such material should be stored in an area separate from similar material procured to other specifications. All material removed from storage should be inspected to verify it is the correct material in conformance with the work order which should accompany the parts though all processing.

In those cases where fracture toughness testing of each part is required, the tests should be conducted on the raw material for each part, and a serial number assigned to relate the individual set of test data to the particular piece of material. This number should be stamped on the raw material and recorded on the work order. During fabrication, the number should be transferred to the part using a permanent marking procedure, such as air grit marking, which is not likely to create sources of crack initiation. In this way, each part can always be identified with the particular set of raw material test data.

b. Parts Traceability - Material acquisition, manufacturing, inspection, and service usage should ensure traceability of the components. Techniques outlined above ensure traceability through manufacture. However, landing gears can be removed from the airframe, disassembled, re-worked, re-assembled using components from different gears, and installed on a different aircraft. Hence, there is potential difficulty tracking individual gear components through service usage. For components that are placed on the critical parts lists, service tracking may have to be performed on an individual part basis. This requires a part number and serial number be permanently marked on each

part using a process such as grit marking. If reworking of the part requires removal of the serial number, the number should be retained by tagging the part and remarking after rework. The expense of individual part tracking must limit the number of parts to be tracked.

c. Critical Process Control - Critical processes such as heat treatment, plating, griding, and corrosion protection application should be controlled by specification. MIL-STD-1587 outlines materials and process requirements for Air Force aircraft.

4. NON-DESTRUCTIVE INSPECTION

a. Manufacturing Quality Assurance - The choice of NDI procedures and acceptance criteria should be based upon criticality, inspectability, stress level, flaw growth rate, and initial flaw size which will grow to failure in the time period established by aircraft specification. In order to reduce NDI costs, engineering drawings should be zoned to concentrate more restrictive and costly acceptance levels to the more critical areas of parts. The primary loading direction should be indicated on the drawing so that inspection procedures can be defined to detect defects perpendicular to the loading direction. Finished part inspection should be used to detect flaws which could grow to critical size during the life of the gear, since surface finishes on forged parts do not provide the required smoothness for the necessary level of ultrasonic inspection. Forgings could be ultrasonically inspected to detect the presence of larger flaws which would result in scrappage after machining.

A combination of ultrasonic, penetrant, and magnetic particle inspection could be used to ensure that the gear has acceptable quality, as indicated in Figure 93. A flaw with a length twice the material thickness will probably penetrate the surface of the part, and thus for relatively thin sections, a flaw can be found by penetrant or magnetic particle inspection alone. In areas of greater thickness, where an embedded flaw of critical initial size has a reasonable probability of occurring, an ultrasonic inspection is utilized, as well as a penetrant or magnetic particle inspection.

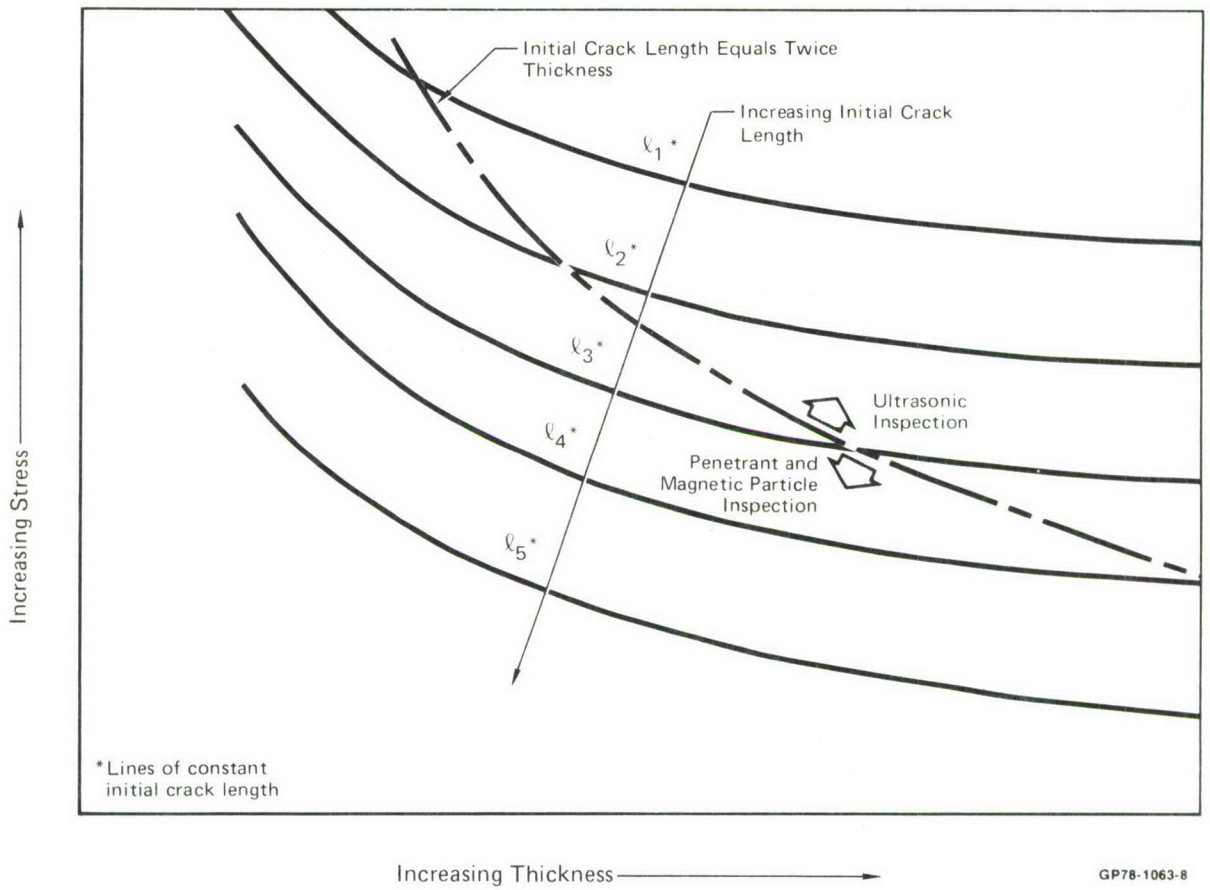

Figure 93
Establishment of NDI Requirements for Finished Part Inspection

The dividing line between the penetrant and ultrasonic inspection techniques is outlined in Figure 93. This division is determined using an initial flaw length that is twice the material thickness and calculating the flaw growth for several thicknesses at different spectrum stress levels. The solid lines in Figure 93 represent the initial crack size that will grow to failure in the time period established by aircraft specification. Below the dashed line critical flaws will probably penetrate the surface and be detectable by penetrant or magnetic particle inspection. Above the line it is possible that an embedded flaw of critical initial size would require ultrasonic inspection for detection.

The NDE procedures should be demonstrated to insure that the flaws requiring detection have a high probability of being located. Production inspection personnel, equipment, and materials should be used in the demonstration. The program should be extensive enough to establish probability of flaw detection as a function of NDE method, material, and flaw size. The probabilities could then be used to establish the sizes of initial flaws which might not be detected by NDE techniques during inspection. Initial flaws of those sizes should be assumed to exist in the structure for purposes of establishing in-service inspection intervals.

b. In-Service Evaluations: In-service inspection intervals should be determined for critical parts by assuming initial flaw sizes consistent with the results of the NDE demonstration program, and predictions of crack growth using environmental conditions and design usage loading spectra. An inspection interval for a part would be considerably less than the predicted life to failure so that multiple inspections would be expected during the time a flaw would grow to failure.

If the gears were instrumented and the instrumentation made a portion of the flight loads monitoring systems, the inspection interval for individual fleet aircraft could be based on actual usage.

An NDE manual should be prepared including non-destructive inspection instructions, procedures, and techniques for critical components. Techniques should be defined for inspection of critical areas for potential service defects (cracking, corrosion, wear, deformation).

5. DURABILITY AND DAMAGE TOLERANCE ANALYSES

a. Materials Data - If an initiation/propagation approach is taken, the S-N data and da/dN data are required. Spectrum loading tests should be performed to validate prediction methodology on the design loads spectrum for the gear.

If a fracture mechanics approach is taken, the data needed comprises da/dN, K_c, F_{ty}, and a measure of crack growth retardation caused by overloads. The crack growth data (da/dN, and ef-

fects of overloads) should be obtained for both inert and aggressive environments. Much of this data is available in literature. This report characterizes four candidate landing gear alloys. Spectrum loading crack growth tests should be based on the design load spectrum for the gear. Basic properties (da/dN, K_c, F_{ty}) should be determined using the same lots of materials used for the spectrum crack growth tests performed with the design usage load spectrum. This will permit comparisons between the fracture mechanics properties of the specific lots of material used for spectrum fatigue testing, with the values used for the numerous growth predictions required in detail design.

b. Detail Stress Analysis - Detail stress levels of durability critical parts should be established on spectrum life predictions, and validated by testing using the design load spectrum. Stress levels of fracture critical parts should be based on crack growth analysis and spectrum crack growth tests of flawed specimens. Single load path and non-inspectable critical areas should be designed such that initial manufacturing or material defects existing at fastener holes or other areas of stress concentration will not propagate to failure in a time period established by aircraft specification. For purposes of design, the size of the initial flaw should be consistent with the results of the NDI demonstration program. Factors such as access for inspectability, fail safe versus safe-life structure, criticality, and ease of replacement should be considered in the establishment of initial flaw sizes.

In order to perform accurate analyses of crack initiation and flaw growth, detailed knowledge of the component stress distributions is required. Good estimates of stresses can be obtained through the use of finite element analyses. These analytic stress estimates should be confirmed by a strain survey of the gear. This can be accomplished by surveying a full scale gear using strain gages. An alternative is to manufacture a model of the gear using photo-elastic material. The latter technique has been useful in confirming stress analysis of landing gear.

c. Stress Spectrum - Prediction of stress time histories requires knowledge of the applied loads. The loading of landing gear includes several conditions (turning and pivoting - left and right, medium and hard braking, taxiing, and landing) at a wide range of aircraft gross weights. The conversion of external gear loads to component stress must be performed for each loading condition. The result of the process is a landing-by-landing stress history for the area being analyzed.

MIL-A-8866, the current specification basis for developing load spectra, requires assumptions as to sequence of conditions, aircraft gross weight, and load duration times. As indicated above there is need for a program to track usage of the gear in a fleet to validate MIL-A-8866 (or provide the data for updating that specification) and provide data for developing load sequences, and duration times.

d. Environment - The chemical environment for landing gear includes dry and moist air, hydraulic fluid, water, and salt water. The durability and crack growth analyses should be performed assuming the presence of the more aggressive environment to which the individual critical parts may be subjected. Critical part selection is outlined in Paragraph 2.d. The selection of corrosion resistant metals reduces the acceleration of crack initiation and growth caused by the environment, as well as the need for precise definition of the environment.

The service temperatures experienced by landing gear are moderate, the gear does not experience the elevated temperatures of mold-line structure. However, for materials that are sensitive to chemical crack growth acceleration, even modest changes in temperature can cause significant changes in chemical acceleration (Reference 2). Accurate prediction of growth would require accurate knowledge of temperature, but the selection of corrosion resistant metals reduces the need for this accurate knowledge.

e. Durability and Crack Growth Analysis Procedures - Durability analyses include predictions of crack initiation life and of crack growth. Prediction procedures for crack initiation have been available for a comparatively long time, in contrast to

the more recently developed crack growth prediction procedures for crack initiation have been available for a comparatively long time, in contrast to the more recently developed crack growth prediction methodology. An objective of this program was the development of crack growth prediction procedures for gear components, considering environmental acceleration. The Willenborg model was used in this program for prediction of growth caused by environment and sustained load. The sustained load growth data required by the linear superposition model of environmentally accelerated crack growth is inferred by subtraction of the growth rates (da/dN) for cyclic load tests performed at two significantly different frequencies. These procedures are outlined in Section IV.

The procedures outlined in Section IV have been shown in this program to predict growth with reasonable accuracy. An exception is the long delay of crack growth at the start of several tests. This delay has been conjectured to be the result of improper initial flaws that were not elliptical in shape, or were not sharpened by the precracking. The observed and predicted inaccuracy in predicted growth is caused by growth delay, and appears to be a problem in creating the proper initial flaw and not a problem in prediction methodology.

6. TESTING

a. Material Testing - Tests using standard specimens, e.g. notched fatigue specimens, and center-crack panels or WOL crack growth specimens should be performed to permit material selection, and spectrum crack initiation and growth predictions. The data required consists of F_{tu}, F_{ty}, S-N, K_{IC}, K_C, da/dN in inert and aggressive environments, and spectrum crack initiation and growth.

For a limited number of components, damage tolerance requires a minimum guaranteed toughness material. For those components, fracture toughness and tensile tests should be conducted. Current practice by the material producers is to guarantee toughness only if the purchase order authorizes tests of each material lot. The expense of these tests must be considered in specifying minimum toughness.

b. Sub-Component Testing - Durability and damage tolerance of landing gear should initially be substantiated by sub-component tests. These tests will permit evaluation of the selected design stress levels and critical design details. They should be performed by subjecting sub-components to design spectrum loads. Data from these tests will provide substantiation of the spectrum crack initiation and growth prediction procedures, including input material data, growth retardation parameters, and stress intensity solutions.

The damage tolerance tests could be performed by providing semi-elliptic surface flaws in the test specimens. As indicated in Section V, it is apparently difficult to prepare repeatable small initial flaws typical of landing gear components.

There is a need for a program to develop procedures to repeatably prepare these small initial flaws. It should evaluate approaches and demonstrate repeatability by test.

An alternate to performance of tests with intentional initial flaws could be durability tests performed with nominally unflawed structure. Fractographic examination of cracks detected after test would permit preparation of crack growth curves. The curves would be used to verify the accuracy of growth prediction methodology.

This alternate approach reduces the number of required test articles (separate durability and damage tolerance tests are not required.) Nor does it require pretest estimates of which areas are the most fatigue critical. Finally, the preparation of intentional flaws is not required, eliminating the preparation problems discovered in this program.

c. Component Testing - The durability and damage tolerance of the gear should be substantiated by spectrum fatigue tests of the complete gear. The damage tolerance tests could be performed by placing semi-elliptic flaws in critical areas, and subjecting the gear to spectrum loads. An alternate is the use of fractographic examination of cracks detected after durability testing, as described above.

The need has previously been discussed for programs to improve knowledge of landing gear loads experienced in service, to improve the definition of initial flaws sizes, and to develop procedures to prepare these small initial flaws. Meaningful durability and damage tolerance tests of the complete gear are contingent upon such programs.

7. SUPPLEMENTARY CRITERIA

The need for further criteria, research, or development to permit implementation of the durability/damage tolerance control plan was evaluated. The outboard trunnion of the F-15 landing gear was used as a basis for this evaluation.

Areas in the control plan that could have significant cost and weight penalties include material selection, initial flaw size specification, load spectrum development, and parts tracking. Before any control plan for landing gear is initiated, programs in the areas of materials development, initial flaw characterization, and load spectrum measurement should be performed.

a. Current Structural Design Criteria and Strength Analysis - The F-15 landing gear is designed to the ultimate strength requirements of MIL-A-8862A and the repeated loads requirements of MIL-A-8866A.

The structural area used as a basis for development of the fatigue spectrum in this study (Section 5) is shown in Figure 68. The majority of the gear design including this outboard trunnion, is controlled by ultimate strength requirements. The location indicated in Figure 68 is critical for two-point braked roll (Paragraph 3.3.1.1 of MIL-8862A), and the margin of safety is 0.02 for that ultimate strength condition. The maximum stress, computed elastically, for ultimate loads is 427 ksi. Plasticity of the material prevents this stress from being developed and results in the positive (0.02) margin of safety. The maximum stress in the fatigue spectrum results from a high sink rate landing, and is 248 ksi. This is less than the stress (285 ksi computed elastically) at limit load caused by the ultimate

strength condition. The ability of the gear to withstand ultimate applied loads and fatigue spectrum was demonstrated in ground tests.

b. Additional Criteria, Research, and Development - The alloy currently used in the trunnion is 300M steel. Data developed in this program indicates 300M to have low toughness, and exhibit environmental acceleration of crack growth. There is need for a high strength steel with a better balance of strength and damage tolerance.

The current design criteria for landing gear are discussed in Paragraph 2. Damage tolerance requirements for airframe are specified in MIL-STD 1530, and MIL-A-83444. A statement in MIL-A-83444 excludes application of that specification to landing gear. Modifications that are suggested before it can be applied to landing gear are outlined in Paragraph 2. That paragraph also identifies the need for further definition of initial flaw depths to be used for landing gear components. The values of 0.008 inches in steel and 0.010 inches in aluminum were used for testing in this program, based on the study reported in Reference 1.

MIL-A-8866 is the current basis for developing load spectra for landing gear. The need to review its realism and the desirability of a tracking program to measure service usage of landing gear has been described in Paragraph 2.

In-service inspection intervals should be determined for critical parts by assuming initial flaw sizes consistent with the results of an NDE demonstration program, and crack growth predictions. A usage-tracking program would permit the inspection interval for individual aircraft to be based on actual usage.

This program has resulted in crack growth predictions which appear to be reasonably accurate, for a known load spectrum. Improved definition of the load spectrum based on a usage tracking program would increase prediction accuracy for behavior of fleet aircraft.

Damage tolerance tests of elements should be performed by providing semi-elliptic surface flaws. During testing using this type of flaw, several specimens exhibited long delay of crack growth. It is believed this delay resulted from initial flaws being rectangular and not pre-cracked on the entire flaw periphery. There is need for a program to develop procedures to repeatably prepare small initial surface flaws.

APPENDIX A

STRESS INTENSITY SOLUTIONS FOR ELLIPTIC SURFACE FLAWS

SUMMARY OF RESULTS - Stress intensity solutions computed from a slice synthesis model and NASTRAN three dimensional finite element results were compared with those obtained from three dimensional finite element analyses of Raju and Newman, Reference 1, to substantiate the model. Results of these comparisons are shown in Figures A-1 and A-2. Good agreement is obtained for the stress intensity at the flaw depth, Figure A-1, and reasonable agreement is obtained for the stress intensity at the surface for all but deep flaws, Figure A-2. The results reported in Reference 1 are based on the most detailed model employed thus far in the analysis of the surface flaw.

Figure A-3 presents the results developed by other investigators, References 2, 3, and 4. The results obtained by Rice and Levy, Reference 2, are based on a line spring model similar to the slice synthesis model. The solutions obtained by Smith and Sorensen, Reference 3, and Kobayashi, Reference 4, are based on extensions of Schwartz's alternating method for solving two-dimensional boundary value problems. As shown in Figure A-3, all of these predictions are in general agreement, except for those obtained by Smith and Sorensen.

Because good agreement is shown between the results of Raju and Newman, and the slice synthesis model, as shown in Figures A-1 and A-2, the slice synthesis model results are expected to be reasonably accurate. The slice synthesis model has the advantage that finite width as well as thickness can be included in the analysis.

In order to readily use these results in crack growth prediction computer routines, equations relating stress intensity to crack shape, and depth to plate thickness ratio, have been empirically established based on the slice synthesis model results:

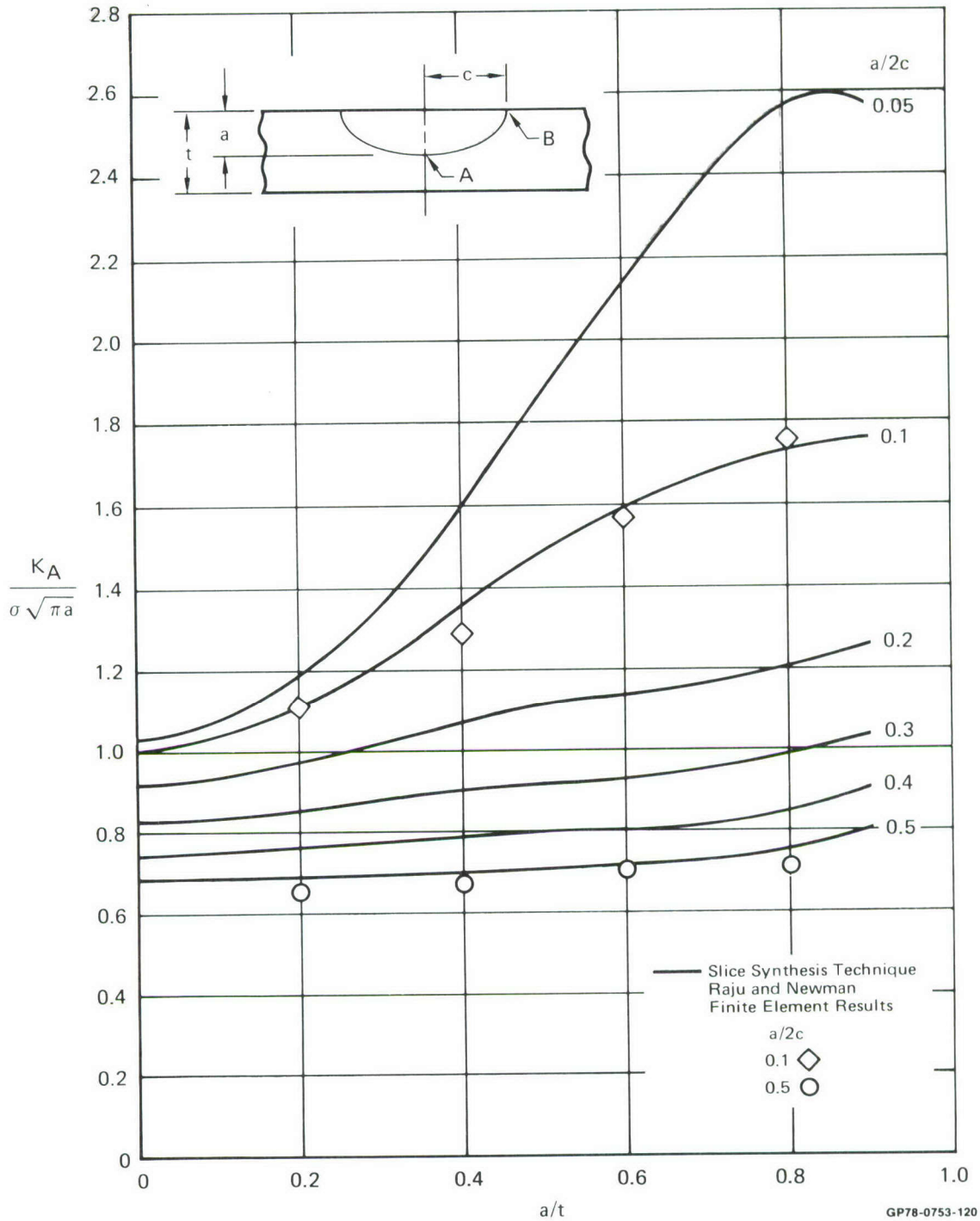

Figure A-1
Surface Flaw Stress Intensity Solution at Depth

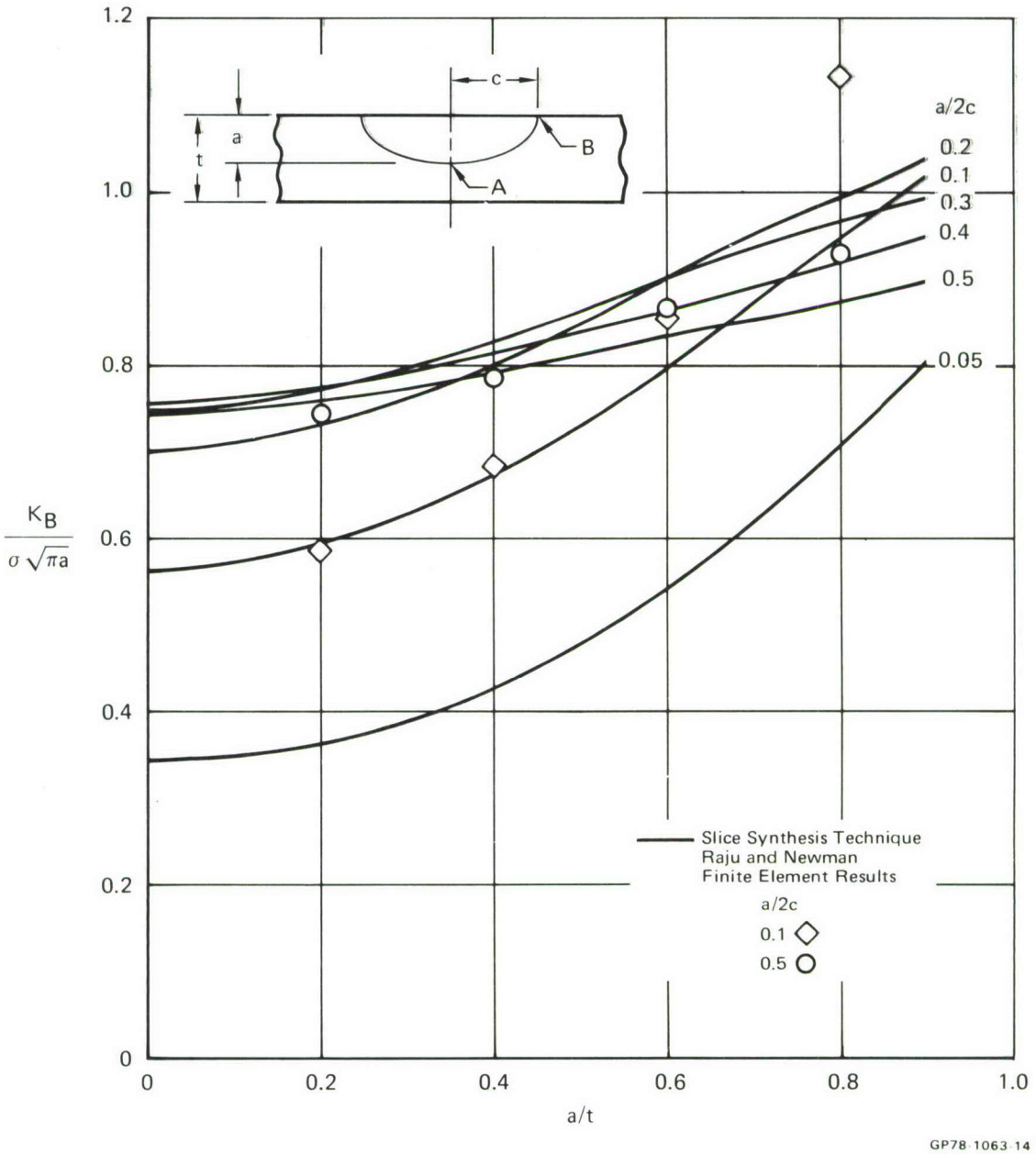

Figure A-2
Surface Flaw Stress Intensity Solution at Surface

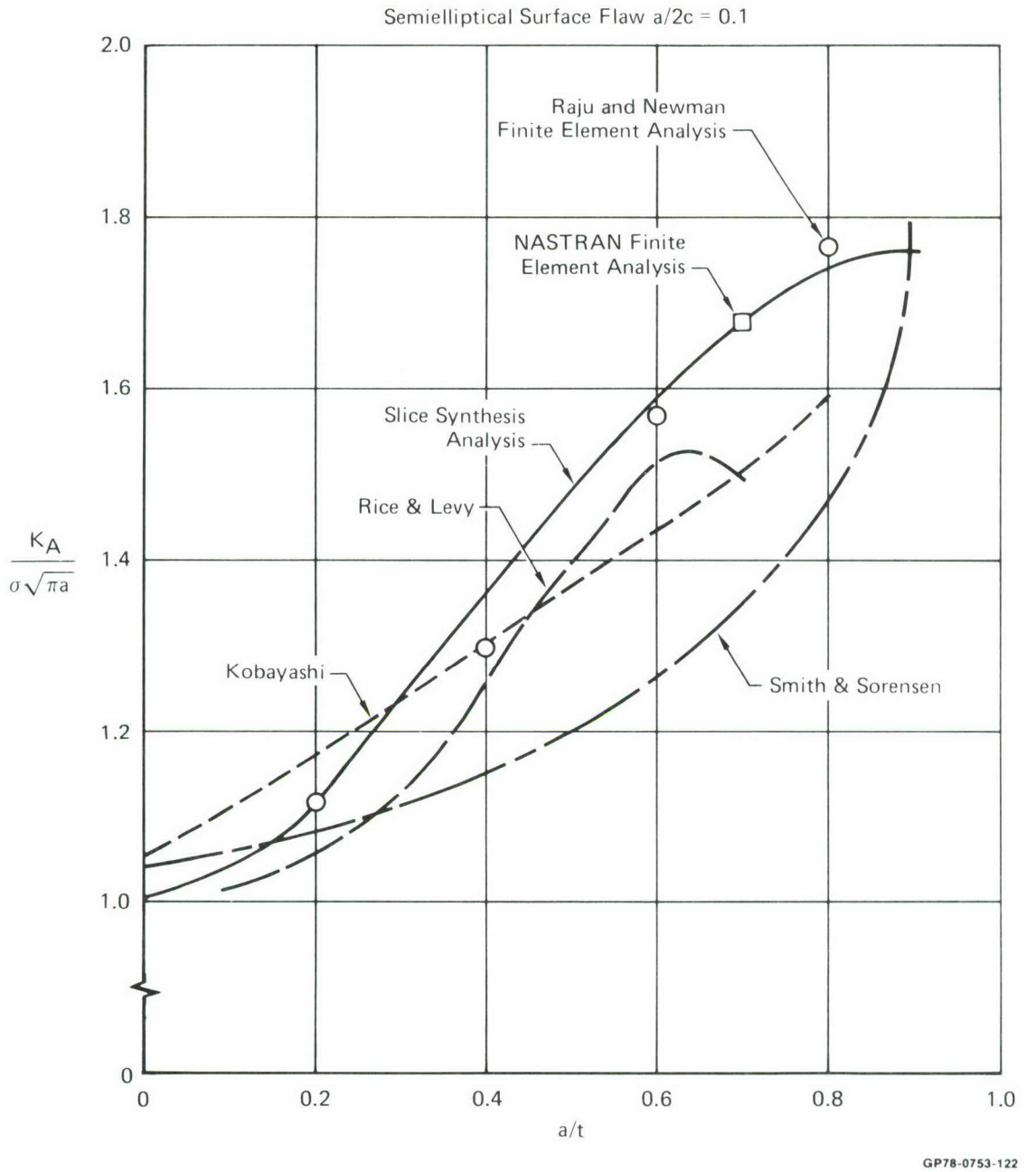

Figure A-3
Comparison of Surface Flaw Stress Intensity Solutions

$$K_A = \sigma\sqrt{\pi a} \sum_{i=0}^{3} \sum_{j=0}^{3} A_{ij} \left(\frac{c}{a}\right)^{i/2} \left(\frac{a}{t}\right)^{j} \qquad \text{(A-1)}$$

$$K_B = \sigma\sqrt{\pi a} \sum_{i=0}^{3} \sum_{j=0}^{3} B_{ij} \left(\frac{c}{a}\right)^{i/2} \left(\frac{a}{t}\right)^{j} \qquad \text{(A-2)}$$

where K_A = stress intensity at depth
K_B = stress intensity at surface
σ = applied stress
a = crack depth
c = half surface length
t = plate thickness

Figures A-4 and A-5 compare the results obtained with these equations with the original data used to establish the equations. Good agreement is apparent, and the maximum discrepancy is 2.3%. The coefficients A_{ij} and B_{ij} are presented in Table A-1.

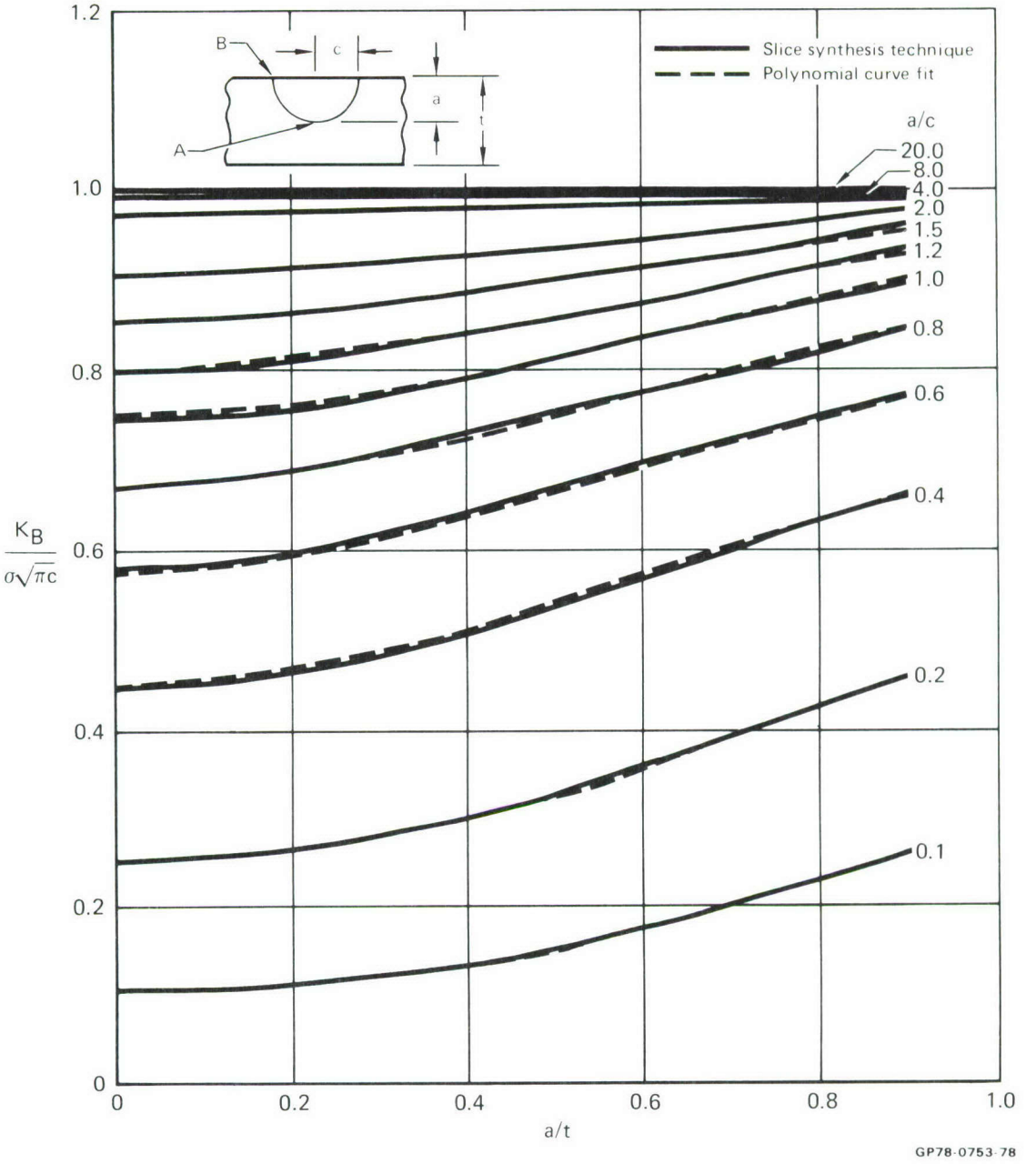

Figure A-4
Polynomial Curve Fit to Surface Flaw Stress Intensity at Surface

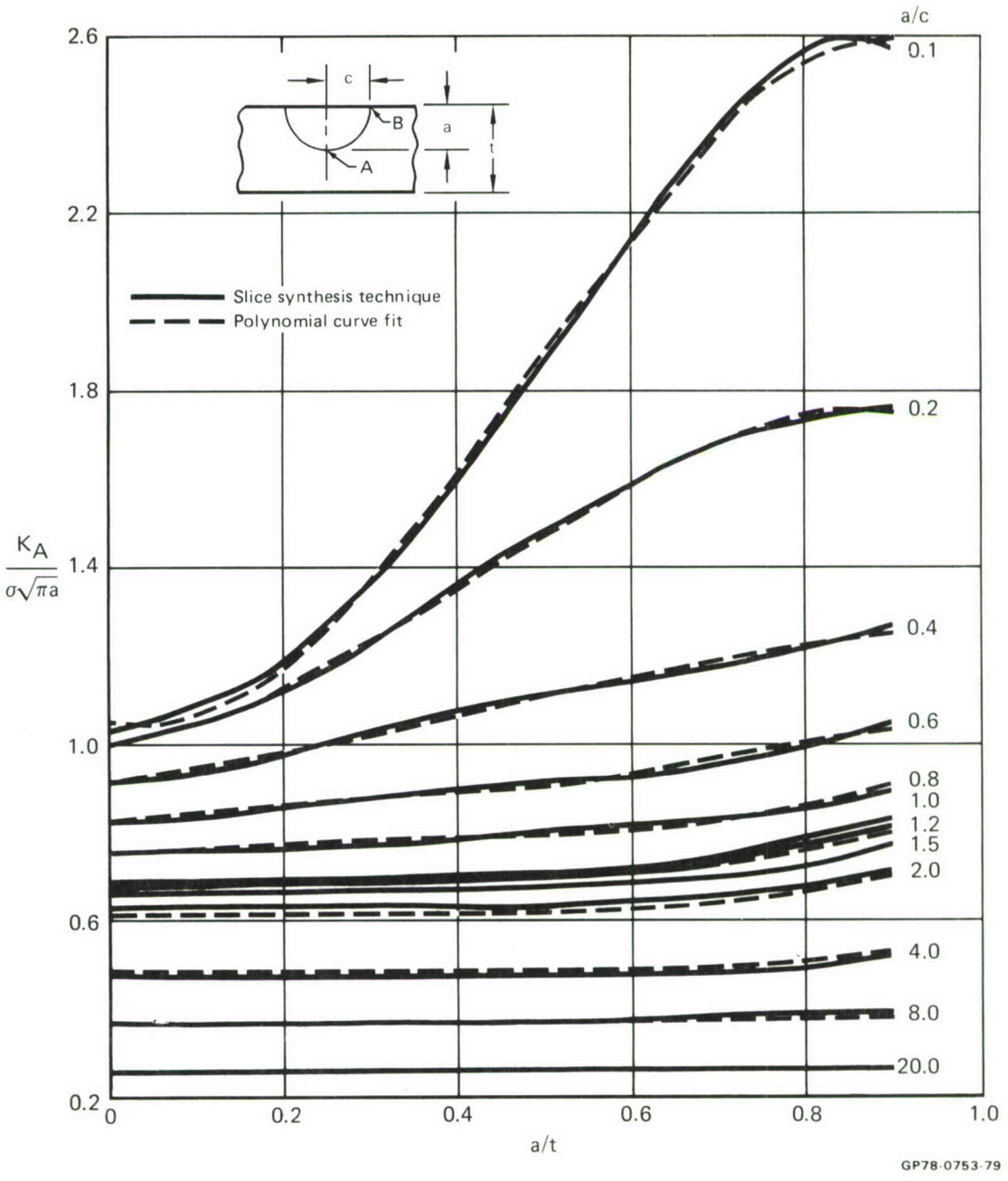

Figure A-5
Polynomial Curve Fit to Surface Flaw Stress Intensity at Depth

TABLE A-1
POLYNOMIAL COEFFICIENTS FOR EVALUATING SURFACE FLAW STRESS INTENSITIES

$$K_A = \sigma\sqrt{\pi a}\sum_{i=0}^{3}\sum_{j=0}^{3} A_{ij}\left[\frac{c}{a}\right]^{i/2}\left[\frac{a}{t}\right]^{j}$$

$$K_B = \sigma\sqrt{\pi a}\sum_{i=0}^{3}\sum_{j=0}^{3} B_{ij}\left[\frac{c}{a}\right]^{i/2}\left[\frac{a}{t}\right]^{j}$$

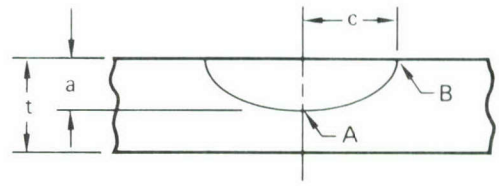

$a \leqslant c$								
i	j							
	A				B			
	0	1	2	3	0	1	2	3
0	−0.333	−1.047	4.618	−3.547	0.426	0.044	−2.109	1.889
1	1.516	1.735	−9.740	8.120	0.654	0.090	3.329	−3.108
2	−0.581	−0.590	5.441	−4.824	−0.385	−0.121	−1.089	1.273
3	0.076	0.026	−0.669	0.669	0.054	0.027	0.096	−0.150

$a > c$								
i	j							
	A				B			
	0	1	2	3	0	1	2	3
0	0.0955	−0.0892	0.358	−0.28	0.000788	0.0154	0.00607	0.0177
1	0.634	0.511	−1.875	1.232	0.956	−0.0992	−0.0396	−0.116
2	0.624	−0.681	1.698	−0.1787	0.281	0.167	−0.0356	0.258
3	−0.676	0.385	−0.55	−0.341	−0.494	−0.0426	0.314	−0.268

GP78-0753-76

SOLUTION DEVELOPMENT

Slice Model - The slice synthesis approach used herein was developed by W. T. Fujimoto, Reference 5. Application of the approach to computation of surface flaw stress intensities is summarized herein.

As shown in Figure A-6, the three dimensional surface flaw is idealized as a system of slices in the xy plane, each containing a center crack whose length is determined by the locations thru the thickness at which the slice was taken. Each slice is considered to react independently to the applied stress, σ, but are coupled through the introduction of pressure distribution, p*, acting on the faces of the cracks. The pressure p*, is determined by a second system of slices in the zy plane. Each of the zy slices contains an edge crack of depth a(x) over which the pressure, p*, acts in opposition to that applied to the center crack slices.

Thus there are two slice systems: center cracks, and edge cracks. These systems are coupled by the pressure distribution p* acting on the crack surfaces of each system and causing the displacements of the two systems to be equal.

Using the crack face pressure distribution, stress intensity factors at A and B can be determined:

$$K_A = \int_o^{a_o} p^* (o,z)\ g(z,a_o)_{e.c.}\ dz \qquad (A\text{-}3)$$

$$K_B = \int_{-c_o}^{c_o} \{(\sigma - p^* (x,o)\}\ g(x,c_o)_{c.c.}\ dx \qquad (A\text{-}4)$$

where for the surface flaw we have assumed

$$p^* (x,z) = A + Bx + Cx^2 + Dz + Ez^2 + Fxz + Gx^2z + Hxz^2 + Ix^2z^2 \qquad (A\text{-}5)$$

and the coefficients A, B, ...I are determined by the requirements for continuity of displacements, through the expression,

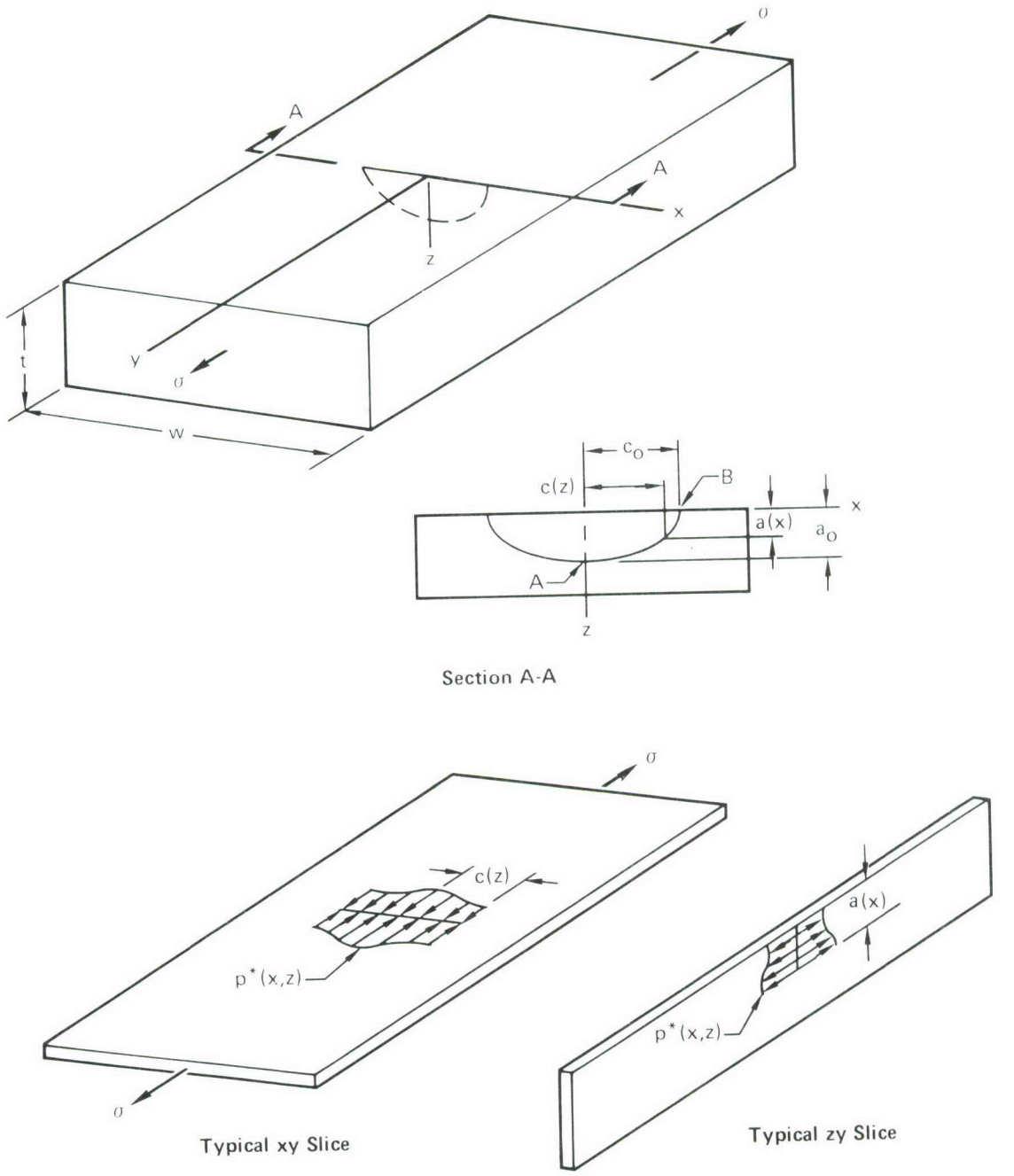

Figure A-6
Surface Flaw Idealization

$$\frac{1}{E}\int_{x}^{c(z)}\int_{-\xi}^{\xi}\{\sigma - p^*(u,z)\}\, g(u,\xi)_{c.c.}\, du\, g(x,\xi)_{c.c.}\, d\xi$$

$$= \frac{1}{E_s}\int_{z}^{a(x)}\int_{o}^{\xi} p^*(x,u)\, g(u,\xi)_{e.c.}\, du\, g(z,\xi)_{e.c.}\, d\xi \qquad \text{(A-6)}$$

where Fujimoto, Reference 5, defines the modulus of the edge crack slices as,

$$\frac{E_s}{E} = \left\{\frac{1}{1-\mu^2}\int_{o}^{\pi/2}\left[\sin^2\phi + \left(\frac{c_o}{a_o}\right)^2\cos^2\phi\right]^{1/2} d\phi - 1\right\}\frac{a_o}{c_o} \qquad \text{(A-7)}$$

and μ is Poisson's ratio.

The function $g(x,\xi)$ used in Equations A-3 to A-6 above is the universal weight function for the center crack, $g_{c.c.}$, or the edge crack, $g_{e.c.}$. The weight function is defined as

$$g(x,\xi) = \frac{E}{K(\xi)}\frac{\partial v(x,\xi)}{\partial \xi} \qquad \text{(A-8)}$$

where $K(\xi)$ is the stress intensity factor for any given fixed load distribution acting on the given flaw type having length, ξ, and $v(x,\xi)$ is the crack surface displacement at any point, x, corresponding to the same fixed load distribution. For a center crack of length 2a in a plate of width, W, the stress intensity factor due to an applied uniform stress, σ, and corresponding displacement at any x are given by Sneddon and Lowengrub, Reference 6, as

$$K(a) = \sigma\sqrt{W\tan\frac{\pi a}{W}}$$

$$v(x,a) = \frac{2W\sigma}{\pi E}\left[\log\left(\cos\frac{\pi x}{W} + \sqrt{\cos^2\frac{\pi x}{W} - \cos^2\frac{\pi a}{W}}\right)\right.$$

$$\left. -\log\left(\cos\frac{\pi a}{W}\right)\right] \qquad \text{(A-9)}$$

The weight function for the center crack is

$$g(x,a)_{c.c.} = \frac{E}{K(a)} \frac{\partial v(x,a)}{\partial a}$$

$$= 2 \left\{ \frac{\cos \frac{\pi a}{W} \sin \frac{\pi a}{W}}{\cos \frac{\pi x}{W} \sqrt{\cos^2 \frac{\pi x}{W} - \cos^2 \frac{\pi a}{W}} - \cos^2 \frac{\pi x}{W} + \cos^2 \frac{\pi a}{W}} \right. \tag{A-10}$$

$$\left. + \tan \frac{\pi a}{W} \right\} / \sqrt{W \tan \frac{\pi a}{W}}$$

For the edge crack slices, the weight function developed by Fujimoto, Reference 5, was used. This solution allows the edge crack slices to bend as the crack approaches the back face, thus predicting an out of plane deformation of the plate for deep cracks. To eliminate this bending, another weight function was developed based on the double edge crack stress intensity factor and displacement solutions of Tada, Reference 3. The weight function in this case was formulated in the same manner as that of Fujimoto.

The solution scheme to find p* is the same as that of Fujimoto; p* is expressed as a power series (from Equation A-5)

$$p^*(x,z) = \sum_{i=0}^{2} \sum_{j=0}^{2} \alpha_{ij} x^i z^j \tag{A-11}$$

and Equation A-6 can be rewritten as

$$Y(x,z) = \sum_{i=0}^{2} \sum_{j=0}^{2} \alpha_{ij} X(x,z)_{ij} \tag{A-12}$$

where

$$Y(x,z) = \sigma \int_{x}^{c(z)} \int_{-\xi}^{\xi} g(u,\xi)_{c.c.} \, du \, g(x,\xi)_{c.c.} \, d\xi \tag{A-13}$$

$$X(x,z)_{ij} = \int_{x}^{c(z)} \int_{-\xi}^{\xi} x^i z^j \, g(u,\xi)_{c.c.} \, du \, g(x,\xi)_{c.c.} \, d\xi \tag{A-14}$$

$$+ \frac{E}{E_s} \int_{z}^{a(x)} \int_{o}^{\xi} x^i z^j \, g(u,\xi)_{e.c.} \, du \, g(z,\xi)_{e.c.} \, d\xi$$

To assure that the coefficients, α_{ij}, represent the displacements over the entire crack face, the continuity expression is evaluated at 13 points described by Figure A-7. Then a multiple linear regression scheme is used to determine α_{ij}. Once α_{ij} are found, the stress intensity factors at A and B become (from Equations A-1 and A-2).

$$K_A = \frac{E}{E_s} \sum_{j=0}^{2} \int_{o}^{a_o} \alpha_{oj} z^j g(z,a_o)_{e.c.} \, dz \qquad \text{(A-15)}$$

$$K_B = \sigma\sqrt{W \tan \frac{\pi c}{W}} - \sum_{i=0}^{2} \int_{-c_o}^{c_o} \alpha_{io} x^i g(x,c_o)_{c.c.} \, dx \qquad \text{(A-16)}$$

ANALYSIS OF PLATE RESTRAINT

Because shear stresses acting on the faces of the "free" edge crack slice are ignored in the slice synthesis model, these slices displace as shown in Figure A-7. In reality, these types of displacements do not occur because of plate stiffness. Thus the model requires an estimate of the effect of plate stiffness in restraining out of plane deflection of "free" edge crack slices. The following paragraphs describe a development of a restrained edge crack element based on analyses using NASTRAN three dimensional finite element results.

Analyses were performed to determine the effect of rotational restraint offered by the plate to the edge crack slices. As shown in Figure A-8, the stress intensity, and hence displacements, for a "free" edge crack can be represented as

$$K_{free} = K_{fixed} + K_m \qquad \text{(A-17)}$$

where

K_{free} is the stress intensity for a "free" edge crack slice

K_{fixed} is the stress intensity for a "fixed" edge crack slice

and K_m is the stress intensity for an edge crack slice subjected to moments representing load eccentricity

Values of stress intensity intermediate to free and fixed can be represented as

$$K_{restrained} = K_{fixed} + K_m' \qquad \text{(A-18)}$$

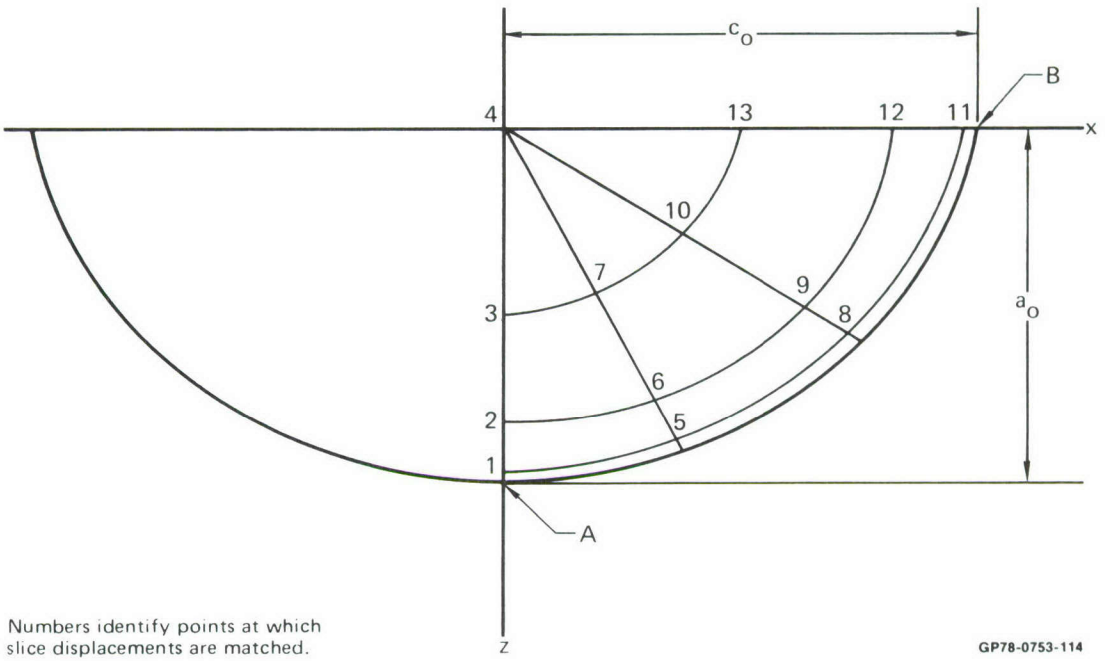

Figure A-7
Surface Flaw Model

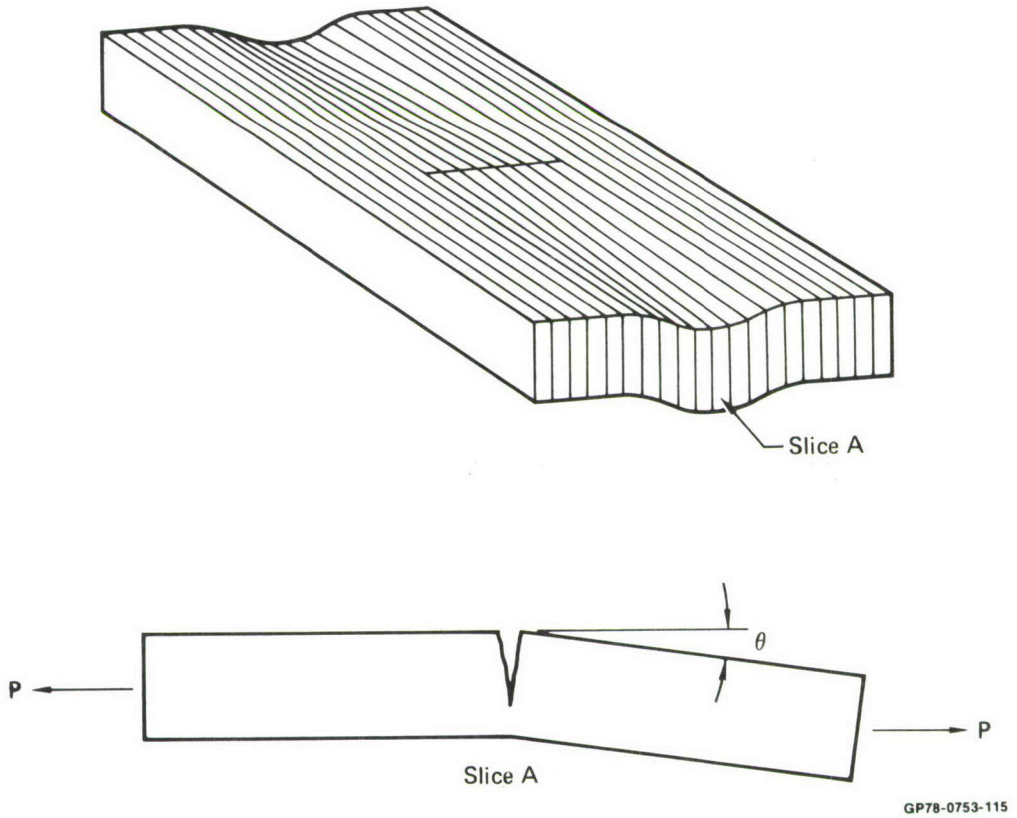

Figure A-8
Deflection of Edge Crack Slices Without Moment Restraint

where K_m' is between zero, the value representing 'fixed' edge crack behavior, and the value representing 'free' edge crack behavior.

$$K_{fixed} = \sigma \lambda_1 \lambda_2 \qquad \text{(A-19)}$$

$$\text{with } \lambda_1 = \sqrt{\frac{2t}{\pi a} \tan \frac{\pi a}{2t}}$$

$$\lambda_2 = 1. + 0.122 \cos^4 \frac{\pi a}{2t}$$

$$K_m' = \sigma \lambda_1 \frac{(\lambda_3 - \lambda_2)}{1 + \frac{\lambda_7 \lambda_5 t}{c}} \qquad \text{(A-20)}$$

$$\text{with } \lambda_3 = 1.122 - 3.367 \frac{a}{t} + 1.8276 \left(\frac{a}{t}\right)^2 + 2.5959 \left[\tan \frac{\pi a}{2t}\right]^{1.014}$$

$$\lambda_5 = \left(\frac{a/t}{1-a/t}\right)^2 [5.93 - 19.69 \left(\frac{a}{t}\right) + 37.14 (a/t)^2 - 35.84 \left(\frac{a}{t}\right)^3 + 13.12 \left(\frac{a}{t}\right)^4]$$

$$K_{restrained} = K_{fixed} + K_m' = \sigma \lambda_1 [\lambda_2 + (\lambda_3 - \lambda_2)/(1 + \frac{\lambda_7 \lambda_5 t}{c})] \qquad \text{(A-21)}$$

If λ_7 is zero, the stress intensity is that for a "free" edge crack slice and if λ_7 is very large, the stress intensity approaches that for a "fixed edge" crack slice. Analyzing the surface flaw geometry shown in Figure A-9, using Equation A-21 to determine the stress intensities and displacements for the edge crack slices, curves are obtained, labeled "FREE" and "FIXED".

To obtain an estimate of the restraint offered by the plate to the surface flaw displacements, three NASTRAN finite element analyses were performed. These three dimensional analyses were performed for an embedded circular flaw in a large plate, a semi-circular surface flaw in a large plate, and for a surface

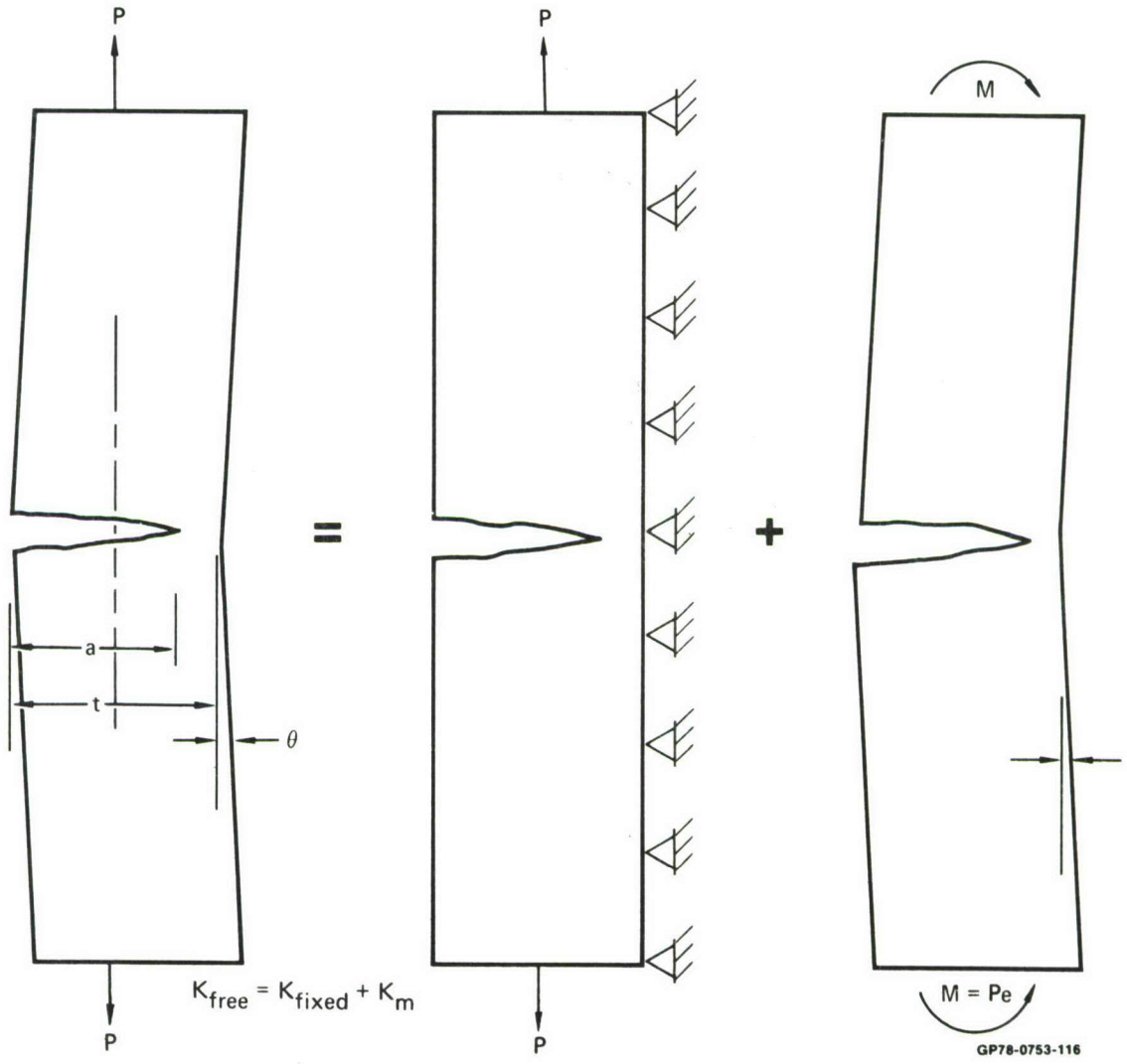

Figure A-9
Stress Intensity Computation for a Free Edge Crack Slice

flaw having a/2c = 0.1 and a/t = 0.7. The first two analys were used to show correlation with accepted stress intensit solutions for these problems, the third analysis was used t determine restraint to crack surface displacement provided the plate and allowing λ_7 to be determined.

NASTRAN finite element results are summarized in Tabl Estimates of stress intensity were developed through analy the crack surface displacements. A displacement function form

$$v = [Ax + Bx^2 + Cx^3]^{1/2} \tag{A-22}$$

was assumed, and the terms A, B, and C, evaluated by least-squares linear regression analysis. The stress intensity was evaluated by use of the relationship

$$K = \frac{1}{2}\sqrt{\pi r_o}\,\frac{E}{(1-\nu^2)} \tag{A-23}$$

where r_o is the radius of curvature at x=0

$$r_o = \frac{[1 + (\frac{dv}{dx})^2]^{3/2}}{\frac{d^2v}{dx^2}} = \frac{1}{2}A \tag{A-24}$$

$$K = \sqrt{\frac{\pi}{8}A}\,\frac{E}{(1-\nu^2)} \tag{A-25}$$

$$\frac{K}{\sigma\sqrt{\pi a}} = \sqrt{\frac{A}{8a}}\,\frac{E}{\sigma(1-\nu^2)} \tag{A-26}$$

Estimates using this procedure are summarized in Table A-2 The theoretical stress intensity for a circular flaw in a solid is $\frac{K}{\sigma\sqrt{\pi a}} = \frac{2}{\pi} = 0.0637$. Table A-2 indicates the value obtained from the NASTRAN analysis is 0.608, an error of 4.77%. The analysis results for the other problems solved with NASTRAN were normalized by $\frac{2}{\pi}/0.608$, bringing the stress intensity estimate for the circular flaw in agreement with the theoretical value. The NASTRAN estimate for the semi-circular surface flaw, after normalizing by this factor, is in good agreement with other solutions for this problem. The estimate obtained from the NASTRAN analysis is $\frac{K}{\sigma\sqrt{\pi a}} = 0.647$, from Smith and Sorensen (Reference 3) is 0.653, from Hartranft and Sih (Reference 8) is 0.668, and from Tracey (Reference 9) is 0.662.

TABLE A-2
NASTRAN FINITE ELEMENT RESULTS
NORMALIZED STRESS INTENSITY

Flaw Geometry	Location	$\frac{K}{\sigma\sqrt{\pi a}}$	$\frac{K_{Norm}}{\sigma\sqrt{\pi a}}$
Circular Flaw in Solid	–	0.608	0.637
Semicircular Surface Flaw, a/t = 0.7	Depth	0.618	0.647
	Surface	0.741	0.776
Semi-elliptic Surface Flaw, a/t = 0.7, a/2c = 0.1	Depth	1.601	1.676
	Surface	0.479	0.502

GP78-1063-7

The NASTRAN analysis results for the surface flaw with a/2c = 0.1 and a/t = 0.7 was used as a basis to select λ_7 in the slice synthesis model. When this was accomplished, the value $\lambda_7 = 0.75$ was found by trial and error to yield results consistent with the NASTRAN analysis, as demonstrated in Figure A-10. This value of λ_7 was used in all other analyses, and good agreement with Raju and Newman's results was obtained, as evidenced by Figures A-1, A-2, and A-10.

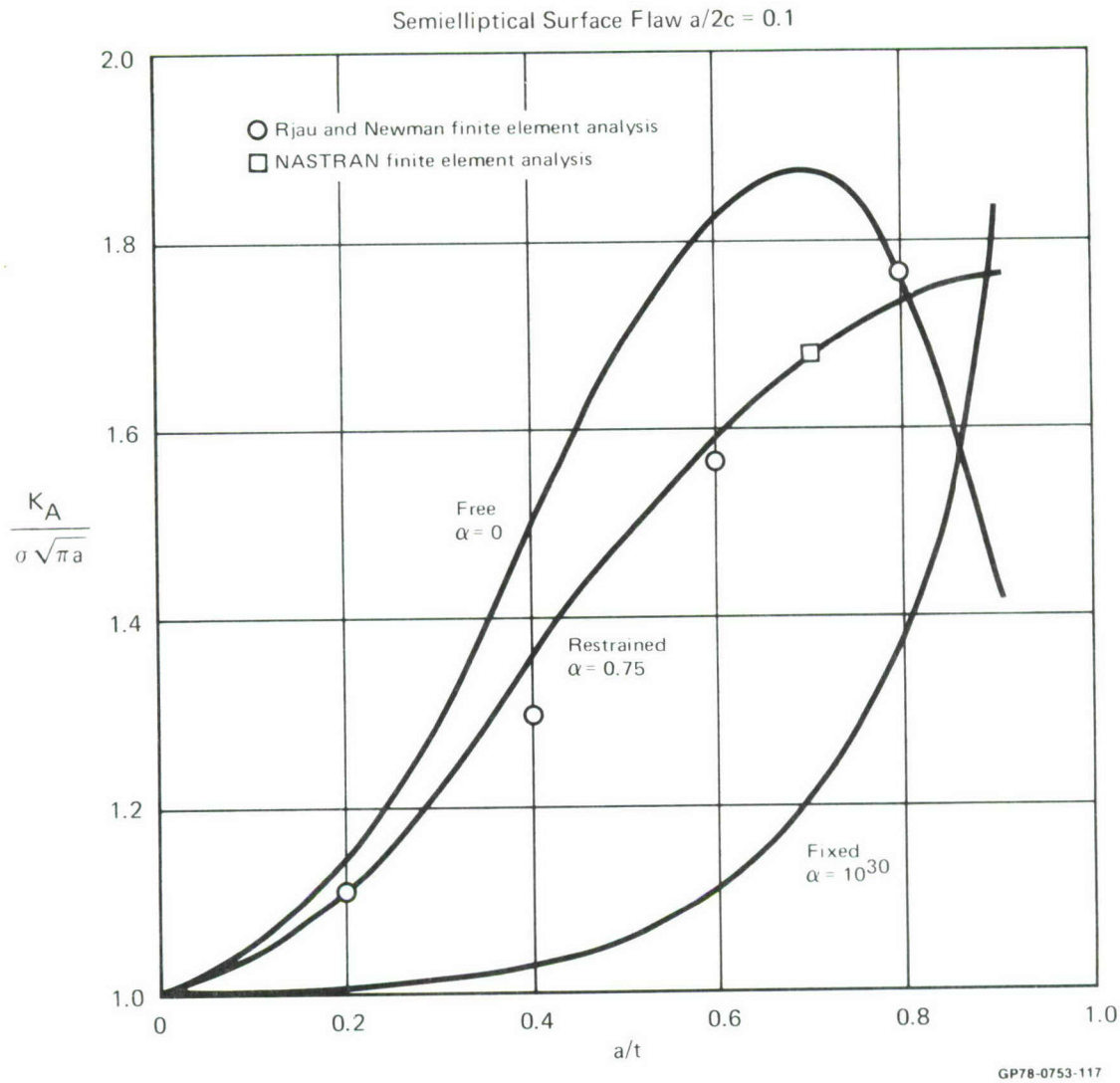

Figure A-10
Selection of Plate Restraint Coefficient to Match Finite Element Results

REFERENCES

1. Raju, I. S. and Newman, J. C., Jr., "Improved Stress-Intensity Factors for Semi-Elliptical Surface Cracks in Finite-Thickness Plates", NASA TM X-7285, August 1977.

2. Rice, J. R. and Levy, N., "The Part-Through Surface Crack in an Elastic Plate", Trans. ASME. J. Appl. Mech. Paper No. 71-APM-20, 1970.

3. Smith, F. W., and Sorensen, D. R., "The Semi-Elliptical Surface Crack - A Solution by the Alternating Method", International Journal of Fracture, Vol. 12, No. 1, February 1972

4. Kobayashi, A. S., "Surface Flaws in Plates in Bending", Proceedings of the 12th Annual Meeting of the Society of Engineering Science, Austin, Texas, October 1975.

5. Fujimoto, W. T., "Determination of Crack Growth and Fracture Toughness Parameters for Surface Flaws Emanating from Fastener Holes", MDC Report A4093, 17 March 1976, Presented at the AIAA; ASME/SAE 17th SDM Meeting, Valley Forge, Pa., 4-7 May 1976.

6. Sneddon, I. N., and Lowengrub, M., Crack Problems in the Classical Theory of Elasticity, John Wiley and Sons, 1969.

7. Tada, H., Paris, P. C., and Irwin, G. R., The Stress Analysis of Cracks Handbook, Del Research Corporation, Hellertown, Pa., 1973.

8. Hartranft, R. J., and Sih, G. C., "Solving Edge and Surface Crack Problems by an Alternating Method", Mechanics of Fracture-1-Methods of Analysis and Solutions of Crack Problems, G. C. Sih Editor, 1973.

9. Tracey, D. M., "3-D Elastic Singularity Element for Evaluation of K Along an Arbitrary Crack Front", International Journal of Fracture, Vol. 9, No. 3, September 1973.

APPENDIX B

SURFACE FLAW GROWTH ANALYSIS ROUTINE

INPUT DEFINITIONS

The computer program has the following inputs:

1. title describing material and product form for reference (TITLE)
2. critical stress intensity factor (KSUBC)
3. number of points in da/dN table (NDADN)
4. stress intensity factor range and crack growth rate for each point in da/dN table (DK(I), DADNA (I)).
5. initial surface flaw depth and length, material thickness, width and maximum stress in spectrum of interest (A, C, T, W, SMAX)
6. number of cycles analyzed between printout of stress intensity factor and crack growth (NPRNT).

DESCRIPTION OF OUTPUT

The program outputs include title, A, C, T, W, SMAX, and a summary of a, β_A, K_A, and c, β_B, K_B printed at the end of each specified print interval. The print interval is reduced by a factor of ten where a exceeds 0.8t and again when transition to a through crack occurs. The stress intensity correction factors, β_A, and β_B are defined as

$$\beta_A = \frac{K_A}{\sigma\sqrt{\pi a}}$$

$$\beta_B = \frac{K_B}{\sigma}\sqrt{\frac{\cos\frac{\pi c}{W}}{\pi c}}$$

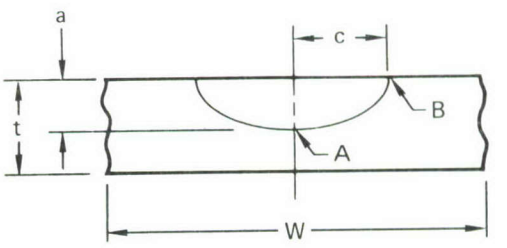

GP78-0753-80

LISTING OF PROGRAM

```
C     THIS PROGRAM COMPUTES CRACK GROWTH AT SURFACE AND THROUGH DEPTH
C     FOR A SEMIELLIPTICAL SURFACE FLAW. STRESS INTENSITY FACTORS
C     ARE BASED ON MCAIR SLICE SYNTHESIS MODEL RESULTS. CRACK
C     FRONT PENETRATION OF BACK FACE IS PREDICTED BY LINEAR EXTRAPOLATION
C     OF STRESS INTENSITY FACTOR RESULTS. ASSUMED LOADING IS CONSTANT
C     AMPLITUDE, R=0., SINUSIODAL LOADING. PROGRAM WAS DEVELOPED BY
C     C.R.SAFF OF MCDONNELL AIRCRAFT CO., ST. LOUIS, MISSOURI,
C     TELEPHONE (314) 232-3356.
C
      INTEGER TITLE(20)
      REAL AC(4,4),BC(4,4),AD(4,4),BD(4,4),DADNA(25),DK(25),KSUBC
      DATA AC/-0.333,1.516,-0.581,0.076,-1.047,1.735,-0.59,0.026,
     &4.618,-9.74,5.441,-0.669,-3.547,8.12,-4.824,0.669/
      DATA BC/0.426,0.654,-0.385,0.054,0.044,0.09,-0.121,0.027,
     &-2.109,3.329,-1.089,0.096,1.889,-3.108,1.273,-0.15/
      DATA AD/0.0955,0.634,0.624,-0.676,-0.0892,0.511,-0.681,
     &0.385,0.358,-1.875,1.698,-0.550,-0.280,1.232,-0.1787,-0.341/
      DATA BD/0.000788,0.956,0.281,-0.494,0.0154,-.0992,0.167,-0.0426,
     &0.00607,-.0396,-0.0356,0.314,0.0177,-0.116,0.258,-0.268/
      PI=3.14159265
C
C      INPUTS ARE - TITLE
C                   KSUBC
C                   NDADN
C                   DK(25),DADNA(25)
C                   A,C,T,W,SMAX
C                   NPRNT
C
C     MATERIAL PARAMETERS
C
C     TITLE DESCRIBES MATERIAL & PRODUCT FORM FOR REFERENCE
C     KSUBC=CRITICAL STRESS INTENSITY FACTOR FOR MATERIAL THICKNESS
C     NDADN=NO. OF POINTS IN DA/DN TABLE
C     DK(I)=DELTA K VALUES OF POINTS IN DA/DN TABLE
C     DADNA(I)=DA/DN VALUES OF POINTS IN DA/DN TABLE
C
C     GEOMETRIC PARAMETERS
C
C     A=INITIAL SURFACE FLAW DEPTH
C     C=INITIAL SURFACE FLAW HALF LENGTH
C     T=MATERIAL THICKNESS - CRACK DEPTH DIRECTION
C     W=MATERIAL WIDTH - CRACK SURFACE DIRECTION
C     SMAX=MAXIMUM SPECTRUM STRESS APPLIED
C
C     NPRNT=NO. OF CYCLES BETWEEN PRINTOUT OF K DATA AND GROWTH
C
      READ(5,1000) TITLE
      WRITE(6,1010) TITLE
      READ(5,1020) KSUBC
```

```
      READ(5,1030) NDADN
      DO 10 I=1,NDADN
      READ(5,1020) DK(I),DADNA(I)
      DK(I)=ALOG10(DK(I))
   10 DADNA(I)=ALOG10(DADNA(I))
      READ(5,1020) A,C,T,W,SMAX
      READ(5,1030) NPRNT
      WRITE(6,1040) A,C,T,W,SMAX
      ICHK=0
      IBRK=0
      CYC=0.
      NP=0
      WRITE(6,1050)
C
C     DO LOOP 80 COMPUTES STRESS INTENSITY FACTORS AND GROWTH AT
C     DEPTH AND SURFACE OF FLAW
C
      DO 80 I=1,100000
      CYC=CYC+1
      IF(ICHK.EQ.1) GO TO 40
      BETAA=0.
      BETAB=0.
      DO 20 J1=1,4
      J=J1-1
      DO 20 K1=1,4
      K=K1-1
      ACOEF=AC(J1,K1)
      BCOEF=BC(J1,K1)
      IF(A.GT.C) ACOEF=AD(J1,K1)
      IF(A.GT.C) BCOEF=BD(J1,K1)
      BETAA=BETAA+ACOEF*(C/A)**(J/2.)*(A/T)**K
   20 BETAB=BETAB+BCOEF*(C/A)**(J/2.)*(A/T)**K
      BETAB=BETAB*SQRT(A/C)
C
C     STRESS INTENSITY FACTOR EXPRESSIONS ARE ASSUMED GOOD UNTIL
C     FLAW DEPTH EXCEEDS 90% OF THICKNESS. VALUES AT A/T=0.8 AND
C     A/T=0.9 ARE USED FOR EXTRAPOLATIONS BEYOND A/T=0.9.
C
      IF(A.LT.0.8*T) GO TO 50
      NPRNT=NPRNT/10
      IF(NPRNT.LT.1) NPRNT=1
      ICHK=1
      A1=0.8*T
      A2=0.9*T
      BA1=0.
      BA2=0.
      BB1=0.
      BB2=0.
      DO 30 J1=1,4
      J=J1-1
      DO 30 K1=1,4
      K=K1-1
      ACOEF=AC(J1,K1)
      BCOEF=BC(J1,K1)
      IF(A.GT.C) ACOEF=AD(J1,K1)
      IF(A.GT.C) BCOEF=BD(J1,K1)
```

```
      BA1=BA1+ACOEF*(C/A)**(J/2.)*(A1/T)**K
      BA2=BA2+ACOEF*(C/A)**(J/2.)*(A2/T)**K
      BB1=BB1+BCOEF*(C/A)**(J/2.)*(A1/T)**K
   30 BB2=BB2+BCOEF*(C/A)**(J/2.)*(A2/T)**K
      BB1=BB1*SQRT(A/C)
      BB2=BB2*SQRT(A/C)
   40 BETAB=(A-A1)/(A2-A1)*(BB2-BB1)+BB1
      BETAA=BETAB*BA1/BB1
   50 AK=BETAA*SMAX*SQRT(PI*A)
      BK=BETAB*SMAX*SQRT(PI*C/COS(PI*C/W))
      IF(IBRK.NE.1) GO TO 60
      WRITE(6,1070) CYC,A,BETAA,AK,C,BETAB,BK
      WRITE(6,1100)
      IBRK=IBRK+1
      GO TO 70
   60 IF(I.LT.NP) GO TO 70
      NP=NP+NPRNT
      WRITE(6,1070) CYC,A,BETAA,AK,C,BETAB,BK
C
C     FRACTURE IS ASSUMED TO OCCUR WHENEVER THE STRESS INTENSITY
C     FACTOR AT EITHER THE SURFACE OR THE DEPTH EXCEEDS KSUBC.
C
   70 IF(AK.GT.KSUBC) GO TO 120
      IF(BK.GT.KSUBC) GO TO 130
C
C     DA/DN LOOK UP IS LOG(DA/DN) VS. LOG(DELTA K). CRACK GROWTH RATE
C     CURVE IN THE DEPTH DIRECTION IS ASSUMED SAME AS ALONG SURFACE.
C
      AK1=ALOG10(AK)
      BK1=ALOG10(BK)
      CALL TLU(DK,DADNA,NDADN,AK1,ADADN)
      CALL TLU(DK,DADNA,NDADN,BK1,BDADN)
      ADADN=10.**ADADN
      BDADN=10.**BDADN
      A=A+ADADN
      C=C+BDADN
C
C     CRACK IS ASSUMED TO GROW AT A FIXED A/C RATIO AFTER CRACK
C     FRONT BREAKTHROUGH UNTIL BETAB EXCEEDS 1. THEN FLAW IS TREATED
C     AS A CENTER CRACK OF LENGTH 2C.
C
      IF(BETAB.GE.1.) GO TO 90
      IF(A.LT.T) GO TO 80
      IF(IBRK.GE.1) GO TO 80
      WRITE(6,1060)
      IBRK=IBRK+1
   80 CONTINUE
   90 WRITE(6,1080)
      WRITE(6,1070) CYC,A,BETAA,AK,C,BETAB,BK
      A=C
      WRITE(6,1090)
      WRITE(6,1070) CYC,A
      DO 110 I=1,100000
      CYC=CYC+1
```

```
      CK=SMAX*SQRT(PI*A/COS(PI*A/W))
      IF(ICYC.LT.NP) GO TO 100
      WRITE(6,1070) CYC,A
      NP=NP+NPRNT-1
  100 IF(CK.GT.KSUBC) GO TO 140
      CK=ALOG10(CK)
      CALL TLU(DK,DADNA,NDADN,CK,DADN)
      DADN=10.**DADN
      A=A+DADN
  110 CONTINUE
      STOP
  120 WRITE(6,1110)
      WRITE(6,1070) CYC,A,BETAA,AK,C,BETAB,BK
      STOP
  130 WRITE(6,1120)
      WRITE(6,1070) CYC,A,BETAA,AK,C,BETAB,BK
      STOP
  140 WRITE(6,1130)
      WRITE(6,1070) CYC,A
      STOP
 1000 FORMAT(20A4)
 1010 FORMAT(1H1,/20A4)
 1020 FORMAT(5F10.0)
 1030 FORMAT(I10)
 1040 FORMAT(/'     A0 = ',F8.3,'     C0 = ',F6.3,
     &/'      T = ',F8.3,'      W = ',F6.3,/'  SMAX = ',F8.3)
 1050 FORMAT(/T4,'CYC',T16,'A',T24,'BETAA',T34,'KA',T44,'C',T52,
     &'BETAB',T62,'KB')
 1060 FORMAT(' CRACK FRONT PENETRATES BACK FACE AT')
 1070 FORMAT(F8.0,2F10.4,F8.2,2F10.4,F8.2)
 1080 FORMAT(' SURFACE CRACK BECOMES THROUGH CRACK AT')
 1090 FORMAT(//' EQUIVALENT THROUGH CRACK LENGTH IS'/,
     &T4,'CYC',T16,'A')
 1100 FORMAT(1H )
 1110 FORMAT(/' FRACTURE AT A')
 1120 FORMAT(/' FRACTURE AT C')
 1130 FORMAT(/' THROUGH CRACK FRACTURE')
      END
C
C
C
      SUBROUTINE TLU(X,Y,N,XVAL,YVAL)
      DIMENSION X(N),Y(N)
      IF(X(N).GE.XVAL) GO TO 10
      I=N
      GO TO 30
   10 DO 20 I=1,N
      IF(X(I).GE.XVAL) GO TO 30
   20 CONTINUE
   30 IF(I.EQ.1) I=2
      YVAL=(Y(I)-Y(I-1))/(X(I)-X(I-1))*(XVAL-X(I-1))+Y(I-1)
      RETURN
      END
```

SAMPLE INPUT

```
HP 9-4-.30 STEEL IN SALT WATER AT 10 CPS
 120.0000  212.0000  212.0000
       17        10.
  13.0000   0.87E-6
  14.0000   1.06E-6
  16.0000   1.45E-6
  18.0000   2.05E-6
  20.0000   2.80E-6
  22.5000   4.00E-6
  25.0000   5.40E-6
  30.0000   9.00E-6
  35.0000   1.30E-5
  40.0000   1.85E-5
  45.0000   2.40E-5
  50.0000   3.00E-5
  60.0000   4.50E-5
  70.0000   6.20E-5
  80.0000   8.90E-5
  90.0000   1.45E-4
 100.0000   3.00E-4
    0.008     0.011       0.26         1.       185.
      100
```

OUTPUT FOR SAMPLE INPUT

HP 9-4-.30 STEEL IN SALT WATER AT 10 CPS

AO = .008 CO = .011
T = .260 W = 1.000
SMAX = 185.000

CYC	A	BETAA	KA	C	BETAC	KB
1.	.0080	.7747	22.73	.0110	.6412	22.06
100.	.0084	.7703	23.18	.0114	.6467	22.64
200.	.0089	.7662	23.67	.0118	.6520	23.24
300.	.0093	.7624	24.18	.0123	.6570	23.87
400.	.0098	.7589	24.71	.0128	.6616	24.51
500.	.0104	.7556	25.27	.0133	.6659	25.18
600.	.0110	.7526	25.85	.0139	.6700	25.88
700.	.0116	.7498	26.47	.0145	.6738	26.60
800.	.0122	.7473	27.12	.0151	.6773	27.35
900.	.0129	.7450	27.80	.0159	.6806	28.13
1000.	.0137	.7429	28.52	.0167	.6837	28.95
1100.	.0145	.7410	29.28	.0175	.6866	29.80
1200.	.0154	.7393	30.08	.0184	.6893	30.70
1300.	.0163	.7377	30.91	.0194	.6919	31.63
1400.	.0173	.7362	31.79	.0205	.6944	32.60
1500.	.0184	.7350	32.70	.0216	.6967	33.61
1600.	.0195	.7339	33.66	.0228	.6988	34.66
1700.	.0207	.7330	34.67	.0241	.7008	35.76
1800.	.0221	.7324	35.73	.0256	.7026	36.90
1900.	.0235	.7319	36.85	.0271	.7043	38.11
2000.	.0250	.7315	38.04	.0288	.7059	39.38
2100.	.0267	.7312	39.29	.0307	.7075	40.73
2200.	.0286	.7308	40.62	.0327	.7093	42.16
2300.	.0306	.7305	42.00	.0348	.7112	43.66
2400.	.0327	.7303	43.45	.0372	.7129	45.23
2500.	.0350	.7302	44.97	.0397	.7148	46.88
2600.	.0375	.7302	46.57	.0424	.7166	48.61
2700.	.0402	.7303	48.24	.0454	.7184	50.43
2800.	.0431	.7306	50.00	.0485	.7203	52.34
2900.	.0462	.7310	51.86	.0520	.7221	54.36
3000.	.0496	.7315	53.82	.0558	.7240	56.50
3100.	.0533	.7322	55.90	.0599	.7261	58.79
3200.	.0573	.7329	58.11	.0644	.7283	61.23
3300.	.0616	.7336	60.45	.0693	.7309	63.84
3400.	.0664	.7345	62.93	.0746	.7337	66.64
3500.	.0716	.7355	65.59	.0805	.7367	69.65
3600.	.0773	.7371	68.46	.0870	.7398	72.92
3700.	.0835	.7396	71.65	.0944	.7426	76.50
3800.	.0905	.7426	75.24	.1028	.7461	80.57
3900.	.0986	.7479	79.55	.1132	.7490	85.33
4000.	.1086	.7561	85.10	.1266	.7520	91.35
4100.	.1230	.7750	94.34	.1488	.7529	100.79
FRACTURE AT C						
4177.	.1501	.8084	113.01	.1908	.7632	120.30

APPENDIX C

CRACK GROWTH ANALYSIS ROUTINE INCLUDING ENVIRONMENT-LOAD INTERACTION EFFECTS

INPUT DEFINITIONS

The computer program has the following inputs:

Analysis inputs include

1. title identifying problem (TITLE)
2. threshold stress intensity factor (DELKTH)
3. initial crack length (AZERO)
4. stress ratio correction parameter, plastic zone size correction factor, and shut-off overload ratio (ALPHA, ROOT, OLMAX)
5. stress intensity correction factor type (ICOR)
6. for single and double cracks from holes (ICOR = 1 or 2, respectively), radius of the hole and shortest distance perpendicular to the load from hole center to the plate edge (RADIUS, ECCEN) are input; for constant shape semi-elliptical surface flaws (ICOR = 3) the flaw aspect ratio, plate thickness, and shortest distance from crack center to plate edge, (A, C, THICK, ECCEN) are input; and for a through crack (ICOR = 4), the shortest distance from the crack center to plate edge (ECCEN) is input.
7. if a stress intensity factor correction table is to be used, the number of points in the table (NPTS), and the crack length and K correction factors for each point (TABLEA(I), TABLEB(I)), are input.
8. number of spectrum repetitions to be analyzed (NBLKS)
9. design limit stress (DLS)
10. number of flights between printouts of accumulated time, crack length, and reference K (PRTFLTS)
11. index for consideration of environmental effects, 0 if no load-environment interaction is to be considered, 1 if load-environment interaction will be considered

Material data inputs include one data set if load-environment interaction is not considered, two data sets if load-environment interaction is considered. The two data sets describe high frequency, sinusoidal wave crack growth rate data and low frequency, trapezoidal wave data. The single data set used for analysis without load-environment interaction is the same as the first of the following sets.

High frequency, sinusoidal wave data (used with or without load-environment interaction effects)

1. title identifying material, product form, and loading (TITLE)
2. critical stress intensity factor for material thickness, monotonic tensile yield stress, cyclic tensile yield stress (KSUBC, TYLD, CYLD)
3. number of points in da/dN table and sine wave frequency (NDADNA, FA)
4. ΔK and da/dN values of points in table (DKA(I), DADNA(I))

Low frequency, trapezoidal wave data (used only for load-environment interaction effects)

1. title identifying material, product form, and loading (TITLE 2)
2. critical stress intensity factor for material thickness, monotonic tensile yield stress, cyclic tensile yield stress (KSUBC, TYLD, CYLD)
3. number of points in da/dN table and trapezoidal wave frequency (NDADNB, FB)
4. ΔK and da/dN values of points in table (DKB(I), DADNB(I))

Spectrum inputs include:

1. title identifying spectrum (TITLE)
2. number of stress levels in spectrum and number of flights (landings) represented by spectrum (NLYR, FLTS)
3. stress level and time increment for each half cycle (SMAX(I), TIME (I))

DESCRIPTION OF OUTPUT

The program outputs include titles of analysis, material, and spectrum input data sets, design limit stress (DLS), initial flaw length (AZERO), and a table of elapsed flights (landings), crack length, and reference stress intensity factor printed at the interval specified by PRTFLTS. When K_{max} exceeds K_c, fracture is predicted to occur and the flight in the spectrum, crack length at fracture, and K_{max} is printed.

LISTING OF PROGRAM

```
C     THIS PROGRAM COMPUTES SPECTRUM CRACK GROWTH
C     INCLUDING ACCELERATION DUE TO SUSTAINED LOADING
C     IN AN AGGRESSIVE ENVIRONMENT.  THE WILLENBORG
C     MODEL IS USED TO PREDICT SPECTRUM LOAD
C     INTERACTION EFFECTS.  A LINEAR SUMMATION APPROACH
C     IS USED TO PREDICT ENVIRONMENTAL ACCELERATION.
C     CYCLE-BY-CYCLE ANALYSIS IS USED.  PROGRAM WAS
C     DEVELOPED BY C.R.SAFF OF MCDONNELL AIRCRAFT CO.,
C     ST. LOUIS, MISSOURI, TELEPHONE (314) 232-3356.
C
      DIMENSION SMAX(1000),TIME(1000),CARRAY(100),SNARAY(100)
      INTEGER RETARD,TITLE(20)
      REAL KMAX,KMIN,KSUBC,KMXEFF,KMNEFF
      COMMON/A/A,RADIUS,ECCEN,AOC,THICK,NPTS,TABLEA(50),TABLEB(50)
      PI=3.14159265
      RETARD=0
C
C     READ AND ECHO INPUT DATA
C
C     ANALYSIS INPUTS INCLUDE-
C
C     TITLE WHICH IDENTIFIES PROBLEM
C     DELKTH=THRESHOLD STRESS INTENSITY FACTOR
C     AZERO=INITIAL CRACK LENGTH
C     ALPHA=STRESS RATIO CORRECTION
C     ROOT2=PLASTIC ZONE SIZE FACTOR
C     OLMAX=SHUT-OFF OVERLOAD RATIO
C     ICOR=STRESS INTENSITY FACTOR CORRECTION TYPE
C          1=SINGLE CRACK FROM HOLE
C          2=DOUBLE CRACK FROM HOLE
C          3=SEMI-ELLIPTICAL SURFACE FLAW (FIXED A/C)
C          4=THROUGH CRACK
C     RADIUS=RADIUS OF CRACKED HOLE
C     ECCEN=SHORTEST DISTANCE PERPENDICULAR TO LOAD
C           FROM HOLE CENTER TO PLATE EDGE
C     AOC=RATIO OF SURFACE CRACK DEPTH TO HALF LENGTH
C     THICK=PLATE THICKNESS
C     ECCEN=SHORTEST DISTANCE FROM CRACK CENTER TO PLATE EDGE
C     NPTS=NO. OF POINTS IN STRESS INTENSITY FACTOR CORRECTION TABLE
C     TABLEA(I),TABLEB(I)=CRACK LENGTH AND K-CORRECTION
C                         FACTOR VALUE FOR TABLE
C     NBLKS=NO. OF SPECTRUM REPETITIONS TO BE ANALYZED
C     DLS=DESIGN LIMIT STRESS
C     PRT FLTS=NO. OF FLIGHTS BETWEEN PRINTOUTS OF ACCUMULATED
C              TIME,CRACK LENGTH,AND REFERENCE K
C     NEN=INDEX FOR CONSIDERATION OF ENVIRONMENTAL EFFECTS
C         0=SINGLE DA/DN CURVE IS TO BE USED
C           NO FREQUENCY EFFECT CONSIDERED
```

```
C          1=ENVIRONMENTAL EFFECT WILL BE CONSIDERED
C            INPUT HIGH FREQ. SINE WAVE DATA &
C            LOW FREQ. TRAPEZOIDAL WAVE DATA
C
      READ(1,2200)  TITLE
      READ(1,1000) DELKTH
      READ(1,1000) AZERO
      READ(1,1000) ALPHA,ROOT2,CLMAX
      IF(ALPHA.LT.-1.85) ALPHA=-1.85
      READ(1,2000) ICOR
      OUTPUT, ICOR
      GO TO (10,10,20,30),ICOR
   10 READ(1,1000) RADIUS,ECCEN
      GO TO 40
   20 READ(1,1000) AOC,THICK,ECCEN
      GO TO 40
   30 READ(1,1000) ECCEN
   40 READ(1,2000) NPTS
      IF(NPTS.LE.0) GO TO 60
      OUTPUT,NPTS
      DO 50 I=1,NPTS
   50 READ(1,1000) TABLEA(I),TABLEB(I)
   60 READ(1,2000) NBLKS
      READ(1,1000) DLS
      READ(1,1000) PRTFLTS
      READ(1,2000) NEN
      WRITE(6,2300) TITLE
C
C     READ MATERIAL GROWTH RATE DATA
C
C     COMPUTE DA/DT AND DA/DN
C
      IF(NEN.EQ.0) GO TO 80
      CALL ENVIR(CARRAY,SNARAY,NDADN,KSUBC,TYLD,CYLD,
     &AA,BB,CC,DD)
      DO 70 I=1,NDADN
      SNARAY(I)=ALOG10(SNARAY(I)*(KSUBC-CARRAY(I))/KSUBC)
   70 CARRAY(I)=ALOG10(CARRAY(I))
      GO TO 100
C
C     DA/DN INPUTS INCLUDE-
C
C     TITLE DESCRIBES MATERIAL & PRODUCT FORM FOR REFERENCE
C     KSUBC=CRITICAL STRESS INTENSITY FACTOR FOR MATERIAL THICKNESS
C     TYLD=MONOTONIC YIELD STRESS
C     CYLD=CYCLIC YIELD STRESS
C     NDADN=NO. OF POINTS IN DA/DN TABLE
C     DK(I)=DELTA K VALUES OF POINTS IN DA/DN TABLE
C     DADNA(I)=DA/DN VALUES OF POINTS IN DA/DN TABLE
C
   80 READ(2,2200) TITLE
      READ(2,1000) KSUBC,TYLD,CYLD
      READ(2,1000) NDADN
      DO 90 I=1,NDADN
      READ(2,1000) CARRAY(I),SNARAY(I)
      SNARAY(I)=ALOG10(SNARAY(I)*(KSUBC-CARRAY(I))/KSUBC)
```

```
   90 CARRAY(I)=ALOG10(CARRAY(I))
      WRITE(6,2350) TITLE
C
C     READ SPECTRUM INPUT DATA
C
C     SPECTRUM DATA INPUTS INCLUDE-
C
C     TITLE WHICH IDENTIFIES SPECTRUM INPUT
C     NLYR=NO. OF STRESS LEVELS IN SPECTRUM
C     FLTS=NO. OF FLIGHTS (LANDINGS) REPRESENTED BY SPECTRUM
C     SMAX(I)=STRESS LEVEL FOR EACH HALF CYCLE
C     TIME(I)=TIME INCREMENT FOR EACH HALF CYCLE
C
  100 READ(4,2200) TITLE
      READ(4,2000) NLYR,FLTS
      DO 110 I=1,NLYR
      READ(4,1000) SMAX(I),TIME(I)
      SMAX(I)=SMAX(I)*DLS/100.
  110 CONTINUE
      WRITE(6,2350) TITLE
      WRITE(6,3460) NBLKS,DLS
C
C     SET UP FOR CYCLIC GROWTH ANALYSIS
C
      ZK=0.33045+0.15164*ALPHA-0.01476*ALPHA**2
      FR=CYLD/TYLD-1.
      ZK=ZK*(1.+0.6*FR-0.156*FR**2)
      SIGMAX=CYLD
      A=AZERO
      ASUBP=AZERO
      CALL BETA(ICOR,BETAT)
      WRITE(6,4300) A
      PFLTS=0.
      ILAN1=625
      ILAN2=250
      WRITE(6,3500)
C
C     CYCLIC GROWTH ANALYSIS
C
      SMIN=0.
      DO 230 J1=1,NBLKS
      DO 220 J4=1,NLYR
      DADN=0.
      SIGMAX=SMAX(J4)
C
C     THE FOLLOWING LINES WERE ADDED TO PROGRAM TO
C     MODIFY SPECTRUM INPUT FOR INFREQUENT HIGH LOADS
C
      IF(J4.NE.30) GO TO 130
      IF(J1.NE.ILAN2) GO TO 120
      SIGMAX=0.818*DLS
      ILAN2=J1+500
  120 IF(J1.NE.ILAN1) GO TO 130
      SIGMAX=DLS
      ILAN1=J1+1250
```

```
C
C     COMPUTE KMAX & KMIN
C
  130 IF(SIGMAX.LT.SMIN) GO TO 210
      KMIN=SMIN*SQRT(PI*A)*BETAT
      R=SMIN/SIGMAX
      IF(KMIN.LT.SKMIN) SKMIN=KMIN
      KMAX=SIGMAX*SQRT(PI*A)*BETAT
      RETARD = 1
      IF(A.GE.ASUBP) GO TO 160
C
C     COMPUTE EFFECTIVE KMAX & KMIN
C
      SIGREF=(SIGMAY*SQRT(2.*(ASUBP-A)/A))/BETAT/SQRT(ROOT2)
      SIGRED=SIGREF-SIGMAX
      IF(OLMAX.NE.0.) GO TO 140
      PHI=1.
      GO TO 150
  140 THRSLD=DELKTH*(1.-R**2)
      PHI=(1.-THRSLD/KMAX)/(OLMAX-1.)
      SIGRED=PHI*SIGRED
  150 IF(SIGRED.LT.0.) SIGRED=0.
      SIGMAX=SIGMAX-SIGRED
      IF(SIGMAX.LE.0.) GO TO 210
      KMNEFF=KMIN-SIGRED*SQRT(PI*A)*BETAT
      IF(KMNEFF.LT.0.) KMNEFF=0.
      KMXEFF=SIGMAX*SQRT(PI*A)*BETAT
      REFF=KMNEFF/KMXEFF
C
C     COMPARE EFFECTIVE PLASTIC ZONE INTERFACE WITH PREVIOUS
C     INTERFACE
C
      RSUBY1=(KMAX**2-3./32.*SKMIN**2)/2./PI*ROOT2/SIGMAY**2
      IF(A+RSUBY1.LT.ASUBP) GO TO 170
C
C     THIS CYCLE IS NOT RETARDED
C
  160 RETARD=0
      RSUBY=(KMAX**2-3./32.*SKMIN**2)/2./PI*ROOT2/SIGMAY**2
      ASUBP=A+RSUBY
      SKMIN=1.E20
      KMXEFF=KMAX
      KMNEFF=KMIN
      REFF=KMIN/KMAX
C
C     COMPUTE DA/DN
C
  170 IF(KMXEFF.LE.KMNEFF) GO TO 180
      IF(KMAX.GE.KSUBC) GO TO 240
      THRSLD=DELKTH*(1.-R**2)
      DELTAK=KMXEFF*(1.-REFF)
      IF(DELTAK.LE.THRSLD) GO TO 180
      DELK=(1.-REFF)*(1.-(1.-REFF)*ZK)/(1.-ZK)*KMXEFF
      IF(REFF.LT.0.) DELK=(1.-ZK*EXP(0.1*REFF))*KMXEFF/(1.-ZK)
      DELTAK=ALOG10(DELK)
```

```
      CALL TLU(CARRAY,SNARAY,NDADN,DELTAK,DADN)
      DADN=10.**DADN*KSUBC/(KSUBC-KMAX)
C
C     COMPUTE ENVIRONMENTAL ACCELERATION
C
  180 IF(NEN.EQ.0) GO TO 210
      IF(TIME(J4).EQ.0.) GO TO 210
      F=0.5/TIME(J4)
      IF(R.GT.0.9) GO TO 190
      DADTL=CC+DD/KMXEFF
      GO TO 200
  190 DADTL=AA+BB/KMXEFF
      F=1./TIME(J4)
  200 IF(DADTL.LT.-99.) DADTL=-99.
      EDADN=10.**DADTL/F
      DADN=DADN+EDADN
C
C     INCREMENT A AND COMPUTE STRESS INTENSITY CORRECTION
C
  210 A=A+DADN
      SMIN=SMAX(J4)
      IF(DADN.LE.0.) GO TO 220
      IF(RDADN.LT.DADN) RDADN=DADN
      CALL BETA(ICOR,BETAT)
      REFK=DLS*SQRT(PI*A)*BETAT
      IF(RETARD.EQ.0) ASUBP=ASUBP+DADN
  220 CONTINUE
C
C     PRINT RESULTS
C
      CFLTS=FLTS*J1
      IF(CFLTS-PFLTS.LT.PRTFLTS) GO TO 230
      PFLTS=PFLTS+PRTFLTS
      WRITE(6,4400) CFLTS,A,REFK
  230 CONTINUE
      GO TO 250
  240 WRITE(6,4100)
      CFLTS=FLTS*J1
      WRITE(6,4200) CFLTS,A,REFK
  250 STOP 1776
 1000 FORMAT(5F10.0)
 2000 FORMAT(I10,5F10.0)
 2200 FORMAT(20A4)
 2300 FORMAT(1H1,/20A4)
 2350 FORMAT(/1X,20A4)
 3460 FORMAT(/T2,I8,' BLOCKS AT ',E12.5,' PSI DESIGN LIMIT STRESS')
 3500 FORMAT('   FLIGHTS     A      REFK'/)
 4100 FORMAT(/68(1H*)/1X,'KMAX EXCEEDS KSUBC. PROBLEM ',
     +'TERMINATED'/68(1H*)/,1X,'LAST CALCULATED VALUES ARE'/)
 4200 FORMAT(1X,'FLIGHT IN SPECTRUM ',F16.2/
     +       1X,'CRACK LENGTH       ',E16.8/
     +       1X,'REFK               ',E16.8)
 4300 FORMAT(//' BEGIN SPECTRUM CRACK GROWTH ANALYSIS, A =',F10.5/)
 4400 FORMAT(F8.0,F10.5,F10.5)
      END
```

```
C
C
C
      SUBROUTINE TLU(X,Y,N,XVAL,YVAL)
C
C     TABLE LOOK UP ROUTINE
C
      DIMENSION X(N),Y(N)
      IF(X(N).GE.XVAL) GO TO 10
      I=N
      GO TO 30
   10 DO 20 I=1,N
      IF(X(I).GE.XVAL) GO TO 30
   20 CONTINUE
   30 IF(I.EQ.1) I=2
      YVAL=(Y(I)-Y(I-1))/(X(I)-X(I-1))*(XVAL-X(I-1))+Y(I-1)
      RETURN
      END
C
C
C
      SUBROUTINE BETA(ICOR,BETAT)
C
C     STRESS INTENSITY FACTOR CORRECTIONS
C
      COMMON/A/A,RADIUS,ECCEN,AOC,THICK,NPTS,TABLEA(50),TABLEB(50)
      DATA PI/3.14159265/
      GO TO (10,20,30,40),ICOR
C
C     SINGLE THROUGH CRACK FROM OPEN HOLE
C
   10 AA1=1./COS(PI*(A+2.*RADIUS)/2./(2.*ECCEN-A))
      IF(AA1.LE.0.) AA1=1.E20
      BOWIE=0.6762062+(0.8733015/(0.3245442+A/RADIUS))
      BETAT=BOWIE*SQRT(AA1)
      GO TO 50
C
C     DOUBLE THROUGH CRACK FROM OPEN HOLE
C
   20 AA1=1./COS(PI*(A+RADIUS)/2./ECCEN)
      IF(AA1.LE.0.) AA1=1.E20
      BOWIE=0.9438510+(0.6805078/(0.2771965+A/RADIUS))
      BETAT=BOWIE*SQRT(AA1)
      GO TO 50
C
C     NEWMAN'S SEMI-ELLIPTICAL SURFACE FLAW CORRECTION
C
   30 AT=A/THICK
      IF(AT.GT.0.95) GO TO 35
      XMW=1./SQRT(COS(PI*A/2./AOC/ECCEN))
      XM1=1.13-0.1*AOC
      Q=1.+1.47*AOC**1.64
      XME=XM1+SQRT(Q/AOC-XM1)*AT**(2.+8.*AOC**3)
      BETAT=XMW*XME/SQRT(Q)
      GO TO 50
```

```
   35 A=(SQRT(AOC)+1.)**2*BETAT**2*A/4.
      ICOR=4
C
C     CENTER CRACK -FINITE WIDTH
C
   40 AA1=1./COS(PI*A/2./ECCEN)
      IF(AA1.LT.0.) AA1=1.E20
      BETAT=SQRT(AA1)
C
C     TABULAR CORRECTION
C
   50 IF(NPTS.EQ.0) GO TO 60
      CALL TLU(TABLEA,TABLEB,NPTS,A,COR1)
      BETAT=BETAT*COR1
   60 RETURN
      END
C
C
C
      SUBROUTINE ENVIR(DKA,DADNA,NDADNA,KSUBC,TYLD,CYLD,
     &AA,BB,CC,DD)
C
C     COMPUTATION OF SUSTAINED LOAD GROWTH DATA
C     FOR AGGRESSIVE ENVIRONMENT
C
      DIMENSION AK(32),DADNA(50),DADNB(50),DKA(50),DKB(50)
      DIMENSION DADT(32),DKC(32),DKD(50),DADND(50)
      INTEGER TITLE1(20),TITLE2(20)
      REAL KSUBC
      DATA AK/1.,2.,3.,4.,5.,6.,7.,8.,9.,10.,12.,14.,16.,18.,20.,22.5,
     &25.,30.,35.,40.,45.,50.,60.,70.,80.,90.,100.,110.,120.,130.,
     &140.,150./
C
C
C     READ DA/DN DATA FOR 10 CPS , R=0, SINE WAVE
C
C     INPUT FOR SINUSOIDAL WAVE DATA INCLUDES-
C
C     TITLE1 WHICH IDENTIFIES MATERIAL  & PRODUCT FORM FOR REFERENCE
C     KSUBC=CRITICAL STRESS INTENSITY FACTOR FOR MATERIAL THICKNESS
C     TYLD=MONOTONIC TENSILE YIELD STRESS
C     CYLD=CYCLIC TENSILE YIELD STRESS
C     NDADNA=NO. OF POINTS IN DA/DN TABLE (SINE WAVE)
C     FA=SINE WAVE FREQUENCY
C     DKA(I)=DELTA K VALUES OF POINTS IN DA/DN TABLE
C     DADNA(I)=DA/DN VALUES OF POINTS IN DA/DN TABLE
C
C
      READ(2,1000) TITLE1
 1000 FORMAT(20A4)
      READ(2,1000) KSUBC,TYLD,CYLD
      READ(2,2000) NDADNA,FA
 2000 FORMAT(I10,5F10.0)
      DO 10 I=1,NDADNA
      READ(2,3000) DKA(I),DADNA(I)
```

```
 3000 FORMAT(8F10.4)
      DKA(I)=ALOG10(DKA(I))
   10 DADNA(I)=ALOG10(DADNA(I))
      WRITE(6,1100) TITLE1
 1100 FORMAT(1H1/,' DA/DT IS DETERMINED FROM '/,20A4)
C
C     READ DA/DN DATA FOR 0.1 CPS, R=0, TRAPEZOIDAL WAVE
C
C     INPUT FOR TRAPEZOIDAL WAVE DATA INCLUDES-
C
C     TITLE2 WHICH IDENTIFIES MATERIAL & PRODUCT FORM FOR REFERENCE
C     KSUBC=CRITICAL STRESS INTENSITY FACTOR FOR MATERIAL THICKNESS
C     TYLD=MONOTONIC TENSILE YIELD STRESS
C     CYLD=CYCLIC TENSILE YIELD STRESS
C     NDADNB=NO. OF POINTS IN DA/DN TABLE (TRAPEZOIDAL WAVE)
C     FB=TRAPEZOIDAL WAVE FREQUENCY
C     DKB(I)=DELTA K VALUES OF POINTS IN DA/DN TABLE
C     DADNB(I)=DA/DN VALUES OF POINTS IN DA/DN TABLE
C
C
      READ(3,1000) TITLE2
      READ(3,3000) KSUBC,TYLD,CYLD
      READ(3,2000) NDADNB,FB
      DO 20 I=1,NDADNE
      READ(3,3000) DKB(I),DADNB(I)
      DKB(I)=ALOG10(DKB(I))
   20 DADNB(I)=ALOG10(DADNB(I))
      WRITE(6,1200) TITLE2
 1200 FORMAT(/' AND'/,20A4//)
C
C     DETERMINE DA/DT
C
      DNLIM=DKA(1)
      IF(DNLIM.LT.DKB(1)) DNLIM=DKB(1)
      UPLIM=DKA(NDADNA)
      IF(UPLIM.GT.DKB(NDADNB)) UPLIM=DKB(NDADNB)
      DO 40 J=1,32
      DO 30 I=1,32
      BK=ALOG10(AK(I))
      IF(BK.LT.DNLIM) GO TO 30
      IF(BK.GT.UPLIM) GO TO 45
      CALL TLU(DKA,DADNA,NDADNA,BK,DADN1)
      CALL TLU(DKB,DADNB,NDADNB,BK,DADN2)
      DADN1=10.**DADN1
      DADN2=10.**DADN2
      IF(DADN2.LE.DADN1) GO TO 30
      GO TO 35
   30 CONTINUE
   35 DADT(J)=(DADN2-DADN1)*FB
      DKC(J)=10.**BK
      DNLIM=ALOG10(AK(I+1))
   40 CONTINUE
   45 NDADT=J-1
      IF(NDADT.GT.0) GO TO 46
      AA=-30.
```

```
      BB=0.
      CC=-30.
      DD=0.
      GO TO 140
C
C     MAKE SURE DA/DT IS MONOTONIC
C
   46 N=NDADT
      NN=N-1
      DO 100 I=1,NN
      IF(I.GT.N-1) GO TO 100
   60 IF(DADT(I).LT.DADT(I+1)) GO TO 100
      M=I+1
      N=N-1
      IF(I.EQ.1) GO TO 80
      IF(M.GT.N) GO TO 100
      DO 70 J=M,N
      DKC(J)=DKC(J+1)
   70 DADT(J)=DADT(J+1)
      GO TO 60
   80 DO 90 J=1,N
      DKC(J)=DKC(J+1)
   90 DADT(J)=DADT(J+1)
      GO TO 60
  100 CONTINUE
      NDADT=N
C
C     CURVE FIT LOG10(DA/DT)
C
      DO 120 I=1,NDADT
  120 DADT(I)=ALOG10(DADT(I))
      CALL LSTSQR(DKC,DADT,NDADT,AA,BB)
C
C     INTEGRATE DA/DT FOR R=0, 1 CPS SINE WAVE
C
      N=1+KSUBC/10.
      IF(N.GT.10) N=10
      DO 130 I=1,N
      DKX=10.*(I-1)
      IF(I.EQ.1) DKX=5.
      CALL GAUSS(AA,BB,DKX,CC)
      DADND(I)=ALOG10(CC)
      DKD(I)=DKX
  130 CONTINUE
C
C     CURVE FIT LOG10(DA/DN)
C
      CALL LSTSQR(DKD,DADND,N,CC,DD)
  140 CONTINUE
C
C     REMOVE DA/DT FROM HIGH FREQUECY DA/DN
C
      DO 150 I=1,NDADNA
      DADN1=10.**DADNA(I)
      DKA(I)=10.**DKA(I)
```

```
      DADN2=10.**(CC+DD/DKA(I))/FA
      DADNA(I)=DADN1-DADN2
  150 CONTINUE
  999 RETURN
      END
C
C
C
      SUBROUTINE LSTSQR(X,Y,NDA,AA,BB)
C
C     LEAST SQUARES CURVE FIT OF Y=A+B/X. ROUTINE WRITTEN BY
C     H.T.YOUNG, MCDONNELL AIRCRAFT CO. ST. LOUIS MO.
C
      DIMENSION Y(100),X(100),A(20),B(400)
      DO 10 J=1,2
      DO 10 K=1,2
          L = 2 * (K-1) + J
      A(J)=0.0
      B(L)=0.0
      DO 10 M=1,NDA
      A(J) = A(J) + 1./X(M)**(J-1) * Y(M)
      B(L) = B(L) + 1./X(M)**(J-1) * 1./X(M)**(K-1)
 10   CONTINUE
      CALL SIMUL(B, A, 2, 1)
      AA=A(1)
      BB=A(2)
      RETURN
      END
C
C
C
      SUBROUTINE SIMUL(A,B,N,KS)
C
C     SIMULTANEOUS EQUATION SOLUTION
C
      DIMENSION A(1),B(1)
      TOL=0.0
      KS=0
      JJ=-N
      DO 65 J=1,N
      JY=J+1
      JJ=JJ+N+1
      BIGA=0
      IT=JJ-J
      DO 30 I=J,N
      IJ=IT+I
      IF(ABS(BIGA)-ABS(A(IJ))) 20,30,30
   20 BIGA=A(IJ)
      IMAX=I
   30 CONTINUE
      IF(ABS(BIGA)-TOL) 35,35,40
   35 KS=1
      RETURN
   40 I1=J+N*(J-2)
      IT=IMAX-J
```

```
      DO 50 K=J,N
      I1=I1+N
      I2=I1+IT
      SAVE=A(I1)
      A(I1)=A(I2)
      A(I2)=SAVE
   50 A(I1)=A(I1)/BIGA
      SAVE=B(IMAX)
      B(IMAX)=B(J)
      B(J)=SAVE/BIGA
      IF(J-N) 55,70,55
   55 IQS=N*(J-1)
      DO 65 IX=JY,N
      IXJ=IQS+IX
      IT=J-IX
      DO 60 JX=JY,N
      IXJX=N*(JX-1)+IX
      JJX=IXJX+IT
   60 A(IXJX)=A(IXJX)-(A(IXJ)*A(JJX))
   65 B(IX)=B(IX)-(B(J)*A(IXJ))
   70 NY=N-1
      IT=N*N
      DO 80 J=1,NY
      IA=IT-J
      IB=N-J
      IC=N
      DO 80 K=1,J
      B(IB)=B(IB)-A(IA)*B(IC)
      IA=IA-N
   80 IC=IC-1
      RETURN
      END
C
C
C
      SUBROUTINE GAUSS(AA,BB,X4,CC)
C
C     10 POINT GAUSS' RULE INTEGRATION ROUTINE
C
      DIMENSION U(5),R(5)
      DATA U/0.0744371695,0.216697697,0.339704784,0.432531683,
     &0.486953264/
      DATA R/0.147762112,0.13463336,0.109543181,0.0747256746,
     &0.0333356722/
      DATA PI/3.14159265/
      A=0.
      B=0.5
      C1=0.5*(B+A)
      C2=B-A
      S=0.
      DO 20 I=1,5
      W=C2*U(I)
      X=C1+W
      J=1
   10 XK=X4/2.*(1.-COS(2.*PI*X))
```

```
      IF(AA+BB/XK.GT.-99.) GO TO 12
      Y=0.
      GO TO 14
   12 Y=10.**(AA+BB/XK)
   14 S=S+R(I)*Y
      IF(J.EQ.2) GO TO 20
      X=C1-W
      J=2
      GO TO 10
   20 CONTINUE
      CC=S*C2
      RETURN
      END
```

SAMPLE INPUT

ANALYSIS FILE

```
SURFACE FLAW ANALYSIS
 0.0000
 0.0195
-0.5500     0.1000     3.5000
      4
 0.5000
      8
 0.0110     0.6412
 0.0126     0.6597
 0.0172     0.6857
 0.0315     0.7066
 0.0796     0.7328
 0.1216     0.7554
 0.2089     0.8104
 0.3237     0.8668
 100000
    185
    250
      1
```

HIGH FREQUENCY, SINE WAVE DA/DN DATA FILE

```
 HP 9-4-.30 STEEL IN SALT WATER AT 10 CPS
120.0000  212.0000  212.0000
      17        10.
 13.0000   0.87E-6
 14.0000   1.06E-6
 16.0000   1.45E-6
 18.0000   2.05E-6
 20.0000   2.80E-6
 22.5000   4.00E-6
 25.0000   5.40E-6
 30.0000   9.00E-6
 35.0000   1.30E-5
 40.0000   1.85E-5
 45.0000   2.40E-5
 50.0000   3.00E-5
 60.0000   4.50E-5
 70.0000   6.20E-5
 80.0000   8.90E-5
 90.0000   1.45E-4
100.0000   3.00E-4
```

LOW FREQUENCY, TRAPEZOIDAL WAVE DA/DN DATA FILE

```
 HP 9-4-.30 STEEL IN SALT WATER AT 0.1 CPS
120.0000  212.0000  212.0000
      17       0.1
 13.0000   1.45E-6
 14.0000   1.85E-6
 16.0000   2.65E-6
 18.0000   3.50E-6
 20.0000   4.50E-6
 22.5000   5.75E-6
 25.0000   7.10E-6
 30.0000   9.90E-6
 35.0000   1.30E-5
 40.0000   1.65E-5
 45.0000   2.15E-5
 50.0000   2.70E-5
 60.0000   4.20E-5
 70.0000   6.10E-5
 80.0000   8.80E-5
 90.0000   1.25E-4
100.0000   1.75E-4
```

SPECTRUM FILE

```
F15 MAIN GEAR OUTER TRUNNION STRESS HISTORY
      88     2.0000
 63.5000     2.0800
 63.5000    13.6000
 29.9000     1.0000
 46.2000     1.3300
 46.2000    27.2000
 29.9000     1.0000
 46.2000     1.3300
 46.2000    27.2000
 29.9000     1.0000
 46.2000     1.3300
 46.2000    27.2000
 -3.9000     3.5800
 29.5000      .7500
 25.6000      .3300
 37.1000      .2000
 20.5000      .4000
 37.1000      .7300
 20.5000      .4000
 37.1000      .7300
 20.5000      .4000
 37.1000      .7300
 20.5000      .4000
 37.1000      .7300
 20.5000      .4000
 25.6000      .2000
 25.6000      .3300
  0.0000      .0300
 41.6000      .0500
 16.2000      .0300
 23.5000      .4300
 13.8000      .2000
 47.5000     1.4300
 47.5000    10.9000
 20.5000     1.0000
 35.0000     1.3300
 35.0000    21.8000
 20.5000     1.0000
 35.0000     1.3300
 35.0000    21.8000
 20.5000     1.0000
 35.0000     1.3300
 35.0000    21.8000
 -4.5000     3.5800
 73.0000     2.0800
 73.0000    13.6000
 29.9000     1.0000
```

53.1000	1.3300
53.1000	27.2000
29.9000	1.0000
53.1000	1.3300
53.1000	27.2000
-4.5000	3.5800
29.5000	.7500
25.6000	.3300
37.1000	.2000
20.5000	.4000
37.1000	.7300
20.5000	.4000
37.1000	.7300
20.5000	.4000
37.1000	.7300
20.5000	.4000
37.1000	.7300
20.5000	.4000
25.6000	.2000
25.6000	.3300
0.0000	.0300
35.0000	.0500
16.2000	.0300
23.5000	.4300
13.8000	.2000
23.5000	.5300
13.8000	.2000
54.4000	1.4300
54.4000	10.9000
20.5000	1.0000
39.7000	1.3300
39.7000	21.8000
20.5000	1.0000
39.7000	1.3300
39.7000	21.8000
-4.9000	4.3300
20.2000	.3300
-4.9000	2.2500

OUTPUT FOR SAMPLE INPUT

```
   SURFACE FLAW ANALYSIS

 DA/DT IS DETERMINED FROM
   HP 9-4-.30 STEEL IN SALT WATER AT 10 CPS

 AND
   HP 9-4-.30 STEEL IN SALT WATER AT 0.1 CPS


    F15 MAIN GEAR OUTER TRUNNION STRESS HISTORY

   100000 BLOCKS AT    .18500E+03 PSI DESIGN LIMIT STRESS


 BEGIN SPECTRUM CRACK GROWTH ANALYSIS, A =     .01950

   FLIGHTS      A       REFK

    250.     .02379  35.21902
    500.     .02939  39.63150
    750.     .03669  44.70988
   1000.     .04615  50.60169
   1250.     .05847  57.67840
   1500.     .07444  66.21555
   1750.     .09588  77.05014
   2000.     .12534  91.53994
   2250.     .16994 114.49061

**********************************************************************
 KMAX EXCEEDS KSUBC. PROBLEM TERMINATED
**********************************************************************
 LAST CALCULATED VALUES ARE

 FLIGHT IN SPECTRUM          2440.00
 CRACK LENGTH          .25650853E+00
 REFK                  .16639628E+03
```

REFERENCES

1. Fujimoto, W. T., and Gallagher, J. P., "Summary of Landing Gear Initial Flaws", AFFDL-TR-77-125, December 1977.
2. Ryder, J. T., and Pickel, F. M., "Effect of Temperature on Stress Corrosion Cracking of 300M Steel", Journal of Testing and Evaluation, Vol, 6, No. 2, March 1978, pp. 129-133.
3. "Damage Tolerant Design Handbook", MCIC HB-01, Part 1, January 1975.
4. Forman, R. G., Kearney V. E., and Engle, R. M., "Numerical Analysis of Crack Propagation in Cylic-Loaded Structures", Journal of Basic Engineering, September 1967.
5. Dill, H. D., and Saff, C. R., "Spectrum Crack Growth Prediction Method Based on Crack Surface Displacement and Contact Analyses", Fatigue Crack Growth Under Spectrum Loads, ASTM STP 595, American Society for Testing and Materials, 1976, pp 306-319.
6. Wei, R. P., and Landes, J. D., "Correlation Between Sustained-Load and Fatigue Crack Growth in High Strength Steels", Materials Research and Standards, Vol. 9, No. 7, pp 25-28, July 1969.
7. Willenborg, J., Engle, R. M., and Wood, H. A., "A Crack Growth Prediction Model Using an Effective Stress Concept", AFFDL-TM-71-1-FBR, 1971.
8. Gallagher, J. P., and Hughes, T. F., "Influence of Yield Strength on Overload Affected Fatigue Crack Behavior in 4340 Steel", AFFDL-TR-74-27, March 1974.
9. Probst, E. P., and Hillberry, B. M., "Fatigue Crack Delay and Arrest Due to Single Peak Tensile Overloads", AIAA Paper 73-325, AIAA Dynamics Specialists Conference, Williamsburg, Va., March 19-20, 1973.
10. Wei, R. P., and Shih, T. T., "Delay in Fatigue Crack Growth", International Journal of Fracture, Vol. 10, No. 1, March 1974, pp 77-85.

11. Alzos, W. X., Skat, A. C., Jr. and Hillberry, B. M., "Effect of Single Overload/Underload Cycles on Fatigue Crack Propagation", Fatigue Crack Growth Under Spectrum Loads, ASTM STP 595, American Society for Testing and Materials, 1976, pp 41-60.
12. McGee, W. M., and Hsu, T. M., "Effects of Underloads on Fatigue Crack Growth", AFFDL-TR-77-2, March 1977.
13. Gallagher, J. P., and Stalnaker, H. D., "Methods for Analyzing Fatigue Crack Growth Rate Behavior Associated with Flight-by-Flight Loading", AIAA Paper 74-367, presented at the 15th Structure, Structural Dynamics and Materials Conference, April 17-19, 1974.
14. Engle, R. M., "CRACKS II, User's Manual", AFFDL-TM-74-173.
15. Dill, H. D., and Saff, C. R., "Effect of Fighter Attack Spectrum on Crack Growth", AFFDL-TR-76-112, March 1977.
16. Hsu, T. M., and Lassiter, L. W., "Effects of Compressive Overloads on Fatigue Crack Growth", AIAA Paper No. 74-365, AIAA/ASME/SAE Structures, Structural Dynamics and Materials Conference, Las Vegas, Nevada, April 17-19, 1974.
17. Fujimoto, W. T., "Determination of Crack Growth and Fracture Toughness Parameters for Surface Flaws Emanating from Fastener Holes", MCAIR Report A4093, 17 March 1976; Presented at the AIAA/ASME/SAE Structure, Structural Dynamics, and Materials Conference, Valley Forge, Pa, 4-7 May 1976.

☆U.S.Government Printing Office: 1979 — 657-002/ 353